

# **STUDY OF MACHINING CHARACTERISTICS IN WIRE ELECTRICAL DISCHARGE MACHINING OF NICKEL BASED ALLOY**

**Thesis**

*submitted in the fulfillment of the requirement of*

**DOCTOR OF PHILOSOPHY**

to

**YMCA UNIVERSITY OF SCIENCE & TECHNOLOGY**

**By**

**VINOD KUMAR**

Registration No. YMCAUST/ Ph31/2K11

**Under the Supervision of**

**Dr. Vikas Kumar**

Professor

Mechanical Engineering Deptt.

**Dr. Kamal Kumar**

Assistant Professor

Mechanical Engineering Deptt.



Department of Mechanical Engineering

Faculty of Engineering and Technology

**YMCA University of Science & Technology**

**Sector-6, Mathura Road, Faridabad, Haryana, India**

**August 2016**

## **CANDIDATE'S DECLARATION**

---

I hereby declare that this thesis entitled **“STUDY OF MACHINING CHARACTERISTICS IN WIRE ELECTRICAL DISCHARGE MACHINING OF NICKEL BASED ALLOY”** is being submitted in fulfillment of the requirements for the Degree of Doctor of Philosophy in Mechanical Engineering under Faculty of Engineering and Technology of YMCA University of Science & Technology, Faridabad, during the academic year 2011-2016, is a bonafide record of my original work carried out under the supervision of **Dr Vikas Kumar**, Professor, Mechanical Engineering Department, YMCAUST and **Dr. Kamal Kumar**, Assistant Professor, Mechanical Engineering Department, PEC University of Technology, Chandigarh and has not been presented elsewhere.

I further declare that this thesis does not contain any part of any work which has been submitted for the award of any degree either in this university or in any other university.



**(Vinod Kumar)**

**(YMCAUST/ Ph31/2K11)**

## CERTIFICATE OF THE SUPERVISORS

---

This is to certify that this thesis entitled “**STUDY OF MACHINING CHARACTERISTICS IN WIRE ELECTRICAL DISCHARGE MACHINING OF NICKEL BASED ALLOY**” by **VINOD KUMAR**, submitted in fulfilment of the requirement for the Degree of Doctor of Philosophy in Mechanical Engineering under Faculty of Engineering and Technology of YMCA University of Science & Technology, Faridabad, during the academic year 2011-2016, is a bonafide record of work carried out under our supervision.

We further declare that to the best of our knowledge, this thesis does not contain any part of any work which has been submitted for the award of any degree either in this university or in any other university.



**Dr. Vikas Kumar**

(Supervisor)

Professor

Mechanical Engineering Department  
YMCA University of Science and  
Technology, Faridabad, Haryana, India



**Dr. Kamal Kumar**

(Co-supervisor)

Assistant Professor

Mechanical Engineering Department  
PEC University of Technology,  
Chandigarh, India

Dated: 19/8/16

## ACKNOWLEDGEMENT

---

I would like to express my sincere gratitude to my supervisors Dr. Vikas Kumar and Dr. Kamal Kumar for giving me the opportunity to work in this area. It would never be possible for me to take this thesis to this level without their innovative ideas and to relentless support and encouragement.

It is my sincere thank to Dr. Dinesh Kumar, Vice Chancellor, YMCA University of Science and Technology (YMCAUST), Faridabad, Haryana, India for his truthful support.

I am also grateful to Dr. Sandeep Grover, Dean, Faculty of Engineering & Technology, YMCAUST, Faridabad, India for his sincere advice and support.

I am very much thankful to Dr. M. L. Aggarwal, Chairman, Mechanical Engineering Department, YMCAUST, Faridabad for his consistent support.

I am also thankful to all the faculty members of the department for their support and encouragement to achieve this goal. I am also thankful to all the staff members of the Department of Mechanical Engineering, YMCAUST, Faridabad, India and to all my well wishers for their inspiration and help.

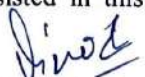
I wish to thank Sh. Santosh Yadav, owner of Ganpati Tools, MCF-4107, Sector 23, industrial area, Faridabad, Haryana, India for his valuable help in conducting the experiments on WEDM.

My special thanks and gratitude to Dr. Ram Bahadur Patel, Professor, Chandigarh College of Engineering and Technology, Sector 26, Chandigarh.

I would also like to give a special thank to my parents. Without their support and encouragement, it could not possible for me to fully dedicate myself to the research work. With my heart, I love them.

I feel deep sense of gratitude and reverence to my dear brothers and sisters for their blessing and endeavour to keep my moral high throughout the period of my work. I would like to thank my wife, Ms. Suman, and two loving kids, Shubham and Yashika for their patience and being source of my energy.

I want to express my sincere thanks to all those who directly or indirectly helped me at various stages of this work. Finally, Thanks to everyone who assisted in this research.

  
**Vinod Kumar**



## ABSTRACT

---

Materials used in the manufacture of aero-engine components generally comprise of nickel and titanium base alloys. These materials offer serious challenges for cutting tool materials during machining due to their unique combinations of properties such as high temperature strength, hardness, toughness and chemical wear resistance. These materials are referred to as difficult-to-cut since they possess a greater challenge to manufacturing engineers due to the high temperatures and stresses generated during machining. Therefore, non traditional techniques of machining are providing effective solutions to the problems imposed by the increasing demand for high strength temperature resistant alloys, the requirement of parts with intricate and compacted shapes and materials so hard as to challenge machining by conventional methods. Wire Electrical Discharge Machining (WEDM) is a non-conventional machine and proved more efficient and economic machining complex and difficult profiles in high strength and high heat resisting materials.

The objective of present research work is to study and optimized the various process parameters for different machining characteristics in machining of Nimonic 90 on WEDM. Using Response Surface Methodology (RSM), four discharge parameters namely peak current ( $I_p$ ), pulse-on time ( $T_{on}$ ), pulse-off time ( $T_{off}$ ) and servo voltage (SV) are investigated and modelled for three performance characteristics namely cutting speed (CS), surface roughness (SR) and radial overcut (RoC). In present experimentation, quadratic model is suggested for all three performance characteristics. Analysis of Variance (ANOVA) shows that  $I_p$ ,  $T_{on}$ ,  $T_{off}$  and SV are significant parameters affecting the CS and SR while  $I_p$ ,  $T_{on}$  and SV are highly significant parameters affecting the RoC. Desirability function is employed to optimize the multi-performance characteristics. Using SEM micrographs and micro-hardness profile, effect of discharge energy on surface morphology is examined. Trim cutting operations are performed after a rough cutting operation with different wire offset values for machining of Nimonic-90 with steel alloy, tungsten carbide composite and Monel-400 alloy. Results show that surface finish is improved significantly after trim cut operation irrespective of rough cutting operation. It is also noticed that multi-trim cutting operations are not much effective.

Trim cutting operation in WEDM is performed on Nimonic 90. Two machining characteristics namely surface roughness (SR) and dimensional shift ( $D_s$ ) are modelled and analysed using RSM in trim cutting operation. Four process parameters namely  $T_{on}$ , SV,  $W_d$  and FR are selected as variable parameters; while other parameters are kept fixed at their optimal setting in trim cutting operation.

Quadratic model is proposed to determine the optimal combination of surface roughness and dimensional shift. Using response surface graphs, the developed mathematical models are able to explain the effect of variables on performance characteristics efficiently. Increasing the value of  $T_{on}$ ,  $W_d$  and FR increases the surface roughness and dimensional shift but increases of SV decreases the both surface roughness and dimensional shift.

Using desirability function, a scale free quantity called desirability is obtained for two performance characteristics to optimize multi-performance characteristics. Corresponds to highest desirability, the optimal combination of discharge parameters is  $T_{on}$  110  $\mu$ s; SV 40V;  $W_d$  10  $\mu$ m and FR 2 L/min. Confirmation experiments prove the goodness of the proposed models and desirability function. Using SEM micrographs, effect of discharge energy on surface morphology is examined.

Using Al and Si metal powders in dielectric fluid, a remarkable modification is obtained for surface textures after trim cut. Using metal powder in dielectric fluid, the recast layer becomes smooth and dense and hence micro hardness increases. EDS analysis confirmed the presences of Al and Si elements on machined surface after trim cut.

Machining of Nimonic-90 with WEDM at optimized setting yields better performance and more economic as compared to conventional processes that proves the potential of WEDM in aerospace industries. Present research approach is useful for achieving high productivity while maintain surface roughness and geometrical accuracy within desire limits for machining complex and intricate shapes in hard and exotic materials.

This study is adding an opportunity for future research on powder mixed WEDM. In future work, WEDM parameters namely  $T_{on}$ ,  $I_p$ ,  $T_{off}$ , SV and WO using different concentration of metal powders may be investigated more precisely. Detailed investigation using high concentration of different metal powders may be carried out to modify the morphology of machined surface.

## TABLE OF CONTENTS

---

CANDIDATE'S DECLARATION	I
CERTIFICATE OF THE SUPERVISORS	II
ACKNOWLEDGEMENT	III
ABSTRACT	IV
TABLE OF CONTENTS	VI
LIST OF FIGURES	XI
LIST OF TABLES	XVIII
LIST OF ABBREVIATIONS	XX
 <b>CHAPTER 1: INTRODUCTION</b>	 <b>1-17</b>
1.1 INTRODUCTION	1
1.2 WIRE ELECTRICAL DISCHARGE MACHINING (WEDM)	4
1.2.1. WORKING PRINCIPAL OF WEDM	5
1.3 APPLICATIONS OF WEDM PROCESS	9
1.4 ADVANTAGES OF WEDM PROCESS	9
1.5 DISADVANTAGES OF WEDM PROCESS	10
1.6 WEDM PROCESS: A CURRENT VIEW	11
1.6.1 Optimizing the Process Variables	11
1.6.2 Monitoring and Controls the Process	11
1.6.3 Developments in WEDM Process	12
1.7 MOTIVATION	13
1.8 OBJECTIVES	13
1.9 WORK CARRIED OUT	14
1.10 ORGANISATION OF THE THESIS	16
 <b>CHAPTER 2: LITERATURE REVIEW</b>	 <b>18-32</b>
2.1 INTRODUCTION	18
2.2 MACHINING OF NICKEL BASED ALLOYS BY CONVENTIONAL MACHINES	18
2.3 MACHINING OF NICKEL-BASED ALLOYS BY NON-	22



	CONVENTIONAL MACHINES (WEDM AND EDM)	
2.4	OPTIMIZATION OF THE MACHINING PARAMETERS IN WEDM	25
2.5	TRIM CUTTING OPERATION IN WEDM	27
2.6	POWDER MIXED EDM	28
2.7	IDENTIFIED GAPS IN THE LITERATURE	31
2.8	DISCUSSION	32
 <b>CHAPTER 3: EXPERIMENTAL SET-UP AND PROCESS PARAMETERS SELECTION</b>		
		<b>33-58</b>
3.1	INTRODUCTION	33
3.2	MACHINE TOOL	33
3.3	WORK MATERIAL	35
3.4	PROCESS PARAMETERS	36
3.4.1	Discharge Parameters	36
3.4.2	Wire Electrode	37
3.4.3	Dielectric Conditions	38
3.5	MACHINING CHARACTERISTICS AND THEIR MEASUREMENT	40
3.5.1	Cutting Speed (CS)	40
3.5.2	Surface Roughness (SR)	41
3.5.3	Radial over Cut (RoC)	41
3.5.4	Wire off Set (WO)	42
3.5.5	Surface Integrity	42
3.6	TRIAL EXPERIMENTS	44
3.7	EFFECT OF WEDM PARAMETERS ON CS	44
3.7.1	Effect of Peak Current ( $I_p$ )	44
3.7.2	Effect of Pulse on Time ( $T_{on}$ )	46
3.7.3	Effect of Pulse off Time ( $T_{off}$ )	47
3.7.4	Effect of Servo Voltage (SV)	48
3.7.5	Effect of Wire Feed Rate ( $W_F$ )	49
3.8	EFFECT OF WEDM PARAMETERS ON SR	51
3.8.1	Effect of Peak Current ( $I_p$ )	51
3.8.2	Effect of Pulse on Time ( $T_{on}$ )	53



3.8.3	Effect of pulse off Time (Toff)	54
3.8.4	Effect of Servo Voltage (SV)	55
3.8.5	Effect of Wire Feed Rate ( $W_F$ )	56
3.9	RANGE OF PARAMETERS ON THE BASIS OF TRIAL EXPERIMENTATION	57
3.10	DISCUSSION	58

#### **CHAPTER 4: EXPERIMENTAL DESIGN METHODOLOGY AND DISCUSSION**

**59-85**

4.1	INTRODUCTION	59
4.2	RESPONSE SURFACE METHODOLOGY (RSM) AND EXPERIMENTAL DESIGN	59
4.3	CENTRAL COMPOSITE DESIGN (CCD)	61
4.3.1	Axial Points	62
4.3.2	Cube Points	62
4.3.2	Centre Point	63
4.4	CENTRAL COMPOSITE SECOND ORDER FACED CENTRED DESIGN	64
4.5	SELECTION OF PARAMETERS AND ITS RANGE BASED ON TRIAL EXPERIMENTATION	65
4.6	EXPERIMENTAL RESULTS	65
4.7	SELECTION OF ADEQUATE MODEL	68
4.8	RESULT AND ANALYSIS	68
4.8.1	Analysis of CS	72
4.8.2	Analysis of SR	76
4.8.3	Analysis of RoC	80
4.9	DISCUSSION	85

#### **CHAPTER 5: OPTIMIZATION USING DESIRABILITY FUNCTION FOR SINGLE AND MULTI MACHINING CHARACTERISTICS**

**86-113**

5.1	INTRODUCTION	86
5.2	DESIRABILITY FUNCTION	86
5.3	SINGLE RESPONSE OPTIMIZATION USING DESIRABILITY FUNCTION	88

5.3.1	Optimum Solutions	89
5.4	MULTI RESPONSE OPTIMIZATION USING DESIRABILITY FUNCTION	101
5.4.1	Model 1: Cutting Speed (CS) and Surface Roughness (SR)	102
5.4.2	Model 2: Cutting Speed (CS), Surface Roughness (SR) and Radial over Cut (RoC)	106
5.5	DISCUSSION	113

#### **CHAPTER 6: SURFACE INTEGRITY ANALYSIS OF MACHINED SURFACE AFTER ROUGH CUT OPERATION IN WEDM**

**114-123**

6.1	INTRODUCTION	114
6.2	RECAST LAYER	114
6.3	UNMACHINED AREA	118
6.4	DISCUSSION	123

#### **CHAPTER 7: COMPARISON OF ROUGH AND TRIM CUTTING OPERATIONS OF NIMONIC 90 WITH STEEL ALLOY, TUNGSTEN CARBIDE COMPOSITE AND MONEL 400 ALLOY**

**124-133**

7.1	INTRODUCTION	124
7.2	EXPERIMENTATION PROCEDURE	124
7.3	RESULTS AND ANALYSIS	126
7.3.1	Cutting Speed (CS)	126
7.3.2	Surface Roughness (SR)	127
7.3.3	Micro Hardness	130
7.4	DISCUSSION	133

#### **CHAPTER 8: OPTIMIZATION OF TRIM CUTTING OPERATION OF NIMONIC-90 WITH RSM USING DESIRABILITY FUNCTION**

**134-157**

8.1	INTRODUCTION	134
8.2	EXPERIMENTATION PROCEDURE	134
8.3	RESPONSE SURFACE METHODOLOGY (RSM) AND EXPERIMENTAL DESIGN	135
8.4	RESULTS AND ANALYSIS	136
8.4.1	Analysis of Surface Roughness (SR) in Trim Cutting Operation	141

8.4.2	Analysis of Dimensional Shift ( $D_s$ ) in Trim Cutting Operation	147
8.5	MULTI RESPONSE OPTIMIZATION USING DESIRABILITY FUNCTION IN TRIM CUTTING	151
8.5.1	Model 1: Surface Roughness (SR) and Dimensional Shift ( $D_s$ )	152
8.6	DISCUSSION	157
<b>CHAPTER 9: A EXPERIMENTAL STUDY ON ROUGH AND TRIM CUT AND METAL POWDER MIXED DIELECTRIC FOR WEDM OF NIMONIC 90</b>		<b>158-175</b>
9.1	INTRODUCTION	158
9.2	EXPERIMENTATION PROCEDURE	159
9.2.1	Setup for Supplying of Metal Powder Mixed Dielectric Fluid	159
9.2.2	Machined Geometry	160
9.2.3	Machining Conditions	160
9.3	RESULTS AND ANALYSIS	162
9.3.1	Effect on Cutting Speed (CS)	162
9.3.2	Effect on Surface Roughness (SR)	163
9.3.3	Surface Morphology and RCL	164
9.3.4	Micro Hardness	172
9.5	DISCUSSION	174
<b>CHAPTER 10: CONCLUSIONS AND SCOPE FOR FUTURE WORK</b>		<b>176-180</b>
10.1	INTRODUCTION	176
10.2	CONCLUSIONS	176
10.2	LIMITATIONS AND SCOPE FOR FUTURE WORK	180
<b>BIBLIOGRAPHIES</b>		<b>181-191</b>
<b>BRIEF BIO DATA OF THE RESEARCH SCHOLAR</b>		<b>192</b>
<b>LIST OF PUBLICATIONS</b>		<b>193-194</b>

## LIST OF FIGURES

---

Figure No.	Caption	Page No.
1.1	Parts of Combustion Chamber	2
1.2	Classification of Nickel Alloys	3
1.3	Gas Turbine Buckets	3
1.4	Classifications of Non-Conventional Manufacturing Processes	5
1.5	Wire Electrical Discharge Machining (WEDM) Process	6
1.6	Blade Root Slots in Turbine Blade Discs, (b, c) WEDM of Fir- Tree Root Slot	7
1.7	Inner Swirler with Twisted Vanes	8
1.8	Injector with Inner and Outer Swirlers	9
1.9	Classification of WEDM Research Areas	12
2.1	Finished Turbine Blade with EDM'd Cooling Holes and Shaped Diffusers	22
2.2	Cut Section of the Electro Plated Combustion Chamber Wall	24
2.3	Schematic Diagram of Trim Cutting Operation in WEDM Process	28
2.4	Powder Mixed Electrical Discharge Machining (PMEDM)	29
3.1	Machine setup of WEDM, Elektra Sprint Cut (ELPULSE-40)	30
3.2	Machining Parameters in WEDM	36
3.3	Series of Electrical Pulses at the Inter Electrode Gap	37
3.4	Surface Roughness Testers SJ-310	41
3.5	Representation of RoC in WEDM	42
3.6	Scanning Electron Microscope (SEM)	43
3.7	Micro Vickers Hardness Testing Machine HM-210/220	43
3.8	Effect of Variation in $I_p$ on CS at Different Value of $T_{on}$	45
3.9	Effect of Variation in $I_p$ on CS at Different Value of $T_{off}$ and $T_{on}$	46
3.10	Effect of variation in $T_{on}$ on CS	47
3.11	Effect of variation in $T_{off}$ on CS	48



3.12	Effect of Variation in SV on CS	49
3.13	Effect of variation in $W_F$ on CS	50
3.14	Effect of Variation in $I_p$ on SR at Different Value of Toff and Ton	52
3.15	Effect of Variation in $I_p$ on SR at Different Value of Ton	52
3.16	Effect of Variation in Ton on SR	53
3.17	Effect of Variation in Toff on SR	55
3.18	Effect of Variation in SV on SR	56
3.19	Effect of Variation in $W_F$ on SR	57
4.1	Axial points of a Full Factorial Design with Three Input Parameters.	62
4.2	Cube points of a Full Factorial Design with Three Input Parameters.	62
4.3	Generation of a CCD for Two Factors	63
4.4	Qualitative Design Space for a Two Parameter Face Centered Cubic Design	64
4.5	Normal Probability Residuals Plot for CS	73
4.6	Predicted vs. Actual Plot for CS	74
4.7a	Combined Effect of $I_p$ and Ton on CS (Toff: 40 $\mu$ s; SV: 40V)	75
4.7b	Combined Effect of $I_p$ and Toff on CS (Ton: 40 $\mu$ s; SV: 40V)	75
4.7c	Combined Effect of SV and $I_p$ on CS (Ton: 112 $\mu$ s; Toff: 40 $\mu$ s)	76
4.8	Normal Probability Residuals Plot for SR	78
4.9	Predicted vs. Actual for SR	78
4.10 a	Combined Effect of $I_p$ and Ton on SR (Toff: 40 $\mu$ s; SV: 40V)	79
4.10b	Combined Effect of $I_p$ and Toff on SR (Ton: 112 $\mu$ s; SV: 40V)	79
4.10c	Combined Effect of $I_p$ and SV on SR (Toff: 40 $\mu$ s; Ton: 112 $\mu$ s)	80
4.11	Normal Probability Residuals Plot for RoC	82
4.12	Predicted vs. Actual for RoC	82
4.13a	Combined Effect of $I_p$ and Ton on RoC (Toff:40 $\mu$ s; SV:40V)	83
4.13b	Combined Effect of $I_p$ and Toff on RoC (Ton: 112 $\mu$ s; SV:40V)	84
4.13c	Combined Effect of Toff and SV on RoC ( $I_p$ :120 A; Ton:112 $\mu$ s)	84
5.1	Surface Graph of Desirability for CS ( $I_p$ 140 A; SV 30 V)	93
5.2	Surface Graph of Desirability for CS (Ton 118 $\mu$ s; SV 30)	93

5.3	Surface Graph of Desirability for CS (Ton 118 $\mu$ s, Toff 35)	94
5.4	Surface Graph of Desirability for CS (Toff 36 $\mu$ s; SV 30 V)	94
5.5	3D Surface Graph of Desirability for SR (Toff 45 $\mu$ s; SV 50V)	95
5.6	3D Surface Graph of Desirability for SR (Ton 106 $\mu$ s; SV 50V)	95
5.7	3D Surface Graph of Desirability for SR (Ton 106 $\mu$ s; Toff 45 $\mu$ s)	96
5.8	3D Surface Graph of Desirability for SR (Ip 95A; Ton 106 $\mu$ s)	96
5.9	3D Surface Graph of Desirability for RoC (Toff 45 $\mu$ s; SV 30V)	97
5.10	3D Surface Graph of Desirability for RoC (Ton 106; SV 30V)	97
5.11	3D Surface Graph of Desirability for RoC (Ip 96 A; Ton 106 $\mu$ s)	98
5.12	Ramp Function Graph of Desirability for CS	99
5.13	Bar Graph of Desirability for CS	99
5.14	Ramp Function Graph of Desirability for SR	100
5.15	Bar Graph of Desirability for SR	100
5.16	Ramp Function Graph of Desirability for RoC	101
5.17	Bar Graph of Desirability for RoC	101
5.18	Ramp Function Graph of Desirability for CS and SR	103
5.19	Bar Graph of Desirability for CS and SR	104
5.20	3D Surface Graph of Desirability for CS and SR (Toff 37 $\mu$ s; SV 50V)	104
5.21	3D Surface Graph of Desirability for CS and SR (Ip 112A; SV 50V)	105
5.22	3D Surface Graph of Desirability for CS and SR (Ip 112A; Toff 37 $\mu$ s)	105
5.23	Contour Plot for Overall Desirability Function (Toff 37 $\mu$ s; SV 50V)	106
5.24	Bar Graph of Desirability for CR, SR and RoC	108
5.25	Ramp Function Graph of Desirability for CR, SR and RoC	109
5.26	3D Surface Graph of Desirability for CS, SR and RoC (Ip 92A; Toff 45 $\mu$ s)	109
5.27	3D Surface Graph of Desirability for CS, SR and RoC (Toff 45 $\mu$ s; SV 30 V)	110
5.28	3D Surface Graph of Desirability for CS, SR and RoC (Ip 94A; SV 30V)	110

5.29	3D Surface Graph of Desirability for CS, SR and RoC (Ton 108 $\mu$ s; SV 30V)	111
5.30	3D Surface Graph of Desirability for CS, SR and RoC (Ton 108 $\mu$ s; Toff 45 $\mu$ s)	111
5.31	3D Surface Graph of Desirability for CS, SR and RoC (Ip 94A; Ton 110 $\mu$ s)	112
5.32	Contour Plot for Overall Desirability Function (Toff 45 $\mu$ s; SV 30V)	112
6.1a	SEM Image of Machined Surface Corresponding to High DE (Ip 150 A; Ton 118 $\mu$ s; Toff 45 $\mu$ s; SV 30V)	115
6.1b	SEM Image of Machined Surface Corresponding to Medium DE (Ip 90 A; Ton 112 $\mu$ s; Toff 40 $\mu$ s; SV 40V)	116
6.1c	SEM Image of Machined Surface Corresponding to Low DE (Ip 90 A; Ton 106 $\mu$ s; Toff 45 $\mu$ s; SV 50V)	116
6.2a	SEM Image of Transverse Section Corresponding to High DE (Ip 150 A; Ton 118 $\mu$ s; Toff 45 $\mu$ s; SV 30V)	117
6.2b	SEM Image of Transverse Section Corresponding to Medium DE (Ip 90 A; Ton 112 $\mu$ s; Toff 40 $\mu$ s; SV 40V)	117
6.2c	SEM Image of Transverse Section Corresponding to Low DE (Ip 90 A; Ton 106 $\mu$ s; Toff 45 $\mu$ s; SV 50V)	118
6.3	EDS Analysis of Machined Surface for Corresponding to High DE (Ip 150 A; Ton 118 $\mu$ s; Toff 45 $\mu$ s; SV 30V)	119
6.4	Representation of Unmachined Surface Area in WEDM	120
6.5	SEM Image of Unmachined Surface (Ip 90 A; Ton 106 $\mu$ s; Toff 45 $\mu$ s; SV 50V)	120
6.6	SEM Image of Unmachined Surface (Ip 120 A; Ton 106 $\mu$ s; Toff 40 $\mu$ s; SV 50V)	121
6.7	SEM Image of Unmachined Surface (Ip 120 A; Ton 118 $\mu$ s; Toff 30 $\mu$ s; SV 40V)	121
6.8	SEM Image of Unmachined Surface ( Ip 150 A; Ton 118 $\mu$ s; Toff 40 $\mu$ s; SV 30V)	122
6.9	Micro-Hardness Profiles Underneath the Machined Surface at High and Low DE	122



7.1	Effect of Discharge Energy on CS	127
7.2	Effect of Discharge Energy on SR	128
7.3	Machined Surface of WC-Co Composite; (a) at Low D.E. (b) at High D.E.	128
7.4	Machined Surface of HCHCr; (a) at Low D.E. (b) at High D.E.	129
7.5	Machined Surface of Nimonic-90; (a) at Low D.E. (b) at High D.E.	129
7.6	Machined Surface of Monel-400; (a) at Low D.E. (b) at High D.E.	129
7.7	Effect of Trim Cutting Operation on SR	130
7.8a	Microhardness Profile Underneath the Machined Surface of WC-Co Composite	131
7.8b	Microhardness Profile Underneath the Machined Surface of HCHCr	131
7.8c	Microhardness Profile Underneath the Machined Surface of Nimonic 90	132
7.8d	Microhardness Profile Underneath the Machined Surface of Monel 400	132
8.1	Cutting Operations in WEDM Process	135
8.2	Normal probability Residuals Plot for SR in Trim Cutting Operation	140
8.3	Predicted vs. Actual Plot for SR in Trim Cutting Operation	140
8.4a	Combined Effect of SV and Ton on SR ( $W_d$ 20 $\mu$ m; FR 4L/min)	143
8.4b	Combined Effect of $W_d$ and Ton on SR (SV 30V; FR 4L/min)	143
8.4c	Combined Effect of $W_d$ and SV on SR (Ton 108 $\mu$ s; FR 4L/min)	144
8.4d	Combined Effect of FR and Ton on SR (SV 30V; $W_d$ 20 $\mu$ m)	144
8.5	SEM Image of Transverse Section of Sample 3 (Ton 104 $\mu$ s, SV 40V, $W_d$ 10 $\mu$ m, FR 2L/min)	145
8.6	SEM Image of Transverse Section of Sample 4 (Ton 112 $\mu$ s, SV 40V, $W_d$ 10 $\mu$ m, FR 2 L/min)	145
8.7	SEM Image of Transverse Section of Sample 15 (Ton 104 $\mu$ s, SV 40V, $W_d$ 30 $\mu$ m, FR 6 L/min)	146



8.8	SEM Image of Transverse Section of Sample 26 (Ton 108 $\mu$ s, SV 30V, W <sub>d</sub> 20 $\mu$ m, FR 4 L/min)	146
8.9	Normal probability Residuals plot for SR in Trim Cutting Operation	148
8.10	Predicted vs. Actual Plot for SR in Trim Cutting Operation	148
8.11a	Combined Effect of FR and Ton on D <sub>s</sub> (SV 30V; W <sub>d</sub> 20 $\mu$ m)	150
8.11b	Combined Effect of W <sub>d</sub> and SV on D <sub>s</sub> (Ton 108 $\mu$ s; FR 4L/min)	150
8.11c	Combined Effect of FR and W <sub>d</sub> on D <sub>s</sub> (Ton 108 $\mu$ s; SV 30V)	151
8.12	Ramp Function Graph of Desirability for SR and D <sub>s</sub>	153
8.13	Bar Graph of Desirability for SR and D <sub>s</sub>	153
8.14	3D Surface Graph of Desirability for SR and D <sub>s</sub> (W <sub>d</sub> 10 $\mu$ m; FR 2L/min)	154
8.15	3D Surface Graph of Desirability for SR and D <sub>s</sub> (SV 40V; FR 2L/min)	154
8.16	3D Surface Graph of Desirability for SR and D <sub>s</sub> (SV 40V; W <sub>d</sub> 10 $\mu$ m)	155
8.17	3D Surface Graph of Desirability for SR and D <sub>s</sub> (Ton 104 $\mu$ m; FR 2L/min)	155
8.18	3D Surface Graph of Desirability for SR and D <sub>s</sub> (Ton 104 $\mu$ m; SV 40V)	156
8.19	Contour Plot for Overall Desirability Function (W <sub>d</sub> 10 $\mu$ m; FR 2L/min)	156
9.1	Experimental Setup for Powder Mixed WEDM (PWEDM)	159
9.2	Geometry of Wire Path for Rough and Trim Cutting Operation	160
9.3a	Influence of Concentration of Metal Powder on CS for Trim Cut	162
9.3b	Influence of Concentration of Metal Powder in Dielectric Fluid for Trim Cut on SR	164
9.4	Influence of Concentration of Metal Powder in Dielectric Fluid for Trim Cut on SR	164
9.5a	SEM Image of Machined Surface after Rough Cut at High DE	165
9.5b	SEM Image of Machined Surface after Trim Cut (Without Metal Powder)	165
9.5c	SEM Image of Machined Surface after Trim Cut using 3g/L Al	166

	Powder in Dielectric	
9.5d	SEM Image of Machined Surface after Trim Cut using 3 g/L Si Powder in Dielectric	166
9.6a	SEM Image of Transverse Surface after Rough Cut at High DE	167
9.6b	SEM Image of Transverse Surface after Trim Cut (Without Metal Powder)	167
9.6c	SEM Image of Transverse Surface after Trim Cut using 3g/L Al Powder in Dielectric	168
9.6d	SEM Image of Transverse Surface after Trim Cut using 3 g/L Si Powder in Dielectric	168
9.7	Comparison of Different WEDM Operations for Thickness of RCL	169
9.8a	EDS Analysis of Machined Surface after Rough Cut at High DE	170
9.8b	EDS Analysis of Machined Surface after Trim Cut	171
9.8c	EDS Analysis of Machined Surface after Trim Cut using 3g/L Al Powder	171
9.8d	EDS Analysis of Machined Surface after Trim Cut using 3g/L Si Powder	172
9.9a	Micro Indent on Transverse Surface	173
9.9b	Comparison of Micro-Hardness Underneath the Machined Surface under Different Process Conditions	173

## LIST OF TABLES

Table No.	Caption	Page No.
3.1	Specification of the CNC WEDM Machine Tool	34
3.2	Chemical Composition and Mechanical Properties of Nimonic 90	35
3.3	Effect of Variation in $I_p$ on CS	45
3.4	Effect of Variation in $T_{on}$ on CS	46
3.5	Effect of Variation in $T_{off}$ on CS	47
3.6	Effect of Variation in SV on CS	48
3.7	Effect of Variation in $W_F$ on CS	50
3.8	Effect of Variation in $I_p$ on SR	51
3.9	Effect of Variation in $T_{on}$ on SR	53
3.10	Effect of Variation in $T_{off}$ on SR	54
3.11	Effect of Variation in SV on SR	55
3.12	Effect of Variation in $W_F$ on SR	57
3.13	Process Parameters and their Range	58
4.1	Components of Central Composite Second Order Faced Centred Design for Four Variables.	65
4.2	Variables Process Parameters and their Levels	65
4.3	Test Conditions in Face Centered CCD for Four Parameters	66
4.4	Experimental Results of CS, SR and RoC	67
4.5	Selection of Adequate Model for CS	69
4.6	Selection of Adequate Model for SR	70
4.7	Selection of Adequate Model for RoC	71
4.8	ANOVA for CS (after backward elimination)	72
4.9	ANOVA for SR (after backward elimination)	77
4.10	ANOVA for RoC (after backward elimination)	81
5.1	Range of Input Parameters and CS for Desirability	88
5.2	Range of Input Parameters and SR for Desirability	88
5.3	Range of Input Parameters and RoC for Desirability	88

5.4	Set of Optimal Solutions of Desirability for CS	90
5.5	Set of Optimal Solutions of Desirability for SR	91
5.6	Set of Optimal Solutions of Desirability for RoC	92
5.7	Optimal Sets of Process Parameters Using RSM and Desirability Function	98
5.8	Range of Input Parameters and Machining Characteristics for Desirability (CS and SR)	102
5.9	Set of Optimal Solutions of Desirability for CS and SR	103
5.10	Predicted and Confirmatory values of CS and SR	106
5.11	Range of Input Parameters and Machining Characteristics for Desirability (CS, SR and RoC)	107
5.12	Set of Optimal Solutions of Desirability for CS, SR and RoC	108
5.13	Predicted and Confirmatory Values of CS, SR and RoC	113
7.1	Composition and Properties of Work Materials	125
7.2	Values of WEDM Parameters in Rough Cutting Operation	126
8.1	Fixed Machining Parameters in Rough & Trim Cutting Operations	136
8.2	Variable Process Parameters and Their Levels for Trim Cutting Conditions	136
8.3	Layout of Experimental Design for Face CCD of Second Order and Experimental Results in Trim Cutting Operation	137
8.4	Selection of Adequate Model for SR in Trim Cutting Operation	138
8.5	Selection of Adequate Model for $D_s$ in Trim Cutting Operation	139
8.6	ANOVA for SR in Trim cutting Operation	142
8.7	ANOVA for $D_s$ in Trim Cutting Operation	149
8.8	Range of Input Parameters and Responses for Desirability (SR and $D_s$ )	151
8.9	Process Parameters Combination for High Value of Desirability (SR and $D_s$ )	152
8.10	Predicted and Confirmatory Values of SR and $D_s$	157
9.1	Parameters Setting for Rough and Trim Cutting Operations	161



## LIST OF ABBREVIATIONS

---

Symbol	Description
ANOVA	Analysis of Variance
BUE	Built up edge
CCD	Central Composite Design
CS	Cutting speed
DE	Discharge energy
D <sub>s</sub>	Dimensional shift
DOF	Degree of freedom
EDM	Electrical Discharge Machining.
EDS	Energy Dispersive Spectroscopic
FEM	Finite Element Method
FR	Flow rate
GRA	Grey Relational Analysis
HDE	High discharge energy
HAZ	Heat affected zone
HB	Higher is better
I <sub>p</sub>	Peak current/ Discharge current
MR	Machining rate
MRR	Material removal rate
OA	Orthogonal array
PMEDM	Powder mixed Electrical Discharge Machining
RCL	Recast layer
RoC	Radial over cut
RSM	Response Surface Methodology
SEM	Scanning Electron Microscope

SDE	Specific Discharge Energy
SR	Surface roughness
SS	Sum of Square
SV	Servo voltage
Toff	Pulse-off time
Ton	Pulse-on time or pulse duration
TWECSM	Travelling wire electrochemical spark machining
$W_d$	Wire diameter
WEDM	Wire EDM/ Wire Electrical Discharge Machining
$W_F$	Wire feed
WO	Wire offset
$W_T$	Wire tension

## CHAPTER-I

### INTRODUCTION

---

#### 1.1 INTRODUCTION

The industrial and technological growths of mechanical industry have lead to the increases in demand for hard and tough materials. The materials – nano materials, cemented carbides, titanium alloys, stainless steels, ceramics and other heat resisting super alloys, etc., have an attractive properties viz, high bending stiffness, low thermal expansion, good damping capacity and better fatigue life make them potential materials for the current day manufacturing applications. They are finding in wide applications, i.e., nuclear engineering, aerospace, and other industries because of their high strength to weight ratio, hardness and heat resistance quality. The improved thermal, chemical, and mechanical properties of these materials are imparting high strength, heat resistance, corrosion resistance, and wear resistance to product performance and design.

Various alloys of steel, titanium, nickel, aluminium are extensively used in manufacturing of aero engine components. Metal-matrix composites and ceramic are also used in manufacturing of aero engine components. These materials give high temperature properties, low thermal diffusivity and high strength-to-weight ratio to make sure efficient fuel consumption for cost-effective operation of flight and longer functioning life. Nickel-based alloys and titanium alloys show good performance in operation as compared to steel which is very dense, and whose uses are restricted to smaller components. The most important uses of these alloys are in: (i) steam turbine power plants, e.g., blades, bolts, stack gas reheaters; (ii) aircraft gas turbines, e.g., combustion chambers, disks, castings, bolts, blades, shaft exhaust systems and brake disks vanes, etc.; {Figure 1.1} (iii) reciprocating engines, e.g., exhaust valves, turbocharger and hot plugs, etc.; (iv) metal processing, e.g., casting dies, hot work tool and dies,; (v) heat-treating equipments; (vi) medical applications, e.g., prosthetic devices and dentistry uses; (vii) space vehicles; (viii) chemical and petrochemical industries; (ix) nuclear power systems; (x) coal gasification and liquefaction systems and (xi) pollution control equipment; (Ezugwu et al. 2005).





**Figure 1.1:** Parts of Combustion Chamber (<http://spl.ch/products/index.html>)

Nickel based alloys play a very vital role in gas turbine compartments. An aircraft engine makes of three subassemblies, namely combustor, compressor and turbine housed in a titanium or aluminium casing. These materials maintain high mechanical and thermal fatigue, high mechanical and thermal shock and resistance to corrosion, creep and erosion at elevated temperature. Figure 1.2 shows the classification of nickel based alloys.

Nickel based alloys are especially used for the fabricating of turbine blades and buckets, which are operated at elevated temperature (up to  $520^{\circ}\text{C}$ ) and pressure in aero engine. They are designed with series of holes arranged in order to maximise external and internal cooling of blades. Generally turbine buckets are made of RENE 77, Udimet and IN738 {Figure 1.3}. Advanced composite and ceramics materials have high prospective for their applications in various fields of engineering because of their outstanding properties such as good thermal shock, resistance to high compressive strength and wear. Such superior material properties should create new challenges to manufacturing engineers to shape and size these electrically non-conductive materials efficiently and economically.

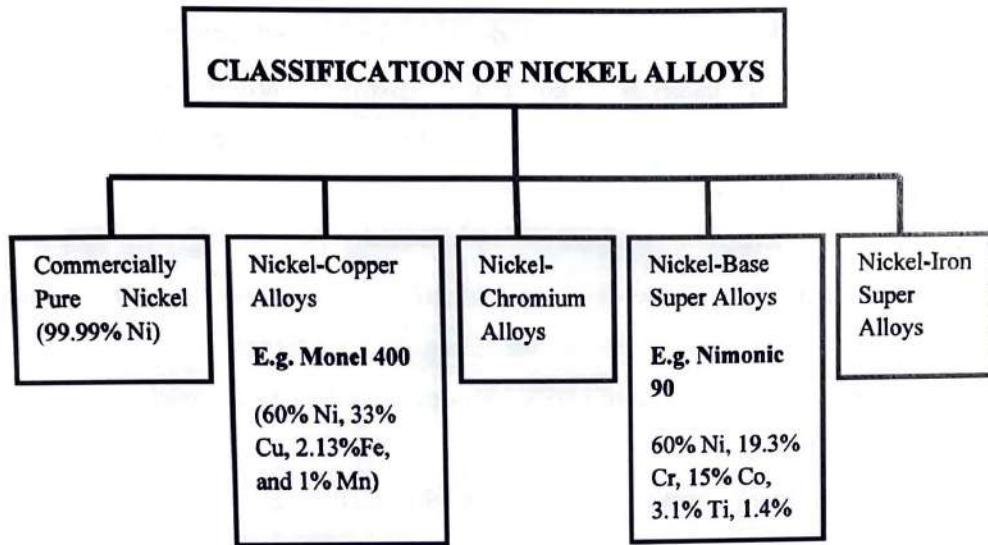


**Figure 1.2:** Classification of Nickel alloys



**Figure 1.3:** Gas Turbine Bucket (<http://unitedsurplusbuyers.com/turbines.htm>)

Machining of these materials with high precision accuracy is the main challenge for manufacturing industries. But, these materials are complicated to machine with conventional machines such as turning, milling, boring and drilling, etc. (Arunachalam et al. 2004; Garcia et al. 2008, Hood et al., 2011; Krain et al., 2007; Sharman et al., 2004; Soo et al., 2011). If it is required to maintain high accuracy and



surface quality excellence, then machining cost is increased. So that these conventional machines are unsuccessful due to excessive tool wear rate resulting poor surface finish and materials removal rate (MRR). Various non conventional machining processes have been developed for finding the efficient and better way of producing intricate geometry with high precision in high hardness and strength materials.

These processes may produce any intricate shape on any workpiece material by suitable control over the various machining parameters of the process. These processes may be classified into various groups according to the basic requirements which are as follow:

- Type of energy required - Mechanical, chemical and electrical, etc.
- Mechanism used in the machining processes - erosion, ionic dissolution and vaporizations, etc.
- Source required for material removal- hydrostatic pressure, high voltage, high current density and ionized materials, etc.
- Means for transfer of energies - high velocity particles, electron electrolyte, and hot gases, etc. On the basis of above requirements, the various processes are classified and given in Figure 1.4.

## **1.2 WIRE ELECTRICAL DISCHARGE MACHINING (WEDM)**

In contrast to conventional machining process, WEDM is proven more efficient and economic for machining the high temperature resistance and super alloys. It is a specialized thermal process which is capable of truly manufacturing complex geometries in hard composite materials that are very difficult to machine by conventional machining process. WEDM technology increases the productivity of fabricating micro tools because of more intricate tool geometries can be easily created with high quality using WEDM (Cheng et al. 2014). Its unique feature of using thermal energy to machine electrically conductive parts regardless of hardness with highest degree of surface finish and dimensional accuracy.



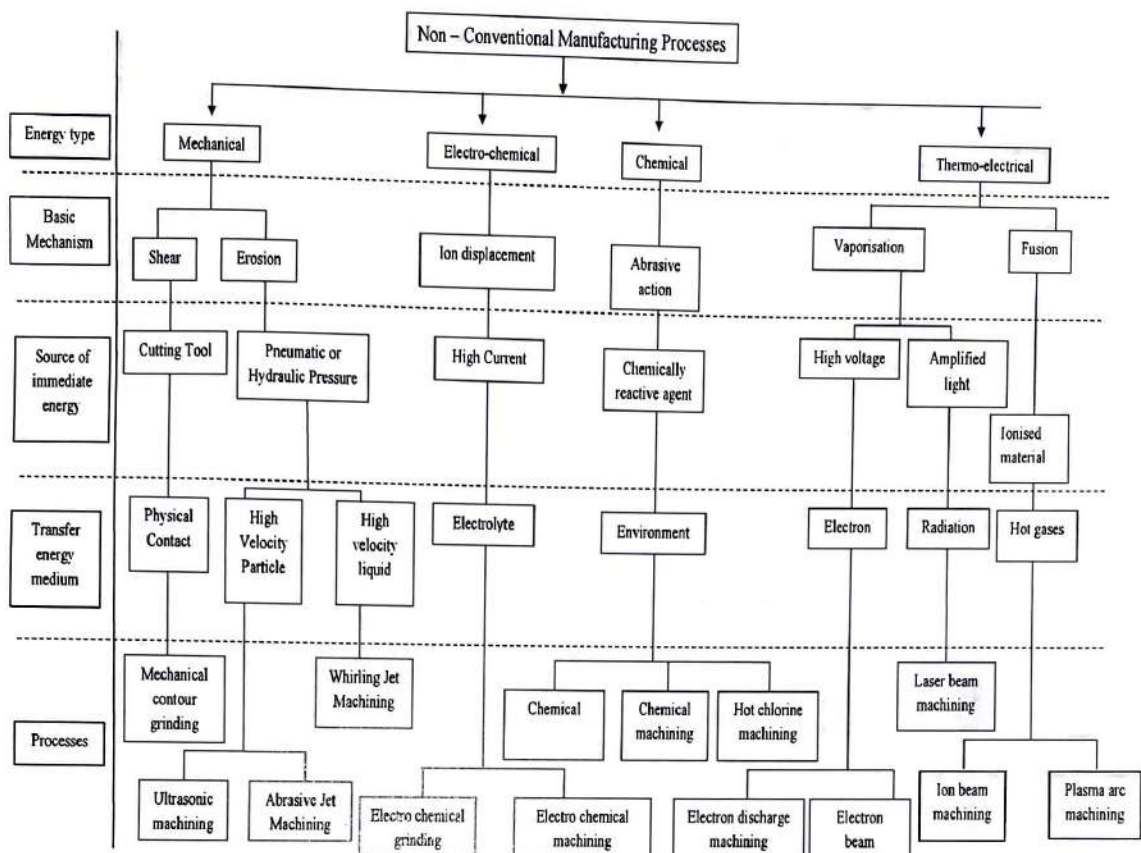


**Figure 1.4:** Classification of Non-Conventional Manufacturing Processes

### 1.2.1. Working Principal of WEDM

WEDM is a thermo electrical process in which a work material is eroded by a series of discrete electrical sparks occurring between electrode (Wire) and work piece as shown in Figure 1.5. The movement of wire is controlled numerically to attain the desire accuracy of the work piece and three dimensional shapes. Dielectric fluid is continuously fed to the machining zone to flush the eroded particles. It consumes a continuously travelling wire electrode made of copper or zinc coated brass wire of diameter 0.05–0.3 mm. It is capable to attain very small corner radii and capability to machine precise, irregular and complex shape with high surface finish and degree of accuracy.

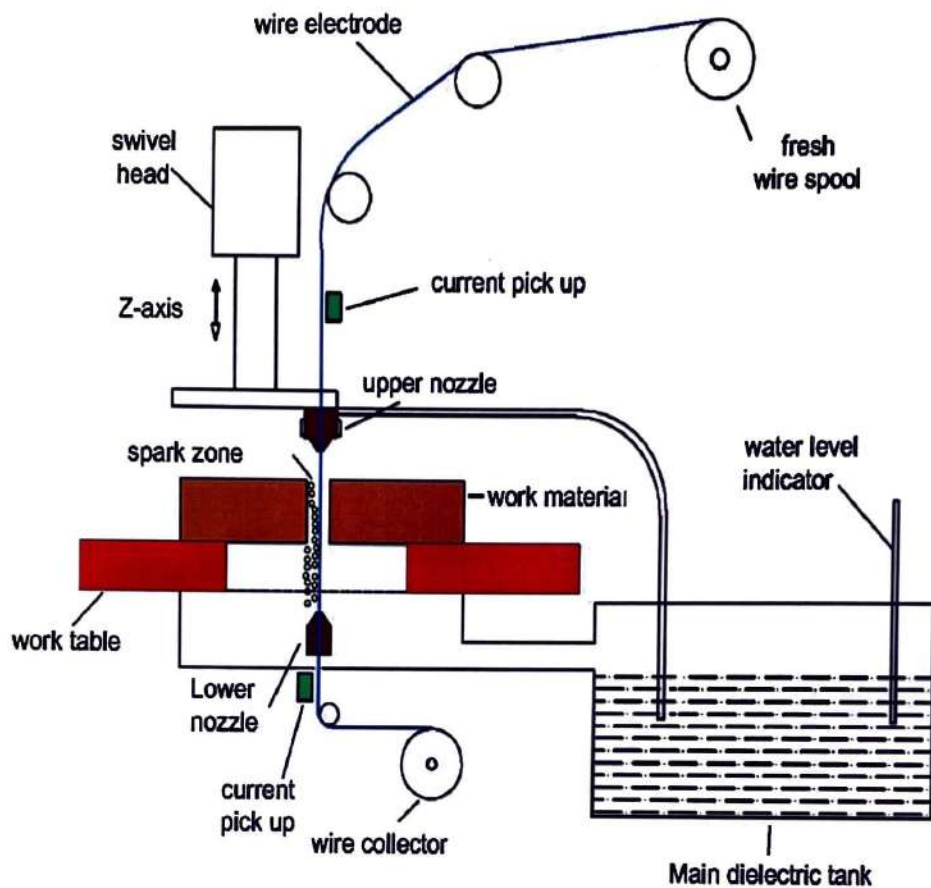


**Figure 1.5: Wire Electrical Discharge Machining (WEDM) Process**

The sparking occurs as a result of ionization of dielectric particles between the electrodes and give rise to extreme temperature rise between  $8000^{\circ}\text{C}$  to  $12000^{\circ}\text{C}$  causing fusion of the metal. Many sparks can be observed at one time. This is because actual discharges can occur more than one hundred thousand times per second, with discharge sparks lasting in the range of  $1/1,000,000$  of a second or less. Product of  $T_{on} * I_p$  may be expressed as the energy content of a single spark discharge. The volume of metal removed during this short period of spark discharge depends on the desired cutting speed (CS) and the surface finish required. These particles (chips) are flushed away from the cut with the help of a stream of dielectric fluid through the top and bottom flushing nozzles.

WEDM uses deionised water as a dielectric fluid instead of hydrocarbon oil which is uses in conventional Electrical Discharge Machining (EDM). WEDM is a

best option for making micro-scale parts with the highest degree of surface finish quality and dimensional accuracy. It may yield better finish and accuracy in fabricating the intricate and complex parts such as blade root slots in turbine discs as shown in Figure 1.6.

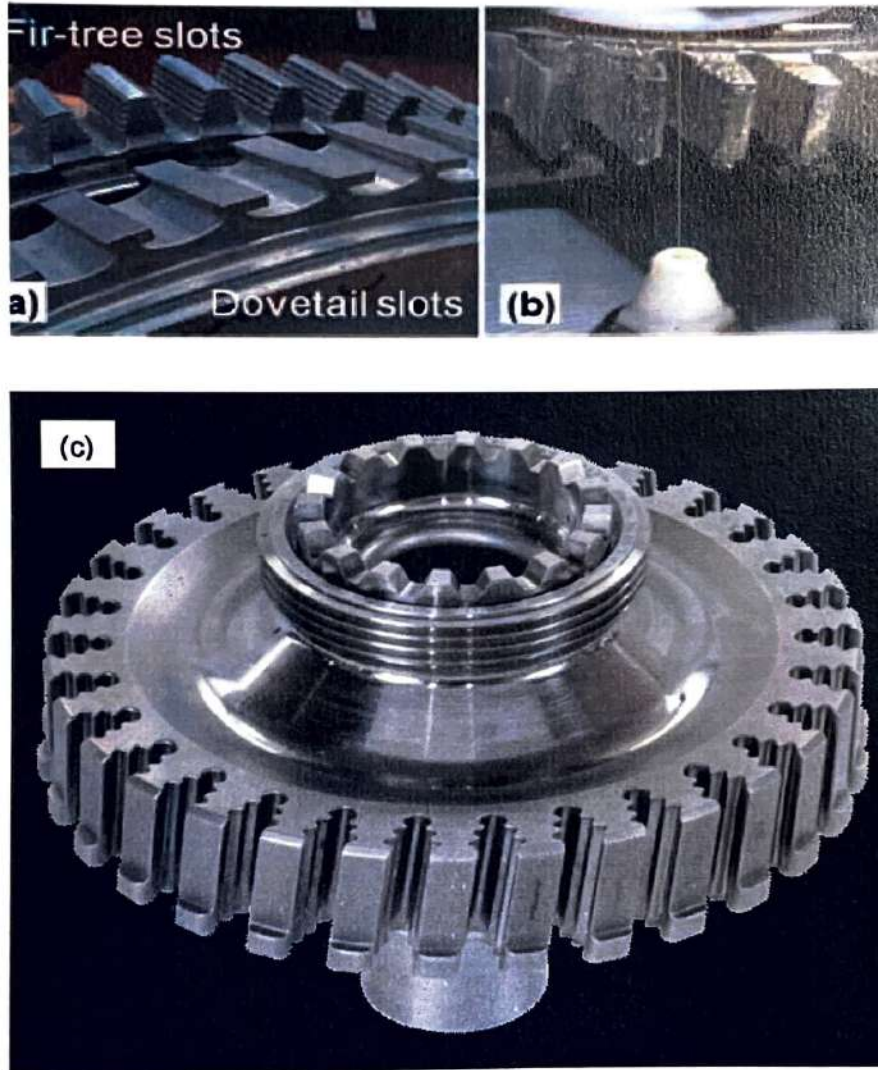


**Figure 1.6:** (a, b) WEDM of Fir-Tree Root Slot (Soo et al., 2013),  
(c) Blade Root Slots in Turbine Blade Discs  
(<http://www.bsel.co.il/Htmls/article.aspx>)

As compared to CNC milling machining, WEDM process is preferred for forming the slot pattern on the swirler blanks whereby material from the blanks is



removed to form the slot pattern as shown in Figures 1.7-1.8. This process presents significant improvement in the cost over former manufacturing methods, and results in producing swirlers that perform well in fuel atomization and combustion for gas turbine engine applications. The machining process involves removing material on single pass at a time along a certain trajectory or profile in a slow turning or profiling mode. It is extremely time consuming process. When, the swirlers are made of high-temperature hardened materials, the milling process becomes costly and also more time-consuming and cost of tooling usually increases considerably due to repeatedly changes of the cutting tools. WEDM process has successfully proved economical machining option to fulfil the demand of machine needs imposed by the growing cost pressures and the short product development cycles. A considerable amount of research has explored the different methodologies of achieving WEDM goals of optimizing the several process parameters analytically with the total abolition of the wire breakage thereby also improving the overall machining reliability.

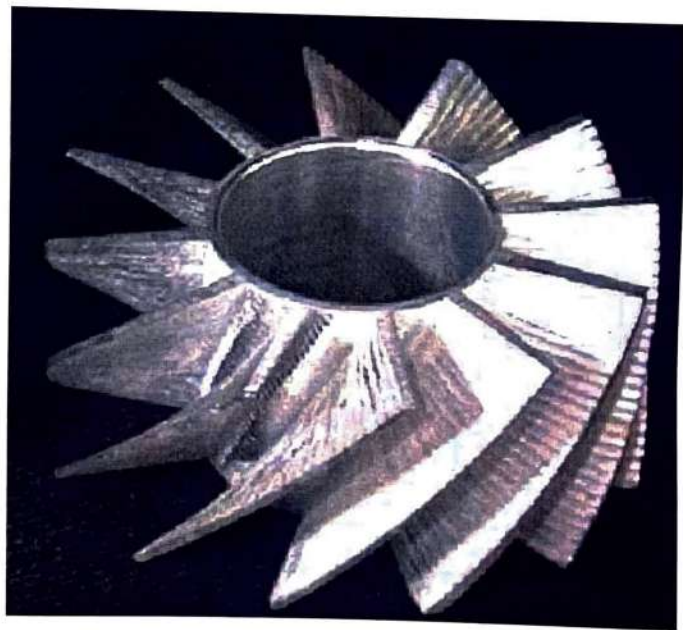


**Figure 1.7:** Inner Swirler with twisted vanes  
([http://www.enme.umd.edu/combustion/underwater\\_propulsion.htm](http://www.enme.umd.edu/combustion/underwater_propulsion.htm))



**Figure 1.8:** Injector with inner and outer Swirlers

([http://www.enme.umd.edu/combustion/underwater\\_propulsion.htm](http://www.enme.umd.edu/combustion/underwater_propulsion.htm))

### **1.3 APPLICATIONS OF WEDM PROCESS**

The present application of WEDM process includes aerospace, automotive, mould, tool and die manufacturing industries, and jewellery industries. Intricate profiles used in prosthetics, bio-medical applications can also be done in WEDM. Fine slits can be made by using a wire electrode. This process is very helpful for making of nozzles, other holes, shapes and profiles on high-temperature harden materials. WEDM helps to achieve accuracy up to 0.005 mm. In case of conventional EDM method, the manufacturing process requires several hours to manufacture electrodes, as well as many hours of manual grinding and polishing.

### **1.4 ADVANTAGES OF WEDM PROCESS**

WEDM process is important for repeatable tooling and higher tolerance parts. High degree of accuracy and tighter tolerances are required in medical, aerospace, injection moulding, and tool and die industries. WEDM process can easily make and duplicate the required specifications. A few advantages of using WEDM are as given below;

- **Efficient Production Capabilities** - Many parts can be more cost-effectively produced, because of the accuracy and high-speed of WEDM machines, rather than with conventional machining.
- **Reliable Repeatability** - WEDM process is more reliable as compared to conventional machining. Because the programs are computer generated and a constant wire diameter electrode is constantly being fed from a spool (the wire electrode is used only one time), the last part is identical to the former part. The cutter wear cannot measure accurately in conventional machining, which affects the final surface characteristics.
- **Unlimited Possibilities** – WEDM process can be economically produced many precious parts, such as: splitting tubes, shaft and collet slots, hexes, cams, gears, internal splines, extrusion moulds, and many other exotic shapes.
- **Exotic Materials** - Many exotic materials can be machined economically using WEDM, viz., Medical grade stainless, Tungsten carbide, Titanium, Nimonic, Monel, Inconel, Superalloys, Hastelloy, Aluminium alloys, Copper, etc. Brittle materials and work hardened metals can be shaped effectively and efficiently by WEDM that are intricate to machine by other conventional machining methods.
- **Elimination of Stress and Distortion** – Distortion of machined component is completely eliminated after heat treating. Because hardened materials can be easily machined by WEDM.
- **Burr-free, Superior Edge Finish** - WEDM shaped work pieces are true and burr-free with outstanding surface finish and ready for instantaneous use as final parts.

## 1.5 DISADVANTAGES OF WEDM PROCESS

WEDM has some disadvantages along with advantages as given below:

- MRR is low as compared to conventional machining processes.
- High cost of wire and machine tool.
- There is a problem regarding the formation of recast layer (RCL) on machined part surface.
- High specific energy consumption (about 50 times that in conventional machining), when forced circulation of dielectric is not possible.



- Surface cracking may occurs in brittle materials at room temperature especially when high energy per pulse is used.

## **1.6 WEDM PROCESS: A CURRENT VIEW**

WEDM process is divided into three main areas, specifically optimizing the process variables, monitoring & control the process and developments in WEDM {Figure 1.9}.

### **1.6.1 Optimizing the Process Variables**

It is a difficult task to optimizing the WEDM process due to the several machining variables. Even a single machining variable changes the process effectively. So that a best possible combination of machining parameters is essential for an optimal machining characteristics involves statistical and analytical methods. It is difficult task to correlate all the process parameters with the output machining characteristics to drive the optimum setting. Because of multi performance characteristics having conflicting nature, obtaining the optimal parameter setting in WEDM is a very tedious job. For example, for obtaining high MRR, high discharge energy (HDE) requires across the wire electrode and work material which results in intense heat generation due to large ionization of the spark gap. But high heat generation adversely affect the surface characteristics and dimensional tolerance of the machined component. Mathematical modelling of the process is an efficient approach to solve a boring problem of co-relating the process parameters to the machining characteristics. Thus matching the process machining parameters with characteristics is always a key area of research in the field of WEDM process optimization (Singh and Khanna, 2011).

### **1.6.2 Monitoring and Controls the Process**

Different monitoring and control systems are used for the WEDM process. Fuzzy control system, wire inaccuracy adaptive controls system and self- tuning adaptive controls systems are used for WEDM process (Liao et al. 2000; Yan and Hsieh, 2014). These systems consider numerous machining variables, identify the important machining factors affecting the process and make changes to the machining condition without using any detailed mathematical model. A fuzzy control strategy is used to improve corner accuracy by increasing the value of pulse off time (Toff) through

reduction of wire lag near corner. On line closed loop, wire tension ( $W_T$ ) control system is used to improve in corner accuracy of product (Lin et al. 2001). Bending of the wire and wire breakage during cutting operation may also reduce the accuracy resulting decreases the accuracy and efficiency of the WEDM process (Liao et al. 1997). Overall productivity is also reduced with the frequent occurrence of wire breakage. Wire bending and static deflection are also affected the geometric accuracy of the machined product. The knowledge of wire lag phenomenon and gap force is very crucial to achieve higher accuracy. Reducing the discharge energy and increasing the machining gap are only solution of wire deflection and wire lag. These are the most important shortcoming in WEDM process efficiency.

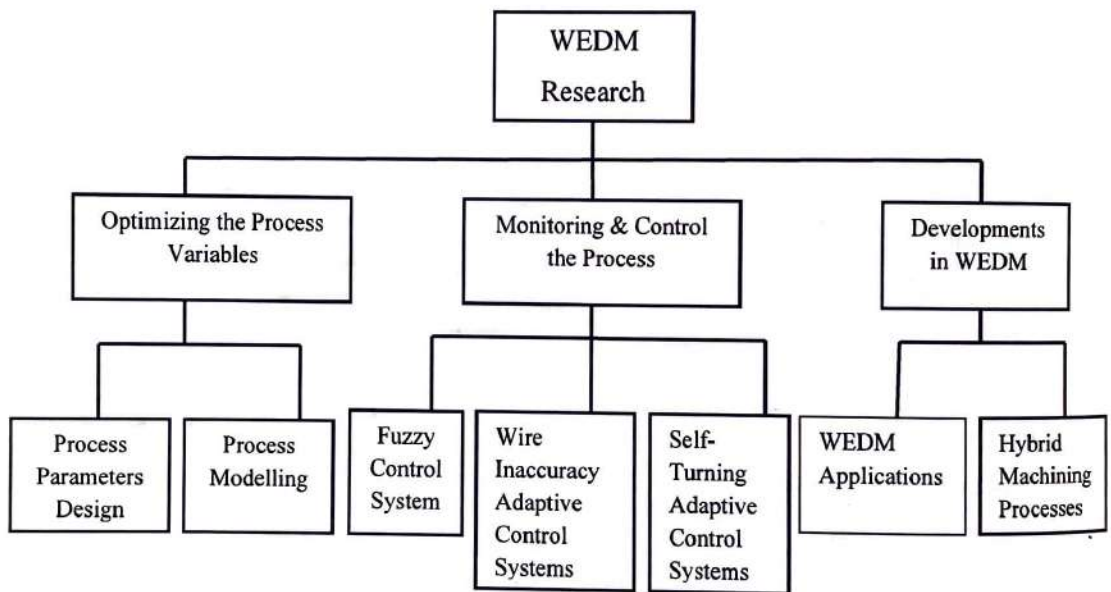


**Figure 1.9:** Classification of WEDM Research Areas (Ho et al. 2004)

### 1.6.3 Developments in

WEDM may be proved more efficient and economic in machining the high temperature resistance and super alloys. Machining of ceramic materials using WEDM process has been completely replaced the conventional machining processes namely ultrasonic and laser beam machining. These conventional machining processes are not only expensive to machines but also harm the surface integrity of materials. WEDM is a non-conventional machining process which has the capability



to produce precisely, intricate shapes and profiles in hard and high strength super alloys. Micro-EDM is also a well-established machining alternative for manufacturing. Consequently, micro electro discharge machining (Micro-EDM) has attracted much research attention. This non-conventional material removal process is extensively used in machining micro-structures. Micro-EDM is capable of machining micro-holes and micro-shafts as small as 5 mm in diameter, and also drills complex three dimensional micro-cavities geometrically complex small parts of hard or super-tough materials.

### **1.7 MOTIVATION**

The present work "Study of Machining Characteristics in WEDM of Nickel Based super alloy" is under taken into consideration due to the following reasons:

- Nickel based alloys are increasingly used in recent manufacturing applications, due to their outstanding properties such as good wear resistance, high toughness, high strength to weight ratio, lower value of coefficient of thermal expansion and capability of operating at very high temperature. They show ineffectiveness in machining by conventional machines such turning, drilling, milling, shaping and grinding, etc. Since it results in poor CS, excessive tool wear and increased surface roughness (SR).
- Nimonic-90 (a nickel-chromium-cobalt alloy) is a most suitable for high temperature applications ( $600^{\circ}\text{C}$  to  $900^{\circ}\text{C}$ ), mainly employed in turbine blades and combustion chamber. As per literature available, a little or negligible research work is found on machinability of Nimonic-90.
- The majority of the research work conducted on WEDM deals with rough cutting operation and a very limited research work have been conducted for trim cutting operation.
- Also, earlier no research work found on metal powders mixed dielectric in WEDM.

### **1.8 OBJECTIVES**

The present state of arts of machining of Nimonic 90 on WEDM suggests that there is a need to study the effect of various machining process parameters for different machining characteristics of it. Further it is also required to analyze the influence of

discharge energy (DE) on machined surface. To achieve this, we outlined the following:

1. Experimental investigation of WEDM process parameters for machining characteristics, namely cutting speed, surface roughness to determine the important parameters and their working range for Nimonic 90, with one parameter at a time approach.
2. Use of Face Centered Composite Design of Experiment to investigate simultaneously the influence of significant WEDM process parameters viz., peak current ( $I_p$ ), pulse on time ( $T_{on}$ ), pulse off time ( $T_{off}$ ), and servo voltage (SV) during rough cut, on the machining characteristics namely cutting speed (CS), surface roughness (SR) and radial over cut (RoC) for machining of Nimonic 90.
3. Development of an empirical relation between input WEDM parameters and machining characteristics using Response Surface Methodology (RSM).
4. Simultaneous optimization of WEDM parameters for multi machining characteristics using Desirability Function.
5. Analysis of surface integrity and micro hardness of machined surface after rough cut operation in WEDM.
6. Comparisons of rough and trim cutting operations of Nimonic-90 with steel alloy, Tungsten carbide composite and Monel-400 alloy.
7. Optimization of trim cutting operation of Nimonic-90 with Response Surface Methodology (RSM) using desirability function.
8. Investigating the Al and Si metal powder additives in dielectric fluid on machining characteristics of WEDM after trim cutting operation.

## **1.9 WORK CARRIED OUT**

In this thesis we studied and optimized the various machining process parameters for different machining characteristics of Nimonic 90 on WEDM. To fulfil the defined objectives, the following works are carried out.

1. Using Response Surface Methodology (RSM), four discharge parameters namely peak current ( $I_p$ ), pulse-on time ( $T_{on}$ ), pulse-off time ( $T_{off}$ ) and servo voltage (SV) are investigated and modelled for three machining characteristics namely cutting speed (CS), surface roughness (SR) and radial overcut (RoC). Quadratic



model is suggested for all three machining characteristics. Analysis of Variance (ANOVA) shows that  $I_p$ ,  $T_{on}$ ,  $T_{off}$  and  $SV$  are significant parameters affecting the  $CS$  and  $SR$  while  $I_p$ ,  $T_{on}$  and  $SV$  are highly significant parameters affecting the  $RoC$ .

2. Desirability function is employed to optimize the multi-performance characteristics. Correspond to highest desirability, the optimal combination of discharge parameters is  $I_p$ : 90A;  $T_{on}$ : 110 $\mu$ s;  $T_{off}$ : 45 $\mu$ s and  $SV$ : 30V and average value obtained for  $CS$ ,  $SR$  and  $RoC$  are 1.75m/min, 1.6 $\mu$ m and 21.61 $\mu$ m, respectively. Confirmation experiments prove the goodness of the proposed models and desirability function.
3. The surface integrity of WEDM surfaces of Nimonic 90 is investigated in case of rough cutting operation. SEM micrographs and micro-hardness profile are used to measure the effect of discharge energy on surface morphology. SEM results are used in comparative study of the surface texture and crater sizes of rough surface of specimens machined at high, medium and low discharge energy (DE). It is observed that recast layer (RCL) has lower hardness, due to which machined surface wear out quickly. These affect the surface quality and dimensional accuracy of the machined components. Therefore, in order to improve the surface integrity of machined surface, Trim cutting operation in WEDM is considered as a probable solution to improve surface characteristics and geometrical accuracy by removing very small amount of work materials from the surface obtained after a rough cutting operation at low DE.
4. Trim cutting operations are performed after a rough cutting operation with different wire offset values for four different materials, viz. Nimonic 90, steel alloy, tungsten carbide composite and Monel 400 alloy. Results show that surface finish is improved significantly after trim cut operation irrespective of rough cutting operation. It is also noticed that multi-trim cutting operations are not much effective. Surface finish may be improved using single trim cut at low DE with appropriate wire off-set value.
5. Trim cutting operation for two machining characteristics namely surface roughness ( $SR$ ) and dimensional shift ( $D_s$ ) are modelled and analyzed for Nimonic 90 using RSM in WEDM. Quadratic model is proposed to determine the optimal

combination of surface roughness and dimensional shift. It is observed that when increasing the value of  $T_{on}$ ,  $W_d$  and FR increases the surface roughness and dimensional shift but increases of SV decreases the both surface roughness and dimensional shift. Desirability function is employed to optimize the multi-performance characteristics. Using SEM micrographs, effect of DE on surface morphology is examined.

6. Using Al and Si metal powders in dielectric fluid in trim cutting operation; a remarkable modification is obtained on textures of machined surface after trim cut. Using metal powder in dielectric fluid, the recast layer becomes smooth and dense and hence micro hardness increases. EDS analysis confirmed the presences of Al and Si elements on machined surface after trim cut.

This study concludes that machining of Nimonic-90 with WEDM at optimized setting yields better performance and more economic as compared to conventional processes that proves the potential of WEDM in aerospace industries. Further, this study gives an opportunity for future research on powder mixed WEDM.

## **1.10 ORGANISATION OF THE THESIS**

The complete thesis is divided into ten chapters, which the work is presented as follows;

**Chapter 1** briefly explores the different nickel based heat resistance alloys and its application in various fields, the classification of non-conventional machining processes, basic principle of WEDM, applications, advantages, limitations and current view of WEDM, objectives of the present research.

**Chapter 2** presents review of machining of nickel based alloy in view of different conventional machines and non conventional machines (EDM and WEDM), modelling of the WEDM process by means of different mathematical techniques, viz., Response Surface Methodology (RSM), Taguchi method, Grey Relational method and Artificial neural network (ANN) model, etc. for different machining characteristics. It also discusses the parameter optimizations techniques for single response and multi-response characteristics. A review related to trim cutting operation in WEDM and concept of Powder mixed Electrical Discharge Machining (PMEDM) is also discussed and identified the gaps in the literature.



**Chapter 3** gives the information about experimental set up, material properties and selection of process parameters and its ranges on the basis of the trial experimentation for optimization studies.

**Chapter 4** explores on design of experiment techniques, i.e., Response surface methodology (RSM) along with Central Composite Design at full fraction. It gives planning and conducting the experiments to investigate the effect of process parameters on the machining characteristics, e.g., cutting speed (CS), surface roughness (SR), and radial over cut (RoC) using RSM. The experimental results are discussed and analyzed.

**Chapter 5** discusses the single and multi response optimization using Desirability Function. It presents optimized response using this technique and the optimal levels of process parameters yielding maximum desirability.

**Chapter 6** presents the surface characteristics of machined surface after rough cut operation in WEDM operation in terms of RCL and unmachined area. Effect of peak energy on surface characteristics including RCL and micro ridges is examined by using Scanning Electron Microscope (SEM) images.

**Chapter 7** gives a comparative study of effect of process parameters on machining characteristics during rough and trim cutting operation of Nimonic 90 in WEDM with three different materials namely WC-Co composite, HCHCr steel alloy and Monel-400.

**Chapter 8** deals with the development of mathematical model using RSM and multi response optimization using Desirability Function for trim cutting operation of Nimonic 90. Using SEM images, effect of discharge energy on surface morphology is also presented.

**Chapter 9** investigates an experimental study on WEDM of Nimonic-90, for rough and trim cutting operations without any metal powder additives and using Al and Si metal powders in dielectric fluid, the effect of mixing of Si and Al metal powders in dielectric fluid on surface morphology of Nimonic 90 during trim cutting operation in WEDM.

**Chapter 10** finally concludes the presented work in this thesis. This chapter also highlights the limitations and scope for future study.



## **CHAPTER-II**

### **LITERATURE REVIEW**

---

#### **2.1 INTRODUCTION**

The investigation of the machining characteristics, such as CS, SR, tool wear, MRR and surface integrity, etc. during machining by conventional and non- conventional machining of nickel based alloys are carried out by many researchers. These investigations are important because nickel based alloys are difficult to machine due to rapid work hardening during machining and their high shear strength and low thermal conductivity, etc. (Choudhury and El-Baradie 1998; Ezugwu et al. 1998; Guo et al. 2009). Surface characteristics of nickel based alloys are investigated using different cutting tool inserts, viz., residual stress, micro surface hardness, and surface roughness (SR) on the machined surface (Sharman et al. 2006). In order to predict the machining characteristics during machining, many researchers modeled the machining parameters using Response Surface Methodology (RSM), Gray Taguchi Method, Finite Element Method (FEM) based simulation using software and Artificial Neural Network (ANN), etc.

Nickel based alloys are currently being applied in the combustion chamber of aircraft engine, because of its unique resistance to thermal fatigue and creep characteristics. In order to understand and access the current status of research in the machining of Nickel based alloys, a review is done which is as follows:

#### **2.2 MACHINING OF NICKEL-BASED ALLOYS BY CONVENTIONAL MACHINES**

In last five decades, different grades of nickel based alloys are commercially available, such as- Inconel, Nimonic, Monel, Rene, Udimet and Pyromet, etc. These alloys may contain the constituents of chromium, titanium, aluminum, molybdenum, cobalt and other elements in varying quantity to give their excellent high temperature strength and intense toughness which create difficulties during machining because of resulting very high cutting forces on tools (Ezugwu et al. 1998). Aerospace industries are consuming nearly two third of nickel based alloys for manufacturing of aircraft engine parts due to capability to maintain high

mechanical and chemical properties at very high temperature (Ezugwu et al. 2005). Reliability is an important measure in the manufacturing of aerospace components, and hence, these component manufacturers need to keep high quality on a regular basis. Machining characteristics of nickel based alloys significantly affect the working life of its components. Several attempts have been made to evaluate the machining characteristics of nickel based alloys with conventional machining methods. Residuals stress profiles on the machined surface developed during the dry face turning negatively affect the fatigue life of machine parts (Kortabarria et al. 2011).

Choudhury and El-Baradie (1998) presented a general review for nickel based alloys on their machinability during turning using different cutting tool materials. It is observed that nickel based alloys are hard to machine, because of chip segmentation resulting in severe tool wear, their rapid work hardening during machining, and their strong tendency to form a built-up edge by welding to the tool material at high cutting temperatures.

These alloys show the poor machinability due to high hardness and toughness, poor thermal conductivity, corrosion resistance, ability to maintain mechanical and thermal shocks, fatigue, creep and erosion at elevated temperature and high strength to weight ratio as compared to stain steel alloy. Due to high heat resisting capacity, nickel based alloys are very intricate to machine with conventional machining processes such as turning, drilling, milling, etc. using ceramic and carbide tools. They have an austenitic matrix structure like stainless steel work is to be hardened rapidly during machining by cutting tools to contributing to notch wear at the tool nose (Choudhury et al. 1998). Presence of hard abrasive carbide in the nickel based alloy, cutting tool suffers high abrasive wear resulting high temperature generated at the tool tip (Ezugwu et al. 1998). A better understanding of different type of cutting tool materials, application of machined components, processing condition and machining time are essential for increasing the productivity, reducing manufacturing cost, without adverse effect on surface finish, the surface integrity and hardness variation of machined components.

Welding of Nickel alloy on to the cutting tool frequently occurs during machining and the poor thermal conductivity of nickel based alloy (about  $15 \text{ W/m}^\circ\text{C}$ ) comparative to conventional machining of cast iron and steels. These properties drastically increase in temperature at the cutting edge of tools and work piece during



machining. Consequently shorten the tool life. The various experimental and theoretical studies show that process characteristics may be improved significantly by selection of right tooling, materials and machining parameters (Mandal et al. 2011).

During machining of Nickel based alloys by different conventional machining processes, cutting tool materials are subjected to extreme mechanical and thermal stresses near to the cutting edge during machining resulting plastic deformation and accelerated tool wear rate. The cutting tool materials should possess adequate hot hardness to withstand a very high temperature due to weakening of inter particles bond strength and resulting accelerated the tool wear rate (Hood et al. 2011). The nickel based alloys are machined by various tools such as cemented tungsten carbide tool, ceramics tool e.g. Alumina and alumina TiC Ceramics, Whisker reinforced alumina ceramics and cubic boron nitride. Carbide tools are not withstood to high temperature. Better thermal properties and toughness of ceramic materials, which enables the tool material to withstand a high temperature and high wear at the cutting edge of tool. CBN is one of the hardest materials available after Diamond. It retains its hardness up to 340 HV during machining. It is most widely recommended for machining Inconel 718 (Ezugwu et al. 2003).

When machining a Nickel based alloy with profiled super abrasive grinding wheels. The tool wear of grinding wheel CBN is lower as compared to diamond (D46) grinding wheel at the high rotation speed with lower value of SR (Aspinwall et al., 2007). Milling or grinding processes may be used as alternatives for EDM process to machine shaped hole in Inconel 718 super heat resistant alloy. The result shows that milling process of Inconel 718 can produce shaped hold with an acceptable SR and geometrically accuracy efficient after optimizing the cutting condition (Wei, 2002; Ulutan and Ozel, 2011). The roughness of end mill specimens achieved up to 0.8  $\mu\text{m}$  when a new tool is to be used. The significant burr increased micro hardness and white layer formation when worn tools are used (Soo. et al. 2011). Flank wear of drilling tools is greatly affected the residual stress distribution and work piece surface integrity for RR1000 (Nickel based super alloy) (Kwong et al. 2009). The machining parameters such as feed rate, CS, geometry of tool, depth of cut, tool materials are greatly affected the tool life and tool wear rate. There is main effect of cutting tools edge geometry on surface integrity and tool life in turning of Nickel based alloy (Sharman et al. 2004).



Ezilarasan et al. (2011) proposed a second order model for generating relation between the cutting parameters (CS, depth of cut and feed rate) on the SR during machining of Nimonic C-263 by using a PVD coated cemented carbide insert. It is found that feed rate is the main process parameters for achieving minimum SR followed by CS and depth of cut. SR increases with increase of feed rate and is greatly affected by cutting edge angle and nose radius. This material showed the tendency to weld with tool material at high temperature. The poor thermal conductivity of these alloys result in focus of high temperatures at the tool work piece interface because of higher cutting conditions resulting significant reduction in the hardness and strength of the cutting tool. This decrease the bonding strength of the tool, thereby accelerating tool wear by mechanical abrasion and thermally related (diffusion and plastic deformation) mechanisms. High pressure generation and chemical affinity of the tool and work piece material are two main factors which are responsible for formation of built up edge (BUE). Work hardening of the work piece surface reduces the tool life due to abrasion (Krain et al. 2007). Haynes 282 is nickel based super alloy used for high temperature structural application, e.g., casing used in gas turbine aero-engine. Tool flank wear was generally uniform at lower operating parameters and most of wear took place on tool corner during drilling of Hayness 282 by using coated carbide tooling with high pressure (50 Bar) cutting fluid (Hood et al.2011). Flank wear is mainly responsible for damaged the machined surfaced during drilling of Nickel alloys. For aerospace applications, the post processing operations such as mill boring or reaming would be essential to remove the re-deposited material and white layer (Popa et al. 2010). A residual stress is considering one of important parameter used for determining the quality of machined surface. During dry machining, when CS increases up to 60m/min, a very high temperature is generated in the primary shear zone. This highly leads to decreases the cutting force. SR has a tendency to decrease with increase in CS in dry condition (Devillez et al. 2011). Formation of RCL and extensive material drag introduced during abusive mechanical drilling operation of Nickel based super alloy RR1000 due to combinations of high intensity of thermal and mechanical effects, i.e., phase transformation from rapid heating and cooling. As a result, very fine grain structure of approximately 50 nm is obtained on RCL. The hardness of white layer is found 455 higher than base material (Herbert et al. 2012). The high pressure coolant supplies approximately 15 MPa during machining of Inconel 718 which gives better

performance in terms of tool life and improved cooling and lubrication at the cutting interface. High cooling rate improve the tool life, effective chip segmentation and offering good lubrication at the tool chip interface. High pressure coolant supplies generally improves the SR. Micro hardness of the base material is lower than the finished surface (Ezugwu et al. 2005). The new developed materials show excellent mechanical and chemical properties at very high temperature. These types of alloys are very difficult to machine precisely with conventional machines due to their very high resistance and low thermal conductivity.

### **2.3 MACHINING OF NICKEL BASED ALLOYS BY NON-CONVENTIONAL MACHINES (WEDM AND EDM)**

EDM/WEDM is a non-conventional machine and proved more efficient and economic for machining complex and difficult profiles in high strength and high heat resisting materials. Since the adoption of EDM/WEDM in manufacturing industries, many successful attempts have been made in last five decades to improve the capability and commercialization of process. Some investigations are carried out on machining of nickel alloys with EDM or WEDM and most of these investigations evaluated the machining of Inconel grade of nickel alloys (In-601, In-718, etc.).



**Figure 2.1:** Finished Turbine Blade with EDM'd Cooling Holes and Shaped Diffusers (<https://commons.wikimedia.org/wiki/File:GaTurbineBlade.svg>)

Various gas turbine components (combustion chambers, blades, bolts, casing, shaft exhaust systems, vanes, etc.) are generally manufactured from nickel based alloy materials. Figure 2.1 shows finished turbine blade with EDM'd cooling holes



and shaped diffusers. Kang et al., (2003) investigated EDM characteristics of Nickel based heat resistance alloy Hastelloy-X. Ton was the most important factors that affect the surface integrity of the work material. In EDM, discharge energy (DE) is greatly affecting the surface integrity of machined surface. With increase of DE resulting formation of wider and deeper micro-cracks on the machined surface resulting increase of SR along with decrease of fatigue life of components.

The cracks are observed on the surface grows vertically into the base materials. Few cracks are found parallel to machined surface at high discharge energy (HDE). Due to ionization of dielectric fluid, carbon reacts with the highly reactive titanium, resulting formation of precipitations of titanium carbides in the melting zones. As a result significantly increase of micro-hardness of the melting zones than the hardness of the unexposed material. The change of microstructure of machine surface after EDM may lead to failure of the components. So, surface needs to be machined by an additional polishing method such as electro chemical polishing (Theisen et al. 2004). Some investigations are conducted to evaluate the effect of input process parameters on machining characteristics of WEDM process on different materials ranging from simple alloy steel to recently developed composite materials (Hascalyk and Caydas, 2004; Delgado et al., 2011). The machining parameter Ton is a main factors that affect the surface integrity of the work material, while machining of Hastelloy-X with EDM (Kang et al., 2003). Rajesha et al. (2011) reported the machining of EDM of Inconel 718 with hollow tubular copper electrodes and investigated the effect of five major parameters namely peak current ( $I_p$ ), duty factor, sensitivity control, gap control and flushing pressure on the machining characteristics (MRR, and SR). It is found that most influential factors are  $I_p$  and duty factor. In WEDM, input parameters may be categorised into three major categories - discharge parameters ( $I_p$ , Ton, Toff, SV), wire electrode (wire material, wire coating, wire diameter,  $W_T$ ,  $W_F$  rate, etc.) and dielectric conditions (dielectric conductivity, flow rate). Discharge parameters affect the heat released across the wire electrode and work material and hence affect MRR and surface characteristics of work material (Liao and Yu, 2004; Li et al., 2013; Spedding and Wang, 1997). Investigations revealed that wire electrode materials must be conductive and should have good tensile strength to bear the requisite  $W_T$ . Coating of wire electrode should possess small work function and high melting point to sustain high DE (Prohaszka et al., 1997). The combustion chamber consists of an



inner copper liner with cooling channels formed by WEDM and an outer shell of electro plated nickel {Figure 2.2}. Hewidy et al. (2005) correlated the various WEDM parameters such as  $I_p$ , duty factor,  $W_T$ , and water pressure with the performance outputs namely MRR, wear ratio and SR in WEDM of Inconel 601. Welling (2014) compared the surface integrity and fatigue life of jet engine components made of Inconel 718 produced by WEDM and a combined process of broaching and grinding. High cycle fatigue test shows the fatigue moment in same magnitude for both the broached and WEDMed specimen, but EDMed and conventional manufactured parts have different characteristics. The effect of voltage, capacitance and magnet polarity on RC- type WEDM of NdFeB permanent magnets are studied by Greer et al. (2014). Both voltage and capacitance affect the slicing rate and only voltage affect the kerf, but polarity of the magnet being machined does not affect the machining process.



**Figure 2.2 :** Cut Section of the Electro Plated Combustion Chamber Wall  
(<http://spl.ch/products/index.html>)

Jangra et al. (2011) evaluated the machinability of Tungsten carbide composite on WEDM. Factors affecting the machinability are grouped in five broad categories - machine tool, work material, tool electrode, cutting conditions, and geometry to be machined. A mathematical model is developed by means of the digraph and matrix method for the performance evaluation of carbide compacting die.

In WEDM, by using coated brass wire, the thickness of recast layer (RCL) in finishing cuts is achieved (approximate  $0.6\mu\text{m}$ ) which is acceptable for the majority of aero-engine parts (Antar et al. 2011). Combination of micro electro discharge machining with high frequency dither grinding improves SR of micro hole machining of high nickel based alloy. This technique eliminates the micro cracks along with reduce SR from 2.12 to  $0.85\mu\text{m}$  Rmax (Liu et al. 2005).  $I_p$  is a important machining parameter which affecting the characteristics of micro holes in high nickel alloy in terms of electrode depletion, micro hole expansion and MRR. A proper  $I_p$  is very important parameter to achieve optimum results. The Taguchi method is used to analysis the significance effect of each parameter, i.e.,  $I_p$ , gap voltage,  $T_{on}$  and duty cycle during machining of Inconel 718 using WEDM with a copper electrode on machining characteristics such MRR, electrode wear rate and radial over cut (RoC) and half taper angle.  $I_p$  much affect the MRR and  $T_{on}$  significantly affects the electrode wear rate (Ghewade and Nipanikar 2011). The discharge parameters of WEDM such as  $T_{on}$ ,  $T_{off}$ , SV and  $I_p$ , etc. are chosen carefully according to the work piece properties to achieve good machining characteristics. Liao et al. (2004) introduces a concept of specific discharge energy for determining the correlation between process parameters and machining characteristics of different materials in WEDM. SDE values of different materials are used for determination of the setting of machining parameters for different materials. Bhuyan& Yadava (2014) investigated the effect of input process variable on MRR and Kerf width during machining of Borosilicate Glass using a hybrid machining process “Travelling wire electrochemical spark machining” (TWECSM). MRR and Kerf width increase with increase in applied voltage,  $T_{on}$  and electrolyte concentration.

## **2.4 OPTIMIZATION OF THE MACHINING PARAMETERS IN WEDM**

Multi machining characteristics are contradictory in nature. It is complicated to obtain the optimal parameter setting in WEDM. For example, to obtain high MRR, requires high DE across the work material and wire electrode. This results in high heat generation due to large ionization of the spark gap. But high heat generation adversely affects the surface characteristics and dimensional tolerance of the machined component. High heat generation causes more melting of work surface resulting into large value of dimensional shift ( $D_s$ ) or RoC which further affects the



dimensional tolerance of the machined component. These facts build a necessity of detailed information of machining parameters setting for each machining characteristic for different work materials. So that, for obtaining good surface quality and dimensional properties, optimized cutting conditions have to be employed and needs a suitable modelling technique for better prediction (Scott et al. 1991; Yang et al. 2012). The optimization is one of the important activities for the economy of manufacture, and to predict the machining characteristics of machining. WEDM process parameters of Incoloy 800 super alloy with multiple machining characteristics such as MRR, SR and kerf are optimized by using Gray – Taguchi method (Kumar et al. 2010).

Jangra et al. (2012) optimized the multi machining parameters in WEDM of Tungsten carbide composite (WC-5.3%Co) using integrated approach of Taguchi, GRA and Entropy method. Six input parameters are investigated for three machining characteristics namely MRR, SR and RoC. Ramakrishnan and Karunamoorthy (2008) developed ANN models to optimize the MRR and SR simultaneously in WEDM of Inconel 718. Authors used Taguchi's L9 orthogonal array for conducting the experiments. Khanna and Singh (2013) developed a mathematical model for cryogenic treated D-3 material by means of RSM and then solved the optimization problem by desirability function. Bobbili et al. (2014) carried out a study for optimizing the WEDM process parameters viz, Ton, Toff,  $W_F$  rate, flushing pressure and SV for the machining of high strength Armor steel. Taguchi methods are used to conducting the experiment and result shows that Ton, Toff and SV are significant variables for both MRR and SR. Gupta and Jain (2014) investigated the behavior of the micro geometry parameters of miniature spur gears produced by WEDM process and optimized the process parameters for minimizing the total profile and accumulated pitch deviation using RSM. Sharma et al. (2013) optimized the process parameters of WEDM using RSM. Desirability approach is adopted for multi response optimization (i.e., CS and dimensional deviation). Ton is the most significant factor for multi response optimization, while two way interactions also played significant role in the process. The various experimental and theoretical studies show that process capability of WEDM is improved significantly by correct selection of machining parameters for a given material.

Previous investigations show that the Ip and Ton are important parameters in WEDM which significantly affect MRR and surface characteristics of the machined



component. In order to obtain high MRR requires high DE which results in high heat generation across the work material and wire electrode. High heat generation results into poorer surface integrity including large RCL, HAZ and several micro-cracks due to either re-solidification of melted materials on the machined surface or generation of high pressure energy in plasma channel across the electrodes which are not flushed quickly out of a narrow spark gap (Li et al., 2013, Jangra K., 2012, Klink et al., 2011; Rebelo et al., 1998). The aero-engine parts are failed due to presence of surface micro-cracks on the machined surface. During roughing, this is a detrimental effect on the fatigue strength. The presence of micro-cracks within RCL is accelerating crack initiations growth. After machining with any convention and non- conventional machining process, the post machining is essential to improve the surface integrity of machined surface components.

In case of WEDM, multi finishing cuts may significantly improved the fatigue life of the aero-engine components through removal of RCL produced during rough machining (Antar et al. 2012). But a post process finishing operation, such as polishing or etching is required for reducing the detrimental influence of WEDM. Surface integrity of a machined component significantly affects its performance such as fatigue life and creep properties. It includes residual stresses, RCL, Heat effected zone (HAZ) and micro-cracks (Klink et al., 2011).

Trim cutting operation is considered as a most excellent option to remove unwanted surface defects for improving the surface integrity of machined surface. A proper discharge parameters and WO should be selected carefully (Huang et al., 1999, Jangra K., 2012; Sarkar et al., 2008; Sanchz et al., 2007). Till date very limited literature is found on trim cutting operation in WEDM.

## **2.5 TRIM CUTTING OPERATION IN WEDM**

In trim cutting or finish cutting operation, wire electrode traces back the same path followed during rough cut path with certain value of Wire offset (WO) at low DE as shown in Figure 2.3. In case of WEDM, several trim cuts passes completely remove RCL. It is observed that there are no micro-cracks on the machined surface. The occurrence of micro-cracks may causes of reduction of components fatigue life. There is no significance change in micro-hardness after trim cuts. The average RCL thickness less than 11  $\mu\text{m}$  found and several trim passes showing no apparent RCL (Jangra et al. 2015).

Aspinwall et al. (2008) employed minimum damage pulse generator technology in rough and finishing process of WEDM on Ti-6Al-4V and Inconel 718 alloys. The average RCL thickness on Inconel 718, after main cut, is found lower than the RCL in Ti-6Al-4V. After several trim passes, no RCL or damage was apparent. Using Taguchi method, the parameters are optimized for depth of material removal and SR in multi pass cutting operation in WEDM machining of WC-5.3% Co composite. A single trim cut with low discharge value with optimal WO improves SR effectively (Jangra 2015).

**Figure 2.3: Schematic Diagram of Trim Cutting Operation in WEDM Process**

## 2.6 POWDER MIXED EDM

Powder mixed EDM (PMEDM) is one of the new contributions for the improvement of capabilities of EDM process as shown in Figure 2.4. In this process, a suitable material (aluminium, chromium, graphite, copper, silicon and silicon carbide, etc.) in the powder form is mixed into the dielectric fluid. When a voltage 80-120V is applied between wire electrode and work piece, an electric field in the range of 105-107 V/m is generated. The powder particles are energized by high electric field and acts as conductors promoting breakdown in the gap. The spark gap filled up with additive particles and the gap distance setup between tool and the work piece is increased. Under the sparking area, these conductive particles form chains at different places under sparking area. The chain formation helps in bridging the discharge gap between wire electrode and work piece material. The interlocking

between the powder particles occurs in the direction of flow of current. Because of bridging effect, the insulating strength of the dielectric fluid decreases resulting in easy short circuit. This causes early explosion in the gap and series of discharge starts under the electrode area. The faster sparking within a discharge causes faster erosion from the work piece surface which increases MRR and at the same time, a series of discharges which are well distributed under the electrode area. This nature of sparks produced shallow craters on the work piece surface and reduces SR (Kansal et al., 2007; Ojha et al. 2011; Singh et al. 2005; Wang et al., 2008). The machining rate increases by the addition of metal powder particles (aluminium, copper, iron) in the dielectric fluid during the machining of mild steel in EDM process (Erden et al. 1980). With the addition of powder particles, a great improvement in the break down characteristics of the dielectric fluid is observed, but after a certain critical concentration of powder short circuiting takes place which causes poor cutting condition. MRR increases with increase in the concentration of powder. At excessive powder concentration, machining becomes unstable due to occurrence of short circuits.

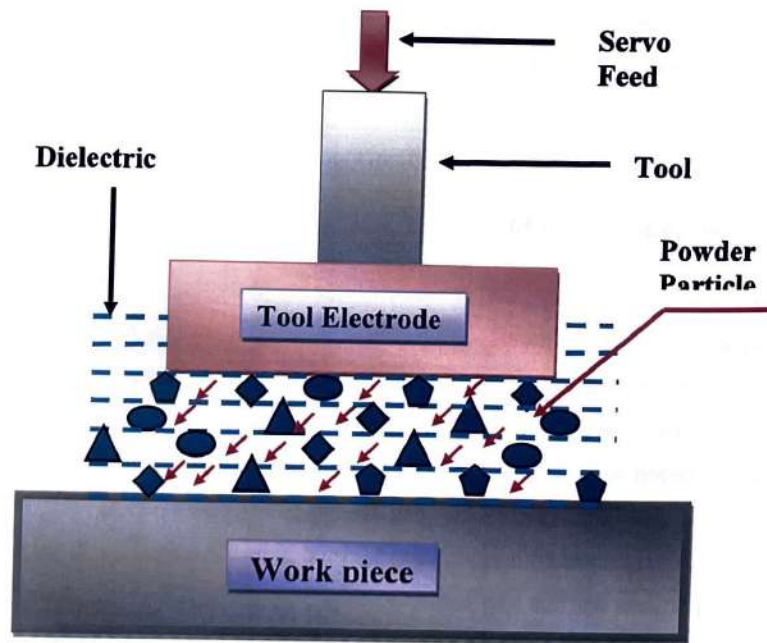


**Figure 2.4:** Powder Mixed Electrical Discharge Machining (PMEDM)



Narumiya et al. (1989) study the effect of addition of silicon, aluminium and graphite as powder materials. In the study powder concentration is considered in the range of 2gm/l to 40gm/l. It is observed that the gap distance increases with the powder concentration and is larger for the aluminium powder. A better result concerning the surface finish is achieved for low powder concentrations levels and that also for silicon and graphite powders. Experimental comparison are carried out using different powders (graphite, silicon (Si), aluminium (Al), crushed glass, silicon carbide (SiC) and molybdenum sulphide) with different grain sizes to obtain near-mirror-finish (Wong et al. 1989). Result shows that Al powder is better finishing for SKH-51 work pieces as compared to SKH-54 work pieces. It is important to know the correct combination of powder and work piece materials to produce superior surface finish. Kobayashi et al. (1992) concluded that Si powder mixed in the dielectric improves the surface finish of SKD-61 tool steel. It is observed that at specific machining conditions in the EDM of steel, Al and graphite powders generate better SR than Si powder. Yan et al. (1993) reported improvement in machining rate (MR) of two different materials SKD11 and Ti-6Al-4V by the use of SiC & Al powders. It is observed that SR also increases with the increase in machining rate. Uno et al. (1997) found that Si powder mixed in kerosene fluid enhances the surface finish. It is concluded that lesser impact force acts on work surface generate small craters resulting in stable machining. EDM process by adding SiC and Al powders into kerosene is carried out for the micro-slit machining of titanium alloy for better MRR (Chow et al, 2000). Tzeng and Chen (2005) found that factors such as particles concentrations, particles size, particle density, electrical resistivity and thermal conductivity of powder play important roles in improving the surface quality of EDM processes. In die sinking EDM, lots of research works are conducted using powder mixed dielectric to improve the MRR and surface characteristics. The electric conductive powder reduces the insulating strength of the dielectric fluid and increases the spark gap between the tool and work-piece. As a result the process becomes more stable thereby improving MRR and surface finish. Kansal et al. (2008) presented the numerical simulation of PMEDM of AISI D2 die steel using FEM. The RSM is used to identify and optimized the most important parameters of PMEDM for maximum MRR and minimum SR. The concentration of added Si powder,  $I_p$  and  $T_{on}$  significantly affect the MRR and SR in PMEDM. Ojha et al. (2011) experimentally investigated MRR and EWR in PMEDM process with

Cr powder suspended dielectric. It is concluded that MRR showed an increasing trend for increase in powder concentration. Bhattacharya et al. (2013) showed improvement in surface properties like micro hardness, wear and corrosion resistance using various powder additives in PMEDM.

For aerospace applications, the surface condition of the machined work piece is of concern because of the role it plays in the useful life of the component under cyclic loading. It is obvious that in order to maintain and/or improve reliability of aerospace components, it is first essential to be aware of the possible damage or surface alterations that are imparted to a material when it is machined. Although it is possible to apply post machining operations such as heat treating or shot peening to impart the conditions which will provide a predetermined desirable surface that may provide consistent desirable mechanical and physical properties. Hence, it is also necessary to control the machining operation to ensure the integrity specifications. Much of the valuable data has been published mostly on machining of Inconel grade of nickel alloys (In-718, In-601 etc) by different conventional and non- conventional machines. However, the comprehensive study on the machinability of the Nimonic 90 in WEDM is not reported.

High strength and toughness over a wide temperature range increase the usage of Nimonic 90 in chemical industries, food processing industry, heat exchanger tubing, nuclear reactors, sub-marine and ship propellers etc. (Lewis et al., 2006). Nimonic-90 is a nickel-chromium-cobalt alloy which is most suitable for high temperature applications (600°C to 900°C). Its high stress rupture strength and creep resistance at high temperature allows using it in turbine blades and combustion chamber components. As per literature available, no significant work is found on machining of Nimonic-90 with EDM or WEDM.

## **2.7 IDENTIFIED GAPS IN THE LITERATURE**

After a comprehensive study of the existing literature, it is found that lot of research work is done in the area of WEDM.

- Several research articles are published on process parameter design and modelling of the WEDM process by means of different mathematical techniques for different response characteristics such as SR, CS or MRR and kerf width or  $D_s$ , etc.



- Several researchers used the fuzzy control system, wire inaccuracy adaptive control and self tuning adaptive system in process monitoring and control.
- In majority of research work, investigation and modeling of WEDM parameters are studied only for rough cutting operation. But only a few research works are reported in the fields of trim or finish cutting operation, WO setting for trim cutting is not fully explored. Determination of WO setting is absolutely essential for achieving a close dimensional tolerance.
- A significant work has not been explored on machining of Nickel based alloy, Nimonic-90 with WEDM.
- Till date, research work on powder mixed dielectric in WEDM is still missing. Therefore, the concept of metal powder mixed dielectric needs to attempt for WEDM.

## **2.8 DISCUSSION**

In this study, problems encountering in machining of the Nickel based alloy in WEDM are considered. Despite the availability of good amount of literature for the machining of Inconel 718 and Inconel 601 super alloy, only few and inconclusive data are available on machining the Nimonic. From the available literature, it is found that no comprehensive and systematic modelling approach with respect to Nimonic 90 is identified. A comprehensive study on micro hardness, surface morphology and RCL in machining Nimonic 90 in WEDM is still missing. It emphasizes that there is a need of more comprehensive scientific work on machining of Nimonic 90 on WEDM. Machining characteristics namely CS, SR and RoC in WEDM of Nimonic-90 are modelled and optimized using RSM with Desirability Function. Also, the literatures revealed the importance of multi response optimization for machining characteristics for economy of the manufacture. An experimental investigation needs to be conducted on rough cut and trim cut using dielectric fluid and trim cut using Al, and Si metal powders in dielectric fluid to evaluate the effect of DE on surface morphology of machined surfaced of Nimonic-90 in WEDM.



## CHAPTER-III

### EXPERIMENTAL SET-UP AND PROCESS PARAMETERS SELECTION

#### 3.1 INTRODUCTION

There is need of experimental investigation of WEDM process parameters for machining characteristics, namely CS and SR to determine the important parameters and their working range for Nimonic 90, with one parameter at a time approach. This chapter gives the information about experimental set up, material properties and selection of process parameters and its ranges on the basis of the trial experimentation for optimization studies.

#### 3.2 MACHINE TOOL

In this study, experiments are performed on 5 axis Elektra Sprint Cut (ELPULS-40) WEDM manufactured by Electronica M/C Tool LTD, India, installed at Ganpati Tools, MCF-4107, Sector 23, Industrial area, Faridabad, Haryana, India. Figure 3.1 shows the machine setup used in presented work.

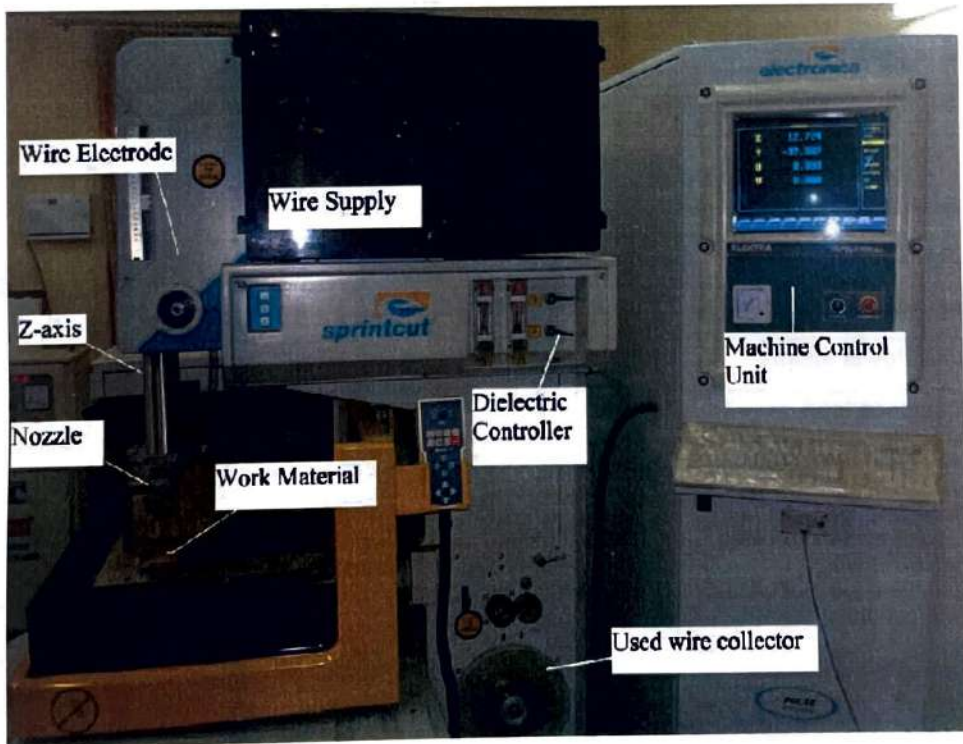


**Figure 3.1:** Machine Setup of WEDM, Elektra Sprint Cut (Electronica Machine Tool Catalogue)

Table 3.1 gives the specification of the CNC WEDM machine tool. Performance of WEDM depends on settings of process parameters. The following section discusses the work materials, machining parameters and experimental design for present investigation.

**Table 3.1** Specification of the CNC WEDM Machine Tool

<b>Descriptions of Machine Tool</b>	<b>Specification</b>
Design	Fixed column, moving table
Table size	440 x 650 mm
Max. workpiece height	200 mm
Max. workpiece weight	500 kg
Main table traverse (X, Y)	300, 400 mm
Auxiliary table traverse (u, v)	80, 80 mm
Max. Taper angle	$\pm 30^\circ/50$ mm
Max. Wire spool capacity	6 kg
Wire electrode diameter	0.25 mm (Standard), 0.15, 0.20mm (optimal)
<b>Pulse Generator</b>	<b>ELPULS-40 A DLX</b>
Pulse peak voltage	1 step
CNC controller	EMT 100W-5
Controlled axes	X, Y, U, V simultaneous / independent
Interpolation	Linear & Circular
Least input increment	0.0001mm
Least command input (X, Y, u, v)	0.0005mm
Input Power supply	3 phase, AC 415 V, 50 Hz
Connected load	10 KVA
Average power consumption	6 to 7 KV
<b>Dielectric Unit</b>	<b>DL 25 P</b>
Dielectric fluid	Deionised water
Tank capacity	250 litres
Filtration	10 $\mu$ Four paper cartridges

### 3.3 WORK MATERIAL

Nickel based alloys are backbone materials for aerospace, petrochemical, medical, submarines, nuclear reactors and steam power plants. Aerospace industry is the main consumer for nickel based alloys along with titanium alloys in fabricating aero-engine parts such as combustion chamber, gas turbine blades, disks, and vanes, etc. This fast growing popularity of nickel based alloys is due to their excellent mechanical properties at every high temperature, high corrosion resistance, thermal shock, resistance to fatigue, creep and erosion. Nimonic-90, a nickel-chromium-cobalt alloy, is the most suitable for high temperature applications (600°C to 900°C). Due to high rupture strength and creep resistance at high temperature (up to 950 °C), it is mainly employed in turbine blades and combustion chamber. The components of this material are mostly fabricated through hot forging process. But WEDM may yield better finish and accuracy in fabricating the intricate and complex parts such as blade root slots in turbine discs. Nimonic 90 hot forged in rectangular sheet of 12.5 mm thickness is selected as workpiece material plate of 150 mm\*100 mm size. Using WEDM, work material is machined and samples are obtained in the form of rectangular punches of dimension 8 mm × 7 mm × 12.5 mm. The chemical composition of this material as obtained by EDS (Electro Dispersive X-ray Spectroscopy) test is shown in Table 3.2.

**Table 3.2** Chemical Composition and Mechanical Properties of Nimonic 90

Work Material	Density	Melting point	Coefficient of Expansion	Modulus of Rigidity	Modulus of Elasticity
Nimonic 90(wt %) ( Ni 60, Cr 19.3, Co 15, Ti 3.1, Al 1.4 )	8.18 g/cm <sup>3</sup>	1370°C	12.7µm/m °C	82.5KN/mm <sup>2</sup>	213KN/mm <sup>2</sup>

### 3.4 PROCESS PARAMETERS

In WEDM, machining parameters are categorised into three major categories such as discharge parameters, wire electrode and dielectric conditions as shown in Figure 3.2.



### 3.4.1 Discharge Parameters

Generally, by increasing the peak energy, one can achieve an increase in the cutting speed. To achieve optimum results of cutting speed and job accuracies, the discharge parameters should be set properly. Lists of peak parameters are peak current, pulse on time, pulse off time and servo voltage.

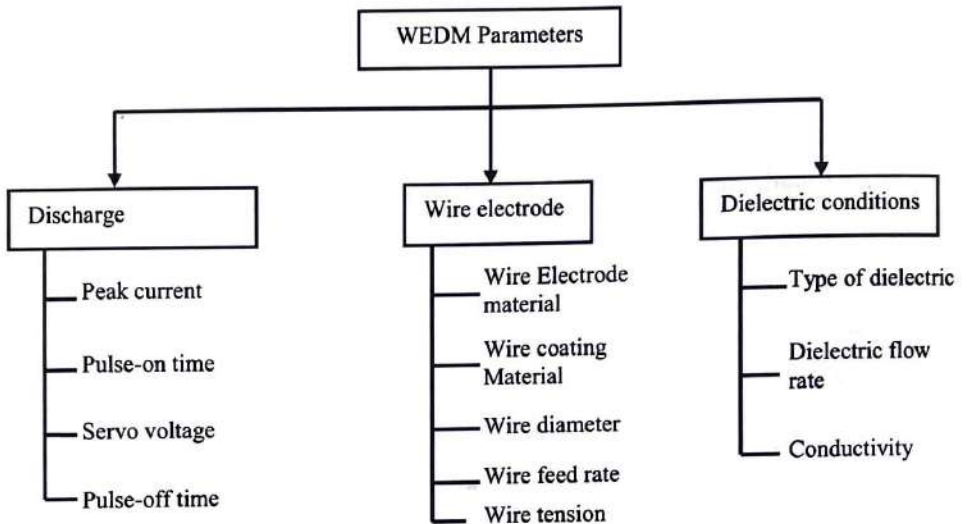


**Figure 3.2: Machining Parameters in WEDM**

#### **(a) Peak Current ( $I_p$ ) Range: 010-230 A (In step of 10)**

Peak current is a significant machining parameter in WEDM. During each pulse on time ( $T_{on}$ ), the current increases until it reaches a preset value, which is expressed as the peak current. In WEDM, maximum amount of average is governed by the surface area of machine cut. Increase in the  $I_p$  value will increase the pulse peak energy which in turn improves the CS. For higher value of  $I_p$ , gap conditions may become unstable with improper combination of  $T_{on}$ ,  $T_{off}$ , SV and SF setting. When the peak condition becomes unstable, one must reduce the  $I_p$  value (and / or increase the  $T_{off}$  period). High  $I_p$  is used in rough cutting operations to achieve maximum CS.

#### **(b) Pulse on Time ( $T_{on}$ ) Range: 100-131 $\mu s$ (in step of 1)**

It represents the duration of time in micro seconds ( $\mu s$ ) for which the current is flowing in each cycle {Figure 3.3}. During this period, the voltage is applied

across the wire electrode and workpiece. Higher the Ton setting, larger is the Ton. The single pulse peak energy increases with increasing Ton period, resulting in higher CS. However with higher values of Ton, SR tends to be higher. The higher value of pulse peak energy may also cause wire breakage.

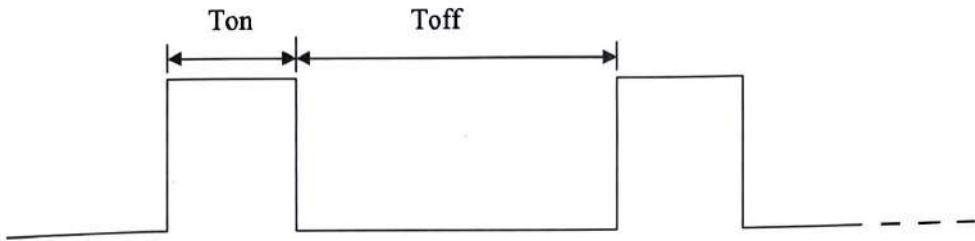


**Figure 3.3: Series of Electrical Pulses at the Inter Electrode Gap**

**(c) Pulse off Time (Toff) Range: 00-63  $\mu$ s (in step of 1)**

It refers to the duration of time in micro 'seconds ( $\mu$ s) between the two simultaneous sparks {Figure 3.3}. Voltage for the gap is absent during this period. Higher the Toff setting, larger is the pulse off period. With a lower value of Toff, there is more number of peaks in a given time, resulting in increase in the sparking efficiency. As a result, the CS also increases. Using the very low values of Toff period, may cause wire breakage which in turn reduces the machining efficiency. As and when the peak conditions become unstable, one can increase the Toff period. This allows lower pulse duty factor and reduces the average gap current.

**(d) Servo Voltage (SV) Range: 0-99 V (in step of 1)**

This is a reference voltage for the actual gap voltage. SV is used for controlling advance and retracts of the wire. If the mean machining voltages is higher than set voltage level, the wire advances, and if it is lower than preset value, the wire retracts. Therefore, a higher value of SV is responsible for widens the gap between the work piece and the electrode resulting decreases the numbers of electrical sparks, stabilizing electrical peak. Hence, cutting speed is slowed down. When a smaller value of SV is set, mean gap become narrow, which leads to increase in numbers of electrical sparks. Hence improve the CS.

### **3.4.2 Wire Electrode**

Wire electrode may be categories in four parts, i.e., wire electrode and coating materials, wire diameter, wire feed rate and wire tension.

#### **(a) Wire Electrode and Coating Materials**

Wire electrode material must be conductive and should have good tensile strength to bear the requisite wire tension. Coating of wire electrode should possess small work function and high melting point to retain high peak energy. The wire electrode material should be Brass/Diffused Brass/ Zinc coated Brass.

#### **(b) Wire Diameter**

The wire electrode is required to have a sufficient tensile strength and should be of uniform diameter and free from kink or twist and breaks even winding. The wire diameter should be within the variation of  $\pm 0.002$  mm with diameter 0.25 mm (Standard), 0.15, and 0.20mm (optimal). Therefore, a zinc coated brass wire having a fixed diameter of 0.25mm is selected as a wire electrode.

#### **(c) Wire Feed Rate ( $W_F$ ) Range: 1-15mm/min (in step of 1)**

Wire feed is the rate at which the wire feed to maximum with less wire breakage and better machining stability. As the wire speed increases, the wire consumption in result the cost of machining increases while low wire speed can cause to wire breakage in high cutting speed. The travelling wire electrode becomes thin and brittle, due to spark erosion.

#### **(d) Wire Tension ( $W_T$ ) Range: 1-15 N (in step of 1)**

Wire tension determines how much the wire is to be stretched between upper and lower guides. High value of  $W_T$  is required for more thickness of job. Improper setting of  $W_T$  may result in wire breakage as well as the job inaccuracies. If the  $W_T$  is high enough the wire stays straight otherwise wire drags behind.

### **3.4.3 Dielectric Conditions**

Dielectric conditions may be expressed in different terms such as type of dielectric, dielectric flow rate, conductivity, dielectric strength of dielectric fluid and flushing.



**(a) Type of Dielectric fluid**

The deionised water is typically used as a dielectric fluid in WEDM because of its environmentally friendly characteristics and makes it suitable to WEDM. The important characteristics are:-

- The use of deionised water as dielectric permits winding of sparks gap to minimize short circuit, resulting in high CS.
- It has good wire electrode cooling effect
- It is non-flammable and its vapours are non-toxic.

**(b) Dielectric Flow Rate (FR)**

High flow rate of dielectric results into complete and quick flushing of the melted debris out of the spark gap those results into high CS and good SR. Therefore, FR is normally kept at high value of 12 litres per minute (L/Min).

**(c) Conductivity of Dielectric**

The conductivity of dielectric plays a very important role in machining efficiency. Lower the conductivity, lower is the gap between workpiece surfaces and wire electrode which resulting the lower the radial over cut. The wire runs closer to top and bottom surface as compared to the middle portion of the workpiece. Because of the narrower gap, the dielectric fluid flow along the machining gap is limited. As a result there is a difficulty in flushing, which may cause wire breakage. The RoC size also will vary from top to bottom surface of the work surface. With very low dielectric conductivity, a serious problem of wire metal deposition on the work surface may result. With very high dielectric conductivity, the water dielectric allows direct current to flow in the gap. With more value of D.C. current, therefore, sufficient peak voltage cannot built-up. As a result, the machining becomes unstable. The machining gap becomes uniform when the required value of conductivity is set. With this condition, the water dielectric wraps the wire uniformly, thereby reducing the wire breakage. The conductivity should be maintained around 20 mho.

**(d) Dielectric Strength of Dielectric Fluid**

Since the insulation characterization of the dielectric fluid decides the RoC, it is very important to keep the conductivity as constant as possible. During

machining, the conductivity of dielectric deionised water changes due to generation of metallic ions and dissolution of ambient gases. The conductivity may be decreased by passing the water through deionizer resin. This is done automatically by the machine.

#### **(e) Flushing**

Flushing is important to achieve a stable machining condition. It plays very role as far as CS is concerned. Both the nozzles (upper and lower) should be just about 0.1 to 0.2 mm away from the workpiece surface, otherwise cutting performance drops significantly. Also both the nozzles should be checked periodically for damages. Purity of the distilled water should be maintained by timely replacement of filters.

### **3.5 MACHINING CHARACTERISTICS AND THEIR MEASUREMENT**

#### **3.5.1 Cutting Speed (CS)**

Cutting speed (CS) or material removal rate (MRR) is used to predict the total machining time on WEDM. Higher the CS/MRR, lower the machining time. CS/MRR can be expressed in terms of weight removal rate (grams/min), volume removal rate ( $\text{mm}^3/\text{min}$ ), surface area removed ( $\text{mm}^2/\text{min}$ ) and linear cutting speed ( $\text{mm}/\text{min}$ ).

In present work, a rectangular Nimonic-90 work plate of dimension 150 mm\*100 mm\*12.5 mm is used. For this heavy work plate, accurate measurement of MRR in terms of grams/min is quite difficult for each experimental trial. Therefore, in present work, CS is measured in terms of linear cutting speed which is observed from machine tool monitor that gives linear cutting speed in terms of mm/min. CS can be expressed in terms of surface area removed per min (i.e.  $\text{mm}^2/\text{min}$ ) by multiplying the linear cutting speed with work piece thickness.

CS increases by selecting the optimal values of process parameters like peak current ( $I_p$ ), pulse on time ( $T_{on}$ ), pulse off time ( $T_{off}$ ), servo voltage (SV) and wire feed rate ( $W_F$ ) etc. Improper selection of these parameters may yield higher CS, but causes frequent wire breakage that reduces the productivity.

### 3.5.2 Surface Roughness (SR)

Surface roughness is an easily measurable parameter which helps a tool manufacturer to make a quick decision about the process parameters setting. SR values,  $R_a$ , are measured using Surface Roughness Testers SJ-310, made of Mitutoyo, Japan installed at National Institute of Technical Teachers Training & Research, Chandigarh {Figure 3.4}.

### 3.5.3 Radial over Cut (RoC)

RoC is the thickness of material removed perpendicular to the tool path direction {Figure 3.5}. It helps to predict the accurate wire offset (WO) in rough cutting operations. RoC can be calculated as;

$$RoC = \frac{\text{kerf width} - \text{wire diameter}}{2}$$



**Figure 3.4:** Surface Roughness Testers SJ-310



Optical microscope is used to measure kerf width. Radial over cut is larger if-

- Machining gap voltage is higher.
- Peak energy is higher.
- Wire tension is lower.
- Guide span is higher.
- Job thickness is higher.
- Dielectric conductivity is higher.
- Machining is unstable.

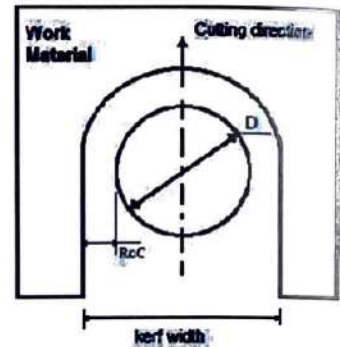


**Figure 3.5:** Representation of RoC in WEDM

### 3.5.4 Wire off set (WO)

Wire off set =  $(0.5 * \text{wire diameter}) + \text{over cut}$ .

Wire offset may be to the Left (G41) or right (G42) of profile depending upon the direction of motion and wire being inside or outside of profile.

### 3.5.5 Surface integrity

Surface characteristics of nickel alloys may significantly affect the working life of its components. So it is essential to analysis the effect of discharge energy (DE) on surface characteristics including RCL, heat affected surfaces, micro-cracks and micro hardness. The specimens are grinded and polished to have mirror finish on the transverse section. Then, machined surface is examined by using Scanning Electron Microscope (SEM) JSM 6510 series manufactured by JEOL LTD, Japan, installed at Thapar University, Patiala {Figure 3.6}. Micro hardness on the transverse section of machined surface is measured using Micro Vickers Hardness testing machine HM-210/220 manufactured by Mitutoyo South Asia Pvt. LTD, installed at National Institute of Technical Teachers Training & Research, Sector 26, Chandigarh {Figure 3.7}. Using micro hardness test, the extent of surface damage due to thermal energy of WEDM process is measured and analysed. Therefore, micro-hardness is measured on transverse section of the machined surface.



**Figure 3.6:** Scanning Electron Microscope (SEM)

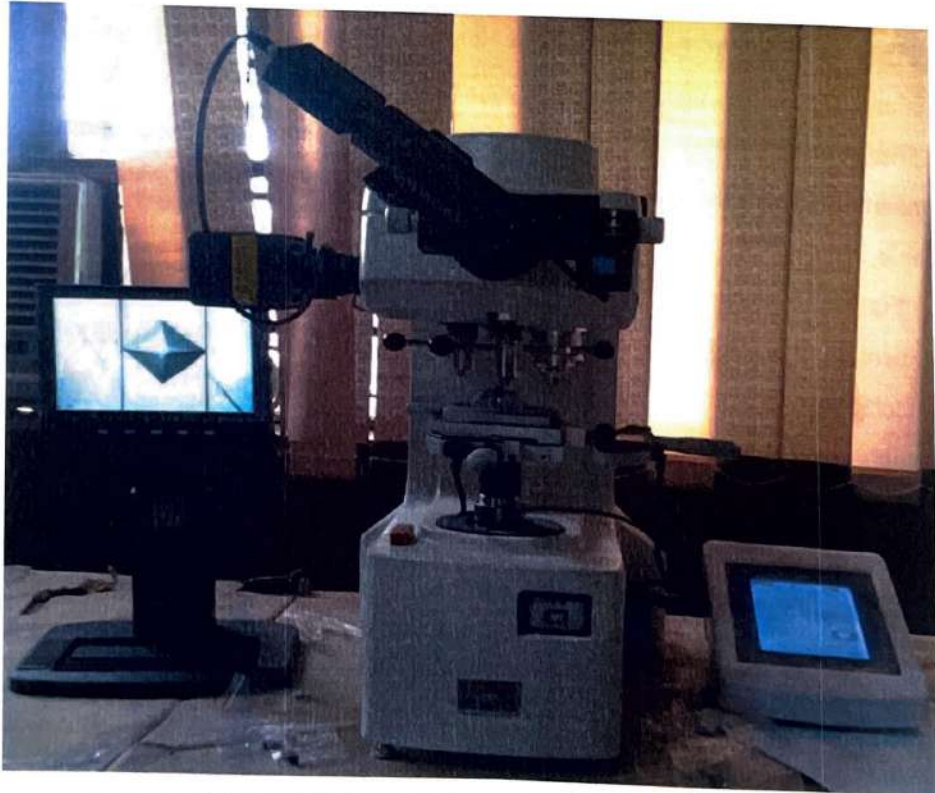


**Figure 3.7:** Micro Vickers Hardness Testing Machine HM-210/220



### 3.6 TRIAL EXPERIMENTS

The trial experiments are performed in order to study the affect of the WEDM process parameters on machining characteristics and also to decide the range of process parameters required for the experimental design methodology used in this research work. 5-Axis Sprint Cut (ELPUSE-40) WEDM is used to conduct the trial experiments. Input parameters such as  $I_p$ , Ton, Toff, SV and  $W_F$  are varied during trial experimental work. One factor at a time approach is used to study the effects of these input parameters on CS and SR. Nimonic-90 is selected as workpiece material. Distilled water having conductivity 20 mho is used in present study. High flow rate of dielectric results into complete and quick flushing of the melted debris; out of the spark gap that result into high CS and good surface finish. Therefore, dielectric flow rate is kept at high value of 12 litres per minute ( $LM^{-1}$ ). In present work, the machining characteristics namely CS and SR are measured.

### 3.7 EFFECT OF WEDM PARAMETERS ON CS

#### 3.7.1. Effect of Peak Current ( $I_p$ )

The effect of  $I_p$  on CS of Nimonic 90 with WEDM is shown in Figure 3.8 and 3.9 under two different setting of Ton (108  $\mu s$  and 120 $\mu s$ ) along with two different setting of Toff (35 $\mu s$  and 45 $\mu s$ ). The other parameters are kept constant such as SV 20V,  $W_T$  10N,  $W_F$  rate 5 m/min., servo feed 2080 and FR 12 litres per min (upper and lower nozzles). The results of the experiments performed at different machining parameters setting are shown in Table 3.3.

Figure 3.8 shows that at low pulse duration (Ton 108 $\mu s$ ), the CS increases slowly with increase of  $I_p$ . But at high pulse duration (Ton 120 $\mu s$ ) there is sharply increase of CS with increase of  $I_p$  from 40A to 80 A. Increase in the  $I_p$  leads to increase in the rate of the heat energy and hence increase the rate of melting and evaporation. When increase in  $I_p$  increased over a certain limit, leads to arcing, which decrease peak number and machining efficiency. Subsequently wire to be break down because of short Toff. The removal time of debris particles from the gap become insufficient.



**Table 3.3:** Effect of Variation in Ip on CS

Ip (A)	CS (mm/min)		
	Toff 35, Ton 108	Toff 45, Ton 120	Toff 35, Ton 120
40	0.39	0.7	0.8
60	0.52	1.21	1.41
80	0.6	1.7	1.8
100	0.6	1.9	Further wire breakage
120	0.79	2.12	
140	0.93	2.27	
160	0.88	2.29	
180	0.76	2.30	
200	0.75	2.34	

Figure 3.9 shows maximum CS occurs due to complete flushing of debris particles with increase of Toff along with Ton and also availability of a complete deionised fluid for the next peak. But further increase in Ip value will leads to increase of CS. Maximum CS of Nimonic 90 with present machine tool occurs at Ip 200 A with Toff 45 $\mu$ s.

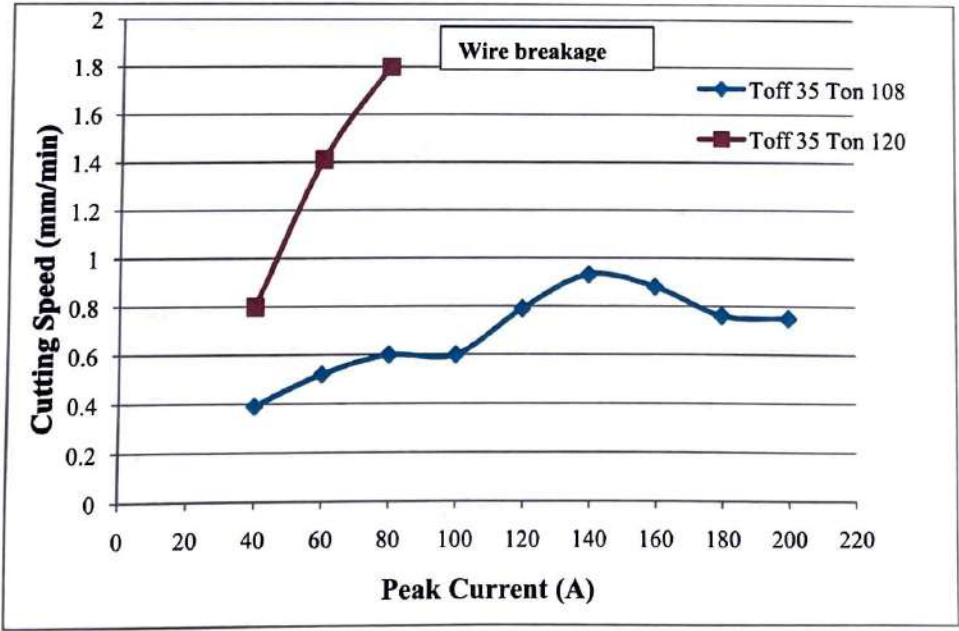


**Figure 3.8:** Effect of Variation in Ip on CS at different value of Ton

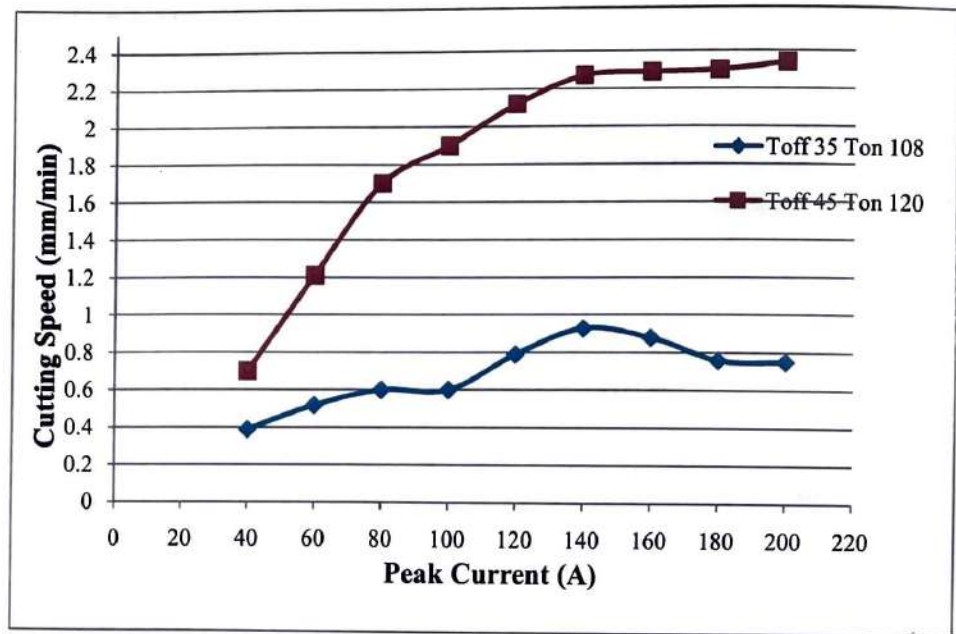


**Figure 3.9:** Effect of Variation in  $I_p$  on CS at different value of Toff and Ton

### 3.7.2 Effect of Pulse on Time (Ton)

The effect of Ton on CS is shown in Figure 3.10 for two different setting of Toff 35  $\mu$ s and Toff 40  $\mu$ s. The other parameters are kept constant under the condition of  $I_p$  120 A, SV 20 V,  $W_F$  rate 5 m /min,  $W_T$  10 N, FR 12 litres per min. and servo feed 2080. The results of the experiments performed at different machining parameters setting are shown in Table 3.4.

**Table 3.4:** Effect of Variation in Ton on CS

Ton ( $\mu$ s)	CS (mm/min)	
	$I_p$ 120, Toff 35	$I_p$ 120, Toff 40
103	0.58	0.49
106	0.85	0.79
109	1.02	1.17
112	1.82	1.51
115	2.17	1.89
118	Further Wire Breakage	2.48

CS increases continuously with increase of Ton. The machining becomes unstable at high pulse duration. At high peak energy, the amount of debris in the gap becomes too

great which form an electrically conductive path between the electrode and workpiece, resulting into development of unwanted arc between them. If Toff increased with Ton then sufficient time is available to flush the debris. Maximum CS of Nimonic 90 occurs at Ton118  $\mu$ s with Toff 40  $\mu$ s.

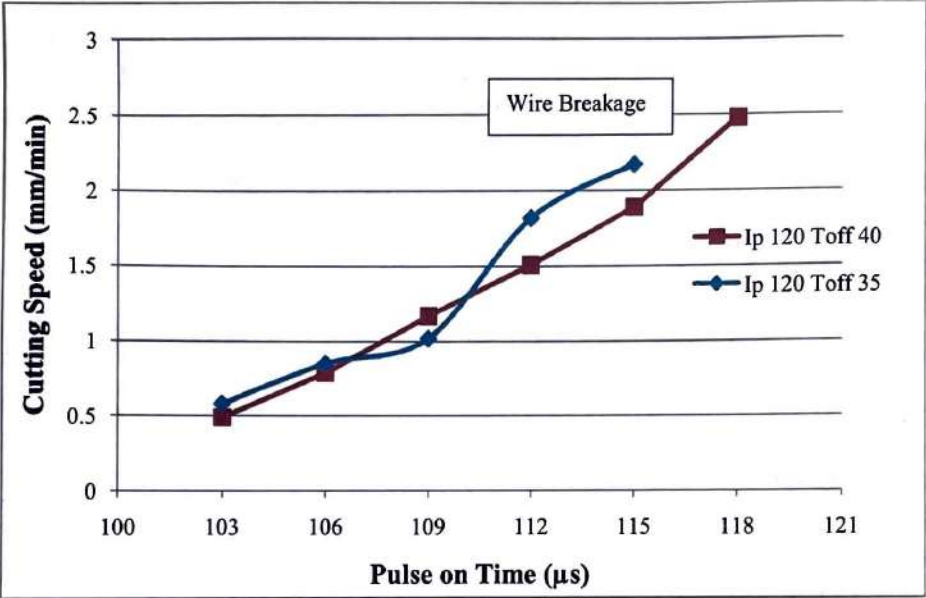


Figure 3.10: Effect of Variation in Ton on CS

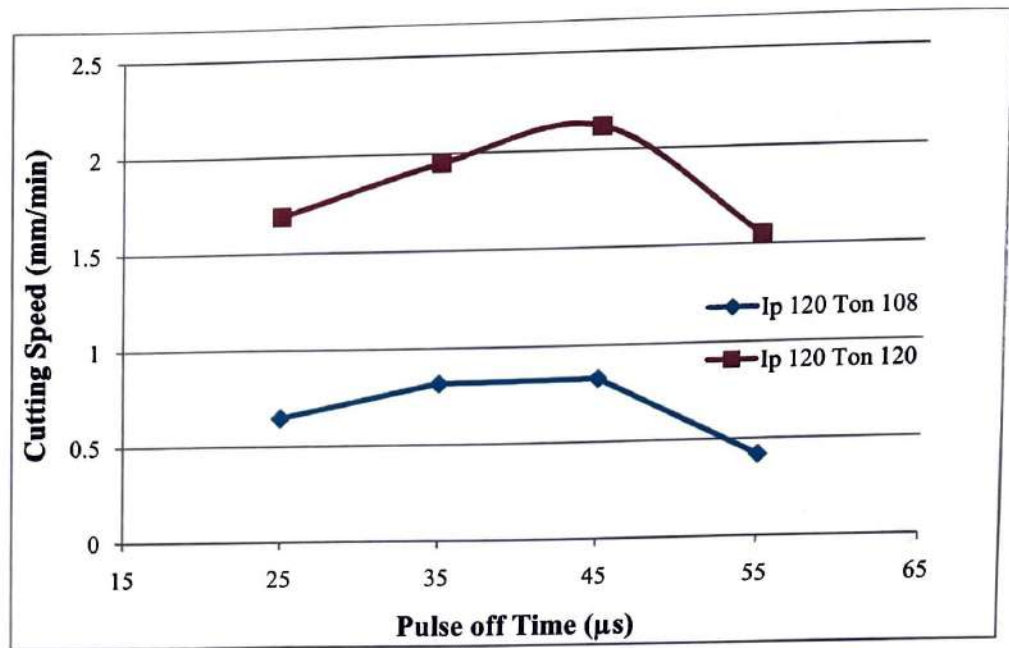
### 3.7.3 Effect of Pulse off Time (Toff)

Figure 3.11 shows the effect of Toff for two machining setting (Ton 108 $\mu$ s and 120 $\mu$ s) with fixed variables Ip 120 A, SV 20 V, FR 12 litres per min, servo feed 2080 ,W<sub>F</sub> rate 5 m/min and W<sub>T</sub> 10N. The CS increases with increases in Toff 25  $\mu$ s to 45 $\mu$ s and after that it decreases rapidly with increase in Toff. The results of the experiments performed at different machining parameters setting are shown in Table 3.5.

Table 3.5: Effect of Variation in Toff on CS

Toff ( $\mu$ s)	CS (mm/min)	
	Ip 120, Ton 108	Ip 120, Ton 120
25	0.65	1.69
35	0.82	1.95
45	0.83	2.12
55	0.42	1.55





**Figure 3.11: Effect of Variation in Toff on CS**

Maximum CS is to be found at Toff 45μs due to complete flushing of debris from the machining zones. After that further increase of Toff, dielectric fluid produces the cooling effect on wire electrode and work material and hence decreases the CS. At high Ton 120μs, the CS increase very fast as compared to low Ton 108μs.

#### 3.7.4 Effect of Servo Voltage (SV)

The effect of SV on CS is shown in Figure 3.12 with two different pulse durations (Ton 108 μs and 120 μs) along with two different values of  $W_F$  rate 5 m/min and 6 m/min keeping other variables fixed such as Toff 35μs, SV 20V, Ip 120 A and servo feed 2080 and  $W_T$  10 N. The results of the experiments performed at different machining parameters setting are shown in Table 3.6.

**Table 3.6: Effect of Variation in SV on CS**

SV (V)	CS (mm/min)	
	Ton 108, $W_F$ 5	Ton 120, $W_F$ 6
20	1.17	2.39
30	1.13	2.42
40	0.9	2.12
50	0.77	1.69
60	0.64	1.60

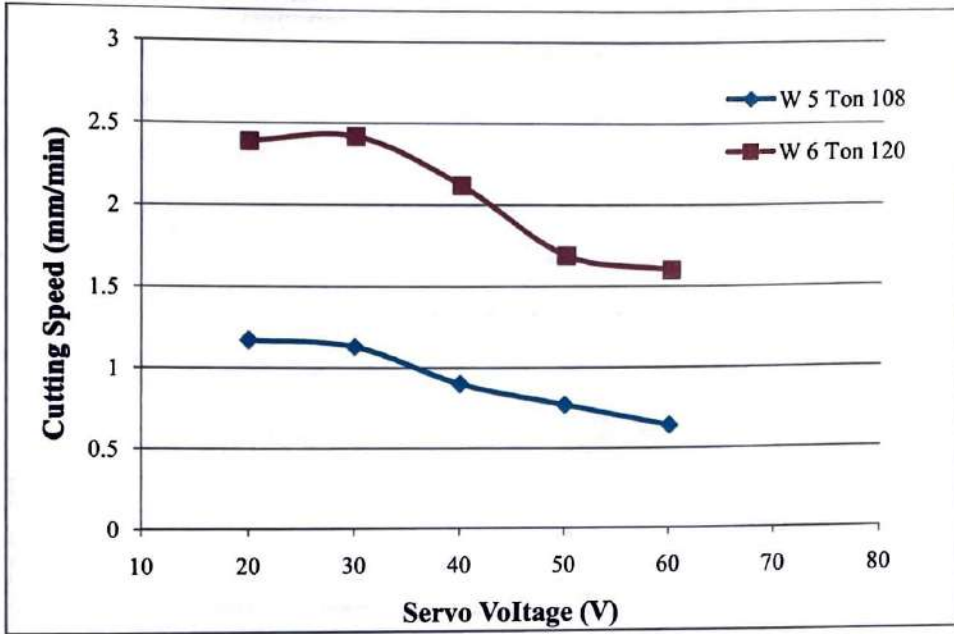


**Figure 3.12:** Effect of Variation in SV on CS

The CS decreases with increase in SV from 20V to 60V for  $W_F$  rate 5 m/min and SV from 20V to 60 V for  $W_F$  rate 6 m/min. Large SV means large ionization of the dielectric fluid between workpiece and wire electrode which results in high peak energy per spark. But further increase of SV will not favour in the CS as the large amount of debris are incapable to clear off the gap for a given  $T_{off}$ .

### 3.7.5 Effect of Wire Feed Rate ( $W_F$ )

The effect of  $W_F$  rate on CS is represented in Figure 3.13 keeping others parameters fixed such as  $T_{on}$  108 $\mu$ s,  $T_{off}$  35 $\mu$ s, SV 20 V,  $I_p$  120A and servo feed 2080,  $W_T$  10 N. The results of the experiments performed at different machining parameters setting are shown in Table 3.7.

**Table 3.7: Effect of Variation in  $W_F$  on CS**

$W_F$ (m/min)	CS(mm/min)
3	0.89
4	1.04
5	1.17
6	1.12
7	1.12
8	1.12
9	1.12

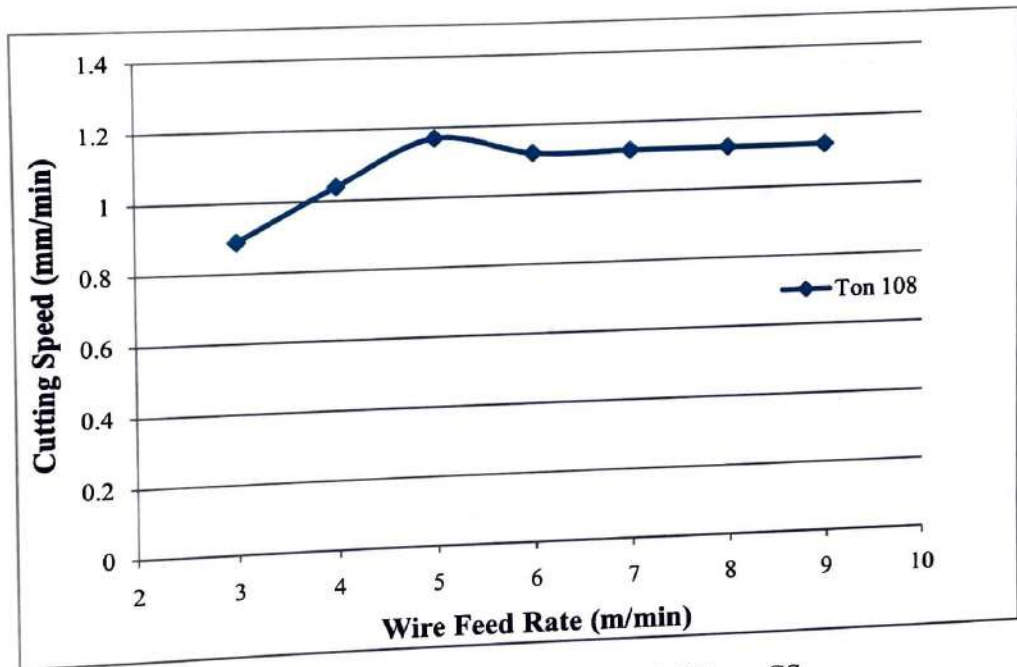


**Figure 3.13: Effect of Variation in  $W_F$  on CS**

Figure 3.13 shows that CS increases with increases of  $W_F$  from 3 m/min to 5 m/min. But further increase of  $W_F$  feed rate has no influence on CS. It implies that with these peak parameters, eroded debris are easily clear off from the spark gap at a  $W_F$  rate of 5m/min.



**3.8 EFFECT OF WEDM PARAMETERS ON SURFACE ROUGHNESS (SR)**

**3.8.1 Effect of Peak Current (Ip)**

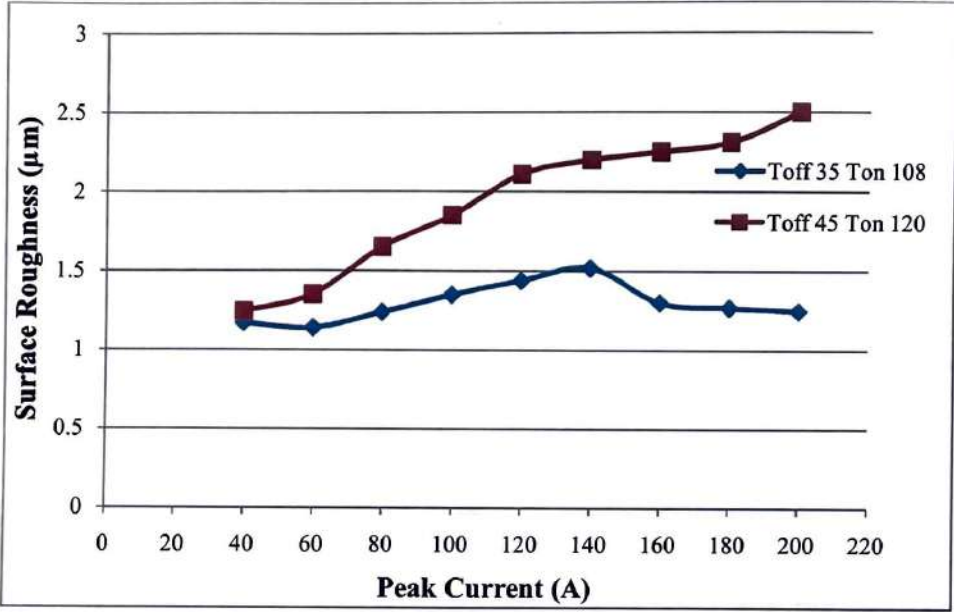
The effect of Ip on SR of Nimonic 90 with WEDM is shown in Figure 3.14 and 3.15 under two different setting of Ton (108  $\mu$ s, 120 $\mu$ s) along with two different setting of Toff (35 $\mu$ s, 45 $\mu$ s). The other parameters are fixed such as SV 20V, WT 10N, WF rate 5 m/min., servo feed 2080 and dielectric flow rate 12 litres per min (upper and lower nozzles). The results of the experiments performed at different machining parameters are shown in Table 3.8.

**Table 3.8:** Effect of Variation in Ip on SR

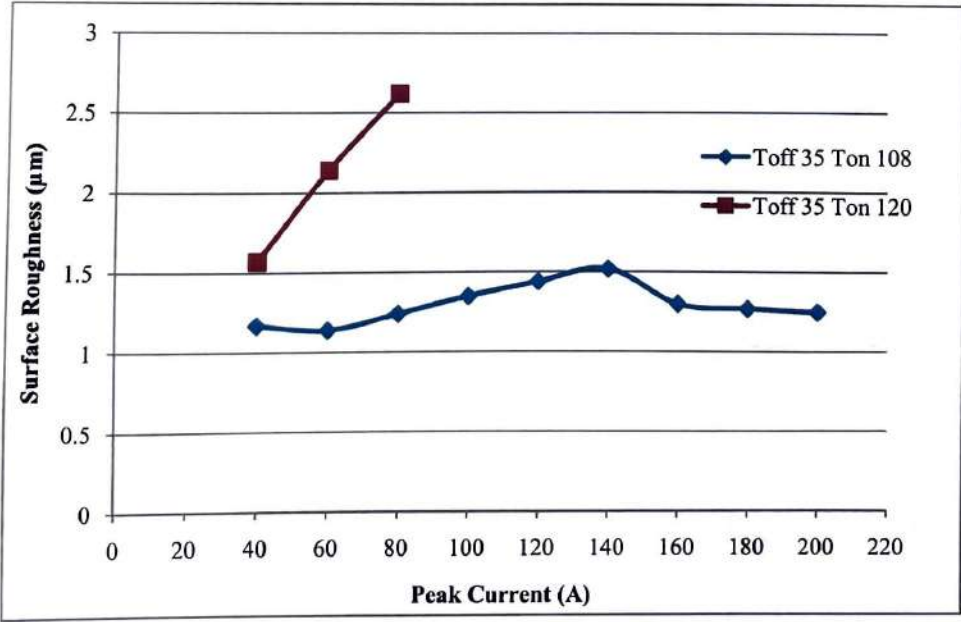
Ip (A)	SR ( $\mu$ m)		
	Toff 35, Ton 108	Toff 45, Ton 120	Toff 35, Ton 120
40	1.17	1.24	1.57
60	1.14	1.35	2.14
80	1.24	1.65	2.62
100	1.35	1.85	Further wire breakage
120	1.44	2.11	
140	1.52	2.2	
160	1.3	2.25	
180	1.27	2.31	
200	1.25	2.50	

Figure 3.14 shows that at low Ton 108 $\mu$ s, SR is increases slowly with increase of Ip value up to a certain limit and then decreases slightly with any increases of Ip. But at the value of Ton 120 $\mu$ s and Toff 40 $\mu$ s, there is increase of SR value with irrespective of CS. There is sharply increase of SR with increase of Ip from 60A to 100 A for Ton 120 $\mu$ s and Toff 35 $\mu$ s {Figure 3.15}. Increase in the Ip leads to increase in the rate of the heat energy and hence in the rate of melting and evaporation. With increasing value of Ip causes an increase in heat energy at the point, where the peaks take place. A pool of molten metal is formed at this point and is overheated. The overheated molten metal evaporates forming gas bubbles that explode when the peak ceases, taking molten metal material away. The

result is the formation of overlapped craters resulting poor SR. But at high Ton 120  $\mu$ s, further increase in the Ip leads to increase in the rate of the heat energy and hence in the rate of melting and evaporation. Increase of Ip value over higher limit leads to arcing, which decreases peak number and machining efficiency. Subsequently wire to be break down because of short Toff. The removal time of debris particles from the gap become insufficient.



**Figure 3.14:** Effect of Variation in Ip on SR at Different Value of Toff and Ton



**Figure 3.15:** Effect of Variation in Ip on SR at Different Value of Ton

3.8.2 Effect of Pulse on Time (Ton)

The effect of Ton on SR is shown in Figure 3.16 for two different setting of Toff (35μs, Toff 40μs) at high value of Ip 120 A .The other parameters are kept constant under the condition of SV 20 V, W<sub>F</sub> rate 5 m/min, W<sub>T</sub> 10 N, FR 12 litres per min. and servo feed 2080. The results of the experiments performed at different machining parameters setting are shown in Table 3.9.

Table 3.9: Effect of variation in Ton on SR

Ton (μs)	SR(μm)	
	Ip 120, Toff 35	Ip 120, Toff 40
103	0.66	0.68
106	0.78	1.23
109	1.42	1.51
112	2.11	2.1
115	2.4	2.37
118	Further Wire Breakage	2.72

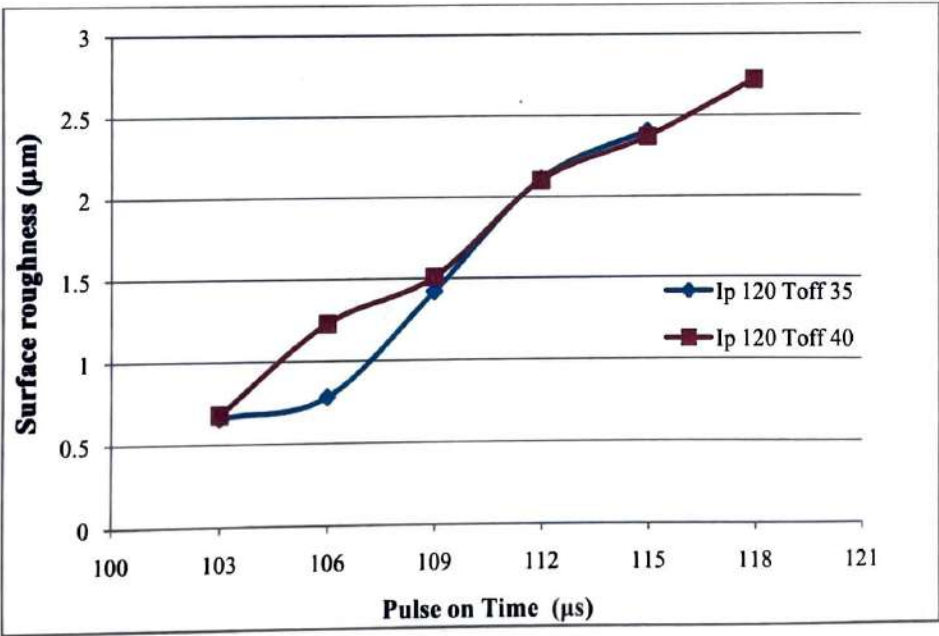


Figure 3.16: Effect of Variation in Ton on SR



According to different research study, Ton is most significant parameter that affects SR. Localized sparking become more frequent as Ton increases. SR increases continuously with increase of Ton. The machining becomes unstable at high pulse duration. At high peak energy, the amount of debris in the gap becomes too great which form an electrically conductive path between the electrode and workpiece, resulting into development of unwanted arc between them. If increase the Toff with increase of Ton, ample time is being available to flush away the debris, hence improve SR.

### 3.8.3 Effect of Pulse off Time (Toff)

Figure 3.17 shows the effect Toff for two machining setting Ton (108 $\mu$ s and 120 $\mu$ s) with fixed variables Ip 120 A, SV 20 V, FR 12 litres per min and servo feed 2080, W<sub>F</sub> rate 5 m/min and W<sub>T</sub> 10 N. The results of the experiments performed at different machining parameters setting are shown in Table 3.10.

**Table 3.10: Effect of Variation in Toff on SR**

Toff ( $\mu$ s)	SR ( $\mu$ m)	
	Ip 120, Ton 108	Ip 120, Ton 120
25	1.08	2.35
35	1.4	2.66
45	1.4	2.74
55	1.26	2.37

SR increases with increases in Toff from 25 to 45 $\mu$ s and after that it decrease sharply with increase in Toff. The higher input power (Ton 120 $\mu$ s, Ip 120A) associate with increase in Toff causes more frequent cracking of dielectric, leading to more frequent melt explosion as compared to low input power (Ton 108 $\mu$ s, Ip 120A). This give rise to higher density of globules accumulated at the close vicinity of machining zone and poor surface finish at high DE as compared to low discharge. SR shows the increasing trends with high value of Ip and Ton with increase of Toff due to increase in surface crater size. However the SR value first increases with increase Toff upto Toff 45 $\mu$ s and then decrease with further increase in value of Toff. This result is attributed to lower DE which does not explode the machined surface at the high value of Toff, hence improve

surface finish. At high value Ton 120 $\mu$ s, SR increase very fast as compared to low value of Ton 108 $\mu$ s.

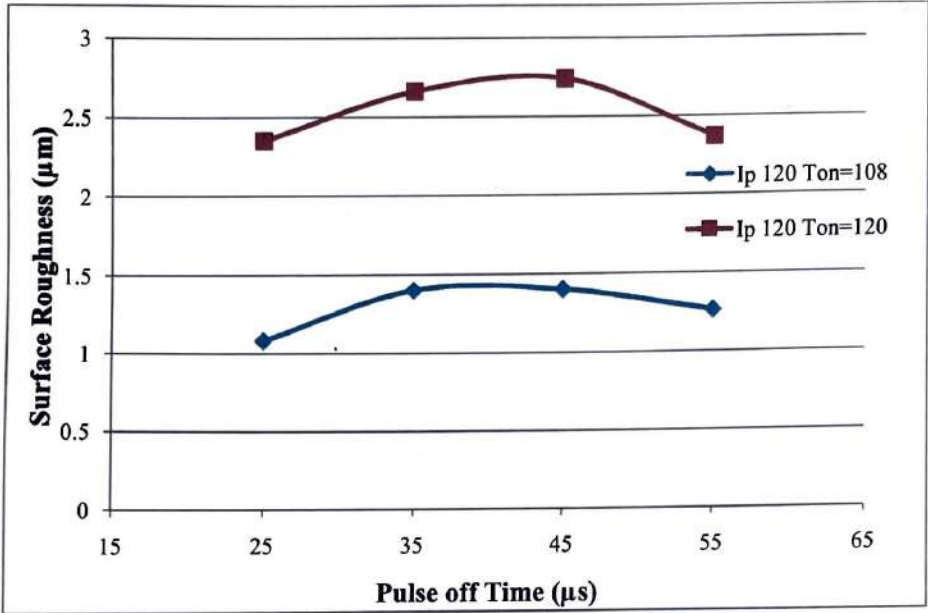


Figure 3.17: Effect of Variation in Toff on SR

### 3.8.4 Effect of Servo Voltage (SV)

The effect of SV on SR is shown in Figure 3.18 with two different values of Ton (108  $\mu$ s, 120  $\mu$ s) along with two different values of  $W_F$  rate (5 m/min, 6 m/min) keeping other variables fixed such as Toff 35 $\mu$ s, Ip 120 A, servo feed 2080 and  $W_T$  10 N. The results of the experiments performed at different machining parameters are shown in Table 3.11.

Table 3.11: Effect of Variation in SV on SR

SV (V)	SR ( $\mu$ m)	
	Ton 108, $W_F$ 5	Ton 120, $W_F$ 6
20	1.38	2.65
30	1.5	2.59
40	1.23	2.57
50	1.14	2.33
60	0.87	2.03

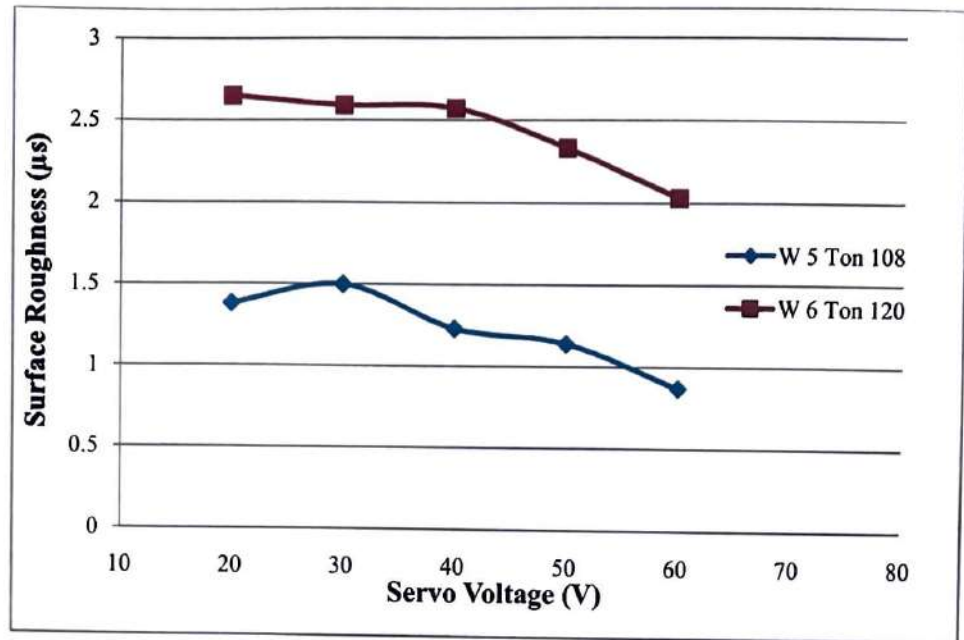


**Figure 3.18:** Effect of Variation in SV on SR

Figure 3.18 show that the increasing the value of SV decreases the SR of machined surface. Higher the value of SR with increasing value of SV for high value of Ton 120μs as compared to low value of Ton 108μs. But further increase of SV favours in the SR as the large amount of debris are able to clear off the gap for a given Toff but an adversely effecting the CS.

### 3.8.5 Effect of Wire Feed Rate ( $W_F$ )

The effect of  $W_F$  rate on SR is shown in Figure 3.19 keeping others fixed parameters such as Ton 108μs, Toff 35μs, SV 20 V, Ip 120A, servo feed 2080 and  $W_T$  10 N. The results of the experiments performed at different machining parameters setting are shown in Table 3.12.

SR increases slowly with increases of  $W_F$  rate from 3 m/min to 5 m/min {Figure 3.19}. But further increase of  $W_F$  rate increases SR very fast which means that the quality is goes down and manufacturing cost is high in term of cost of wire. At optimum value of  $W_F$  rate of 5m/min with these peak parameters, eroded debris are easily clear off from the spark gap.



**Table 3.12:** Effect of Variation in  $W_F$  on SR

$W_F$ (m/min)	SR ( $\mu\text{m}$ )
Ton 108, Toff 35	
3	1.17
4	1.38
5	1.41
6	1.81
7	2.49
8	2.45
9	2.37

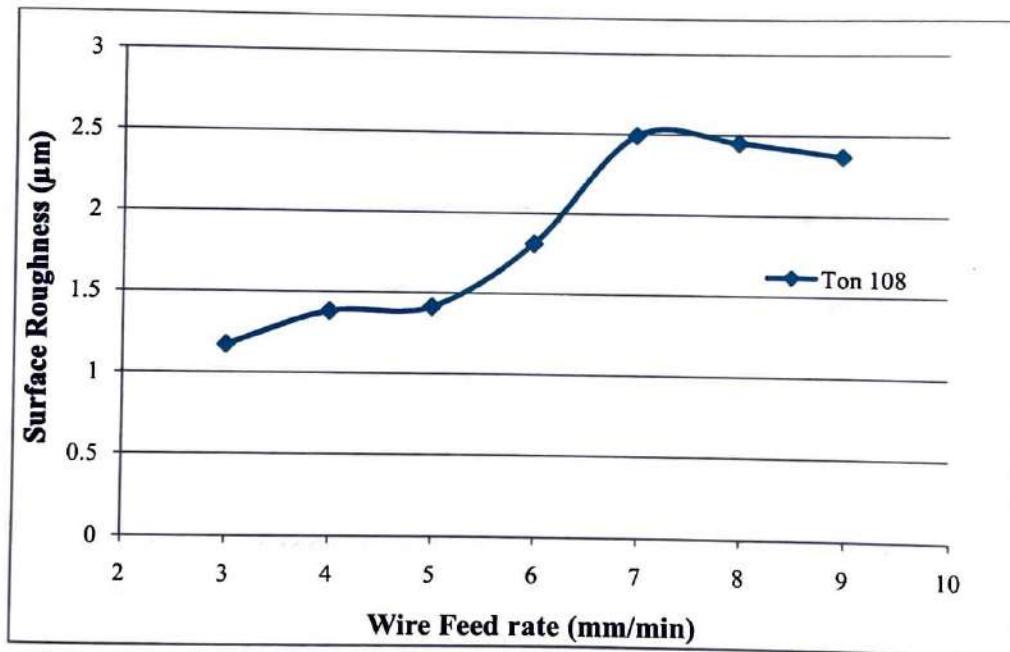


**Figure 3.19:** Effect of Variation in  $W_F$  on SR

### 3.9 RANGE OF PARAMETERS ON THE BASIS OF TRIAL EXPERIMENTATION

Trial experiments are conducted with Zinc coated brass wire. It is observed that wire feed rate do not produce any noticeable influence on WEDM performance. Thus,  $W_F$  rate should be kept at lower value to minimize the machining cost. Therefore, a constant value of 5m/min is assigned to  $W_F$  rate with adequate wire tension of 10N. All experiments are conducted at zero wire offset value.

Peak parameters namely  $I_p$ ,  $T_{on}$ ,  $T_{off}$  and SV controls the peak energy across the wire electrode and work material and hence affect the phenomenon of ionization of spark gap. Peak parameters are mainly controlled by pulse generator. In present machine tool, peak parameters can be varied under the following range;  $I_p$ : 10-230 A;  $T_{on}$ : 101-131 $\mu$ s;  $T_{off}$ : 10-63 $\mu$ s; SV: 0-90V. Based on the trial experiments, only four important variables namely  $I_p$ ,  $T_{on}$ ,  $T_{off}$  and SV are selected in present study.

Based on trial experiments on WEDM of Nimonic-90, it is found that effective working range of  $T_{on}$  is 106  $\mu$ s to 118  $\mu$ s. Beyond 118  $\mu$ s at  $T_{off}$  below 35  $\mu$ s, breakage of wire electrode occurs frequently. Effect of  $I_p$  is noticeable only from 70 A to 160 A, therefore, an effective range of 90 A to 150 A is selected for  $I_p$ . Similarly SV is kept in the range of 30 V to 50 V to provide a noticeable variation in machining characteristics. Selected range of four process parameters are listed in Table 3.13.

**Table 3.13: Process Parameters and their Range**

Parameters	Symbol	Units	Range	
			Low	High
Peak Current	$I_p$	A	90	150
Pulse on Time	$T_{on}$	$\mu$ s	106	118
Pulse off Time	$T_{off}$	$\mu$ s	35	45
Servo Voltage	SV	V	30	50

### 3.10 DISCUSSION

On the basis of trial experiments, important machining parameters namely  $I_p$ ,  $T_{on}$ ,  $T_{off}$  and SV etc. are proposed for further experimental work. Finally, the range and levels of these four variable machining parameters are selected.

## CHAPTER-IV

### EXPERIMENTAL DESIGN METHODOLOGY

---

#### 4.1 INTRODUCTION

A scientific approach is necessary for conducting the experiments efficiently. The design of experiment plan is necessary for an appropriate data collection for experimentation, and statistical analysis for exact findings. Design of experiments (DOE) is a theory concerning the minimum number of experiments needed to develop an empirical model of a research statement and a methodology for setting up the necessary experiments. A statistical methodology is a right approach to analysis a problem comprises data subjected to experimental error. The advantages of design of experiments are as follows:

- Numbers of trials experiments are significantly reduced.
- Offer the best indication that the work is responsible for changes in outcomes.
- Identified the main decision variables which improve and control the performance of the process.
- Find out the most favourable setting of the parameters.
- Qualitative evaluation of parameters may be draw.
- Estimate the experimental error easily.
- Identify the inference regarding the effect of parameters on the characteristics of the process.

In this study experimental work is planned and analysed using Response Surface Methodology (RSM).

#### 4.2 RESPONSE SURFACE METHODOLOGY (RSM) AND EXPERIMENTAL DESIGN

RSM is a collection of mathematical and experimental techniques useful for developing new processes, optimizing and improving their performance. The most common applications of RSM are in social science, industrial, engineering sciences, food science, biological and clinical science. Originally, RSM was developed to model experimental responses (Box and Hunter, 1957), and then migrated into the modelling of numerical experiments. It requires sufficient number of experimental



data to analyse the problem and to develop mathematical models for several independent variables (input variables) and output response characteristics (Kumar et al. 2014). By using the design of experiments and applying regression analysis, the modelling of the desired response ( $Y$ ) to several independent input variables  $x_1, x_2, x_3, \dots, x_k$  can be gained. In RSM, the quantitative form of relationship between desired response and independent input variables may be represented as:

$$Y = \phi(x_1, x_2, \dots, x_k) \pm e_r \quad (4.1)$$

The function  $\phi$  is called response surface or response function. The residual  $e_r$  measures the experimental errors on the response, background noise, effect of other variables, and so on.

$\phi$  is unknown in most RSM problems. In order to develop a proper approximation for  $\phi$ , the experimenter usually a low-order polynomial in some relatively small region of the independent variable space is appropriate. If the response can be defined by a linear function of independent variables, then the approximating function is a first-order model. A first-order model for two independent variables can be expressed as

$$Y = b_0 + b_1x_1 + b_2x_2 + e \quad (4.2)$$

A higher degree polynomial should be used, in case of curvature in the response surface. A second order model is likely to be required in these situations. The approximating function with 2 variables is called a second order model:

$$Y = b_0 + b_1x_1 + b_2x_2 + b_{11}x_1^2 + b_{22}x_2^2 + b_{12}x_1x_2 + e \quad (4.3)$$

The second-order model is widely used in RSM for several regions:

1. It is very elastic and takes on a wide variety of functional forms. It works well for an estimate to the true response surface.
2. It is easy to calculate approximately the parameters in the second-order model.
3. Second order model work well in solving real response surface problems.

In general, all RSM problems use either one or the mixture of the both of these models. In each model, the levels of each factor are independent of the levels of other factors. In order to get the most efficient result in the approximation of polynomials, a proper experimental design must be used to collect data. Once the data are collected, the Method of Least Square is used to estimate the parameters in the polynomials. The response surface analysis is performed by using the fitted surface. The response

surface designs are types of designs for fitting response surface. Therefore, the objective of studying RSM can be accomplished by:

- (1) Understanding the topography of the response surface (local maximum, local minimum, ridge lines).
- (2) Finding the region where the optimal response occurs. The goal is to move rapidly and efficiently along a path to get to a maximum or a minimum response so that the response is optimized.

In RSM, the dependent variable is considered as a surface to which a mathematical model is fitted. For the development of regression equations related to various machining characteristics of WEDM process, the second order response surface is assumed as:

$$Y = b_0 + \sum_{i=1}^k b_i x_i + \sum_{i=1}^k b_{ii} x_i^2 + \sum_{i < j=2}^2 b_{ij} x_i x_j \pm e_r \quad (4.4)$$

This assumed surface  $Y$  contains linear, squared and cross product terms of variables  $x_i$ . The model parameters can be estimated most efficiently only if the data is collected by proper experimental design. Procedure of RSM is as follows:

1. Preliminary experiments are performed.
2. Design the input parameters according to preliminary experiments and output quality characteristics according to experiment.
3. Select the design of experiments.
4. Regression analysis is to be carried out.
5. Analysis of variance is to be found out.
6. If the model is significant.
7. Optimal settings are to be found.
8. At these setting, confirm the predicated values of experiment.
9. If model is not significant, then input parameters screening are to be carried out and repeat the process from Step 3.

#### 4.3 CENTRAL COMPOSITE DESIGN (CCD)

A Box-Wilson Central Composite Design is also named as central composite design. These types of experimental design are frequently used together with response models of the second order. For the further description of the designs, the ranges minimum and maximum values of the control parameters are scaled to  $[-1, +1]$ . The design consists of three types of points:

4.3.1 Axial Points

The  $2 \times n$  axial points are created by a Screening Analysis. An example of a Screening Analysis of a three dimensional parameter space is shown in Figure 4.1. This design spans a star in the  $n$  dimensional parameter space and these points are called star points.

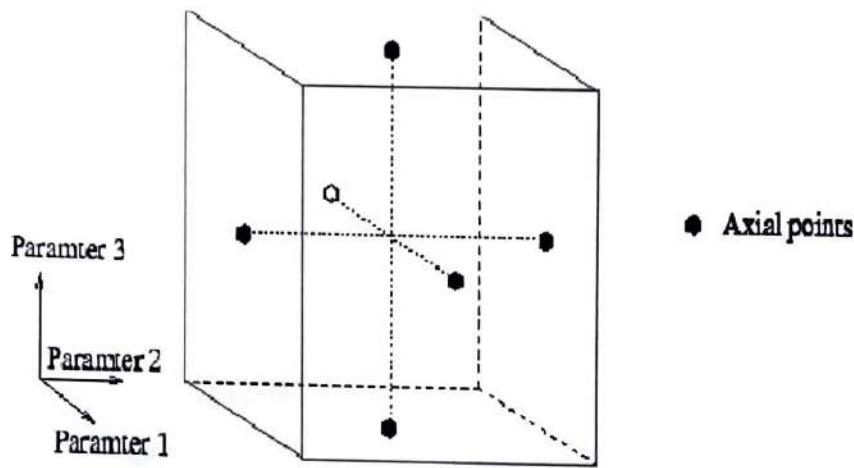


Figure 4.1: Axial points of a Full Factorial Design with Three Input Parameters

4.3.2 Cube Points

The Full Factorial creates  $2^n$  sample points with all possible combination of the minimum and maximum values of the control parameters. An example of a Full Factorial design of a three dimensional parameter space is shown in Figure 4.2. This design spans a hyper cube in the  $n$  dimensional parameter space and these points are called cube points.

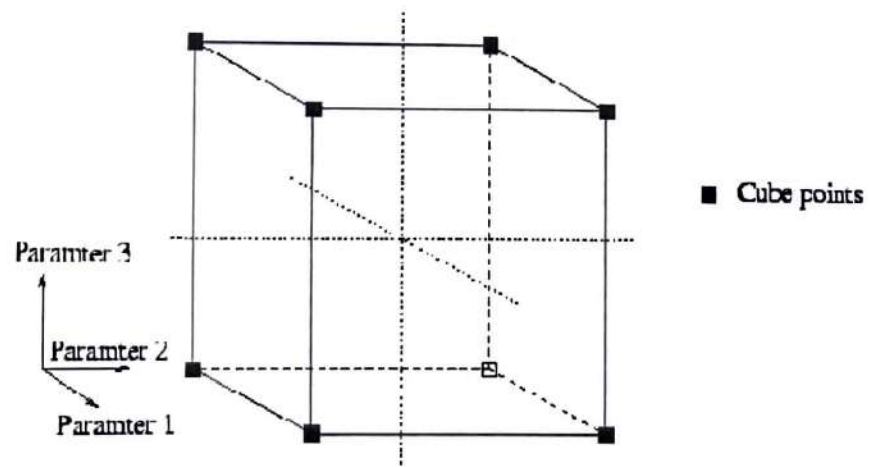


Figure 4.2: Cube points of a Full Factorial Design with Three Input Parameters



### 4.3.3 Centre Point

A single point in the center is created by a Nominal design. The Nominal design consists of one experiment where all control parameters are set to their nominal values. This single set of parameter values is also called a center point. The nominal design is mainly used as part of other designs, or for the testing of assigned parameter values or simulation based evaluations.

CCD contains an imbedded factorial or fractional factorial design with center points that is augmented with a group of 'star points' which allow estimation of curvature. If the distance from the centre of the design space to a factorial point is  $\pm 1$  unit for each factor, the distance from the centre of the design space to a star point is  $|\alpha| > 1$ . The precise value of  $\alpha$  depends on certain properties desired for the design and on the number of factors involved. Similarly, the number of centre point runs the design is to contain also depends on certain properties required for the design. In this design, the star points are at the centre of each face of the factorial space, so  $\alpha = \pm 1$ . This variety requires 3 levels of each factor.

A CCD always contains twice as many star points as there are factors in the design. The star points represent new extreme values (low and high) for each factor in the design. Figure 4.3 shows a diagram of central composites design generation for two factors.

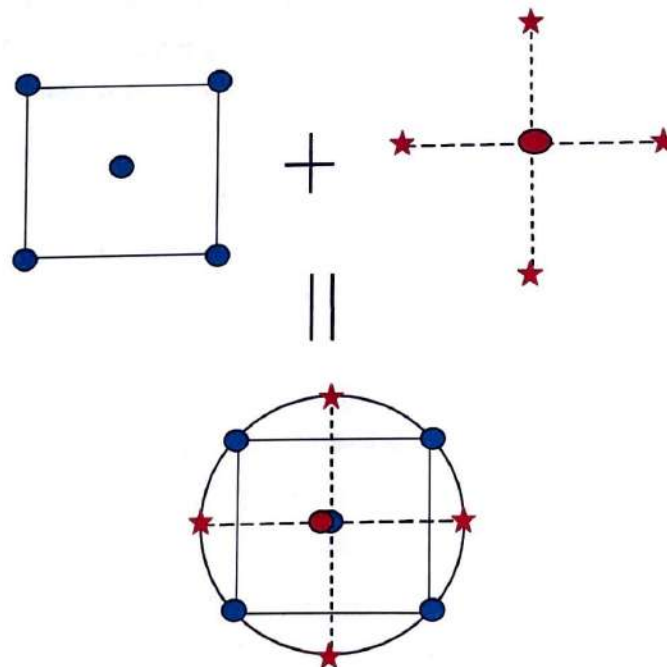


**Figure 4.3:** Generation of a CCD for Two Factors

#### 4.4 CENTRAL COMPOSITE SECOND ORDER FACED CENTRED DESIGN

In this design, the star points are at the centre of each face of the factorial space, so  $\alpha = \pm 1$ . This variety requires 3 levels of each factor. Augmenting an existing factorial design with appropriate star points can also produce this design. A central composite design with axial points set at a normalized distance of one away from the centre, as shown in Figure 4.4.

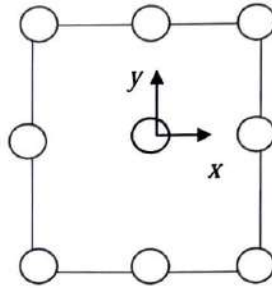


**Figure 4.4:** Qualitative design space for a two parameter face centered cubic design.

The face centered, central composite design contains an imbedded factorial design with center points. It is used to find the best set of values, for a set of factors, giving an optimal response. In this mathematical approach, design helps in exploring quadratic surface responses where each experimental response (Y) can be represented. A polynomial model developed based on the regression analysis of the statistically significant variables enables the study of the effects of each variable factor (x) and their interaction over the considered responses (Y) and hence can be used to predict responses of CS, SR and RoC) values for rough cutting operation in WEDM. Comparison of predicted values for  $Y_1$ ,  $Y_2$  and  $Y_3$  with experimental data is used to test validity of the models. A standard second order experimental design called face centered CCD is adopted for analysing and modelling the machining parameters for different machining characteristic using the minimum possible number of experiments without sacrificing its accuracy. Using Design expert (DX-7) a statistical tool, face centred central composite design is generated for different machining parameters. Each row in the matrix represents an experiment and each experiment represents a set of results. The selected machining parameters are varied up to three levels. Response Surface Methodology is used to develop second order regression equation relating machining parameters and machining characteristics. The components of central composite second order faced centred design for four numbers of variables are given in Table 4.1. Work materials are machined and samples are obtained in the form of rectangular punches of size 6 mm  $\times$  4 mm  $\times$  12.5 mm. A level of four process parameters is listed in Table 4.2.

**Table 4.1:** Components of Central Composite Second Order Faced Centred Design for Four Variables.

Variables (K)	Factorial Points (2 <sup>k</sup> )	Star points (2k)	Center Points (n)	Total Trial (N)
4	16	8	6	30

**Table 4.2:** Variables Process Parameters and their Levels

Parameter	Symbol	Units	Levels		
			Low (-1)	Middle (0)	High (+1)
Peak Current	Ip	A	90	120	150
Pulse on Time	Ton	μs	106	112	118
Pulse off Time	Toff	μs	35	40	45
Servo voltage	SV	V	30	40	50

#### 4.5 SELECTION OF PARAMETERS AND ITS RANGE BASED ON TRIAL EXPERIMENTATION

In present investigation, only discharge parameters namely Ip, Ton, Toff and SV are selected as variable parameters while parameters under the category of wire electrode and dielectric conditions have been assigned a constant value. Experiments are properly planned to fulfil the following necessities:

- Uniformly distributed the data over the entire range of controllable factors to be investigated.
- Minimizing the total number of experiments to be performed.
- To ascertain a relationship between different input variables.

#### 4.6 EXPERIMENTAL RESULTS

Four parameters are set at three levels. Therefore, a standard second order experimental design called face centered CCD is adopted. This design consists of full factorial having 30 runs including 6 central points. Using Design expert (DX-7) a statistical tool, face centered CCD is generated for four input variables as shown in Table 4.3 and average values of machining characteristics are shown in Table 4.4.



**Table 4.3: Test Conditions in Face Centered CCD for Four Parameters**

Trial No.	Ip	Coded value	Ton	Coded value	Toff	Coded value	SV	Coded value
	(A)		( $\mu$ s)		( $\mu$ s)		(V)	
1	90	-1	106	-1	35	-1	30	-1
2	150	1	106	-1	35	-1	30	-1
3	90	-1	118	1	35	-1	30	-1
4	150	1	118	1	35	-1	30	-1
5	90	-1	106	-1	45	1	30	-1
6	150	1	106	-1	45	1	30	-1
7	90	-1	118	1	45	1	30	-1
8	150	1	118	1	45	1	30	-1
9	90	-1	106	-1	35	-1	50	1
10	150	1	106	-1	35	-1	50	1
11	90	-1	118	1	35	-1	50	1
12	150	1	118	1	35	-1	50	1
13	90	-1	106	-1	45	1	50	1
14	150	1	106	-1	45	1	50	1
15	90	-1	118	1	45	1	50	1
16	150	1	118	1	45	1	50	1
17	90	-1	112	0	40	0	40	0
18	150	1	112	0	40	0	40	0
19	120	0	106	-1	40	0	40	0
20	120	0	118	1	40	0	40	0
21	120	0	112	0	35	-1	40	0
22	120	0	112	0	45	1	40	0
23	120	0	112	0	40	0	30	-1
24	120	0	112	0	40	0	50	1
25	120	0	112	0	40	0	40	0
26	120	0	112	0	40	0	40	0
27	120	0	112	0	40	0	40	0
28	120	0	112	0	40	0	40	0
29	120	0	112	0	40	0	40	0
30	120	0	112	0	40	0	40	0

**Table 4.4:** Experimental Results of CS, SR and RoC

<b>Trial No.</b>	<b>CS (mm/min.)</b>	<b>SR (<math>\mu\text{m}</math>)</b>	<b>RoC (<math>\mu\text{m}</math>)</b>
1	1.46	1.41	22.36
2	1.61	1.73	23.24
3	2.65	2.43	27.56
4	2.90	2.73	28.90
5	1.06	1.22	20.80
6	1.22	1.46	22.13
7	2.46	2.27	27.10
8	2.71	2.45	28.60
9	1.16	1.13	22.46
10	1.32	1.32	23.45
11	2.35	2.30	29.71
12	2.59	2.55	32.02
13	0.72	0.97	22.10
14	0.92	1.14	23.46
15	2.18	2.12	31.50
16	2.40	2.37	33.78
17	2.18	1.93	26.10
18	2.39	2.11	27.95
19	1.37	1.35	23.29
20	2.71	2.41	32.11
21	2.46	2.10	27.13
22	2.13	1.79	26.10
23	2.53	2.16	26.10
24	2.23	1.87	28.56
25	2.39	1.95	27.50
26	2.37	2.03	27.00
27	2.36	2.01	27.30
28	2.35	2.00	27.00
29	2.39	2.01	27.10
30	2.38	1.99	27.50

#### **4.7 SELECTION OF ADEQUATE MODEL**

There are three tests, i.e., sequential model sum of squares, lack of fit tests and model summary statistics are performed for deciding the adequacy of the model for three different machining characteristics, i.e., CS, SR and RoC in WEDM process. Table 4.5-4.7 are used to decide an adequate model to fit various machining characteristics. The sequential model is sum of squares test in each table shows how the terms of increasing complexity contribute to the model. It is observed that for all the responses, the quadratic model is appropriate. The “lack of fit” test compares the residual error to the pure error from the replicated design points. The results indicate that the quadratic model in all the characteristics show a non-significant lack of fit, hence confirmed the adequacy of quadratic model. “Model summary statistics” test confirms the quadratic model is the best to fit as it shows low standard deviation, high “R-Squared” values, and a low “PRESS” (Adeq Precision).

#### **4.8 RESULTS AND ANALYSIS**

The experiments are performed as per layout shown in Table 4.3 and machining characteristics are measured. To analyze the experimental data, a statistical tool Design expert (DX7) is used and ANOVA is performed on the experimental data to test the goodness of fit of the model. This includes the test for significance of the regression model, test for significance on model coefficients and test for lack of fit model adequacy (Myers and Montgomery, 1995; Kansal et al. 2005).



**Table 4.5:** Selection of Adequate Model for CS

<b>Sequential Model Sum of Squares Test</b>						
<b>Source</b>	<b>Sum of Squares</b>	<b>Degree of Freedom</b>	<b>Mean Square</b>	<b>F-value</b>	<b>p-value Prob&gt;F</b>	
Mean vs. Total	127.93	1	127.93			
Linear vs. Mean	9.15	4	2.29	33.19	<0.0001	
2F1 vs. Linear	0.055	6	9.156E-004	0.10	0.9950	
Quadratic vs. 2F1	1.67	4	0.42	1878.75	<0.0001	Suggested
Cubic vs. Quadratic	1.678E-003	8	2.098E-004	0.89	0.5666	Aliased
Residual	1.646E-003	7	2.352E-004			
Total	138.81	30	4.63			
<b>Lack of Fit Tests</b>						
<b>Source</b>	<b>Sum of Squares</b>	<b>Degree of freedom</b>	<b>Mean Square</b>	<b>F- Value</b>	<b>p- value Prob &gt; F</b>	
Linear	1.72	20	0.086	322.97	<0.0001	
2F1	1.67	14	0.12	446.67	<0.0001	
Quadratic	1.991E-003	10	1.991E-004	0.75	0.6762	
Cubic	3.129E-004	2	1.565E-004	0.59	0.5903	Suggested
Pure Error	1.333E-003	5	2.667E-004			Aliased
<b>Model Summary Statistics</b>						
<b>Source</b>	<b>Standard Deviation</b>	<b>R-Squared</b>	<b>Adjusted R-Squared</b>	<b>Predicated R-Squared</b>	<b>Press</b>	
Linear	0.26	0.8415	0.8162	0.7748	2.45	
2F1	0.30	0.8466	0.7658	0.4313	6.19	
Quadratic	0.015	0.9997	0.9994	0.9986	0.015	Suggested
Cubic	0.015	0.9998	0.9994	0.9946	0.59	Aliased

**Table 4.6: Selection of Adequate Model for SR**

<b>Sequential Model Sum of Squares Test</b>						
<b>Source</b>	<b>Sum of Squares</b>	<b>Degree of Freedom</b>	<b>Mean Square</b>	<b>F- value</b>	<b>p-value Prob&gt;F</b>	
Mean vs. Total	109.48	1	109.48			
Linear vs. Mean	6.13	4	2.291.53	179.22	<0.0001	
2F1 vs. Linear	0.040	6	9.156E-006.696E-0034	0.73	0.6293	
Quadratic vs. 2F1	0.15	4	0.40.0392	30.93	<0.0001	Suggested
Cubic vs. Quadratic	0.015	8	1.850E-003	3.26	0.0685	Aliased
Residual	3.971E-003	7	5.674E-004			
Total	115.83	30	3.86			
<b>Lack of Fit Tests</b>						
<b>Source</b>	<b>Sum of Squares</b>	<b>Degree of freedom</b>	<b>Mean Square</b>	<b>F- value</b>	<b>p- value Prob &gt; F</b>	
Linear	0.21	20	0.011	14.26	0.0040	
2F1	0.17	14	0.012	16.48	0.0030	
Quadratic	0.015	10	1.509E-003	2.05	0.2219	
Cubic	2.882E-004	2	1.441E-004	0.20	0.8284	Suggested
Pure Error	3.683E-003	6	7367E-004			Aliased
<b>Model Summary Statistics</b>						
<b>Source</b>	<b>Standard Deviation</b>	<b>R-Squared</b>	<b>Adjusted R-Squared</b>	<b>Predicted R-Squared</b>	<b>Press</b>	
Linear	0.092	0.9663	0.9609	0.9506	0.31	
2F1	0.096	0.9726	0.9582	0.9057	0.60	
Quadratic	0.035	0.9970	0.9943	0.9854	0.093	Suggested
Cubic	0.024	0.9994	0.9974	0.9893	0.068	Aliased

**Table 4.7:** Selection of Adequate Model for RoC

<b>Sequential Model Sum of Squares Test</b>						
<b>Source</b>	<b>Sum of Squares</b>	<b>Degree of Freedom</b>	<b>Mean Square</b>	<b>F- value</b>	<b>p-value Prob&gt;F</b>	
Mean vs. Total	21328.53	1	21328.53			
Linear vs. Mean	290.32	4	72.58	71.50	<0.0001	
2F1 vs. Linear	14.52	6	2.42	4.23	0.0072	
Quadratic vs. 2F1	8.55	4	2.14	13.87	<0.0001	Suggested
Cubic vs. Quadratic	1.87	8	0.23	3.71	0.0506	Aliased
Residual	0.44	7	0.063			
Total	21644.24	30	721.47			
<b>Lack of Fit Tests</b>						
<b>Source</b>	<b>Sum of Squares</b>	<b>Degree of freedom</b>	<b>Mean Square</b>	<b>F-value</b>	<b>p- value Prob &gt; F</b>	
Linear	25.10	20	1.26	22.96	0.0013	
2F1	10.59	14	0.76	13.83	0.0045	
Quadratic	2.04	10	0.20	3.73	0.0796	
Cubic	0.17	2	0.084	1.54	0.3019	Suggested
Pure Error	0.27	5	0.055			Aliased
<b>Model Summary Statistics</b>						
<b>Source</b>	<b>Standard Deviation</b>	<b>R-Squared</b>	<b>Adjusted R-Squared</b>	<b>Predicated R-Squared</b>	<b>Press</b>	
Linear	1.01	0.9196	0.9068	0.8688	41.42	
2F1	0.76	0.9656	0.9475	0.8806	37.71	
Quadratic	0.39	0.9927	0.9858	0.9659	10.76	Suggested
Cubic	0.25	0.9986	0.9942	0.9354	20.40	Aliased



**Table 4.8:** ANOVA for CS (after backward elimination)

Source	Sum of Squares	Degree of freedom	Mean Square	F-value	p-value	
Model*	10.87	9	1.21	6904.81	<0.0001	Significant
Ip	0.19	1	0.19	1074.95	<0.0001	
Ton	8.15	1	8.15	46555.45	<0.0001	
Toff	0.40	1	0.40	2314.63	<0.0001	
SV	0.41	1	0.41	2366.63	<0.0001	
(Ip) <sup>2</sup>	0.026	1	0.026	146.28	<0.0001	
(Ton) <sup>2</sup>	0.33	1	0.33	1869.44	<0.0001	
(Toff) <sup>2</sup>	0.020	1	0.020	117.09	<0.0001	
Ip*Ton	5.256E-003	1	5.256E-003	30.04	<0.0001	
Ton*Toff	0.050	1	0.050	282.93	<0.0001	
Residual	3.499E-003	20	1.750E-004			
Lack of fit	2.166E-003	15	1.44E-004	0.54	0.8359	Not significant
Pure error	1.33E-003	5	2.667E-004			
Cor. Total	10.88	29				
Standard deviation = 0.013;      R <sup>2</sup> = 0.9997      R <sup>2</sup> (Adj.) = 0.9995						

#### 4.8.1 Analysis of CS

Table 4.8 shows ANOVA for CS suggests that quadratic model is statistically significant for analysis. A selected model will be statistically significant, if  $p$ -value for the model terms are less than 0.05 (i.e.  $\alpha = 0.05$ , or 95% confidence level) (Kanagarajan et al. 2008). Using backward elimination process, insignificant terms ( $p$ -value > 0.05) is eliminated from the reduced quadratic model. The  $p$ -value for quadratic model is significant which shows that the terms in the model have significant effect on output response. In present case, the value of  $R^2$  and  $R^2(\text{adj.})$ , called coefficient of determination, is over 99%. When  $R^2$  approaches unity, better the response model fits the actual data. Also, test of 'lack of fit' shows insignificant effect, which is desirable for selecting the models (Kansal et al. 2008). Figure 4.5 shows that the residuals are normally distributed about a straight line which means that the errors are normally distributed. Figure 4.6 shows that the predicted vs. actual values plot for CS and all the actual values are following the predicating values.

Hence declared model assumptions are right. Consequently, the proposed model for CS can be considered as significant for fitting and predicting the experimental results.

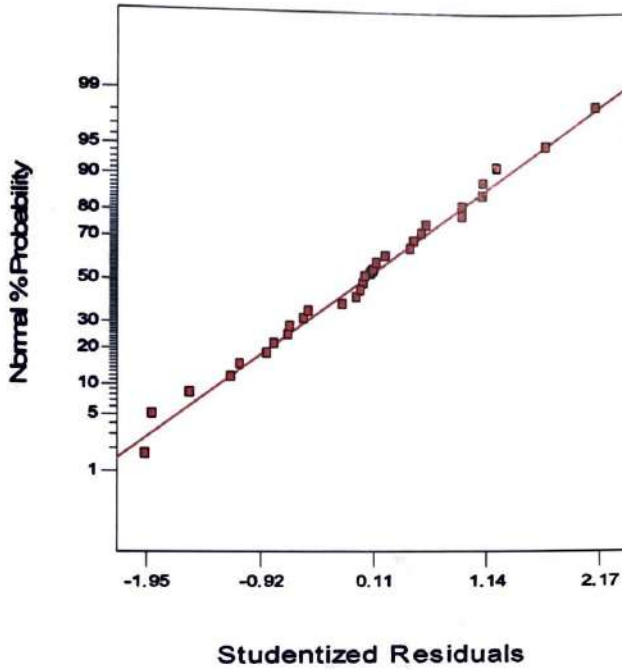


**Figure 4.5:** Normal probability Residuals plot for CS

Table 4.8 shows that the input parameters  $I_p$ ,  $T_{on}$ ,  $T_{off}$ ,  $SV$ , interaction effect of  $I_p$  with  $T_{on}$  and interaction effect of  $T_{on}$  with  $T_{off}$  have significant effect. The other non significant terms are eliminated to fairly fit the quadratic model. The final regression equation for CS is given as below:

**(In coded terms)**

$$CS = 2.38 + 0.10 I_p + 0.67 T_{on} - 0.15 T_{off} - 0.15 SV - 0.095 (I_p)^2 - 0.34 (T_{on})^2 - 0.085 (T_{off})^2 + 0.018 I_p \times T_{on} + 0.056 (T_{on} \times T_{off}) \quad (4.5)$$

**(In terms of actual parameters)**

$$CS = -124.36 + 0.0174 I_p + 2.138 T_{on} + 0.03419 T_{off} - 0.015 SV - 1.055E-004 (I_p)^2 - 9.429E-003 (T_{on})^2 - 3.398 (T_{off})^2 + 1.0069E-004 (I_p \times T_{on}) + 1.85E-003 (T_{on} \times T_{off}) \quad (4.6)$$

In order to analyze the influence of WEDM parameters on CS, response surface graphs are plotted {Figure 4.7a to 4.7c}.

Figure 4.7(a) shows that CS increases with increase in Ton and Ip. But the effect of Ton is highly noticeable as compared to Ip. Increasing Ip and Ton increases the discharge energy across the electrode and hence results into high melting and evaporation of material. High melting and evaporation combined with high dielectric supply results into high CS (Jangra and Grover 2012).

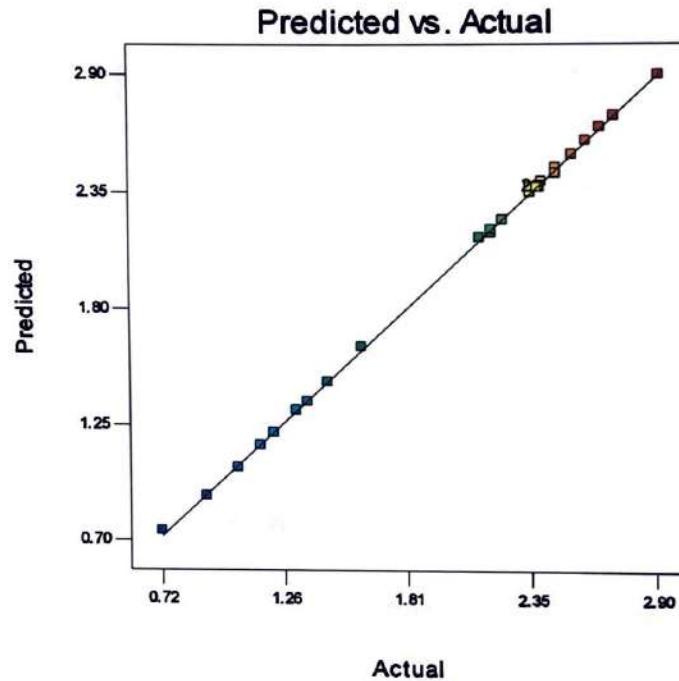


**Figure 4.6:** Predicted vs. Actual Plot for CS

Effect of Toff combined with Ip is depicted in Figure 4.7(b). Increase in value of Toff results into decrease in CS. Increasing Toff value decreases the discharge frequency and increases the cooling effect on work surface due to high flow of dielectric, resulting into decrease in overall machining time. Decreasing SV narrow the spark gap, results into large ionization of dielectric fluid and hence increases CS as shown in Figure 4.7(c). Response surface plots depicts that the maximum value of CS can be obtained with the combination of high value of Ip and Ton and low level of Toff and SV, respectively.



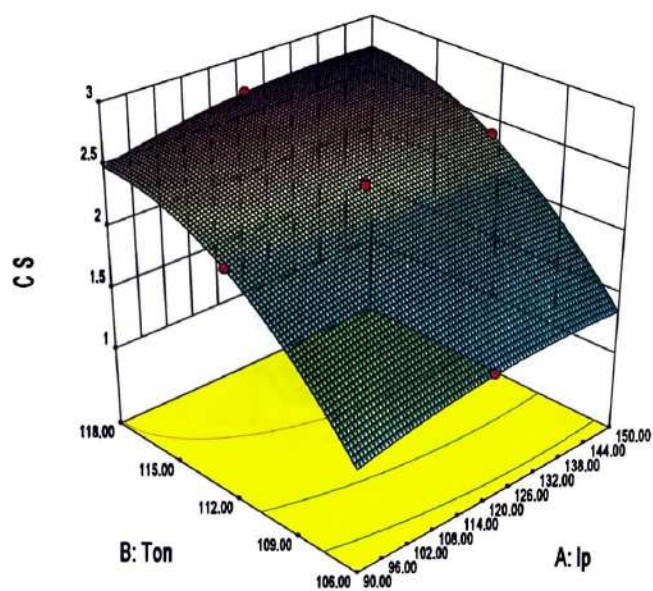


**Figure 4.7(a):** Combined Effect of  $I_p$  and  $T_{on}$  on  $CS$  ( $T_{off}$ :  $40\mu s$ ;  $SV$ :  $40V$ )

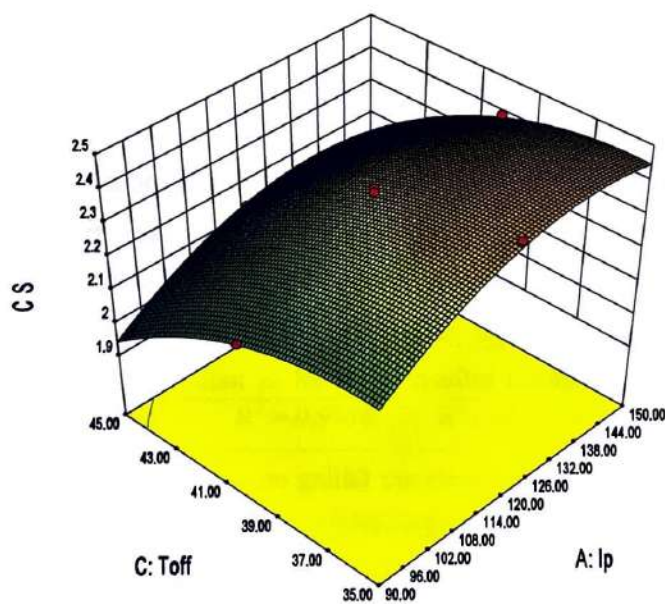


**Figure 4.7 (b):** Combined Effect of  $I_p$  and  $T_{off}$  on  $CS$  ( $T_{on}$ :  $40\mu s$ ;  $SV$ :  $40V$ )

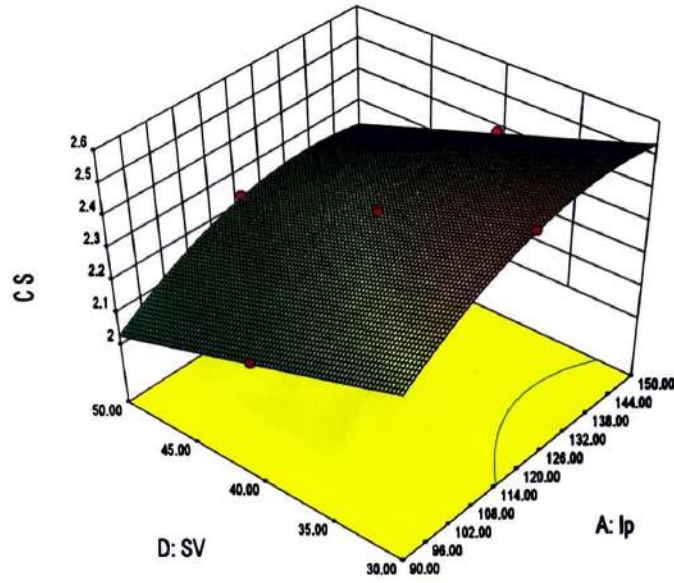


**Figure 4.7 (c):** Combined Effect of SV and Ip on CS (Ton: 112 $\mu$ s; Toff: 40 $\mu$ s)

#### 4.8.2 Analysis of SR

Table 4.9 shows the ANOVA for SR after backward elimination process suggested that quadratic model is statistically significant for analysis. In case of SR, value of  $R^2$  and  $R^2(\text{adj.})$  is greater than 99% which shows that regression model provides an excellent explanation of the relationship between input variables and the response. The  $p$ -value for model is less than 0.05; indicates that the model is statistically significant. The lack of fit is also non-significant. The input parameters namely Ip, Ton, Toff, SV and interaction of Ton with SV have significant influences on SR as indicated by the associated  $p$ -value (less than 0.05).

Figure 4.8 shows that residuals are falling on a straight line which means that the errors are normally distributed. It is observed from Figure 4.9 that all the actual values are following the predicted values. After eliminating the non significant terms, the final response equation for SR is given as follows:

**(In coded terms)**

$$\text{SR} = 2.00 + 0.12 \text{ Ip} + 0.55 \text{ Ton} - 0.11 \text{ Toff} - 0.12 \text{ SV} - 0.11 (\text{Ton})^2 - 0.045 (\text{Toff})^2 + 0.045 (\text{Ton} \times \text{SV}) \quad (4.7)$$

(In terms of actual parameters)

$$SR = -45.261 + 0.00385 I_p + 0.746 Ton + 0.123 Toff - 0.0956 SV - 0.00305 (Ton)^2 - 0.0018 (Toff)^2 + 0.00075 (Ton \times SV) \quad (4.8)$$

**Table 4.9:** ANOVA for SR (after backward elimination)

Source	Sum of Squares	Degree of freedom	Mean Square	F-value	p-value	
Model <sup>a</sup>	6.32	7	0.90	703.53	<0.0001	Significant
Ip	0.24	1	0.24	187.40	<0.0001	
Ton	5.44	1	5.44	4245.36	<0.0001	
Toff	0.20	1	0.20	158.02	<0.0001	
SV	0.24	1	0.24	189.21	<0.0001	
(Ton) <sup>2</sup>	0.042	1	0.042	32.50	<0.0001	
(Toff) <sup>2</sup>	6.975E-003	1	6.97E-003	5.44	0.0293	
Ton*SV	0.032	1	0.032	25.26	<0.0001	
Residual	0.028	22	1.28E-003			
Lack of fit	0.025	17	1.44E-003	1.96	0.2354	Not significant
Pure error	3.683E-003	5	7.367E-004			
Cor. Total	6.34	29				
Standard deviation = 0.036; R <sup>2</sup> = 0.9956 R <sup>2</sup> (Adj.) = 0.9941						

Figure 4.10(a) and 4.10(b) are showing noticeable influence of Ton and Ip on SR. It is observed that SR increases with increasing the value of Ip and Ton. Ton is highly significant factor which can be proved by the sharp curve of Figure 4.10(a) and highest F-value in Table 4.9. High discharge energy due to high value of Ton and Ip results into overheating and evaporation of molten metal forming gas bubbles that explode when the discharge ceases. As a result high pressure energy creates large size craters on work surface. The diameter and depth of crater increases with increasing Ip and Ton and hence increases the SR (Hewidy et al. 2005).



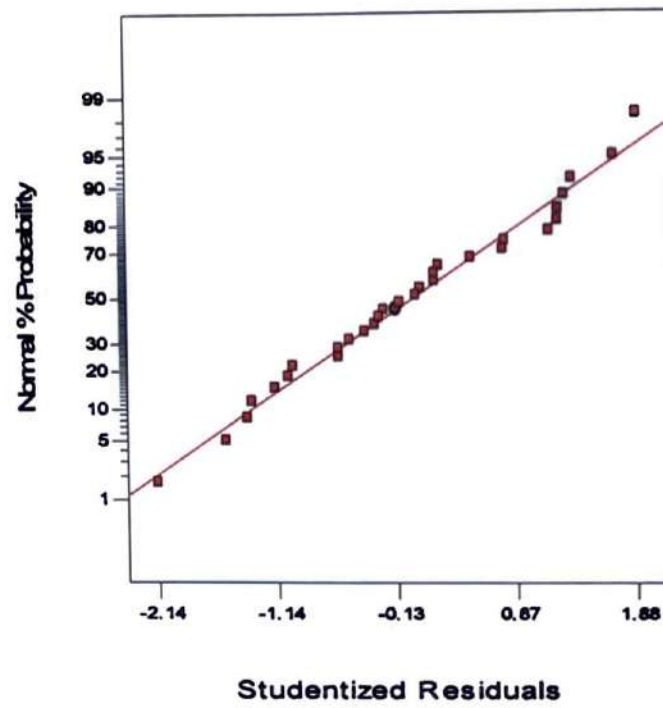


Figure 4.8: Normal probability Residuals plot for SR

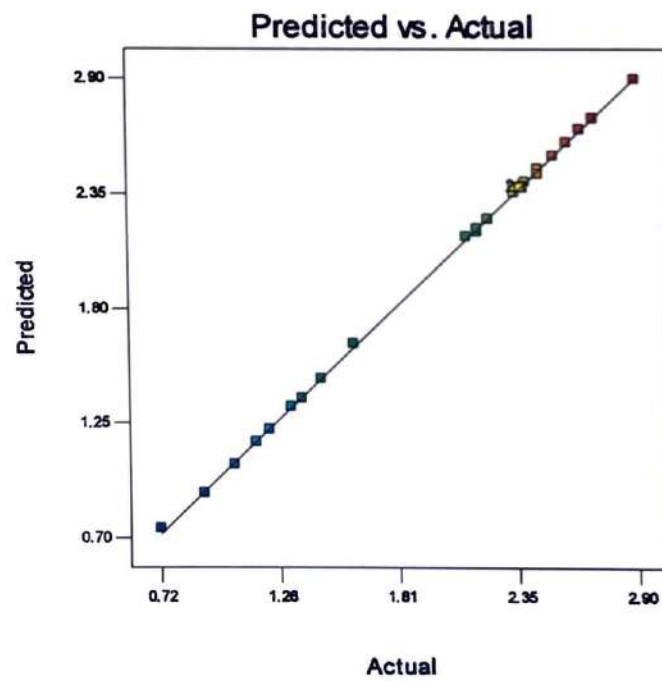
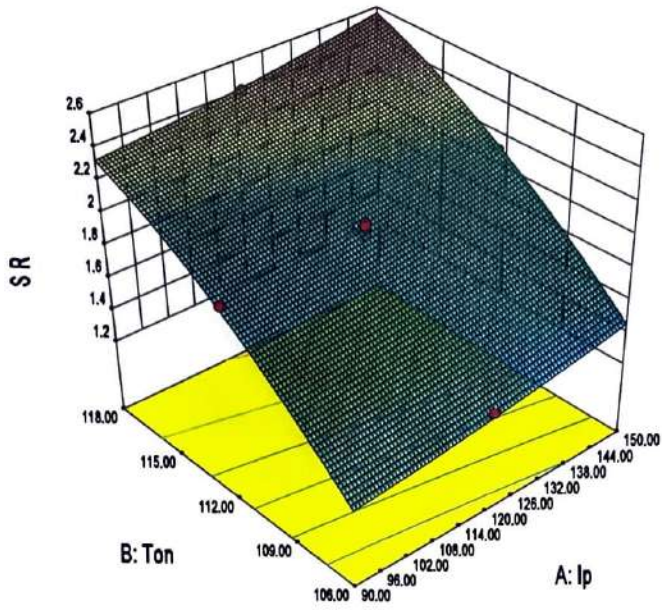
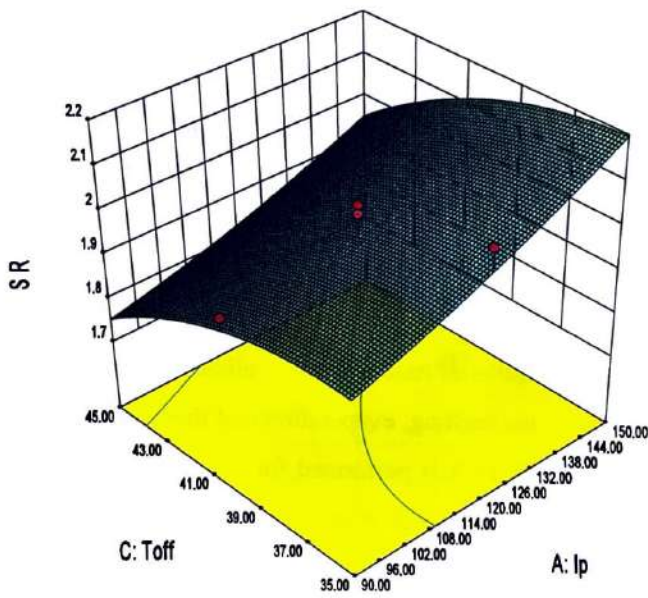


Figure 4.9: Predicted vs. Actual for SR



**Figure 4.10 (a):** Combined Effect of Ip and Ton on SR (Toff: 40 $\mu$ s; SV: 40V)



**Figure 4.10 (b):** Combined Effect of Ip and Toff on SR (Ton: 112 $\mu$ s; SV: 40V)

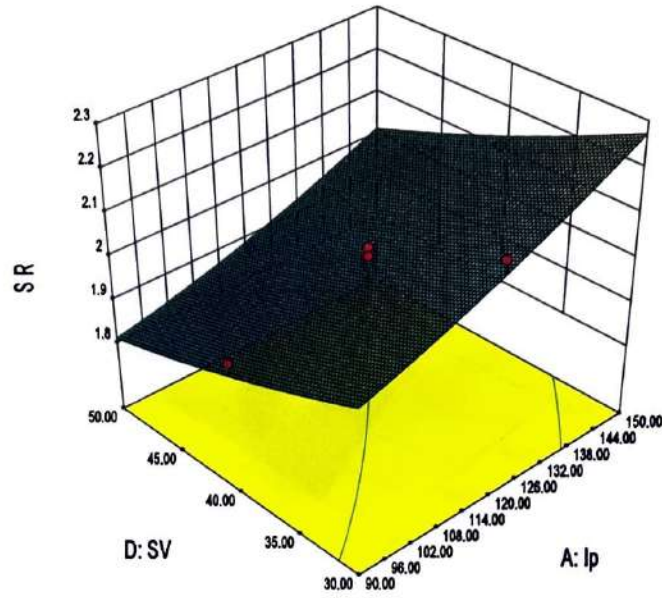


**Figure 4.10(c):** Combined Effect of  $I_p$  and SV on SR (Toff:  $40\mu s$ ; Ton:  $112\mu s$ )

Increasing in the value of Toff decreases the spark frequency and reduces the probability of gas explosion; as a result smooth surface with small crater size is generated. Increasing Toff value results in low recast layer as a result low surface roughness is obtained (Jangra et al. 2012). SR decreases with increase in the value of SV as shown in Figure 4.10(c). Increasing SV increases the gap between work material and wire electrode that results into low ionization of dielectric medium and hence low discharge energy get generated.

#### 4.8.3 Analysis of RoC

RoC is the thickness of material removed perpendicular to the cutting direction of wire electrode. It depends on the melting, evaporation and flushing out of the surface material. Similar to CS and SR, ANOVA is performed for RoC also. Fit summary listed in Table 4.10 suggested that quadratic model is statistically significant for analysis. In case of RoC, value of  $R^2$  and  $R^2(\text{adj.})$  is greater than 99%, the p-value for model is less than 0.05 and the lack of fit is non-significant. The input parameters namely  $I_p$ , Ton, Toff, SV and interaction of Ton with SV have significant influences on RoC as indicated by the associated p-value (less than 0.05). This means the proposed model for RoC may be considered as significant for fitting and predicting the experimental results. Figure 4.11 shows the residuals plot for RoC which are normally distributed along a straight line.



Figure 4.12 presents the predicted values and the actual values relationship. After eliminating the non significant terms, the final response equation for RoC is given as follows:

(In coded terms)

$$\text{RoC} = 27.29 + 0.77 \times \text{Ip} + 3.78 \times \text{Ton} - 0.070 \times \text{Toff} + 1.13 \times \text{SV} - 1.05 \times (\text{Toff})^2 + 0.36 \times (\text{Ton} \times \text{Toff}) + 0.74 \times (\text{Ton} \times \text{SV}) + 0.41 \times (\text{Toff} \times \text{SV}) \tag{4.9}$$

(In terms of actual parameters)

$$\text{RoC} = 5.75991 + 0.02563 \times \text{Ip} - 0.351 \times \text{Ton} + 1.6526 \times \text{Toff} - 1.6085 \times \text{SV} - 0.041922 \times (\text{Toff})^2 + 0.01204 \times (\text{Ton} \times \text{Toff}) + 0.012406 \times (\text{Ton} \times \text{SV}) + 8.2875\text{E-}003 \times (\text{Toff} \times \text{SV}) \tag{4.10}$$

**Table 4.10:** ANOVA for RoC (after backward elimination)

Source	Sum of Squares	Degree of freedom	Mean Square	F-value	p-value	
Model*	311.96	8	38.99	218.57	<0.0001	Significant
Ip	10.64	1	10.64	59.65	<0.0001	
Ton	256.81	1	256.81	1439.50	<0.0001	
Toff	0.088	1	0.088	0.49	0.4897	
SV	22.78	1	22.78	127.69	<0.0001	
(Toff) <sup>2</sup>	7.91	1	7.91	44.33	<0.0001	
Ton*Toff	2.11	1	2.11	11.83	0.0025	
Ton*SV	8.87	1	8.87	49.69	<0.0001	
Toff*SV	2.75	1	2.75	15.40	0.0008	
Residual	3.75	21	0.18			
Lack of fit	3.47	16	0.22	3.97	0.0673	Not significant
Pure error	0.27	5	0.055			
Cor. Total	315.70	29				
Standard deviation = 0.42;      R <sup>2</sup> = 0.988      R <sup>2</sup> (Adj.) = 0.9836						

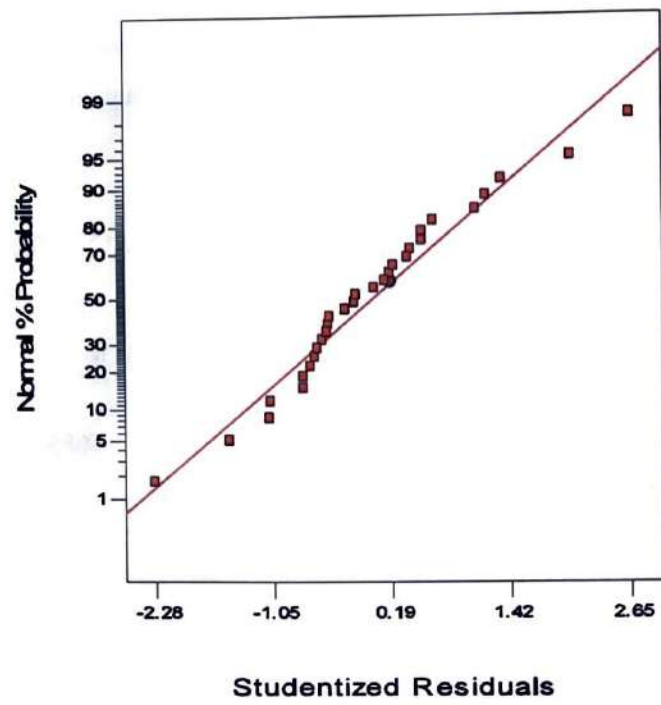


**Figure 4.11:** Normal probability Residuals Plot for RoC

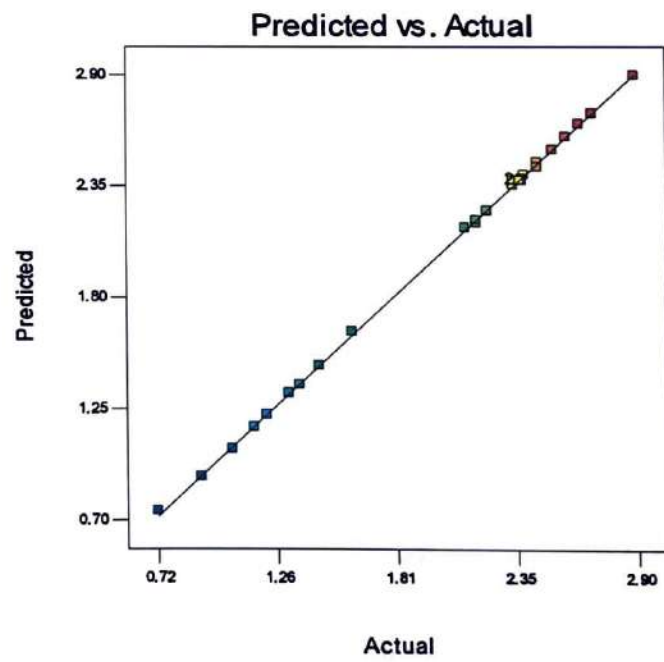


**Figure 4.12:** Predicted vs. Actual for RoC

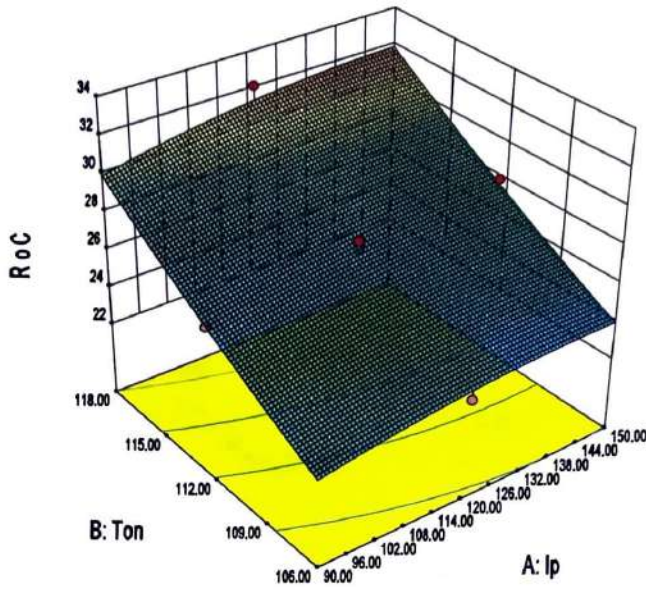


**Figure 4.13 (a):** Combined Effect of  $I_p$  and  $T_{on}$  on RoC ( $T_{off}$ :  $40\mu s$ ;  $SV$ :  $40V$ )

Increase in the value of  $T_{on}$  and  $I_p$  results into high heat generation that increases the melting and evaporation of work material and hence the value of RoC increases as shown by response surface plot in Figure 4.13 (a) and Figure 4.13 (b).

RoC increases with increase in the value of  $SV$  as shown in Figure 4.13(c). The value of RoC is maximum at the mid value of  $T_{off}$  ( $40\mu s$ ) while the value of RoC decreases towards the extreme ends (i.e., at  $35\mu s$  and  $45\mu s$ ). This phenomenon is conflicting in nature. Because at high value of  $T_{off}$ , low discharge frequency results into low melting and erosion of work surface perpendicular to cutting direction. Also high dielectric flushing at high value of  $T_{off}$  results into cooling effect on work material. This causes low value of RoC. At low value of  $T_{off}$  with high value of  $T_{on}$  ( $112\mu s$ ), melted work material is unable to flush out completely through spark gap and re-deposit to work surface. As a result, low value of RoC is obtained. At  $T_{off}$ :  $40\mu s$ , the complete melting and flushing of eroded material takes place that causes increase in the value of RoC.



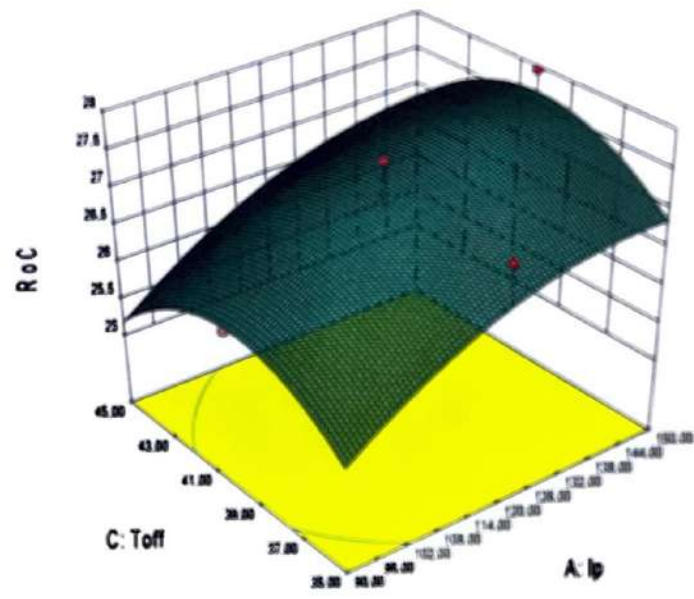


Figure 4.13 (b): Combined Effect of  $I_p$  and  $T_{off}$  on  $R_oC$  ( $T_{on}$ :  $112\mu s$ ;  $SV$ :  $40V$ )

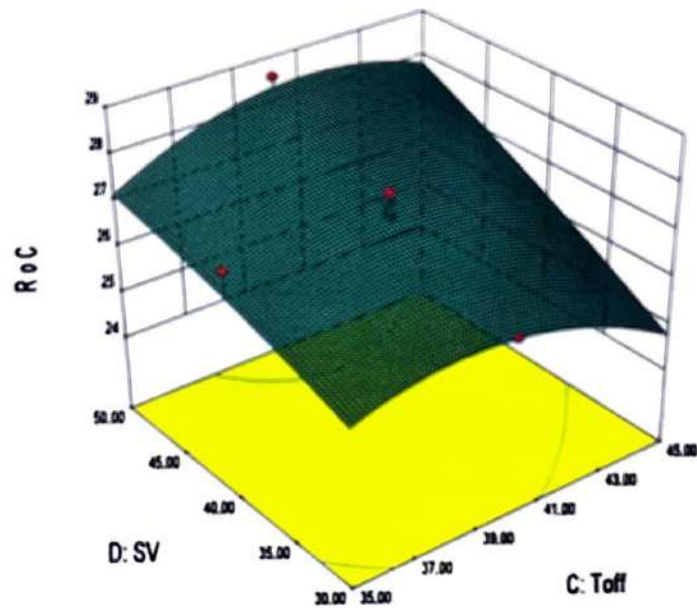


Figure 4.13 (c): Combined Effect of  $T_{off}$  and  $SV$  on  $R_oC$  ( $I_p$ :  $120A$ ;  $T_{on}$ :  $112\mu s$ )

#### 4.9 DISCUSSION

The machining characteristics namely CS, SR and RoC are modelled and analysed using RSM of Nimonic-90 in WEDM. Four discharge parameters namely  $I_p$ , Ton, Toff and SV are selected as variable parameters; while other parameters are kept fixed at their optimal setting. Face centered central composite design is adopted to carry out experimental study.

Quadratic models are suggested for all three machining characteristics. Using response surface graphs, the developed mathematical models are able to explain the effect of variables on machining characteristics efficiently. Increasing the value of  $I_p$  and Ton increases the discharge energy that increases the value of CS and RoC but it adversely affects the SR. Increasing Toff decreases the CS but improves the surface finish by flushing out melted debris completely. Increase in SV, decreases the CS and improves the SR. ANOVA shows that  $I_p$ , Ton, Toff and SV are significant parameters affecting the CS and SR while  $I_p$ , Ton and SV are highly significant parameters affecting the RoC.

## CHAPTER-V

# OPTIMIZATION USING DESIRABILITY FUNCTION FOR SINGLE AND MULTI MACHINING CHARACTERISTICS

---

### 5.1 INTRODUCTION

The machining characteristics namely CS, SR and RoC are conflicting in nature. In order to obtain maximum CS, high value of Ton and Ip and low value of Toff and SV is desirable. This results into generation of high heat energy that causes very poor surface finish. RoC affects the specified dimensional tolerance. For low value of RoC, low value of Ip and Ton and high value of Toff and SV are desirable. This implies the complex nature of WEDM process. Therefore, a trade off is required among different machining characteristics to obtain as a single optimal combination of WEDM parameters. To accomplish this purpose, desirability function is used.

### 5.2 DESIRABILITY FUNCTION

Desirability function is a mathematical approach which is most popularly used for optimization of multi-response characteristics, proposed by Derringer and Suich (1980). It is extensively used methods in industry for the optimization of multiple response processes. It is based on the thought that the "quality" of a product or process that has several quality characteristics, with one of them outside of some "desired" limits, is totally intolerable. Using desirability approach, each response  $y_i(x)$  is converted into an individual desirability function ( $d_i$ ) that ranges between 0 and 1 where 1 is most desirable. If the response  $y_i(x)$  is at its goal or target, then  $d_i=1$ , and if the response is outside an acceptable region,  $d_i=0$ . The numerical optimization finds a point that maximizes the desirability function. Derringer and Suich (1980) defined the three types of desirability function depending on the type of response characteristics which are as follows:

(I) For "larger- the-better" type:

$$d_i = \begin{cases} 0, & y_i \leq y_l \\ \left[ \frac{y_i - y_l}{y_u - y_l} \right]^t, & y_l \leq y_i \leq y_u \\ 1, & y_i \leq y_u \end{cases} \quad (5.1)$$



Where  $y_l$  is the minimum acceptable value of  $y_l$ ,  $y_l'$  is the highest value of  $y_l$ ;  $t$  is the shape function for desirability.

(II) For smaller-the-better type:

$$d_l = \begin{cases} 1, & y_l \leq y_l'' \\ \left[ \frac{y_l' - y_l}{y_l' - y_l''} \right]^r & y_l'' \leq y_l \leq y_l' \\ 0, & y_l \geq y_l' \end{cases} \quad (5.2)$$

Where  $y_l''$  is the lowest value of  $y_l$ ,  $y_l'$  is the maximum acceptable value of  $y_l$ ;  $r$  is the shape function for desirability.

(III) For nominal-the-best type:

$$d_l = \begin{cases} \left[ \frac{y_l - y_l'}{C_l - y_l'} \right]^s & y_l' \leq y_l \leq C_l \\ \left[ \frac{y_l - y_l'}{C_l - y_l'} \right]^t & C_l \leq y_l \leq y_l' \\ 0, & y_l > y_l' \text{ or } y_l' > y_l \end{cases} \quad (5.3)$$

Where  $C_l$  is the most acceptable or target value and  $s$  and  $t$  are the exponential parameters that determines the shape of desirability function.

Overall desirability function of the multi-response system can be measured by combining the individual desirability of the functions. It can be represented as  $D = (d_1^{w_1} \cdot d_2^{w_2} \dots d_n^{w_n})$ ; where  $w_j$  ( $0 < w_j < 1$ ) is the weight value given for the importance of  $j$ th response variable and  $\sum_{j=1}^n w_j = 1$ . The parameters settings with maximum overall desirability value are considered to be the optimal parameter combination.

Desirability function is used to find the optimal parameters setting that maximize the overall desirability function for three machining characteristics namely CS, SR and RoC. Second order central composite experimental design involving four factors (Ip, Ton, Toff and SV) each at three levels is used to determine optimum combination of factors. Desirability function approach is used for single response and multi-response optimizations. Using Design expert (DX-7), optimal solutions are derived for specified design space constraints for single and multi machining characteristics.

### 5.3 SINGLE RESPONSE OPTIMIZATION USING DESIRABILITY FUNCTION

Tables 5.1-5.3 show the ranges of input parameters and individual response characteristics, i.e., CS, SR and RoC for desirability. Limits and goals are established for each response characteristics in order to determine accurate their impact on individuals desirability. A maximum or minimum level is set for each response characteristics which is to be optimized. Equal importance is assigned to each machining characteristics.

**Table 5.1:** Range of Input Parameters and CS for Desirability

Process Parameters	Goal	Lower limit	Upper limit	Importance
Ip	in range	90	150	3
Ton	in range	106	118	3
Toff	in range	35	45	3
SV	in range	30	50	3
CS	maximize	0.72	2.9	3

**Table 5.2:** Range of Input Parameters and SR for Desirability

Process Parameters	Goal	Lower limit	Upper limit	Importance
Ip	in range	90	150	3
Ton	in range	106	118	3
Toff	in range	35	45	3
SV	in range	30	50	3
SR	minimize	0.97	2.73	3

**Table 5.3:** Range of Input Parameters and RoC for Desirability

Process Parameters	Goal	Lower limit	Upper limit	Importance
Ip	in range	90	150	3
Ton	in range	106	118	3
Toff	in range	35	45	3
SV	in range	30	50	3
RoC	minimize	20.8	33.78	3

### 5.3.1 Optimum Solutions

To find out the optimum result, it is necessary to achieve all goals. For finding this, the value of desirability should not be always 1, because the value of desirability depends on how the lower and upper limits are closely set to the actual optimum value. For the specified design space constraints for individual's response characteristics viz., CS, SR and RoC during WEDM processing of Nimonic 90, a set of 20 optimal solutions are derived using a Design Expert 7 (Statistical software). Optimal set of conditions for desired response represent highest value of desirability. Table 5.4-5.6 give the best condition with highest value of desirability for gaining desired response characteristics under specified constraints. By keeping input parameters in range, Desirability 3D-plots are drawn for CS at maximum level and SR and RoC separately keeping their values at minimum level.

Figures 5.1 - 5.4 show plots of desirability function distribution of CS for various machining parameters. Figure 5.1 shows that CS increases with increase of  $T_{on}$  and decreases of  $T_{off}$ . Effect of  $T_{off}$  combined with  $I_p$  is depicted in Figure 5.2. Increase in value of  $T_{off}$  results into decrease in CS. Increasing  $T_{off}$  value decreases the discharge frequency and increases the cooling effect on work surface due to high flow of dielectric, resulting into decrease in overall machining time. Decreasing SV narrow the spark gap, results into large ionization of dielectric fluid and increases the CS {Figure 5.3}.

Figure 5.4 shows that CS increases with increase in  $T_{on}$  and  $I_p$ . But the effect of  $T_{on}$  is highly noticeable as compared to  $I_p$ . Increasing  $I_p$  and  $T_{on}$  increases the discharge energy across the electrode and it results into high melting and evaporation of material. High melting and evaporation combined with high dielectric supply results into high CS (Jangra & Grover, 2012). Desirability 3D plots depicts that maximum value of CS may be obtained with the combination of high value of  $I_p$  and  $T_{on}$  and low level of  $T_{off}$  and SV, respectively.

3D plots of desirability function distribution of SR are shown in Figure 5.5 – 5.8 for various inputs parameters. High discharge energy due to high value of  $T_{on}$  and  $I_p$  results into overheating and evaporation of molten metal forming gas bubbles that explode when the discharge ceases. As a result high pressure energy creates large size craters on work surface. The diameter and depth of crater increases with increasing  $I_p$



and Ton and resulting increases of SR. Increasing Toff value results in low RCL as a result low SR is obtained. SR improves with increasing the value of SV and Toff.

3D plots of desirability function distribution of RoC are shown in Figure 5.9 – 5.12 for various inputs parameters. Increase in the value of Ton and Ip results into high heat generation that increases the melting and evaporation of work material and the value of RoC increases as shown by Figure 5.9. RoC increases with increase in the value of SV. At high value of Toff, low discharge frequency results into low melting and erosion of work surface perpendicular to cutting direction. Also high dielectric flushing at high value of Toff results into cooling effect on work material. This causes low value of RoC.

**Table 5.4:** Set of Optimal Solutions of Desirability for CS

Number	Ip	Ton	Toff	SV	CS	Desirability	
1	134.82	117.24	37.20	30.8	2.91	1.000	<b>Selected</b>
2	143.01	116.95	36.87	31.2	2.90	1.000	
3	136.66	117.49	36.78	31.2	2.91	1.000	
4	138.43	116.63	37.55	30.2	2.91	1.000	
5	141.10	117.79	39.25	30.1	2.91	1.000	
6	138.16	116.86	35.63	30.5	2.91	1.000	
7	145.90	117.70	38.39	30.7	2.91	1.000	
8	133.60	116.99	36.43	30.6	2.91	1.000	
9	137.16	117.48	38.20	30.6	2.91	1.000	
10	132.02	117.25	37.58	30.9	2.90	1.000	
11	138.97	117.97	35.01	30.3	2.90	1.000	
12	135.52	117.93	38.14	31.3	2.90	1.000	
13	132.50	117.64	35.09	30.2	2.91	1.000	
14	143.42	117.18	35.97	30.9	2.90	1.000	
15	137.75	116.81	37.43	30.6	2.91	1.000	
16	130.28	116.88	38.03	30.3	2.90	1.000	
17	139.27	117.58	35.25	30.7	2.90	1.000	
18	136.81	117.51	36.04	31.3	2.90	1.000	
19	137.27	117.43	39.40	30.4	2.90	1.000	
20	90.09	118.00	41.87	30	2.60	0.862	

**Table 5.5:** Set of Optimal Solutions of Desirability for SR

Number	Ip	Ton	Toff	SV	SR	Desirability	
1	96.08	106.00	45.00	50.0	0.97	1.000	<b>Selected</b>
2	90.31	106.01	44.89	49.8	0.97	1.000	
3	90.32	106.00	45.00	48.1	0.98	0.993	
4	101.34	106.00	45.00	49.7	0.98	0.992	
5	103.06	106.00	44.97	50.0	0.99	0.991	
6	107.07	106.00	45.00	50.0	0.99	0.986	
7	90.00	106.26	45.00	50.0	0.99	0.986	
8	117.45	106.00	45.00	50.0	1.02	0.971	
9	90.00	106.00	45.00	43.5	1.04	0.962	
10	129.87	106.00	45.00	50.0	1.06	0.949	
11	130.32	106.00	45.00	50.0	1.06	0.948	
12	90.00	106.00	44.91	40.7	1.08	0.938	
13	95.12	106.00	35.00	50.0	1.13	0.908	
14	90.01	106.00	37.93	48.1	1.14	0.901	
15	90.17	106.00	35.17	48.1	1.15	0.900	
16	111.63	106.00	35.01	50.0	1.18	0.878	
17	116.41	106.00	35.00	49.9	1.20	0.867	
18	90.00	106.00	35.08	43.9	1.21	0.865	
19	149.80	106.00	45.00	41.6	1.25	0.838	
20	130.11	106.00	35.00	50	1.26	0.838	

**Table 5.6:** Set of Optimal Solutions of Desirability for RoC

Number	Ip	Ton	Toff	SV	RoC	Desirability	
1	96.08	106.00	45.00	30.1	20.94	0.989	<b>Selected</b>
2	90.04	106.03	45.00	33.6	21.01	0.984	
3	100.70	106.00	45.00	30.0	21.11	0.976	
4	106.65	106.00	45.00	30.0	21.31	0.961	
5	107.95	106.00	45.00	30.0	21.35	0.957	
6	121.00	106.02	45.00	30.0	21.66	0.934	
7	149.54	106.00	45.00	30.1	21.75	0.927	
8	90.00	106.07	44.99	44.1	21.78	0.925	
9	140.13	106.00	44.98	30.0	21.80	0.923	
10	90.00	106.00	45.00	46.1	21.84	0.920	
11	90.00	106.00	35.06	40.6	22.46	0.872	
12	90.00	106.00	35.03	40.1	22.46	0.872	
13	90.00	106.04	35.00	30.6	22.51	0.868	
14	90.22	106.00	35.00	32.0	22.51	0.868	
15	90.01	106.00	36.23	50.0	22.53	0.867	
16	90.00	106.84	45.00	50.0	22.63	0.859	
17	150.00	106.00	35.24	30.0	23.35	0.803	
18	128.25	106.01	35.00	30.0	23.41	0.799	
19	150.00	106.00	36.21	30.0	23.48	0.794	
20	150.00	106.00	35.00	39.71	23.52	0.791	



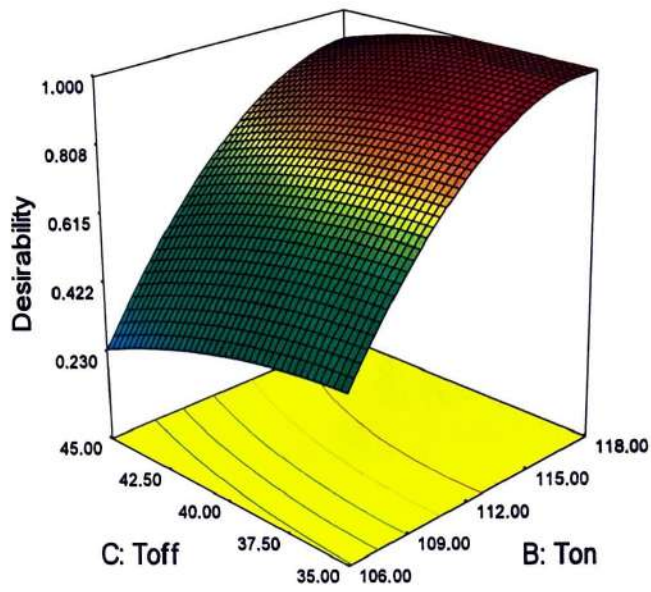


**Figure 5.1:** Surface Graph of Desirability for CS ( $I_p$  140 A; SV 30 V)

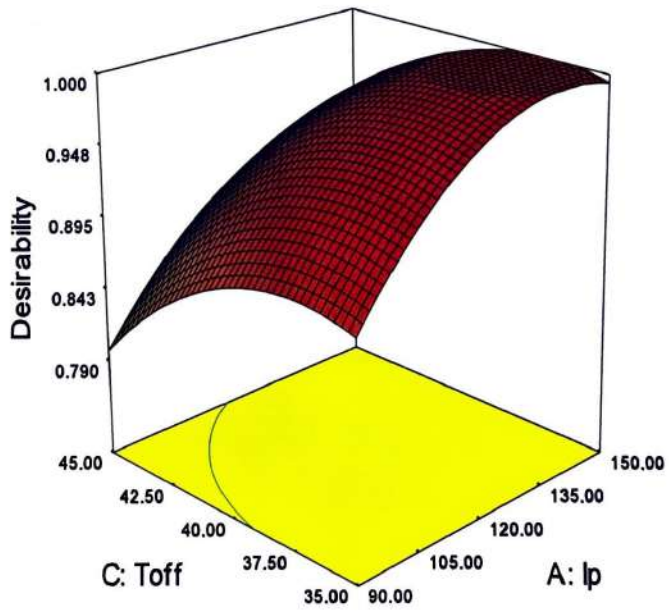


**Figure 5.2:** Surface Graph of Desirability for CS ( $T_{on}$  118 $\mu$ s; SV 30)

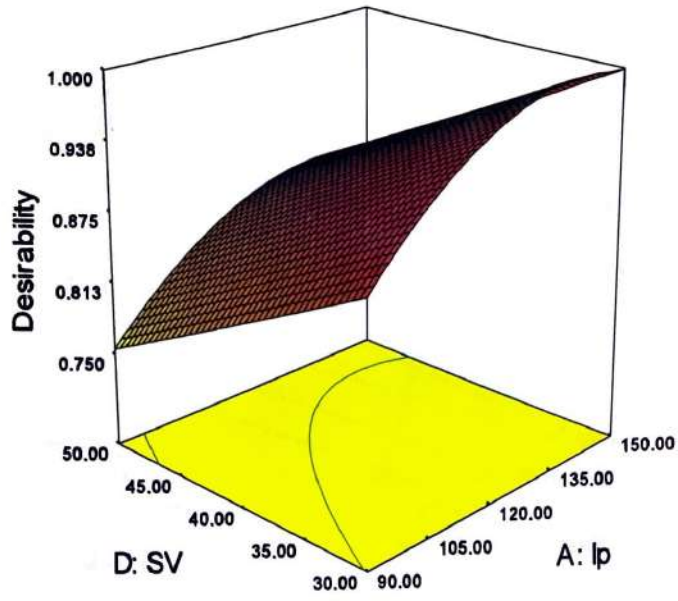


**Figure 5.3:** Surface Graph of Desirability for CS (Ton 118 $\mu$ s, Toff 35)

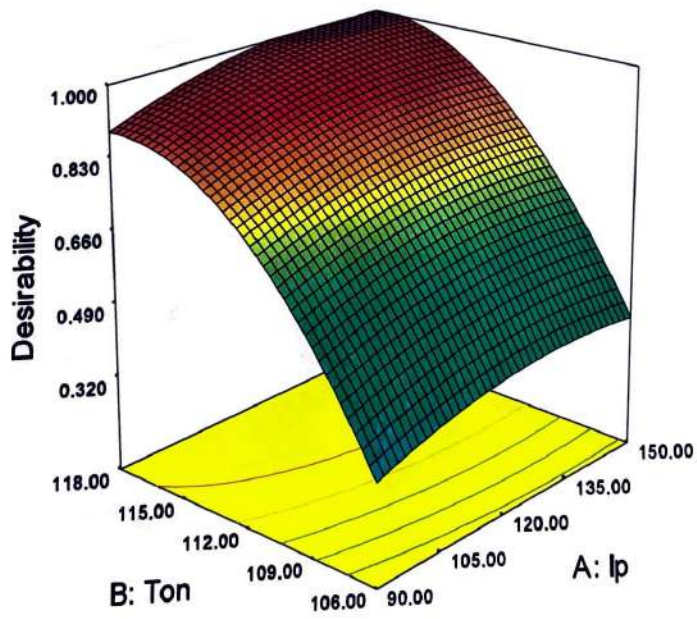


**Figure 5.4:** Surface Graph of Desirability for CS (Toff 36 $\mu$ s; SV 30 V)

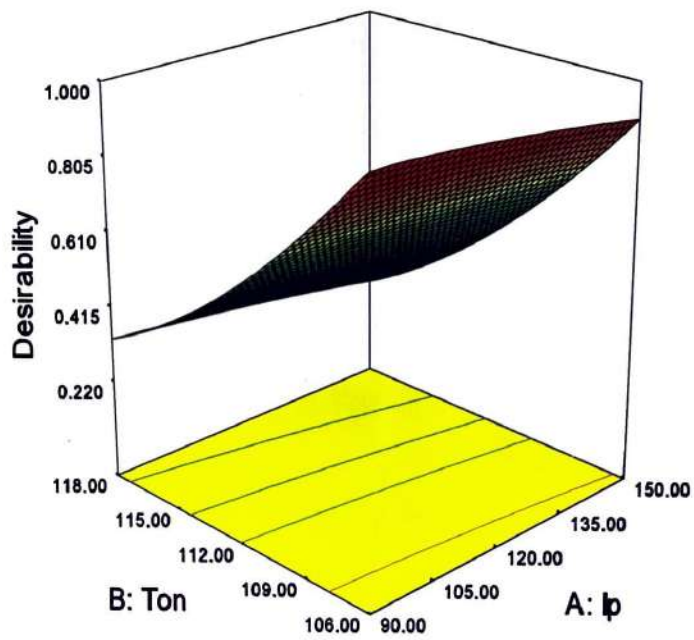


**Figure 5.5:** 3D Surface Graph of Desirability for SR (Toff 45 $\mu$ s; SV 50V)

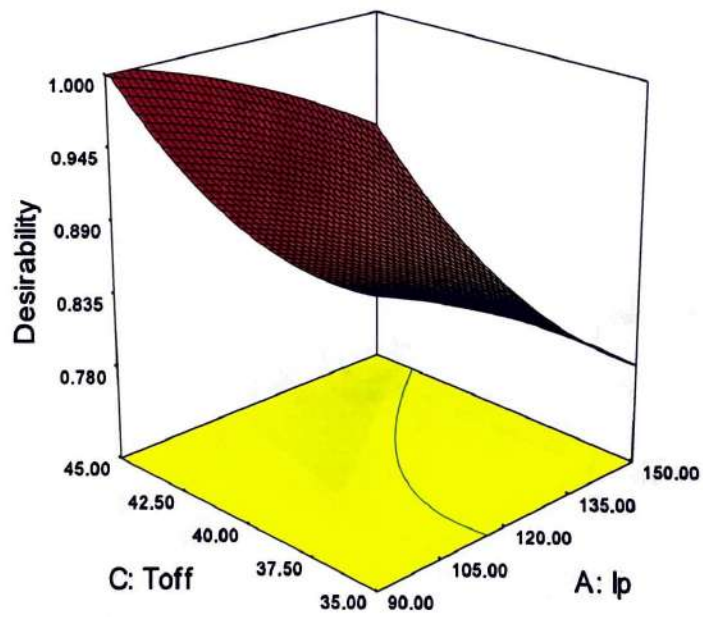


**Figure 5.6:** 3D Surface Graph of Desirability for SR (Ton 106 $\mu$ s; SV 50V)



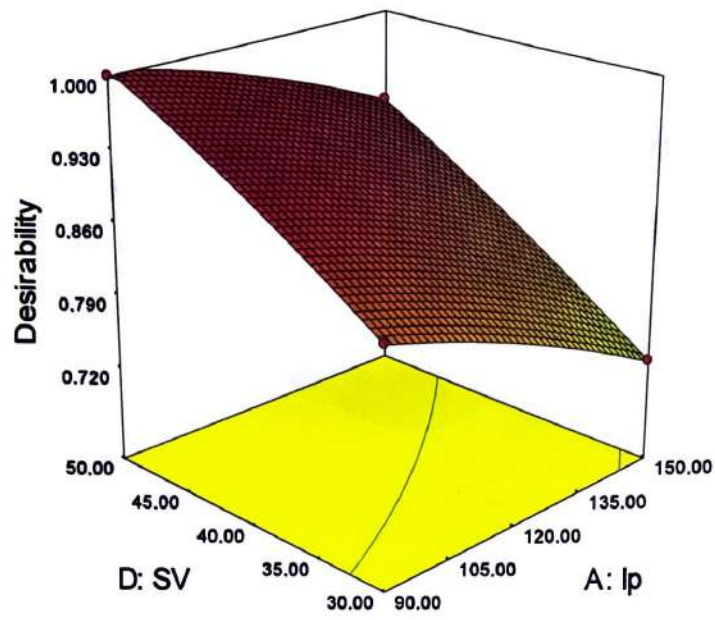


**Figure 5.7:** 3D Surface Graph of Desirability for SR (Ton 106 $\mu$ s; Toff 45 $\mu$ s)

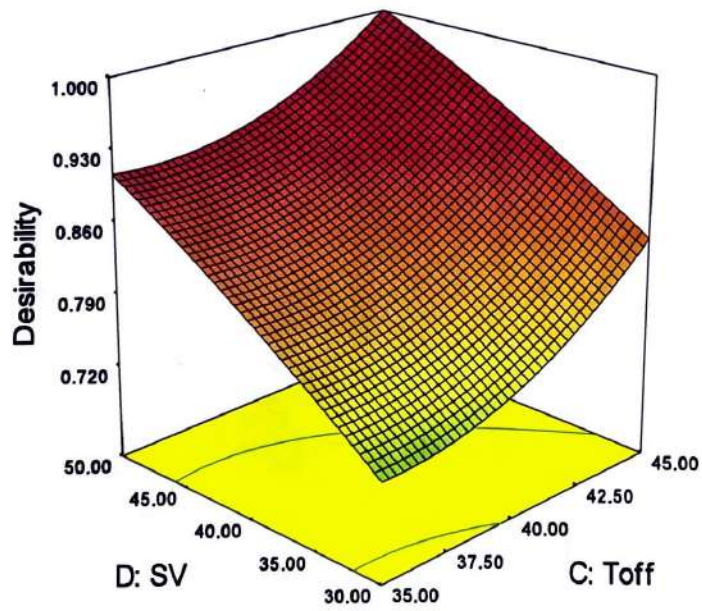


**Figure 5.8:** 3D Surface Graph of Desirability for SR (Ip 95A; Ton 106 $\mu$ s)

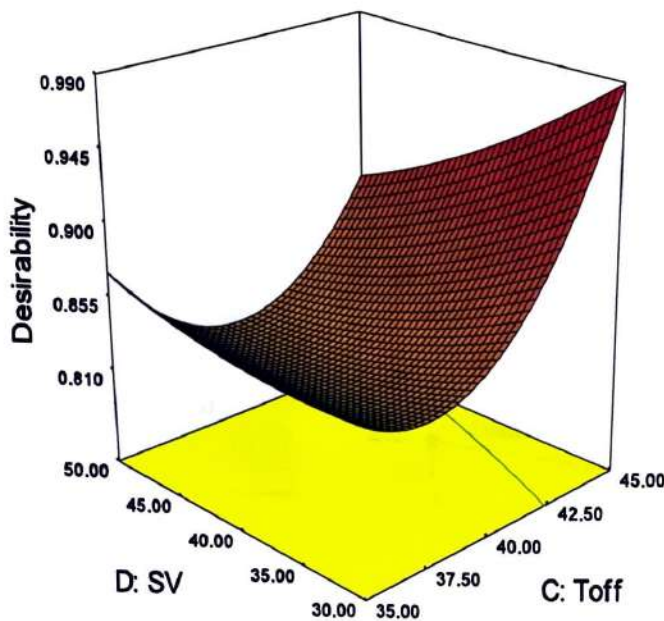


**Figure 5.11:** 3D Surface Graph of Desirability for RoC (Ip 96 A; Ton 106 $\mu$ s)

Design Expert solver is used to draw ramp function graphs and bar graphs which show the desirability for each factor and each response as shown in Figures 5.12 - 5.17. The dot on each ramp indicated the factor setting for response characteristic. The elevation of the dot shows how desirable it is. A linear ramp function is formed between the low value and the goal or the high value and the goal as the weight for each parameter is set equal to one. Bar graphs show the individual/partial desirability functions ( $d_i$ ) of each of the responses (CS, SR and RoC);  $d_i$  varies from 0 to 1 depending upon the nearness of the response towards goal. The bar graph indicate how well each variable satisfies the criterion, values close to one are considered excellent. Table 5.7 represents the optimum levels of various process parameters and the predicted values of various response characteristics.

**Table 5.7:** Optimal Sets of Process Parameters Using RSM and Desirability Function

Response Characteristic	Desirability	A (Ip)	B (Ton)	C (Toff)	D (SV)	Pridicated Optimal Response
CS	1.000	134.82	117.24	37.20	30.8	2.91
SR	1.000	96.08	106.00	45.00	50.0	0.97
RoC	1.000	96.08	106.00	45.00	30.1	20.94

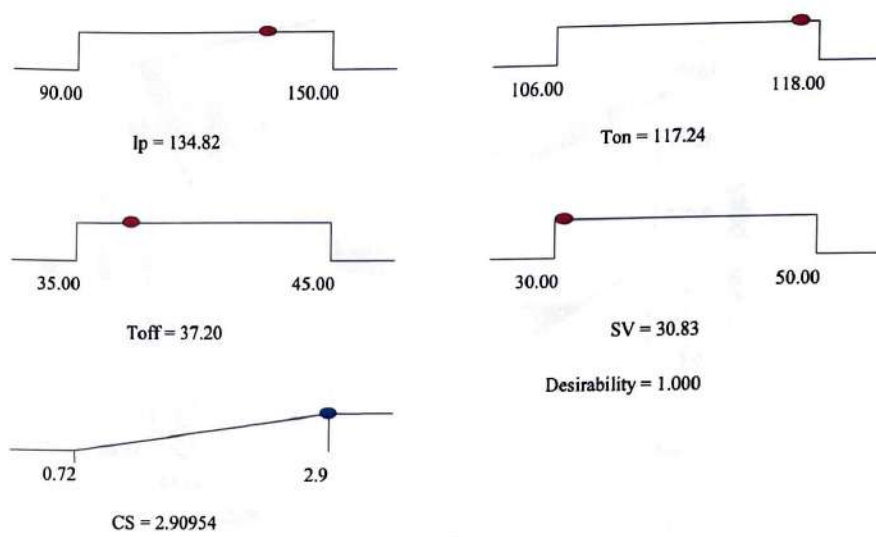


**Figure 5.12: Ramp Function Graph of Desirability for CS**

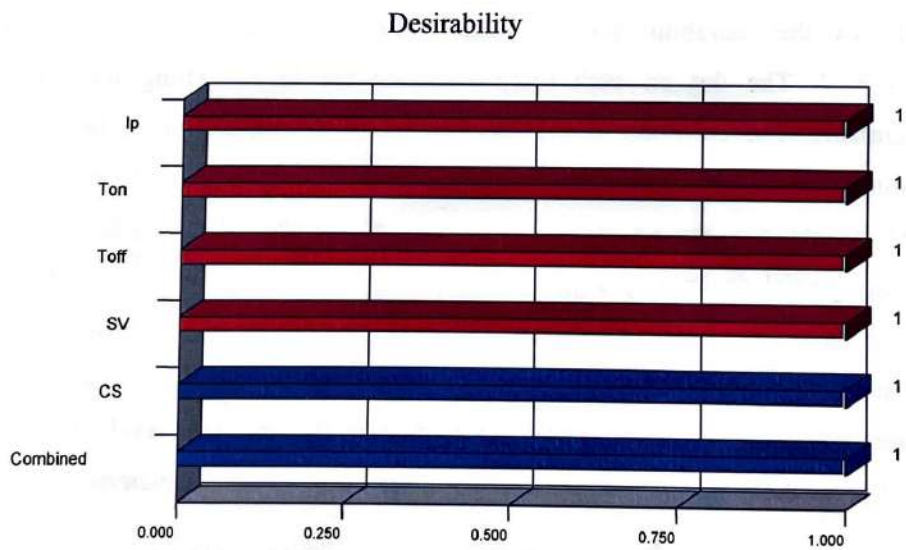


**Figure 5.13: Bar Graph of Desirability for CS**



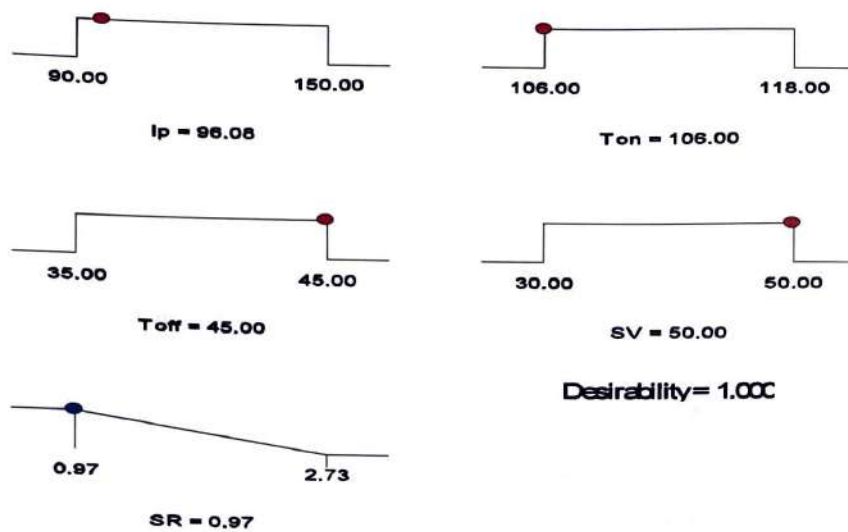


Figure 5.14: Ramp Function Graph of Desirability for SR

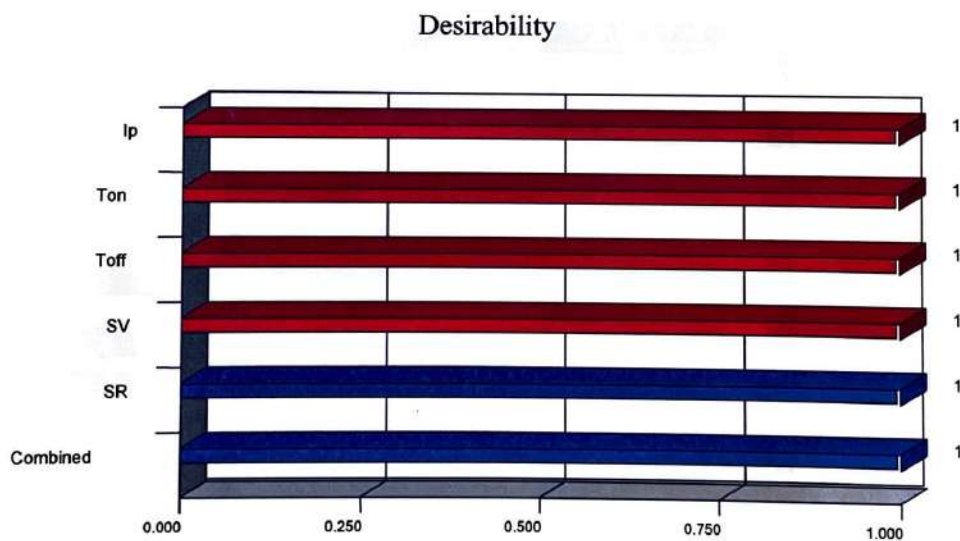


Figure 5.15: Bar Graph of Desirability for SR

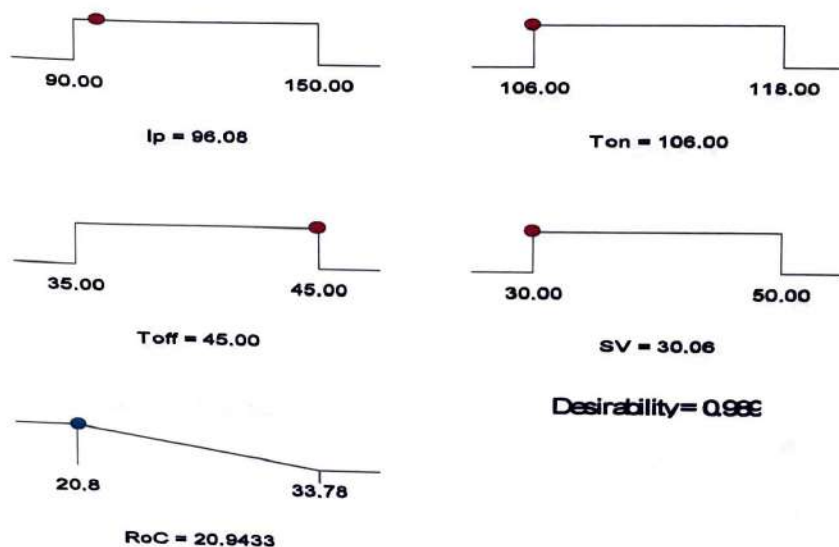


Figure 5.16: Ramp Function Graph of Desirability for RoC

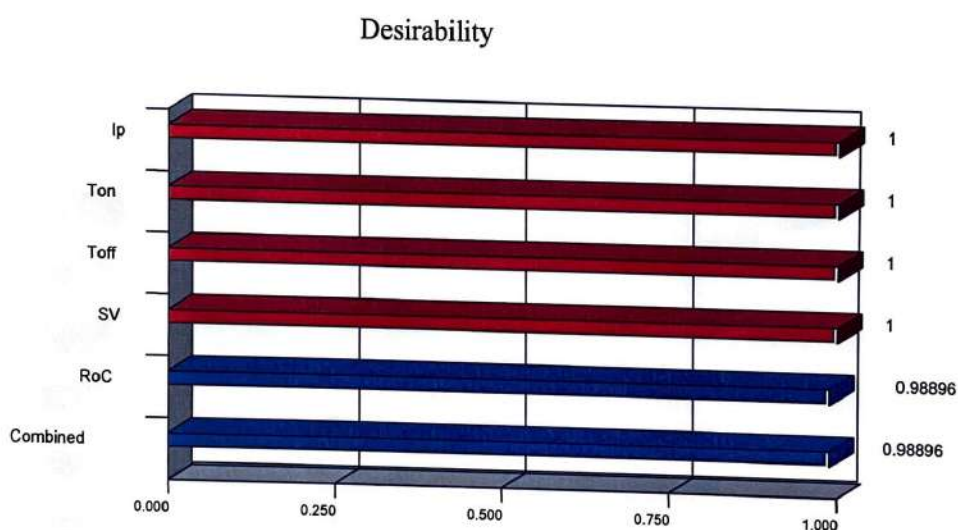


Figure 5.17: Bar Graph of Desirability for RoC

#### 5.4 MULTI RESPONSE OPTIMIZATION USING DESIRABILITY FUNCTION

Multi response optimization is carried out to overcome the problem of conflicting response of single response optimization using desirability function in combination with RSM. Generations of high heat energy increases the CS but causes of poor SR

and low discharge energy causes reduce the productivity. The optimization technique is needed for obtaining higher CS as well as minimum SR. Various multi-characteristic models are developed for solving the problems of multi response optimization. In order to determine accurately their impact on overall desirability, goals and limits are established for each response characteristics. A maximum or minimum level is provided for all response characteristics which are to be optimized. Equal weights are assigned to each response relative to the other responses. Importance varies from minimum (1) to maximum (5).

#### 5.4.1 Model 1: Cutting Speed (CS) and Surface Roughness (SR)

The goals and range of input parameters viz  $I_p$ ,  $T_{on}$ ,  $T_{off}$  and  $SV$  and machining characteristics viz, CS and SR are shown in Table 5.8.

**Table 5.8:** Range of Input Parameters and Machining Characteristics for Desirability (CS and SR)

Name	Goal	Lower Limit	Upper Limit	Lower Weight	Upper Weight	Importance
$I_p$	is in range	90	150	1	1	3
$T_{on}$	is in range	106	118	1	1	3
$T_{off}$	is in range	35	45	1	1	3
$SV$	is in range	30	50	1	1	3
CS	maximize	0.72	2.9	1	1	3
SR	minimize	0.97	2.73	1	1	3

The aim of optimization is to determine best combination of all parameters for finding best results. So that desirability value is completely depend on how closely the lower and upper limits are fixed to get the actual optimum setting. Using Design expert statistical software, a set of 9 optimal solutions is derived for the specified design space constraints and is shown in Table 5.9 for CS and SR. A set of conditions corresponding to highest desirability value is selected as optimum condition for the desired responses.

Using Design Expert solver, the ramp function graph and bar graph {Figure 5.18 – 5.19} are drawn. They showed the desirability for CS and SR. The dot on each ramp indicates the factor setting for response characteristic. The elevation of the dot



shows how desirable it is. A linear ramp function is formed between the low value and the goal or the high value and the goal as the weight for each parameter was set equal to one. Bar graphs show the individual/ partial desirability functions ( $d_i$ ) of each of the responses (CS and SR);  $d_i$  varies from 0 to 1 depending upon the closeness of the response towards target. The bar graph shows how well each variable satisfies the criterion, values close to one are considered excellent.

**Table 5.9:** Set of Optimal Solutions of Desirability for CS and SR

Number	Ip	Ton	Toff	SV	CS	SR	Desirability	
1	111.97	110.15	37.11	50	2.0213	1.7091	0.5884	Selected
2	111.99	110.14	37.05	50	2.0206	1.7085	0.5884	
3	111.97	110.16	37.15	50	2.0223	1.7098	0.5884	
4	112.35	110.14	37.14	50	2.0205	1.7084	0.5884	
5	112.15	110.18	37.28	50	2.0235	1.7108	0.5884	
6	112.69	110.1	36.71	50	2.0217	1.7095	0.5884	
7	111.32	110.11	37.26	50	2.0094	1.6998	0.5884	
8	111.98	110.03	35.68	50	2.0163	1.7067	0.5880	
9	112.44	110.03	35.33	50	2.0204	1.7108	0.5877	

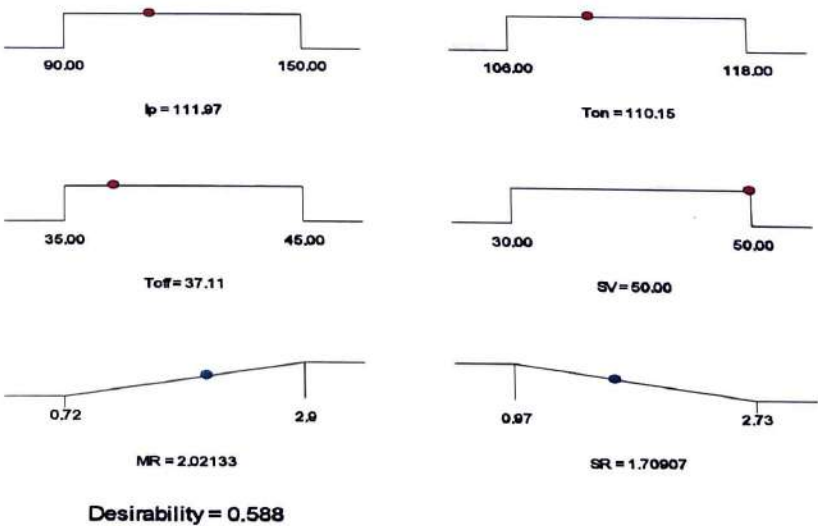


**Figure 5.18:** Ramp Function Graph of Desirability for CS and SR

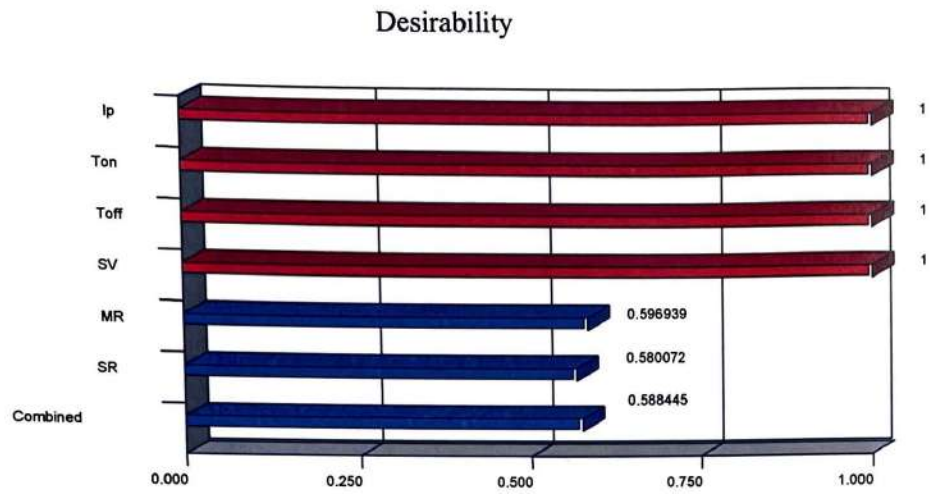


**Figure 5.19:** Bar Graph of Desirability for CS and SR

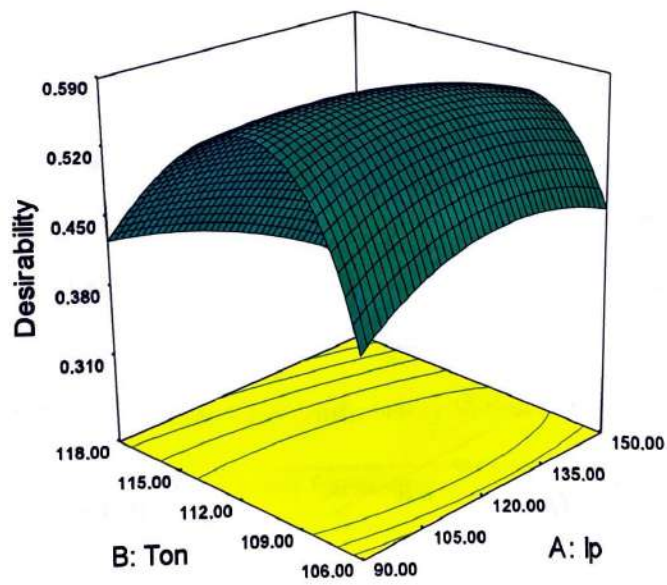


**Figure 5.20:** 3D Surface Graph of Desirability for CS and SR (Toff 37 $\mu$ s; SV 50V)

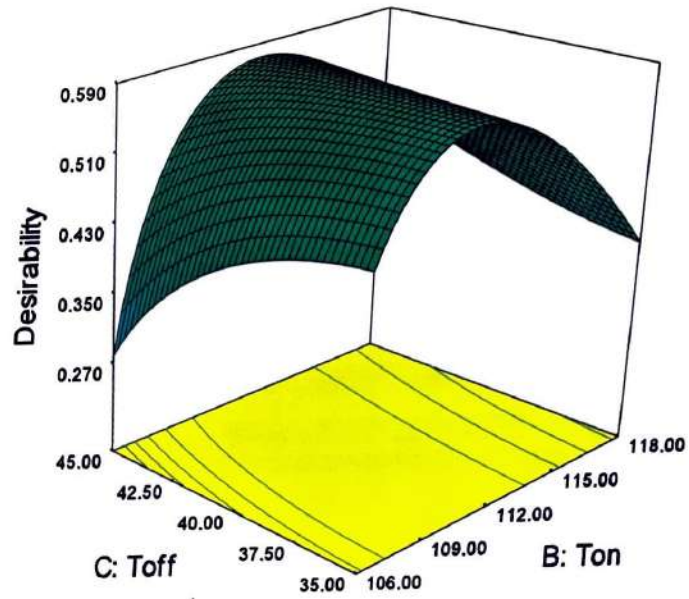


**Figure 5.21:** 3D Surface Graph of Desirability for CS and SR (Ip 112A; SV 50V)

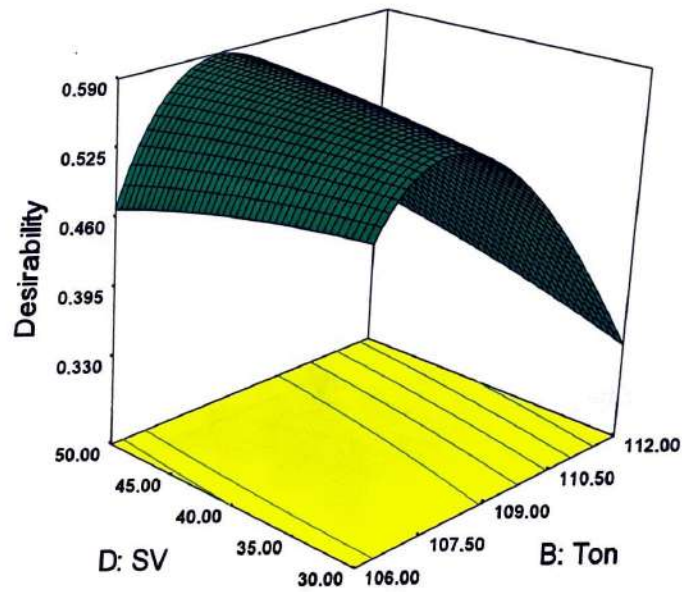


**Figure 5.22:** 3D Surface Graph of Desirability for CS and SR (Ip 112A; Toff 37 $\mu$ s)

Desirability 3D-plots {Figure 5.20-5.22} are first drawn keeping input process parameters in range, CS at maximum and SR at minimum. Figure 5.23 shows the contour plot of overall desirability for multi-machining characteristics. An optimal region is located near to left hand side which has a desirability value of 0.5884. The



near optimal region was located close to the left hand bottom region of the plot, which has overall desirability value greater than 0.5884 that gradually reduced while moving right and upwards. Table 5.9 shows ccorresponding to highest desirability (0.584), optimal combination of WEDM parameters for multi-machining characteristics are selected as Ip: 112 A, Ton: 110  $\mu$ s, Toff: 37  $\mu$ s and SV: 50 V. Confirmation experiments are conducted at this optimal setting and the average experimental values are obtained for CS and SR. The confirmatory results are very close to the predicted values that shows the goodness of the proposed models and desirability approach. Table 5.10 shows predicted and confirmatory values of CS and SR.

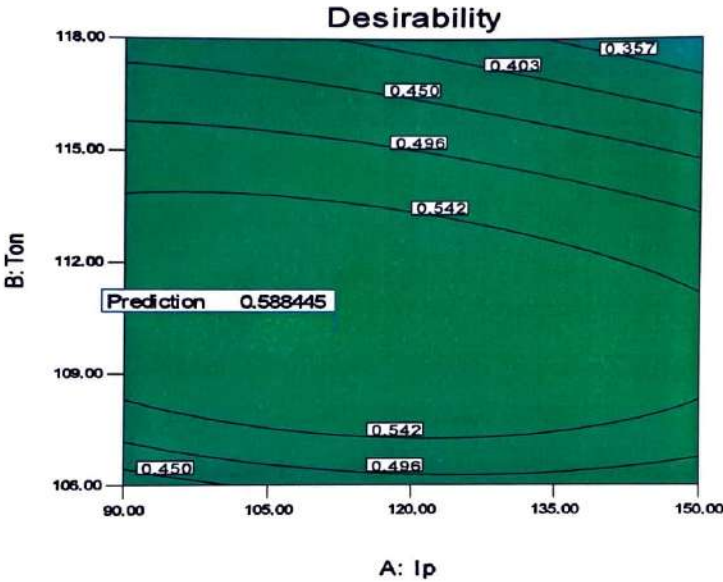


**Figure 5.23:** Contour Plot for Overall Desirability Function (Toff: 37  $\mu$ s, SV: 50 V)

**Table 5.10:** Predicted and Confirmatory Values of CS and SR

	Machining Parameters				Machining Charcteristics	
	Ip	Ton	Toff	SV	CS	SR
Predicted values	111.97	110.15	37.11	50	2.0213	1.7091
Confirmatory values	112	110	37	50	1.92	1.60

### 5.4.2 Model 2: Cutting Speed (CS), Surface Roughness (SR) and Radial over Cut (RoC)

The goals and range of input parameters viz Ip, Ton, Toff and SV and machining characteristics viz. CS, SR and RoC are shown in Table 5.11.

**Table 5.11:** Range of Input Parameters and Machining Characteristics for Desirability (CS, SR and RoC)

Name	Goal	Lower Limit	Upper Limit	Lower Weight	Upper Weight	Importance
Ip	is in range	90	150	1	1	3
Ton	is in range	106	118	1	1	3
Toff	is in range	35	45	1	1	3
SV	is in range	30	50	1	1	3
CS	maximize	0.72	2.9	1	1	3
SR	minimize	0.97	2.73	1	1	3
RoC	minimize	20.8	33.78	1	1	3

The aim of optimization is to determine best combination of all parameters for finding best results. The desirability value totally depends on how closely the lower limit and upper limits are fixed to get the actual optimum setting. Using Design expert statistical software, a set of 15 optimal solutions is derived for the specified design space constraints shown in Table 5.12 for CS and SR. A set of conditions corresponding to highest desirability value is selected as optimum condition for the desired responses. Table 5.12 shows the value of WEDM parameters which give the high value of desirability. Bar graph {Figure 5.24} shows the overall desirability function of the responses. The ramp view drawn using Design Expert software shows the desirability for the output machining characteristics {Figure 5.25}. Desirability 3D-plots {Figures 5.26 - 5.31} are drawn keeping input parameters in range, CS at maximum and SR and RoC at minimum.

**Table 5.12:** Set of Optimal Solutions of Desirability for CS, SR and RoC

Number	Ip	Ton	Toff	SV	CS	SR	RoC	Desirability	
1	93.55	109.89	45	30	1.837	1.675	22.861	0.6369	<b>Selected</b>
2	93.27	109.93	45	30	1.842	1.678	22.871	0.6369	
3	94.43	109.86	45	30	1.840	1.676	22.885	0.6369	
4	93.68	109.8	45	30	1.823	1.667	22.815	0.6369	
5	97.18	109.74	45	30	1.844	1.675	22.940	0.6367	
6	91.6	109.98	45	30.05	1.834	1.676	22.827	0.6367	
7	94.81	109.99	45	30.07	1.863	1.689	22.980	0.6366	
8	100.25	109.63	45	30	1.848	1.675	23.001	0.6363	
9	98.57	109.43	45	30	1.803	1.649	22.825	0.6362	
10	90.05	108.29	35	30	1.897	1.711	23.257	0.6328	
11	90.29	108.3	35	30.03	1.899	1.712	23.271	0.6328	
12	91.92	108.25	35	30.01	1.907	1.714	23.326	0.6326	
13	90	108.28	35.17	30	1.894	1.709	23.277	0.6323	
14	94.44	108.27	35	30.02	1.933	1.726	23.447	0.6322	
15	93.86	107.88	35.02	30	1.859	1.681	23.259	0.6320	

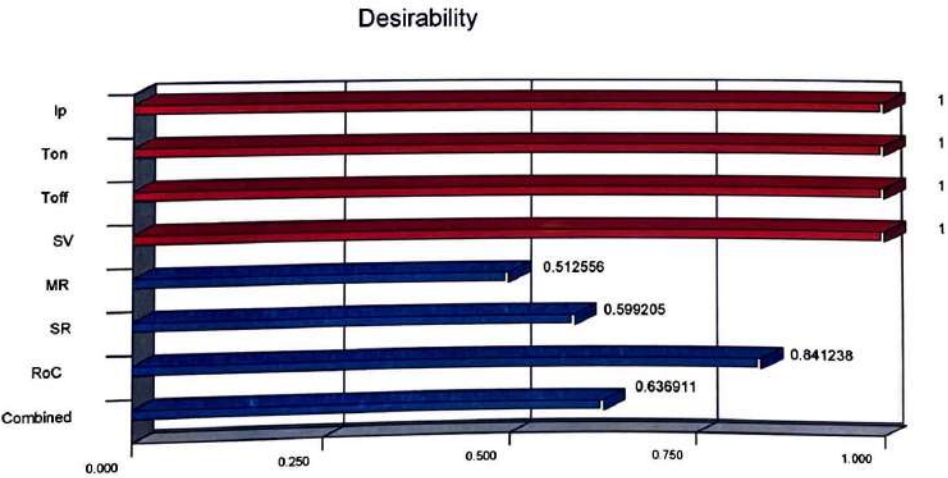


**Figure 5.24:** Bar Graph of Desirability for CR, SR and RoC



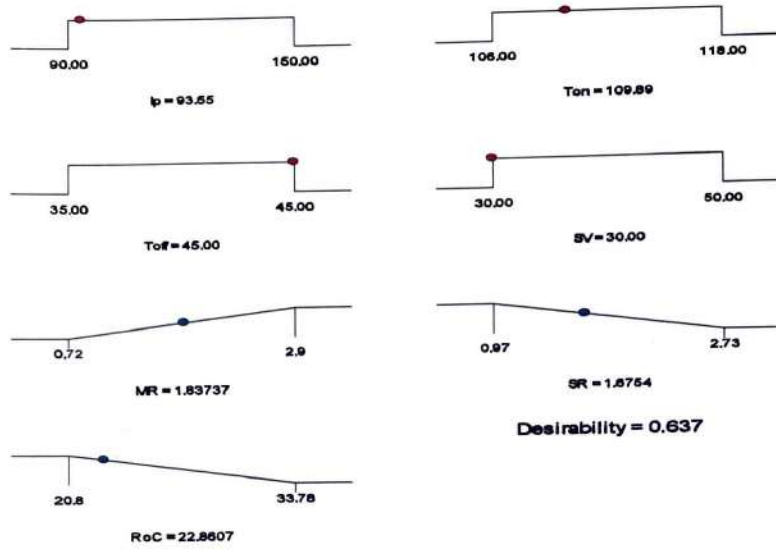


**Figure 5.25:** Ramp Function Graph of Desirability for CR, SR and RoC

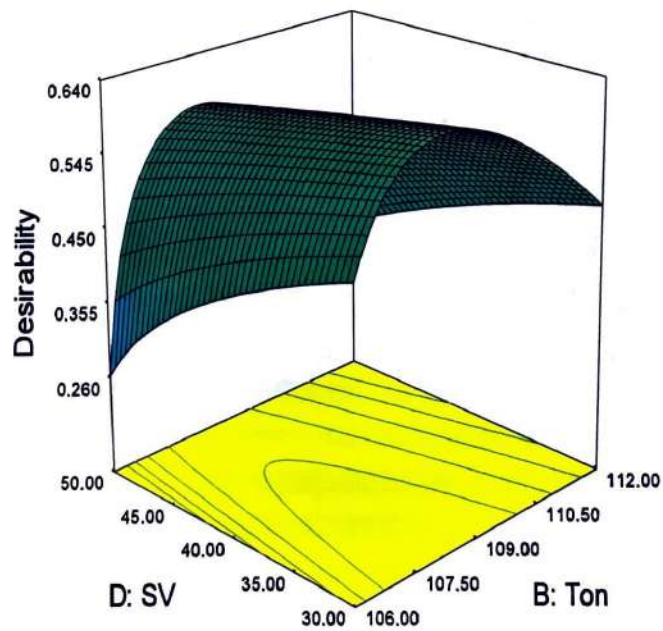


**Figure 5.26:** 3D Surface Graph of Desirability for CS, SR and RoC ( $I_p$  92A;  $T_{off}$  45 $\mu$ s)

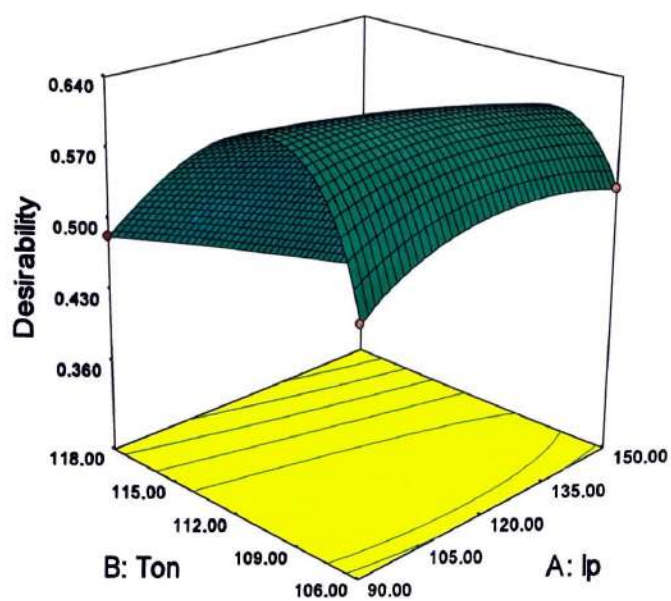


**Figure 5.27:** 3D Surface Graph of Desirability for CS, SR and RoC (Toff 45 $\mu$ s; SV 30 V)

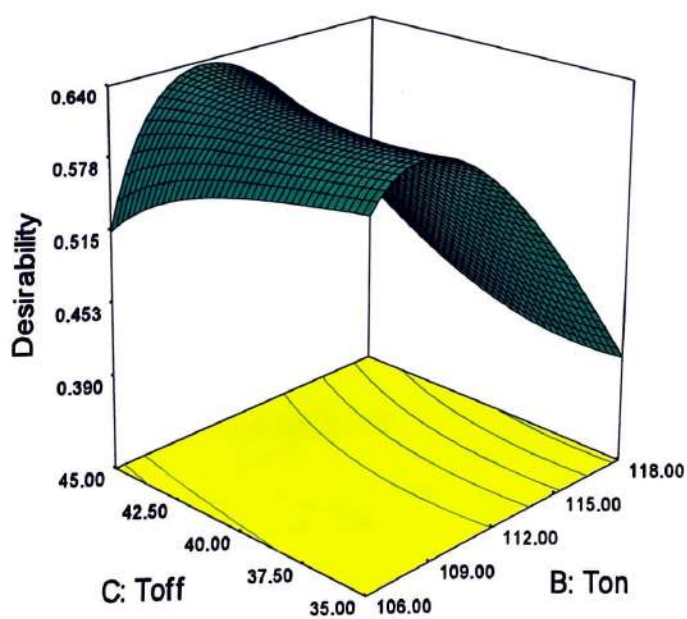


**Figure 5.28:** 3D Surface Graph of Desirability for CS, SR and RoC (Ip 94A; SV 30V)

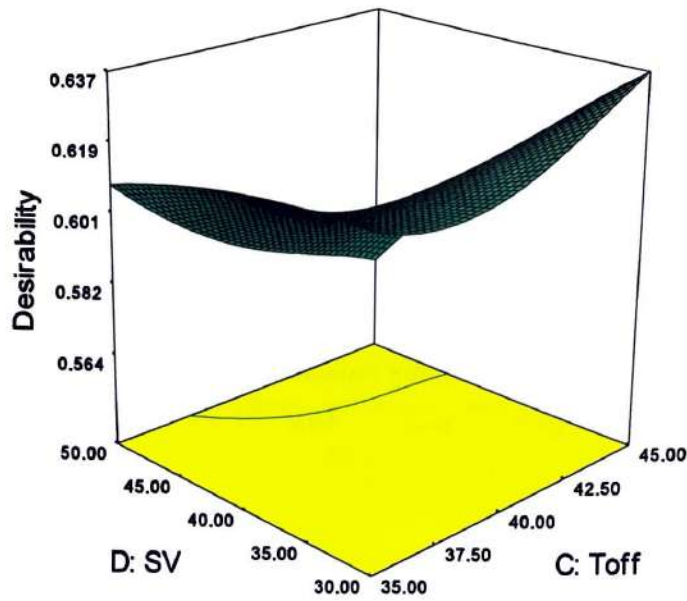


**Figure 5.31:** 3D Surface Graph of Desirability for CS, SR and RoC (Ip 94A; Ton 110 $\mu$ s)

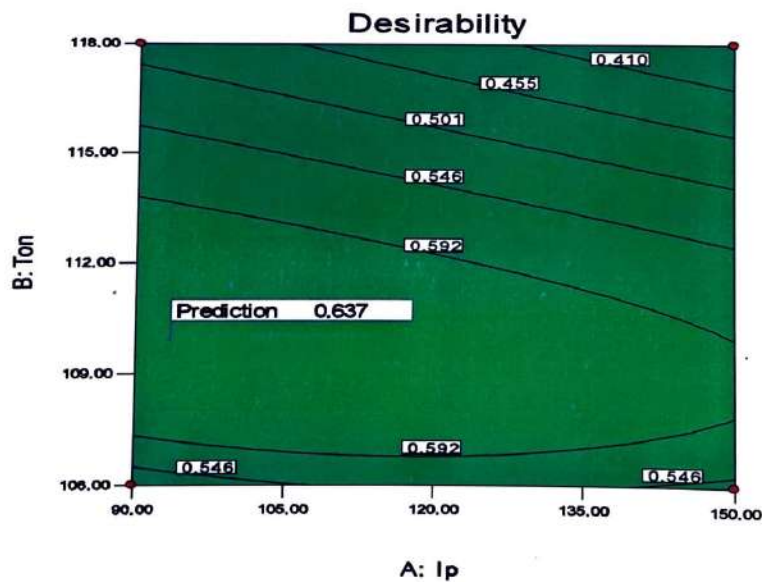


**Figure 5.32:** Contour Plot for Overall Desirability Function (Toff 45 $\mu$ s; SV 30V)

Figure 5.32 shows the contour plot of overall desirability for multi-machining characteristics. The optimal region is located near to left hand side which has a desirability value of 0.6369. Shape of the contour lines represents the sensitivity of the



parameters. Corresponding to highest desirability (0.6369), optimal combination of WEDM parameters for multi-machining characteristics are obtained. Confirmation experiments are conducted at this optimal setting and the average experimental values obtained for CS, SR and RoC. The confirmatory results are very close to the predicted values that shows the goodness of the proposed models and desirability approach. Table 5.13 shows predicted and confirmatory values of CS, SR and RoC.

**Table 5.13:** Predicted and Confirmatory Values of CS, SR and RoC

	Machining Parameters				Machining Characteristics		
	Ip	Ton	Toff	SV	CS	SR	RoC
Predicted values	93.55	109.89	45	30	1.837	1.675	22.861
Confirmatory values	90	110	45	30	1.75	1.60	21.610

## 5.5 DISCUSSION

Using desirability function, a scale free quantity called desirability is obtained for three machining characteristics to optimize multi-machining characteristics. Maximum possible value of CS is found as 2.90 mm/min. while minimum possible values of SR and RoC are 0.97 $\mu$ m and 20.80  $\mu$ m. Correspond to highest desirability, the optimal combination of discharge parameters are Ip: 90A; Ton: 110 $\mu$ s; Toff: 45 $\mu$ s and SV: 30V and average value obtained for CS, SR and RoC are 1.75m/min, 1.6 $\mu$ m and 21.61 $\mu$ m, respectively. Confirmation experiments prove the goodness of the proposed models and desirability function.

## **CHAPTER-VI**

# **SURFACE INTEGRITY ANALYSIS OF MACHINED SURFACE AFTER ROUGH CUT OPERATION IN WEDM**

---

### **6.1 INTRODUCTION**

In WEDM process, material is removed by a series of discrete electrical sparks between the wire electrode and workpiece. These sparks generate craters, recast layers and heat-affected zones on the subsurface of the machined workpiece. Surface integrity on WEDM surfaces involves the extent of surface roughness, depth of heat-affected zone, micro hardness, and size of surface crater. This chapter investigates the surface integrity of WEDM surface and explores possible ways to adjust process parameters for achieving the better surface integrity.

### **6.2 RECAST LAYER (RCL)**

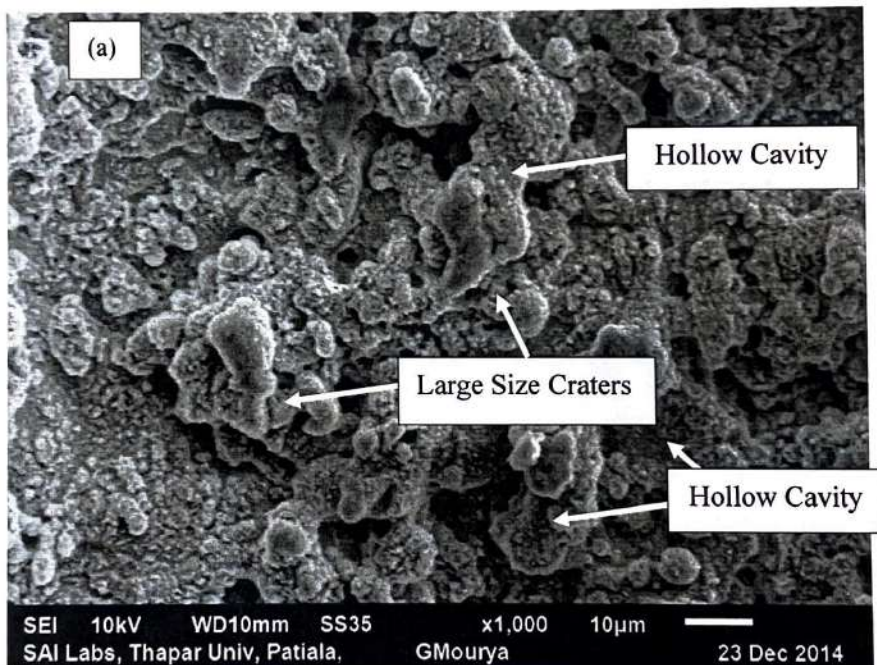
RCL is a hard skin on the work surface formed due to the re-solidification of melted residual material which is not completely expelled during the process (Puri and Bhattacharyya, 2005). It is considered as a major flaw on work (die) surface machined with WEDM because it adversely affects the die performance (Hargrove and Ding, 2007). RCL consist of large size craters, hollow cavities and micro-cracks due to thermal residual stresses. It also consists of shallow craters of varying sizes, globules of debris formed by entrapped gases which make the surface rougher. The morphology of RCL is much different from bulk material and it adversely affects the working life of machined components (Liao et al., 2004; Soo et al., 2013). To analyse the effect of DE on work surface, specimens are grinded and polished to have mirror finish on the transverse section. Surface morphology is studied using Scanning Electron Microscope (SEM).

Figure 6.1 compares the topography and Figure 6.2 shows RCL produced on the machined surface corresponding to high, medium and low DE. It is observed from Figure 6.1a that high DE ( $I_p$ : 150 A;  $T_{on}$ : 118  $\mu$ s;  $T_{off}$ : 35  $\mu$ s; SV: 30V) results in the formation of overlapped and deep craters with large size diameters. These cracks are formed as a result of high thermal stresses prevailing due the rapid heating and cooling in the sparking zone. High density of melted globules gets accumulated at the



machine surface resulting into rough surface. The surface layer is damaged due to the high heat energy, which may be distinguished by the amount of Nickel grains and micro cracks. At high DE, significant amount of melted cobalt is transformed into vapour phase. On cooling, hollow cavities are formed as shown in Figure 6.1a.

Whereas at low DE ( $I_p$ : 90 A; Ton: 106  $\mu$ s; SV: 50V) and high value of Toff (45  $\mu$ s), smaller craters in size and less density of melted globules are found on machined surface {Figure 6b-6c}. At this stage, melted material quickly flushed out without generating any exploding pressure in between plasma channel. Electrical sparks generate smaller craters on the surface. As a result, fine surface; free of micro voids, is generated. It indicates that lower value of  $I_p$  and Ton and higher value of Toff and SV yields good surface characteristics in WEDM of Nimonic 90.



**Figure 6.1a:** SEM Images of Machined Surface Corresponding to High DE ( $I_p$  150 A; Ton 118  $\mu$ s; Toff 45 $\mu$ s; SV 30V)

RCL is observed predominantly at high DE which is discontinuous and non uniform. At high DE, high heating and melting of materials cause of high pressure energy in plasma channel (Li et al., 2013) and a fraction of molten metal flushed away through the narrow spark zone while rest of the material re-solidifies on work surface. At high DE, the average thickness of RCL is found up to 17 $\mu$ m. While at low DE, average thickness of RCL is 6  $\mu$ m. No exploding pressure generates inside the plasma



channel and at high value of Toff, melted and re-solidified debris are quickly flushed out. Thinner RCL exists on specimens machined using shorter Ton and Ip.

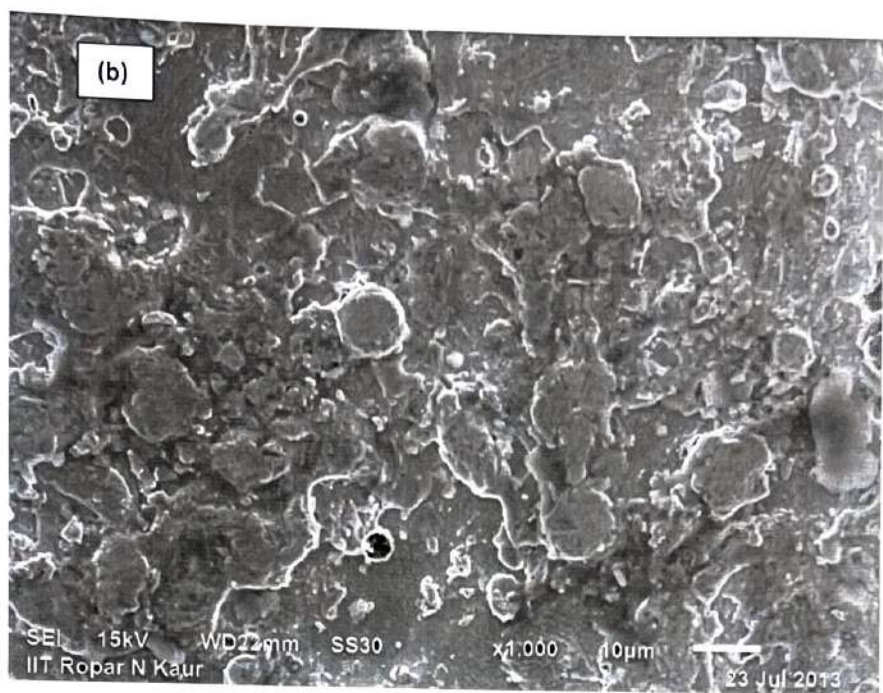


**Figure 6.1b:** SEM Image of Machined Surface Corresponding to Medium DE (Ip 90 A; Ton 112 µs; Toff 40µs; SV 40V)

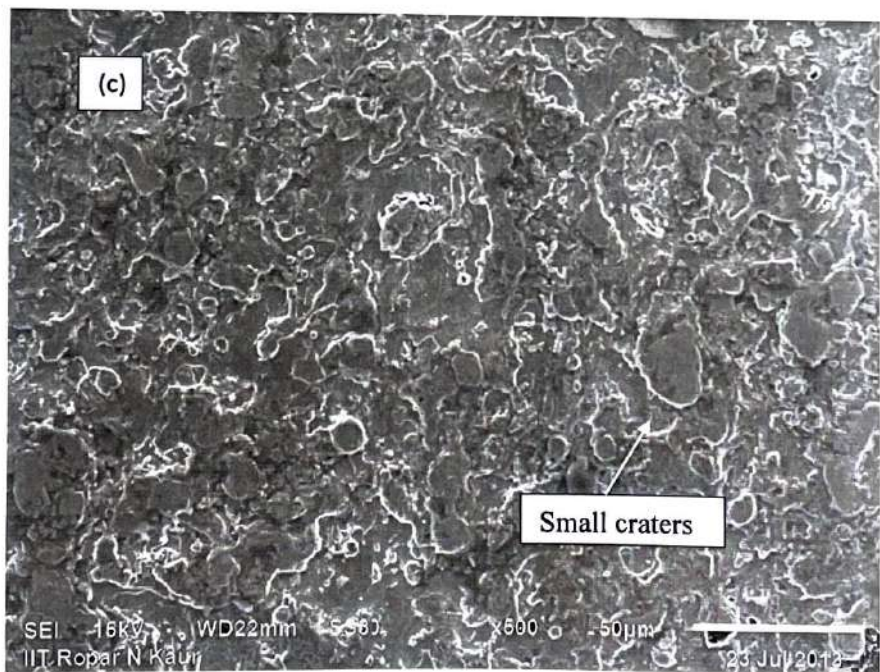


**Figure 6.1c:** SEM Image of Machined Surface Corresponding to Low DE (Ip 90 A; Ton 106 µs; Toff 45µs; SV 50V)

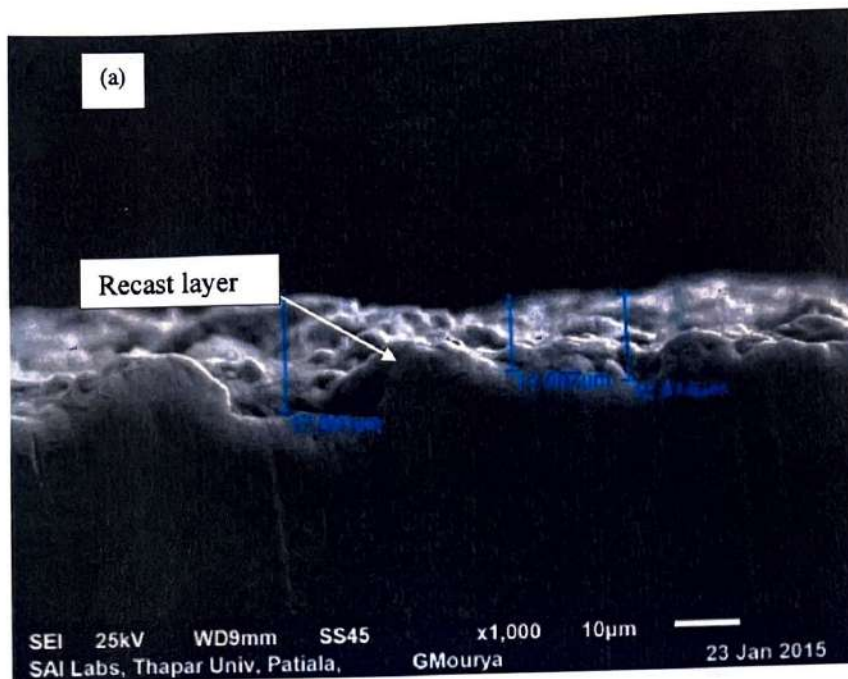


**Figure 6.2a:** SEM Image of Transverse Section Corresponding to High DE (Ip 150 A; Ton 118 µs; Toff 45µs; SV 30V)

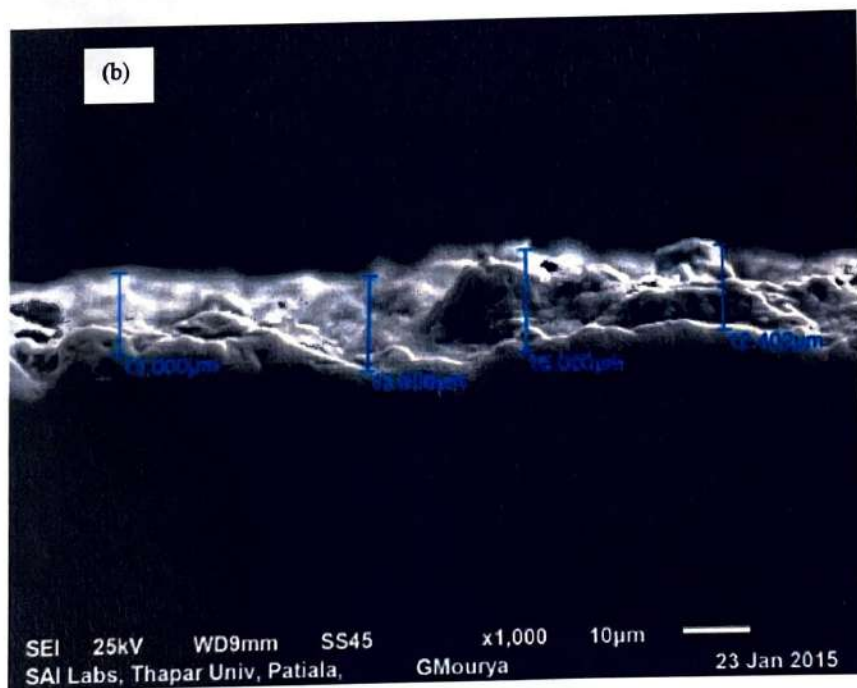


**Figure 6.2b:** SEM Image of Transverse Section Corresponding to Medium DE (Ip 90 A; Ton 112 µs; Toff 40µs; SV 40V)



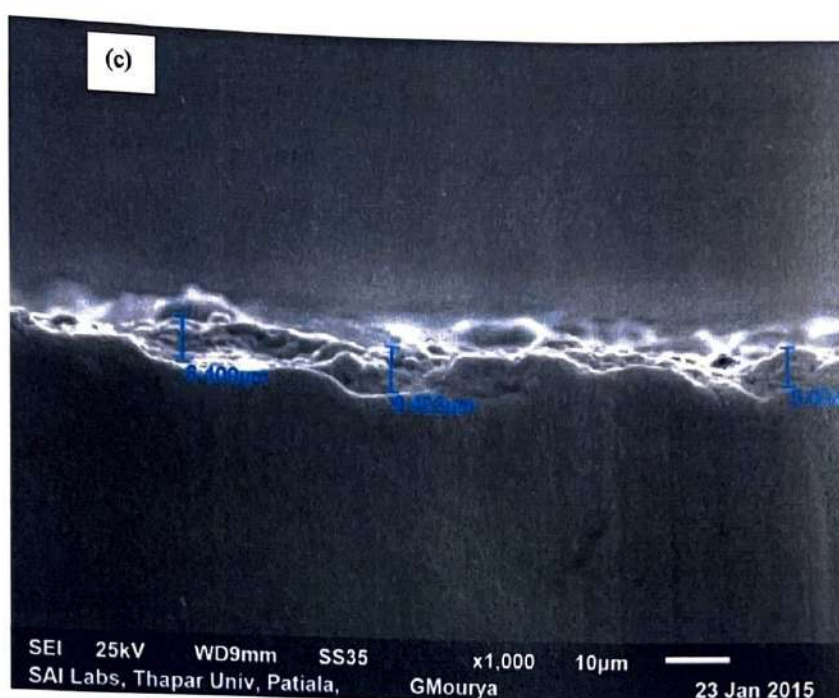


**Figure 6.2c:** SEM Image of Transverse Section Corresponding to Low DE (Ip 90 A; Ton 106 µs; Toff 45µs; SV 50V)

Energy Dispersive Spectroscopy (EDS) analysis of the machined surface at high DE shows that RCL consists of main constituents of work material and no carbon element is present on the top surface {Figure 6.3}. If the WEDM machining of Nimonic-90 is compared with die steel (Kruth et al., 1995) and Tungsten carbide (WC-Co) composite (Saha et al., 2008), less surface damage is observed on Nimonic 90. Unlike steel alloys, due to the absence of C elements in Nimonic-90, quenching in dielectric do not cause micro-cracks in subsurface (Li et al., 2013). Melting point of Nimonic 90 is  $\sim 1370^{\circ}\text{C}$  which is quite low as compared to the temperature generated in plasma channel in WEDM. With uniform melting and evaporation, all constituents get flush out easily and results into better surface characteristics.

### 6.3 UNMACHINED AREAS

In rough cutting operation, it is observed that SEM images show some surface area remains unmachined / uncleared at the end of cut in machine cavity. The movement of wire electrode starting from point 0 is shown by the direction of arrow in Figure 6.4. Wire electrode completes the cutting operation at point B before reaching point A. Therefore, a triangular shape unmachined surface is formed inside the cavity. The



area of the unmachined surface mainly depends on DE across the electrodes. Figure 6.5-6.8 shows SEM images of the top view of inside surface of the cavity.

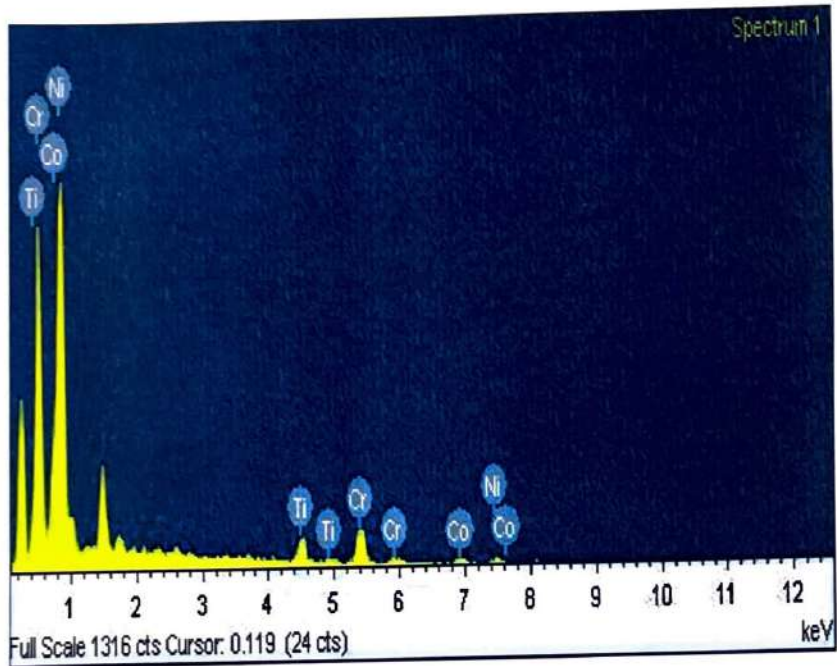


**Figure 6.3:** EDS Analysis of Machined Surface for Corresponding to High DE ( $I_p$  150 A;  $T_{on}$  118  $\mu$ s;  $T_{off}$  45 $\mu$ s; SV 30V)

A triangular shape is appeared of the unmachined top surface area. Its deterioration depends on the discharge conditions, i.e.,  $I_p$  and  $T_{on}$ . At low DE, materials are removed from the machined surface with low CS. So that, a sharp triangular shape is formed with greater height {Figure 6.5-6.6}. Whereas, the increase in  $I_p$  increases the spark diameter which increases the length of ridge line but decreases the height of triangular shape. Increase in  $I_p$  and  $T_{on}$  deteriorate the shape and length of ridge line which is mainly due to large melting and increasing RCL {Figure 6.7-6.8}. Long pulse duration with high  $I_p$  erodes more material from work surface which may cause re-deposition of melted material because of incomplete flushing of debris out of the spark gap, resulting into deteriorated ridge line.

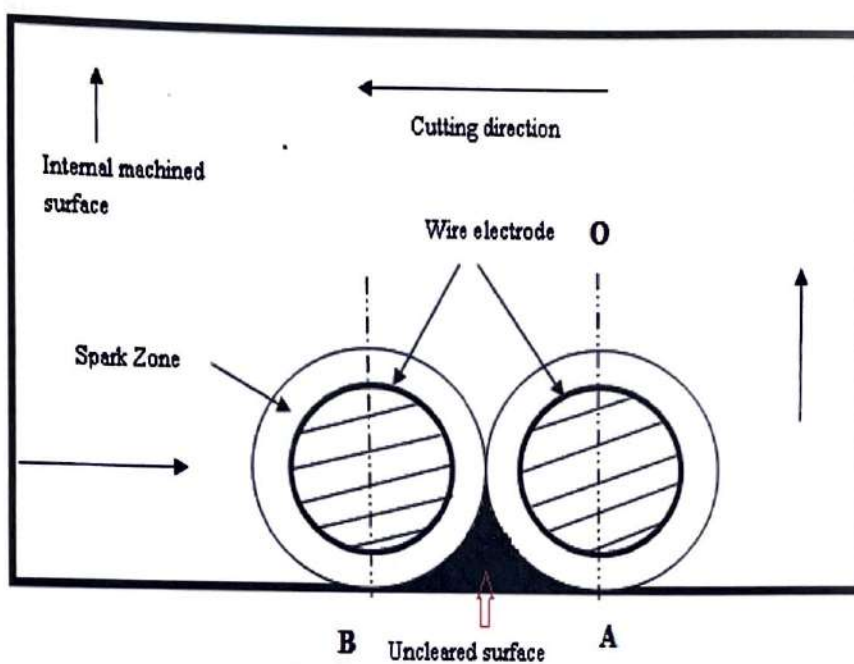


**Figure 6.4:** Representation of Unmachined Surface Area in WEDM

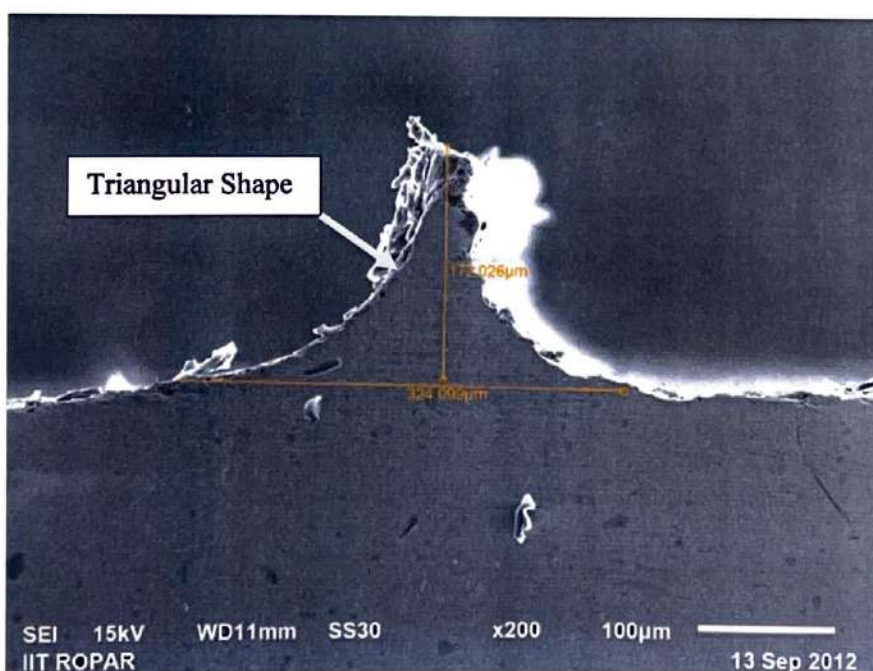


**Figure 6.5:** SEM Image of Unmachined Surface at  $I_p$  90 A;  $T_{on}$  106 µs;  $T_{off}$  45µs; SV 50V)

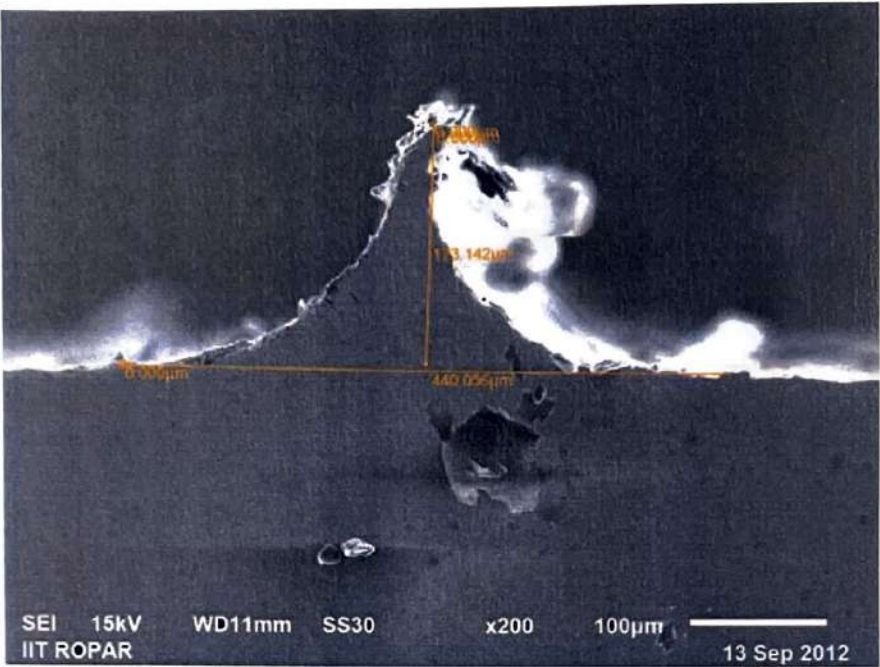


**Figure 6.6:** SEM Image of Unmachined Surface (Ip 120 A; Ton 106  $\mu$ s; Toff 40  $\mu$ s; SV 50V)

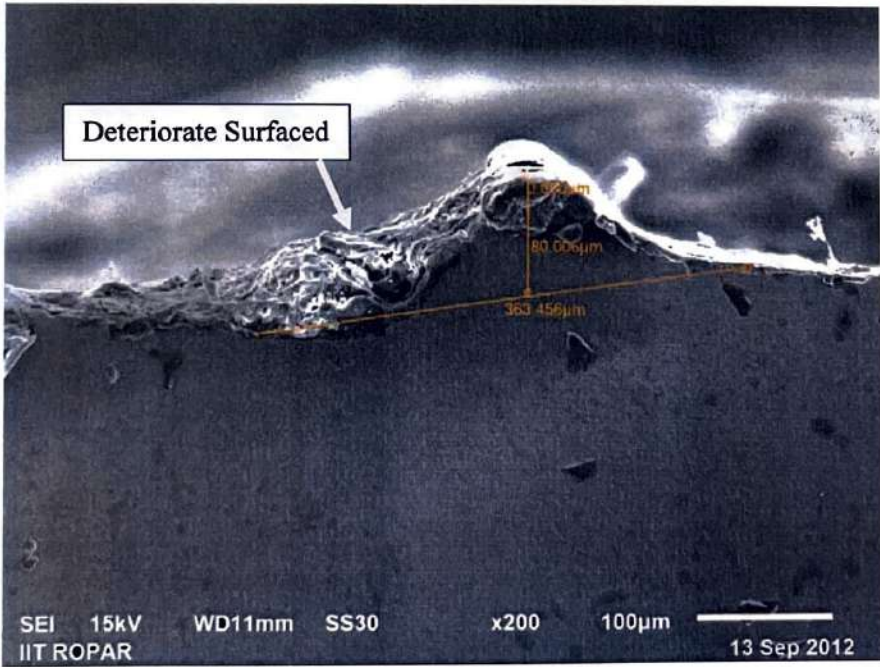


**Figure 6.7:** SEM Image of Unmachined Surface (Ip 120 A; Ton 118  $\mu$ s; Toff 30  $\mu$ s; SV 40V)



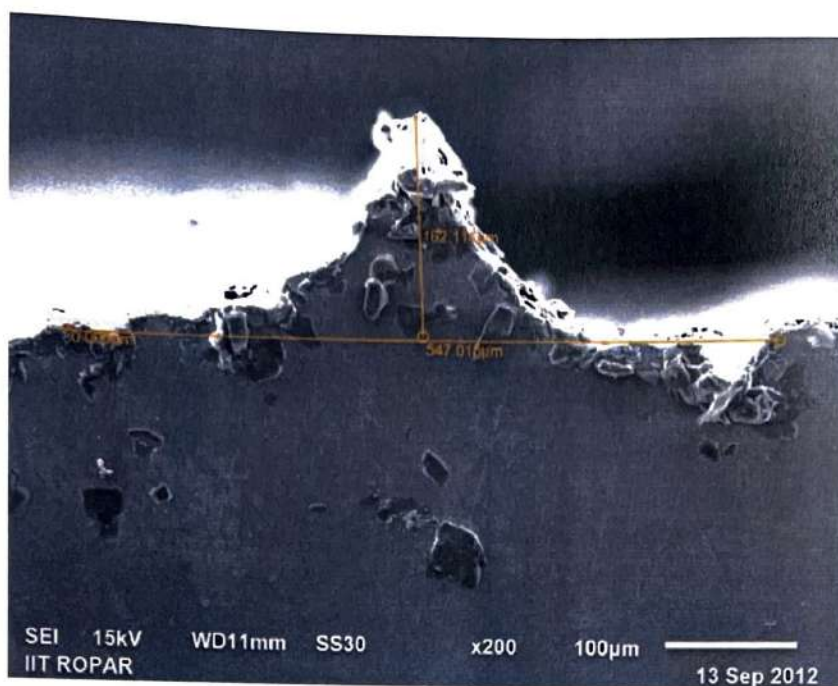


**Figure 6.8:** SEM Image of Unmachined Surface ( Ip 150 A; Ton 118  $\mu$ s; Toff 40  $\mu$ s; SV 30V)

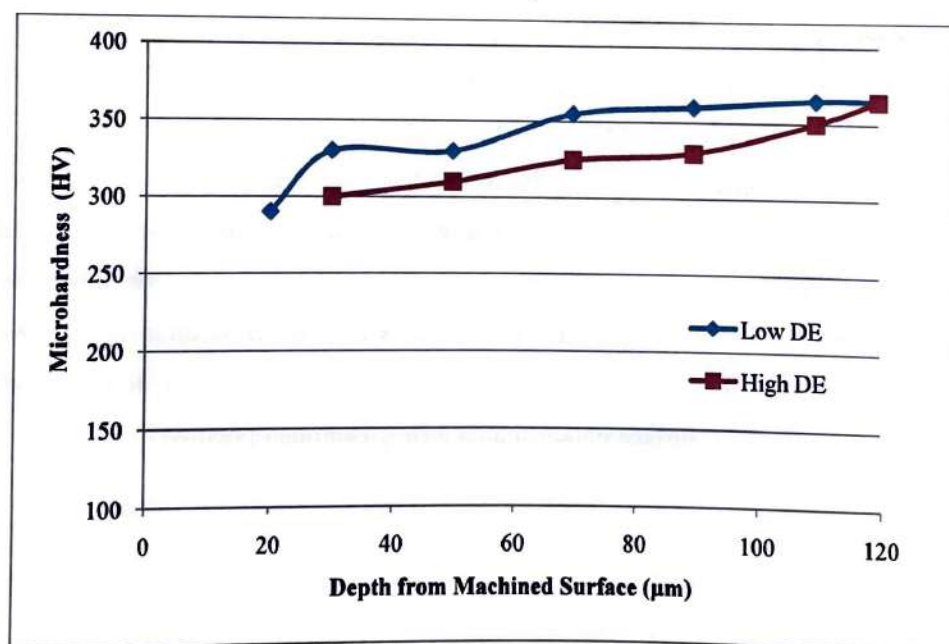


**Figure 6.9:** Micro-Hardness Profiles underneath the Machined Surface at High and Low DE

Figure 6.9 depicts the micro-hardness profile for machined surface at high and low DE. Micro-hardness significantly reduces at the machined top layer as compared to bulk material. This reduction is mainly due to the thermal degradation of top surface (Li et al., 2013) and the depth of degradation increases with increasing DE. At high DE, some part of the thermal energy is transferred to the work material that extends the heat affected zone underneath the machined surface. It is observed that measurement of micro hardness value corresponding to top machined layer is difficult because of the large surface damage at top surface that causes inaccurate impression of micro indent on this region. Therefore, the reading for micro hardness is missing up to 20  $\mu\text{m}$  underneath the top layer in case of High DE.

#### **6.4 DISCUSSION**

The surface integrity of WEDM surfaces of Nimonic 90 is investigated in case of rough cutting operation. SEM results are used in comparative study of the surface texture and crater sizes of rough surface of specimens machined at high, medium and low DE. RCL thickness and length of ridge line are function of two main discharge parameters, i.e.,  $I_p$  and  $T_{on}$ . RCL is mainly due to the incomplete flushing of the eroded carbide material out of the spark gap. Therefore, thickness of RCL increases with increase in  $I_p$  and  $T_{on}$ . RCL and ridge line both degrade the performance of machined surface. RCL has lower hardness, due to which machined surface wear out quickly. These affect the surface quality and dimensional accuracy of the machined components. Therefore, in order to improve the surface integrity of machined surface, Trim cutting operation in WEDM is considered as a probable solution to improve surface characteristics and geometrical accuracy by removing very small amount of work materials from the surface obtained after a rough cutting operation.

## **CHAPTER-VII**

# **COMPARISON OF ROUGH AND TRIM CUTTING OPERATIONS OF NIMONIC 90 WITH STEEL ALLOY, TUNGSTEN CARBIDE COMPOSITE AND MONEL 400 ALLOYS**

---

### **7.1 INTRODUCTION**

In rough cutting operation, damaged surface with poor surface integrity is a major problem because re-solidification of melted debris's that do not flushed quickly out of a narrow spark gap. In rough cutting operation; spark zone is quite large as compared to trim cutting operation. As a result, the volume of molten metal is very high in rough cutting operation which generates large pressure energy in spark zone. It causes large size craters and cracks on work surface. In trim cutting operation, spark zone is influenced by wire offset value and discharge parameters (Sarkar et al., 2010). Therefore, using low discharge energy parameters and accurate value of wire offset in trim cutting operation, damaged surface layer can be minimized or eliminated. The majority of the research work on WEDM deals with rough cutting operation and a very limited research work are conducted for trim cutting operation. Trim cutting operation in WEDM is a best option to remove unwanted surface defects after rough cut in WEDM, with proper discharge parameters and wire offset (Huang et al., 1999; Sarkar et al., 2008; Klink et al., 2011). In this chapter, an experimental study of rough and trim cutting operation of Nimonic 90 with three different materials, i.e., Die steel, Tungsten carbide composite and Monel 400 is presented on WEDM.

### **7.2 EXPERIMENTATION PROCEDURE**

All these materials are machined on 5 axis sprint cut (ELPULSE-40) WEDM. WC-5.3%Co is a difficult to machine material. It possesses high strength and very high hardness which makes it highly suitable for cutting tools, die and other special components. HCHCr die steel is also extensively used for die and mould making. Nimonic 90, a nickel-chromium-cobalt alloy, having high rupture strength and high creep resistance at high temperature (up to 950 °C) and it is mainly employed in turbine blades and combustion chamber. Monel 400 is a nickel copper based alloy,



mostly employed in ships and corrosion resisting applications. Table 7.1 shows the composition and properties of selected work materials.

**Table 7.1: Composition and properties of work materials**

Materials	Nimonic 90	Monel 400	Tungsten Carbide	HCHCr
Composition	60% Ni, 19.3% Cr, 15% Co, 3.1% Ti, and 1.4% Al,	63% Ni, 33% Cu, 2.13% Fe, and 1% Mn	WC-5.3% Co	1.5% C, % 0.6 Mn, 0.6% Si, 1% Co, 12.5 % Cr, 0.9% Mo, 1.10 % V, 0.3% Ni and remaining Fe
Density (g/cm <sup>3</sup> )	8.18	8.8	15.63	7.7
Melting point (°C)	1370	1350	2870	1421
Hardness (HV)	361	199	1990	680
Thermal Conductivity	11.47 W/m °C	22 W/m °C	84.02W/mK	20 W/m °C
Co-efficient of thermal expansion	12.7 µm/°C	13.9 µm/°C	5.8 µm·m <sup>-1</sup> ·K <sup>-1</sup>	10.4µ/°C
Elastic modulus (GPa)	213	115	550	210

Using WEDM, work materials are machined and samples are obtained in the form of rectangular punches of size 8 mm × 7 mm × 12.5 mm. Firstly, effect of discharge energy is evaluated on CS and SR in rough cutting operation. Three levels of discharge energy are selected; low, medium and high. To vary the DE across the work surface, values of discharge parameters namely Ip, Ton, and Toff are varied. Therefore, only three discharge parameters are the variables while the other parameters are kept constant.

Wire electrode and dielectric conditions are assigned a constant value. A zinc coated brass wire is selected as wire electrode. Experiments are conducted at zero WO value. Table 7.2 shows the values of parameters for different level of DE in rough cutting operation. The experiments are performed corresponds to three settings of discharge energy (DE) for each work material and machining characteristics namely CS and SR are observed.

**Table 7.2:** Values of WEDM Parameters in rough cutting operation

DE Level	Values of variable Parameters	Constant Parameters
Low	Ton 106 $\mu$ s, Toff 40 $\mu$ s, Ip 100 A	SV 30V; Wire diameter: 250 $\mu$ m; $W_T$ 10N; $W_F$ 5m/min.; FR 12LM <sup>-1</sup> ; Servo feed 2080.
Medium	Ton 112 $\mu$ s, Toff 40 $\mu$ s, Ip 120 A	
High	Ton 118 $\mu$ s, Toff 35 $\mu$ s, Ip 160 A	

Another set of experiments are performed to examine the effect of trim cutting operations on machining characteristics for each work material. Trim cutting operations are followed after a rough cutting operation that are performed at high level of DE corresponds to the parameters listed in Table 7.2. Trim cutting operations (maximum two numbers) are performed at different wire offset (WO) values of 105 and 85 $\mu$ m but at constant discharge parameters. The values of discharge parameters in trim cutting operation are Ton 105 $\mu$ s; Toff 35 $\mu$ s; Ip 90A; SV 30V;  $W_T$  8N;  $W_F$  2m/min; FR: 3LM<sup>-1</sup>.

### 7.3 RESULTS AND ANALYSIS

Firstly, experiments are conducted to examine the effect of DE and work material properties on machining characteristics of WEDM. CS and SR are observed for these four different work materials after rough cutting operation performed at different levels of DE. After evaluating the effect of DE in rough cutting operation, trim cutting operations are performed and a comparative study for SR and micro-hardness is made.

#### 7.3.1 Cutting Speed (CS)

In WEDM, CS depends on DE across the wire tool electrode and work material. Ip, Ton, Toff and SV are important discharge parameters in WEDM. Low value of Ip, Ton, SV and high value of Toff results into low DE per unit time and vice versa. High DE results in high heat generation across the spark gap and results in large melting and evaporation of work material (Jangra and Grover, 2012; Li et al., 2013). It is seen that CS increases with increase in DE across the electrodes as shown in Figure 7.1.

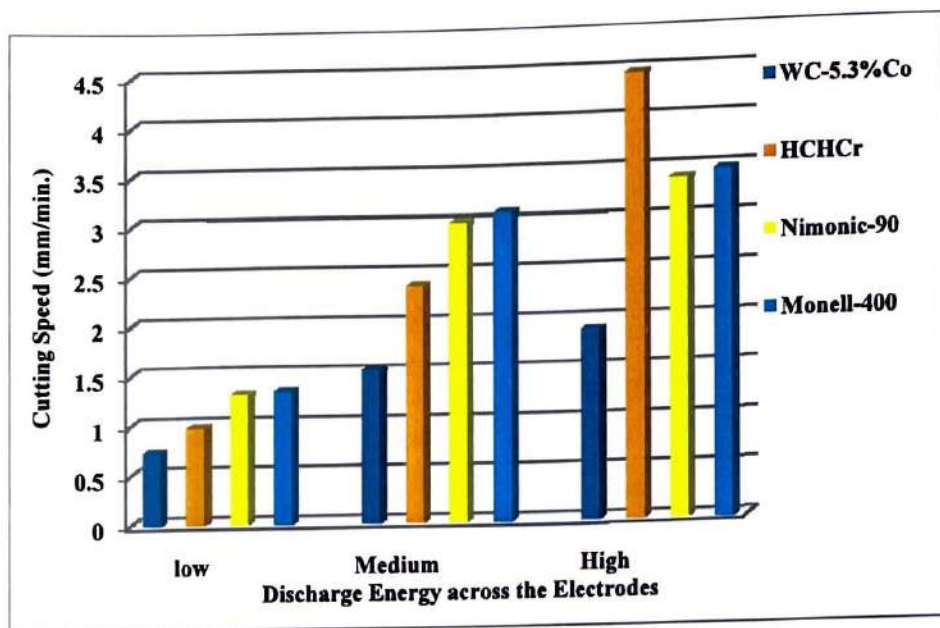


**Figure 7.1: Effect of DE on CS**

With increases in DE, CS increases for all four work materials but in different proportions. The increase in CS is lowest in WC-Co composite while nickel alloys (Nimonic-90 and monel-400) show good increase in CS with increasing of DE. HCHCr steel shows maximum CS corresponds to high level of DE. The melting temperature (nearly  $2800^{\circ}\text{C}$ ) and boiling temperature ( $6000^{\circ}\text{C}$ ) for Tungsten carbide is quite high as compared to other three alloys. Also, WC-Co has higher thermal conductivity which increases the fraction of heat transfer to the bulk material (Jangra K, 2012) and hence less melting and evaporation of WC-Co material take place. As a result, rise in CS for WC-5.3% Co composite is less as compared to other alloys which melts nearly at  $1400^{\circ}\text{C}$ . At high level of DE, Die steel completely melts and evaporates that easily flushed out of the spark gap at high FR.

### 7.3.2 Surface Roughness (SR)

In WEDM process, SR of machined surface is characterized by the size and depth of the craters produced after the melting and expulsion of work material. Therefore, similar to CS, SR is also function of DE across the electrodes. Figure 7.2 shows the effect of DE on SR in rough cutting operation. Result shows that SR increases with increasing DE for all four work materials.



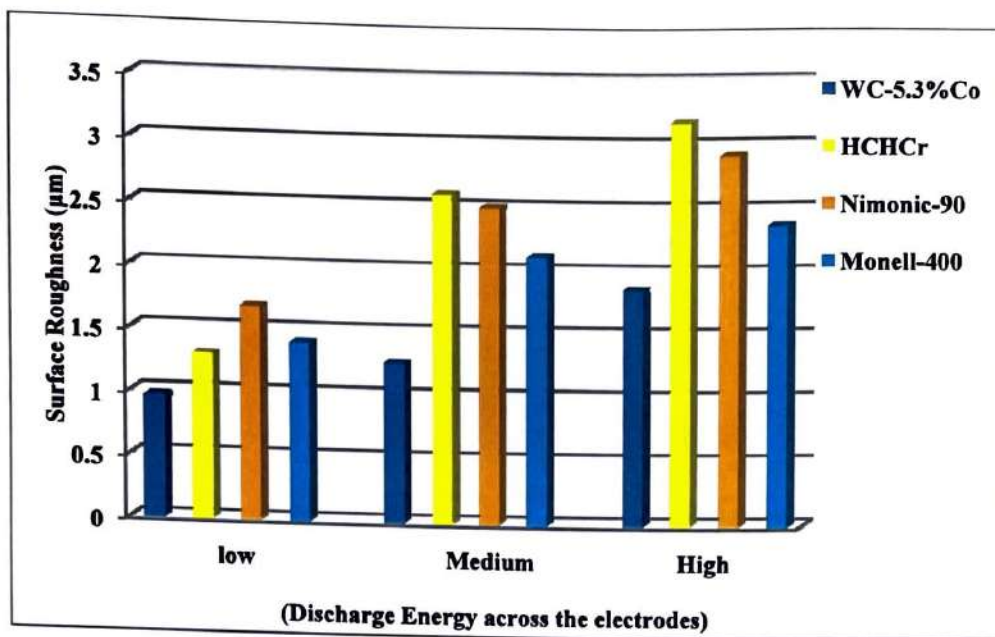


**Figure 7.2: Effect of DE on SR**

SR is least for WC-Co composite while is highest for HCHCr. These results may be confirmed by comparing the machined surface in Figure 7.3-7.6. Machined surface of HCHCr and Nimonic-90 consists of deep and large size craters while WC-Co and Monel-400 has small size craters. Here, thermal conductivity, melting and boiling temperature are the responsible factors. Work materials having low melting and evaporating temperature, high DE causes overheating and evaporation of molten metal forming gas bubbles that explode when the discharge ceases (Han et al. 2007; Li et al., 2013). Resulting high pressure energy creates large size craters on work surface. The diameter and depth of crater increases with increasing DE and a result increases the SR.

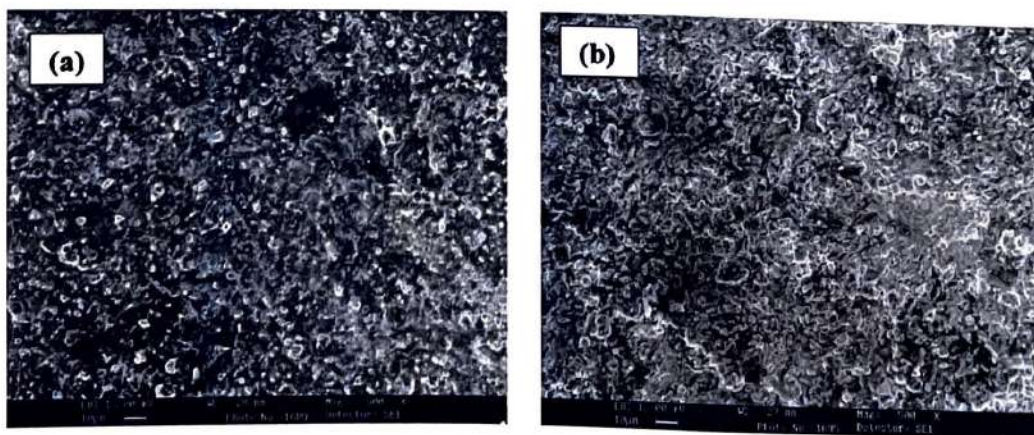


**Figure 7.3: Machined Surface of WC-Co Composite; (a) at Low D.E. (b) at High D.E.**



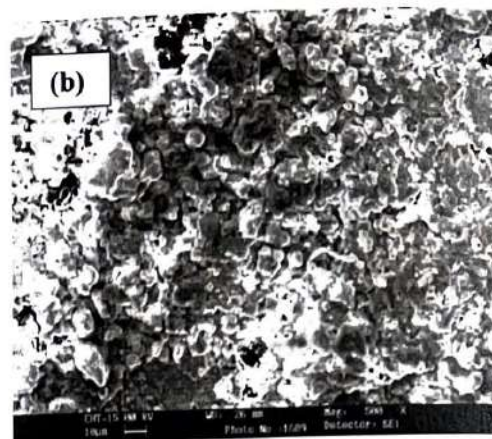
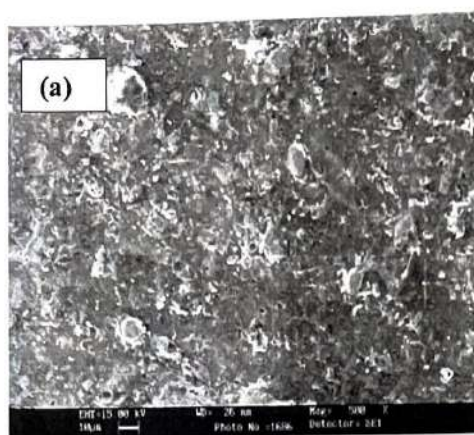


**Figure 7.4:** Machined Surface of HCHCr; (a) at Low D.E. (b) at High D.E.

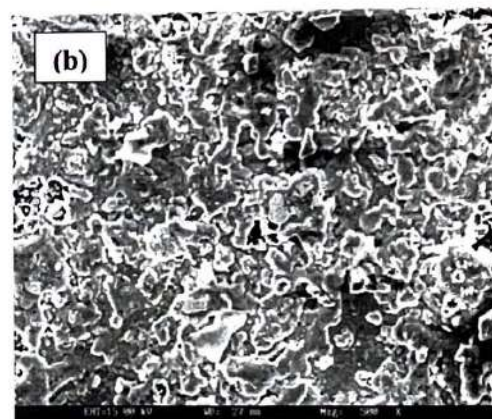
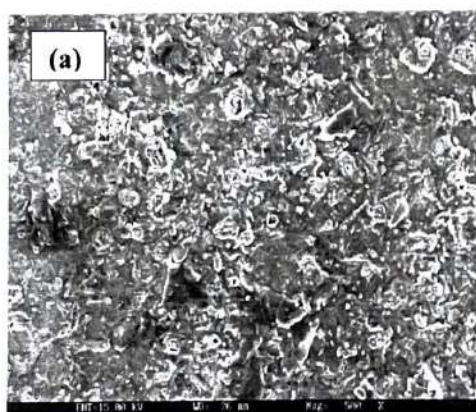


**Figure 7.5:** Machined Surface of Nimonic 90; (a) at Low D.E. (b) at High D.E.

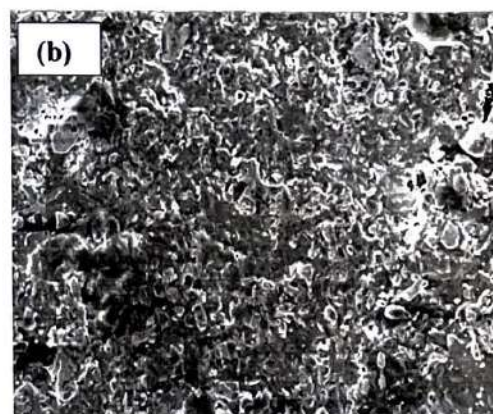
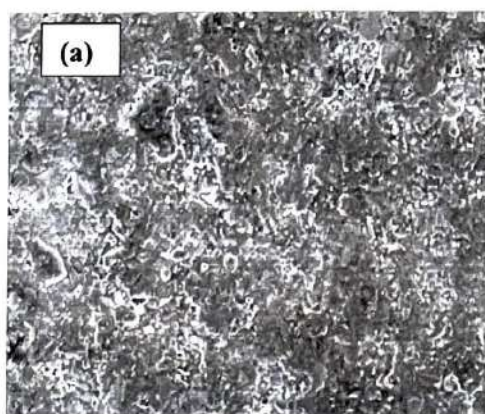


**Figure 7.6:** Machined Surface of Monel 400; (a) at Low D.E. (b) at High D.E.

Figure 7.7 represents the effect of trim cutting operation on SR. Trim cutting operations are conducted for all four work materials under similar discharge parameters but at different values of WO values of 105 and 85 $\mu$ m. Trim cutting operations are conducted after a rough cutting operation that is performed at high level of DE. In trim cutting operation, CS is quite high (10 to 13mm/min.) as compared to rough cutting operation (1-2.5 mm/min.) and it remains nearly same irrespective of the work material.

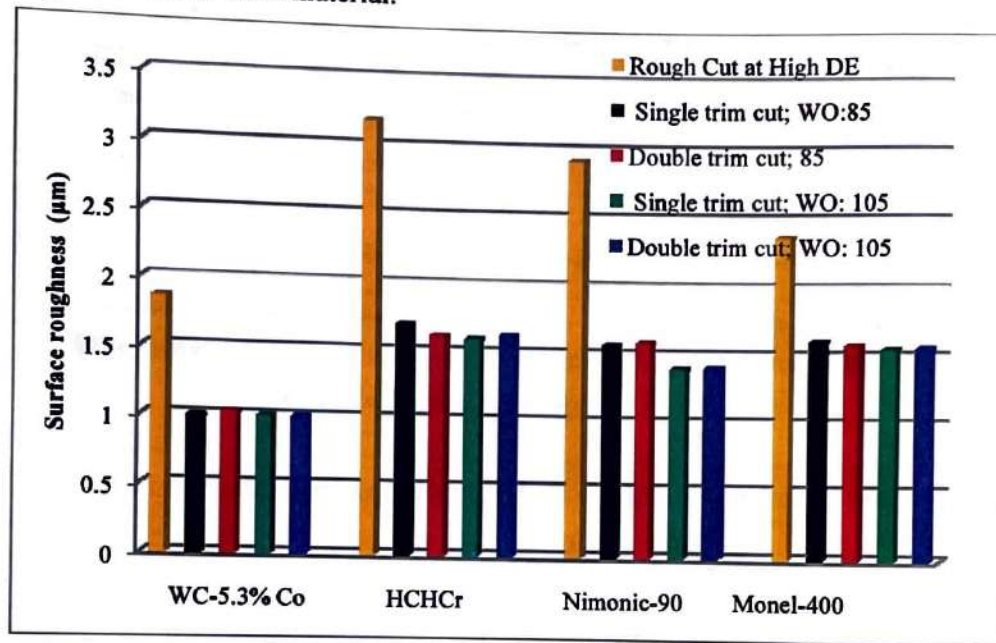


**Figure 7.7: Effect of Trim Cutting Operation on SR**

Trim cutting operation is removed a thin layer of surface material and surface irregularities (peaks). As results, surface finish is improved significantly after trim cutting operation. It is also noticed that multi-trim cutting operations are not much effective. Therefore, surface finish may be improved using single trim cut at low DE with appropriate wire offset value.

### 7.3.3 Micro Hardness

Figure 7.8 (a-d) depict micro-hardness profile underneath the machined surface after rough cutting and single trim cutting operation. Micro-hardness are measured at transverse section to the machined surface. Profiles show that micro-hardness significantly reduced at the machined top layer as compared to bulk material. This reduction is mainly due to the thermal degradation of top or machined surface (Li et



al., 2013) which is predominately due to the high pressure energy generated inside the plasma channel. At high DE, some part of the thermal energy is transferred to the work material that extends the heat affected zone underneath the machined surface.

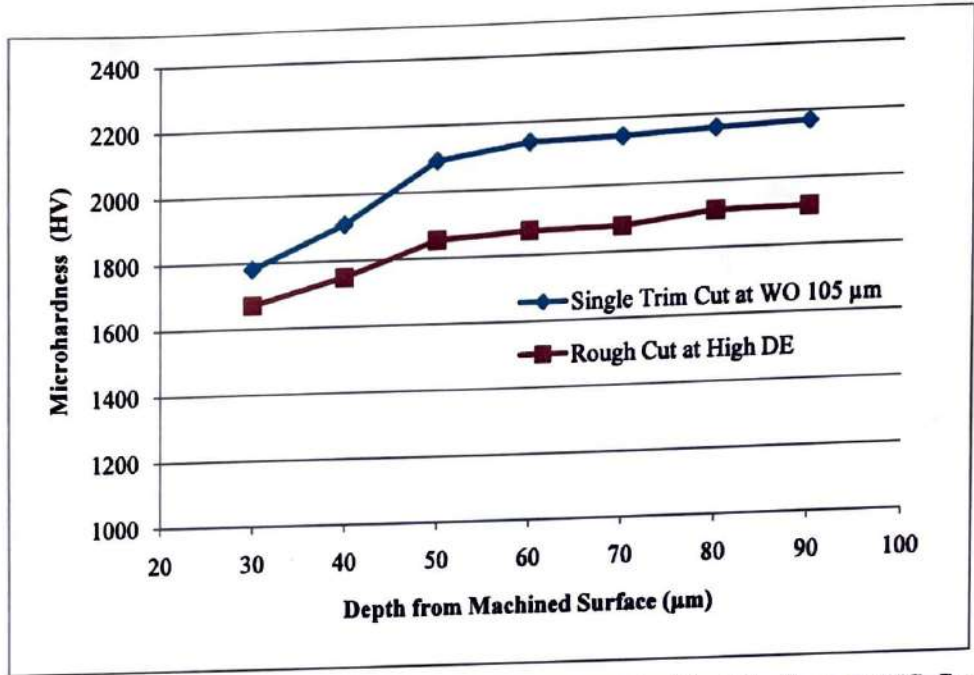


Figure 7.8a: Microhardness Profile Underneath the Machined Surface of WC-Co Composite

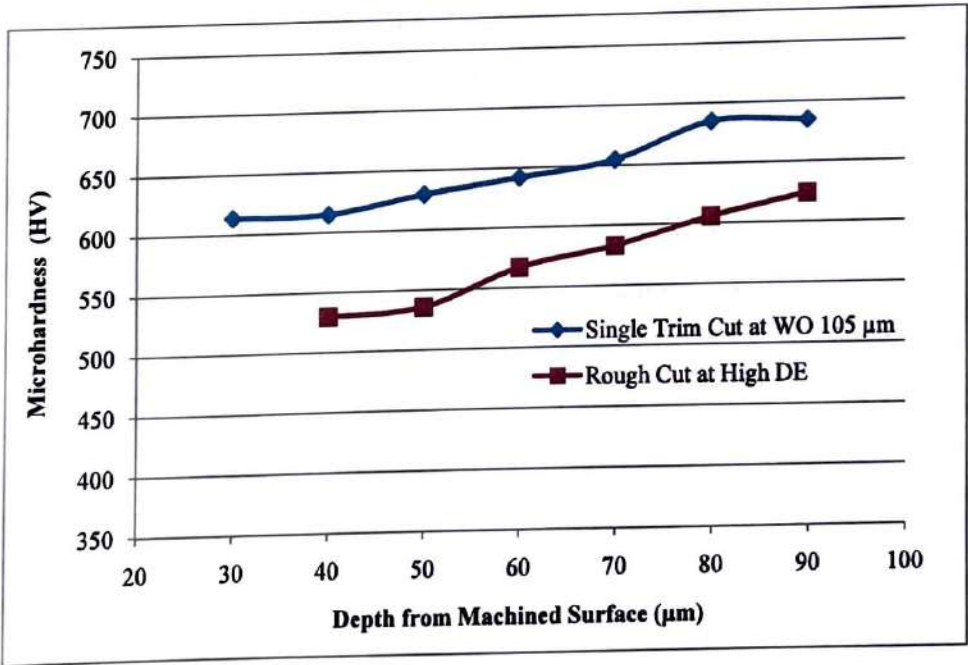
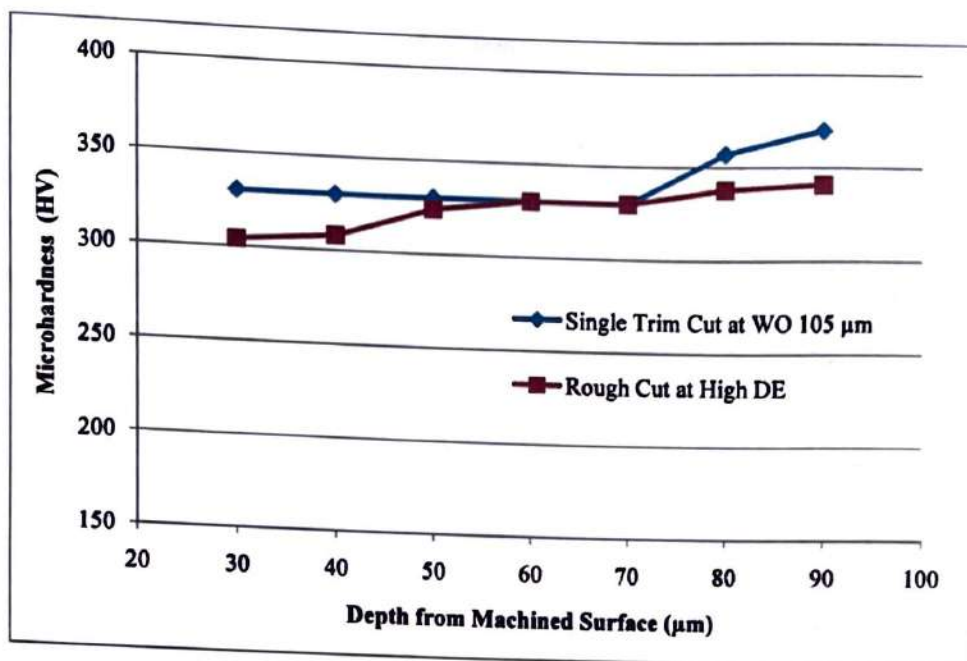
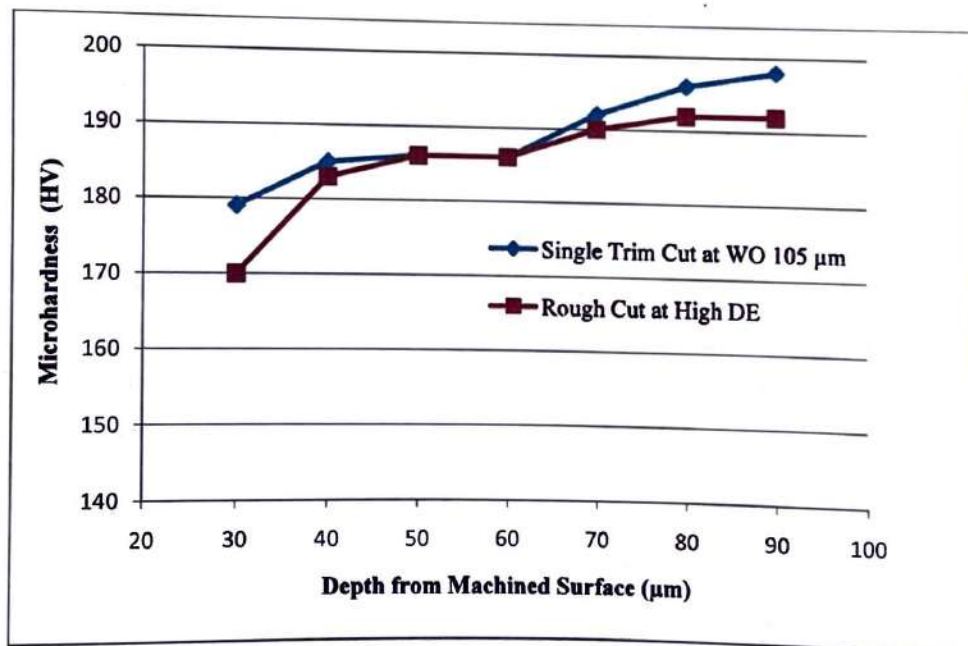


Figure 7.8b: Microhardness Profile Underneath the Machined Surface of HCHCr



**Figure 7.8c:** Microhardness Profile Underneath the Machined Surface of Nimonic 90



**Figure 7.8d:** Microhardness Profile Underneath the Machined Surface of Monel 400

Figures 7.8c and 7.8d show the Nimonic 90 and Monel 400, nearly closed micro hardness profiles are obtained for rough and trim cutting operations underneath the machined surface except up to a depth of 40μm. But in case of WC-Co composite

and HCHCr, a noticeable difference is obtained in micro hardness profiles for rough and trim cutting operation. In WC-Co composite and HCHCr, carbon percentage is more which causes quenching of machined surface due to dielectric fluid and results into micro-cracks in sub-surface (Kruth and Stevens, 1995; Li et al., 2013). Using trim cutting operation, the degraded surface is removed resulting into new surface having lesser numbers of micro-cracks and defects. Therefore, micro-hardness after trim cutting operation increases in WC-Co and HCHCR. It is observed that measurement of micro hardness value corresponding to top machined layer is difficult because of the large surface damage at top surface that causes inaccurate impression of micro indent on this region. Therefore, the reading for micro hardness is missing up to 20  $\mu\text{m}$  underneath the top layer.

#### **7.4 DISCUSSION**

In this chapter, an experimental study of rough and trim cutting operations in WEDM is studied for Nimonic-90 with three hard to machine materials namely Tungsten carbide cobalt (WC-Co) composite, high carbon high chrome (HCHCr) steel alloy and Monel 400. CS, SR and micro-hardness are the performance characteristics. Result shows that with the increase in DE, CS and SR increases which is due to the high heat generation and high rate of melting and evaporation of work material. From SEM images for low and high DE, it is observed that the machined surface of HCHCr and Nimonic-90 consist of deep and large size craters while WC-Co and Monel-400 have small size craters. This may be due to the difference in values of thermal conductivity and melting and boiling temperatures of work materials.

Trim cutting operations are performed after a rough cutting operation (with high level of discharge energy) under the similar discharge conditions but with different wire offset values. Results show that surface finish is improved significantly after trim cut operation irrespective of rough cutting operation. It is also noticed that; multi-trim cutting operations are not much effective. Therefore, surface finish may be improved using single trim cut at low DE with appropriate wire off-set value.

Micro-hardness profiles underneath the machined surface after rough cutting operation showed that at high DE, depth of thermal degradation of top surface increases and thermal degradation is affected by carbon percentage in work material.



## CHAPTER-VIII

# OPTIMIZATION OF TRIM CUTTING OPERATION OF NIMONIC-90 WITH RSM USING DESIRABILITY FUNCTION

---

### 8.1 INTRODUCTION

Trim cutting is considered as a probable solution to improve the surface integrity, geometrical accuracy and fatigue life by removing the degraded materials from the machined surface. In trim cutting operation, wire electrode trace back the same wire path of first cut with low DE and certain values of WO (Huang et al., 1999; Puri & Bhattacharyya, 2003). Wire depth ( $W_d$ ) is the distance travelled perpendicular and inside the work piece during trim cutting operation. The depth of cut is related to WO value. Increasing the WO value decreases the  $W_d$ . Surface finish is improved considerably using single trim cut at low DE with appropriate WO value.

This chapter is presented the investigation on trim cutting operation in WEDM of Nimonic 90. Machining parameters namely Ton, SV, FR and  $W_d$  are investigated on surface characteristics and dimensional shift ( $D_s$ ) in trim cutting operation. A standard second order experimental design called face centered Central Composite Design (CCD) in term of machining parameter is adopted using RSM. Desirability function is employed to optimize two performance characteristics simultaneously.

### 8.2 EXPERIMENTATION PROCEDURE

In the study, 5 axis sprint cut (ELPUSE-40) WEDM is selected for conducting experiments. Trim cutting operations are performed at different combination of process parameters after a rough cut performed at constant parameters. Using WEDM, work material is machined and samples are obtained in the form of rectangular cavity of dimension 10 mm × 6 mm × 12.5 mm. Figure 8.1 shows the schematic diagram of the cutting operation performed in present work. According to path programme {Figure 8.1}, firstly, a rough cut (1-2-3-4-5-2-1) is performed at zero WO value to part-off the material. The machine is halted at point 2 to remove the punch out of the work plate and then trim cut (1-6-7-8-9-10-6-1) are performed according to the experimental plan mentioned in Table 8.3.  $D_s$  is calculated after

measuring the dimensions of die cavity with the help of an optical microscope. It is obtained as

$$D_s = (\text{Die cavity width after trim cut} - \text{Die cavity width after rough cut})/2.$$

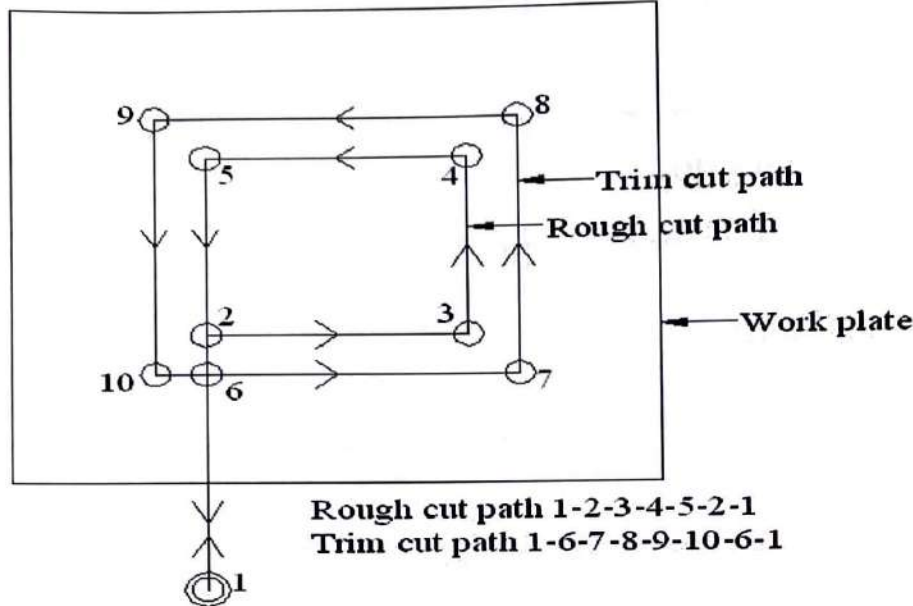


**Figure 8.1: Cutting Operations in WEDM Process**

In case of trim cutting, the prime objective is to improve SR and to reduce dimensional inaccuracy. Therefore, a combination of high DE parameters is provided the maximum CS in rough cutting operation, while in trim cutting operation, low DE parameters resulting, low SR, are selected. Fixed Machining parameters setting for rough and trim cutting operations are shown in Table 8.1. A zinc coated brass wire having a fixed diameter of 0.25mm is selected as wire electrode. The Ton, SV,  $W_d$  and FR are considered as main process parameters in trim cutting operation for investigation.  $D_s$  and SR are considered as machining characteristics. Table 8.2 shows the process parameters and their levels for trim cutting operation. Experiments are performed according to the layout of experimental design for Face CCD of second order shown in Table 8.3.

### 8.3 RESPONSE SURFACE METHODOLOGY (RSM) AND EXPERIMENTAL DESIGN

A standard second order experimental design called face CCD is adopted for analysing and modelling the WEDM parameters for average value of SR and  $D_s$  as shown in Table 8.3. SR is measured in terms of mean absolute deviation (Ra) using

the Digital Surface Tester Mitutoyo 301P. A regression equation is developed for correlating the input process parameters with response parameters using RSM.

**Table 8.1:** Fixed Machining Parameters in Rough and Trim Cutting Operations

Rough cut parameters	Trim cut parameters
Ton 118 $\mu$ s	Toff 30 $\mu$ s
Toff 35 $\mu$ s	Ip 110 A
FR 12L/min	$W_T$ 8N
$W_R$ 5 mm/min	$W_T$ 2m/min
$W_T$ 10 N	Servo feed = 150
Ip 150 Amp	
SV 30 V	
Servo Feed 150	

**Table 8.2:** Variable Process Parameters and their Levels in Trim Cutting Operation

Parameters	Symbol	Units	Levels	
			Low (-1)	High (+1)
Pulse on Time	Ton	$\mu$ s	104	112
Servo voltage	SV	V	20	40
Wire Depth	$W_d$	$\mu$ m	10	30
Flow Rate	FR	L/min	2	6

#### 8.4 RESULT ANALYSIS

To analyze the experimental data, Design expert (DX7), a statistical tool is utilized. There are three tests, i.e., sequential model sum of squares, lack of fit tests and model summary statistics are performed for deciding the adequacy of the model for two different machining characteristics, i.e., SR and  $D_s$  in WEDM process. Table 8.4-8.5 are used to decide an adequate model to fit various machining characteristics. Analysis of Variance (ANOVA) is performed on the experimental data to test the goodness of fit of the model. This includes test for significance of the regression model, significance on model coefficients and lack of fit model adequacy.



**Table 8.3:** Layout of Experimental Design for Face CCD of Second Order and Experimental Results in Trim Cutting Operation

Expt. No.	Ton ( $\mu s$ )	SV (V)	W <sub>d</sub> ( $\mu m$ )	FR (L/min)	SR ( $\mu m$ )	D <sub>s</sub> ( $\mu m$ )
1	104	20	10	2	1.31	14
2	112	20	10	2	2.03	17
3	104	40	10	2	1.1	16
4	112	40	10	2	1.51	14
5	104	20	30	2	1.25	38
6	112	20	30	2	2.45	38
7	104	40	30	2	1.22	43
8	112	40	30	2	2.22	45
9	104	20	10	6	1.18	22
10	112	20	10	6	2.41	29
11	104	40	10	6	1.11	17
12	112	40	10	6	1.97	28
13	104	20	30	6	1.25	40
14	112	20	30	6	2.9	48
15	104	40	30	6	1.3	46
16	112	40	30	6	2.69	54
17	104	30	20	4	1.32	23
18	112	30	20	4	2.53	27
19	108	20	20	4	2.03	23
20	108	40	20	4	1.81	27
21	108	30	10	4	1.86	20
22	108	30	30	4	2.2	47
23	108	30	20	2	1.72	27
24	108	30	20	6	2	36
25	108	30	20	4	2.03	28
26	108	30	20	4	2.08	27
27	108	30	20	4	2.09	27
28	108	30	20	4	2.06	29
29	108	30	20	4	2.08	30
30	108	30	20	4	2.12	27

**Table 8.4:** Selection of Adequate Model for SR in Trim Cutting Operation

<b>Sequential Model Sum of Squares Test</b>						
Source	Sum of Squares	Degree of Freedom	Mean Square	F-value	p-value Prob>F	
Mean vs. Total	103.90	1	103.90			
Linear vs. Mean	6.11	4	1.53	32.22	<0.0001	
2F1 vs. Linear	0.59	6	0.099	3.16	0.0255	
Quadratic vs. 2F1	0.56	4	0.14	53.99	<0.0001	Suggested
Cubic vs. Quadratic	0.018	8	2.254E-003	0.77	0.6425	Aliased
Residual	0.021	7	2.933E-003			
Total	111.20	30	3.71			
<b>Lack of Fit Tests</b>						
Source	Sum of Squares	Degree of freedom	Mean Square	F- value	p- value Prob > F	
Linear	1.18	20	0.059	65.15	0.0001	
2F1	0.59	14	0.042	46.43	0.0002	
Quadratic	0.034	10	3.403E-003	3.75	0.0786	
Cubic	0.016	2	8.000E-004	8.82	0.0229	Suggested
Pure Error	4.533E-003	5	9.067E-004			Aliased
<b>Model Summary Statistics</b>						
Source	Standard Deviation	R-Squared	Adjusted R-Squared	Predicted R-Squared	Press	
Linear	0.22	0.8375	0.8115	0.7422	1.88	
2F1	0.18	0.9186	0.8758	0.7168	2.07	
Quadratic	0.051	0.9947	0.9898	0.9791	0.15	Suggested
Cubic	0.054	0.9972	0.9883	0.7387	1.91	Aliased

**Table 8.5:** Selection of Adequate Model for  $D_s$  in Trim Cutting Operation

Sequential Model Sum of Squares Test						
Source	Sum of Squares	Degree of Freedom	Mean Square	F- value	p-value Prob>F	
Mean vs. Total	27421.63	1	27421.63			
Linear vs. Mean	3112.78	4	778.19	53.95	<0.0001	
2F1 vs. Linear	129.38	6	21.56	1.77	0.1589	
Quadratic vs. 2F1	203.74	4	50.94	27.81	<0.0001	Suggested
Cubic vs. Quadratic	11.72	8	1.47	0.65	0.7203	Aliased
Residual	15.75	7	2.25			
Total	30895.00	30	1029.83			
Lack of Fit Tests						
Source	Sum of Squares	Degree of freedom	Mean Square	F- value	p- Value Prob > F	
Linear	352.59	20	17.63	11.02	0.0072	
2F1	223.21	14	15.94	9.96	0.0096	
Quadratic	19.47	10	1.95	1.22	0.4386	
Cubic	7.75	2	3.87	2.42	0.1839	Suggested
Pure Error	8.00	5	1.60			Aliased
Model Summary Statistics						
Source	Standard Deviation	R- Squared	Adjusted R- Squared	Predicated R- Squared	Press	
Linear	3.80	0.8962	0.8796	0.8448	539.19	
2F1	3.49	0.9334	0.8984	0.8263	603.26	
Quadratic	1.35	0.9921	0.9847	0.9567	150.29	Suggested
Cubic	1.50	0.9955	0.9812	0.4525	1901.64	Aliased



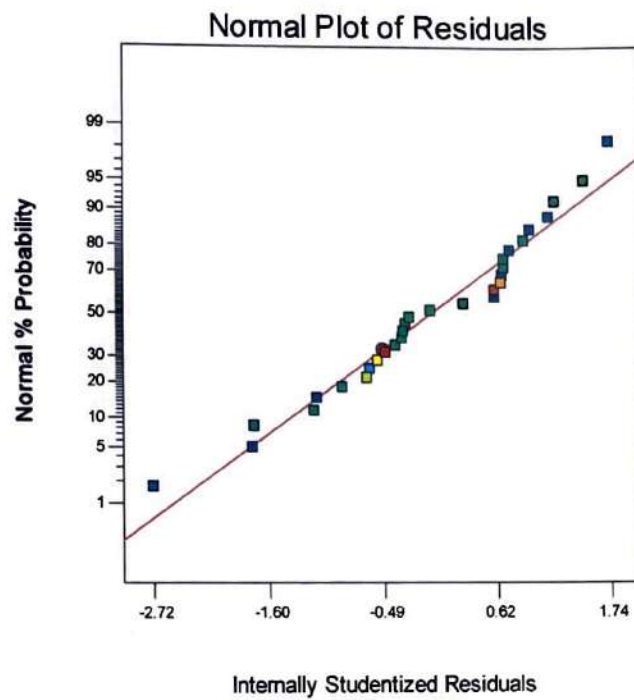


**Figure 8.2:** Normal Probability Residuals Plot for SR in Trim Cutting Operation

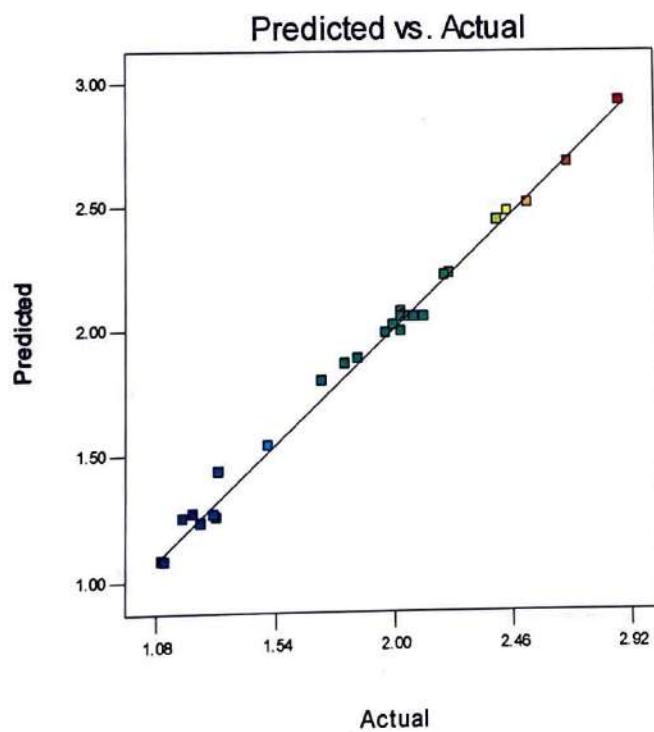


**Figure 8.3:** Predicted vs. Actual Plot for SR in Trim Cutting Operation

#### 8.4.1 Analysis of SR in Trim Cutting Operation

Fit summary for SR suggested that quadratic model is statistically significant for analysis. Table 8.6 shows ANOVA for SR, after backward elimination process. The Model F-value of 232.85 implies that the model is significant. There is only a 0.01% chance that a "Model F-Value", this large could occur due to noise. In this case A, B, C, D, AB, AC, AD, BC, A<sup>2</sup>, B<sup>2</sup>, D<sup>2</sup> are significant model terms. Values greater than 0.05 indicates that the model terms are not significant. A selected model would be statistically significant, if *p*-value for the model terms are less than 0.05 (i.e.  $\alpha = 0.05$ , or 95% confidence level) (Myers & Montgomery, 1995). Using backward elimination process, insignificant terms (*p*-value > 0.05) are eliminated from the reduced quadratic model.

Table 8.4 shows that the *p*-value for quadratic model is significant. The terms in the model have significant effect on output response. In present case, the value of R<sup>2</sup> and R<sup>2</sup> (adj.), called coefficient of determination, is over 99%. When R<sup>2</sup> approaches unity, better the response model fits the actual data. Also, test of 'lack of fit' shows insignificant effect, which is desirable for selecting the models. Figure 8.2 shows that the residuals are normally distributed about a straight line which means that the errors are normally distributed. Figure 8.3 shows that the predicted vs. actual values plot for SR and all the actual values are following the predicating values. Hence declared model assumptions are right. Consequently, the proposed model for SR may be considered as significant for fitting and predicting the experimental results. The final response equation after eliminating the non significant terms for SR is given below:

(In terms of actual parameters)

$$\begin{aligned} \text{Surface roughness} = & -63.92711 + 1.12996 * \text{Ton} + 0.22186 * \text{SV} - 0.33958 * \text{Wd} - 1.17592 * \\ & \text{FR} - 1.78125\text{E-}003 * \text{Ton} * \text{SV} + 3.15625\text{E-}003 * \text{Ton} * \text{Wd} + 0.014063 * \text{Ton} * \text{FR} + \\ & 5.12500\text{E-}004 * \text{SV} * \text{Wd} - 4.91477\text{E-}003 * \text{Ton}^2 - 8.36364\text{E-}004 * \text{SV}^2 - 0.035909 * \text{FR}^2 \end{aligned} \quad (8.1)$$

In order to analyse the influence of WEDM parameters on SR, response surface graphs are shown in Figure 8.4(a-d). These figures show the noticeable influence of process parameters on SR. SR increases with increasing the value of Ton, W<sub>d</sub> and FR while it decreases with increasing value of SV. The influence of FR is non-symmetric. The curved plots show the interaction among the input parameters. The parameter namely Ton, SV, W<sub>d</sub>, FR and their interactions are highly significant for SR.

**Table 8.6: ANOVA for SR in Trim Cutting Operation**

Source	Sum of Squares	Degree of freedom	Mean Square	F-value	p-value	
Model*	7.25	11	0.66	232.85	< 0.0001	Significant
Ton	5.19	1	5.19	1835.66	< 0.0001	
SV	0.2	1	0.2	69.38	< 0.0001	
W <sub>d</sub>	0.5	1	0.5	176.68	< 0.0001	
FR	0.22	1	0.22	78.52	< 0.0001	
Ton*SV	0.081	1	0.081	28.7	< 0.0001	
Ton* W <sub>d</sub>	0.26	1	0.26	90.11	< 0.0001	
Ton*FR	0.2	1	0.2	71.55	< 0.0001	
SV*W <sub>d</sub>	0.042	1	0.042	14.85	0.0012	
(Ton) <sup>2</sup>	0.018	1	0.018	6.2	0.0228	
(SV) <sup>2</sup>	0.02	1	0.02	7.02	0.0163	
(FR) <sup>2</sup>	0.059	1	0.059	20.69	0.0002	
Residual	0.051	18	2.83E-03			
Lack of fit	0.046	13	3.57E-03	3.94	0.0697	Not significant
Pure error	4.53E-03	5	9.07E-04			
Cor. Total	7.3	29				
$R^2 = 0.9930$ $R^2 (\text{Adj.}) = 0.9887$ Pred R-Squared = 0.9773              Adeq Precision = 54.737						

High DE due to high value of Ton results into overheating and evaporation of molten metal resulting into high pressure energy that creates large size craters on work surface. The diameter and depth of crater increases with increasing of Ton which increases SR. Increasing the value of W<sub>d</sub> decreases the gap between wire electrode and work surface which increases the effective sparking on work surface and hence melting and erosion of the surface material increases. This causes increase in SR. SR decreases with increasing the value of SV as shown in Figure 8.4c. Increasing SV increases the gap between work material and wire electrode that result into low ionization of dielectric medium and hence low DE get generated. At low dielectric FR, laminar dielectric flow is maintained that results into effective spark generation



in trim cutting operation which removes the surface irregularities completely after the rough cutting operation. Therefore, low FR results into lower SR.

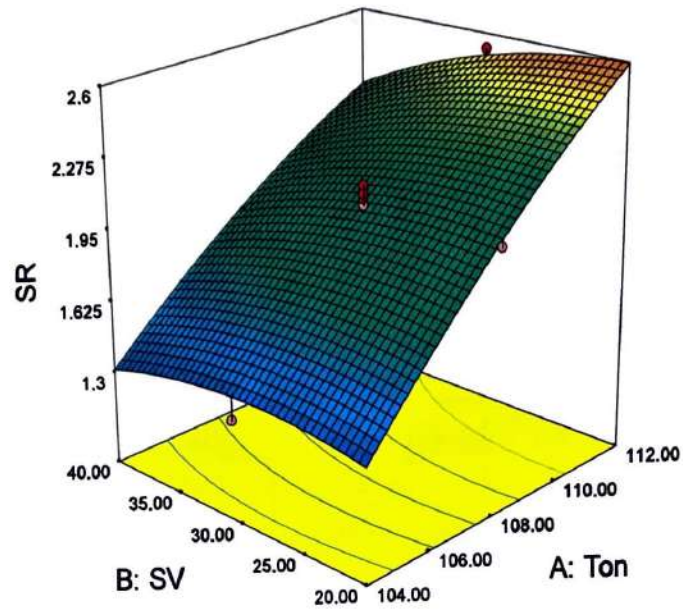


**Figure 8.4a:** Combined Effect of SV and Ton on SR ( $W_d$ : 20 $\mu$ m; FR: 4L/min)

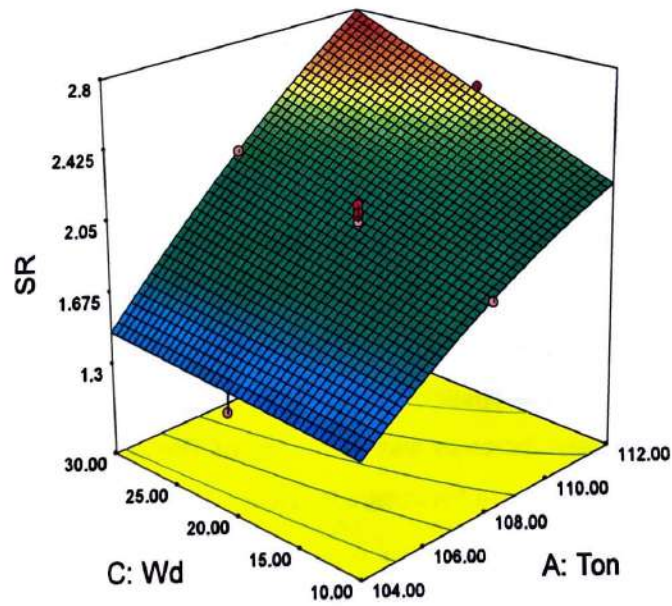


**Figure 8.4b:** Combined Effect of  $W_d$  and Ton on SR (SV: 30V; FR: 4L/min)

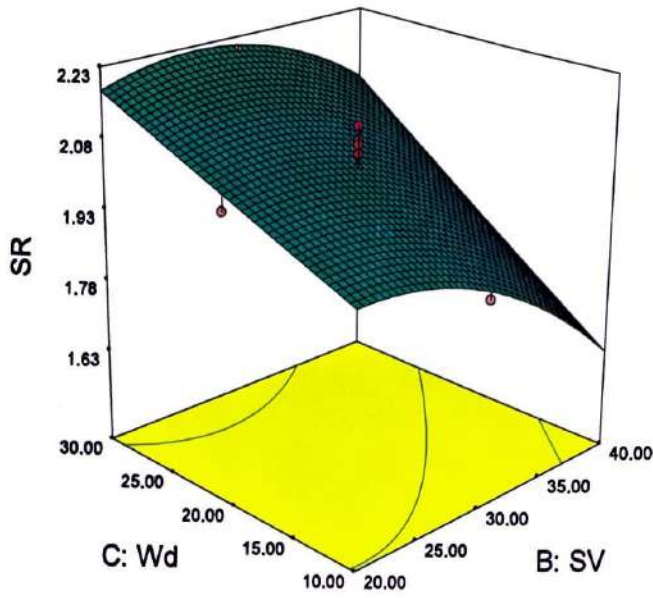


**Figure 8.4c:** Combined Effect of  $W_d$  and SV on SR (Ton:  $108\mu\text{s}$ ; FR: 4L/min)

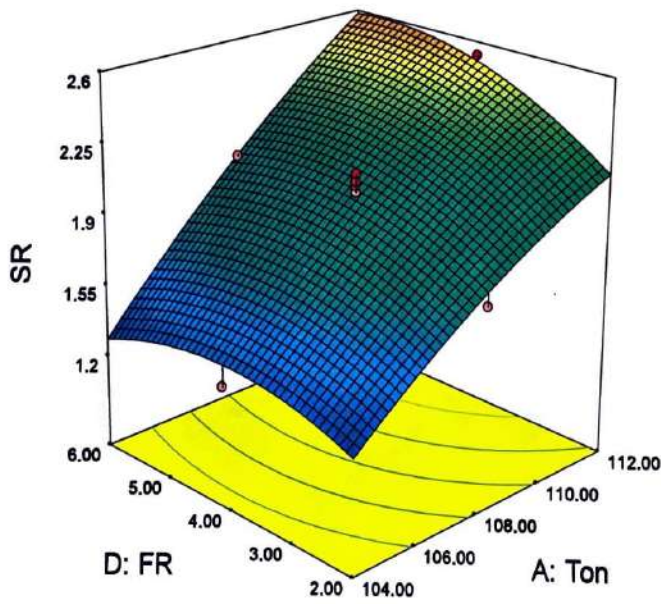


**Figure 8.4d:** Combined Effect of FR and Ton on SR (SV: 30V;  $W_d$ :  $20\mu\text{m}$ )

In order to examine the extent of surface damage (RCL) formed due to the re-solidification of melted residual material which is not completely expelled during the process (Puri & Bhattacharyya, 2005). The morphology of recast layer is much different from bulk material and it adversely affects the working life of machined component (Liao et al., 2004;

Soo et al., 2013). Figures 8.5-8.8 show the SEM images of transverse section of sample correspond to sample no. 3, 4, 15 and 26, respectively.

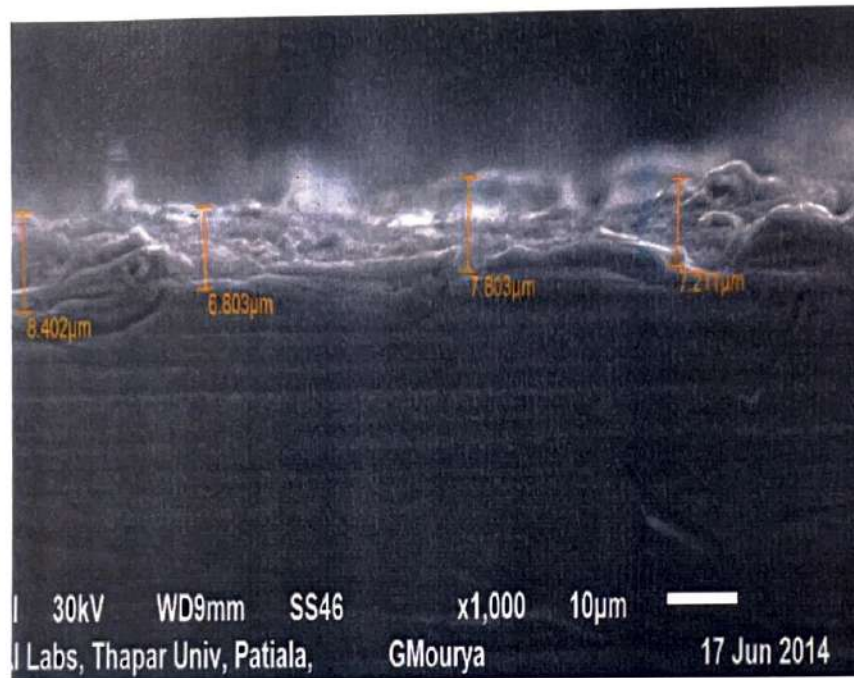


**Figure 8.5:** SEM Image of Transverse Section of Sample 3 (Ton 104μs, SV 40V, W<sub>d</sub> 10μm, FR 2L/min)

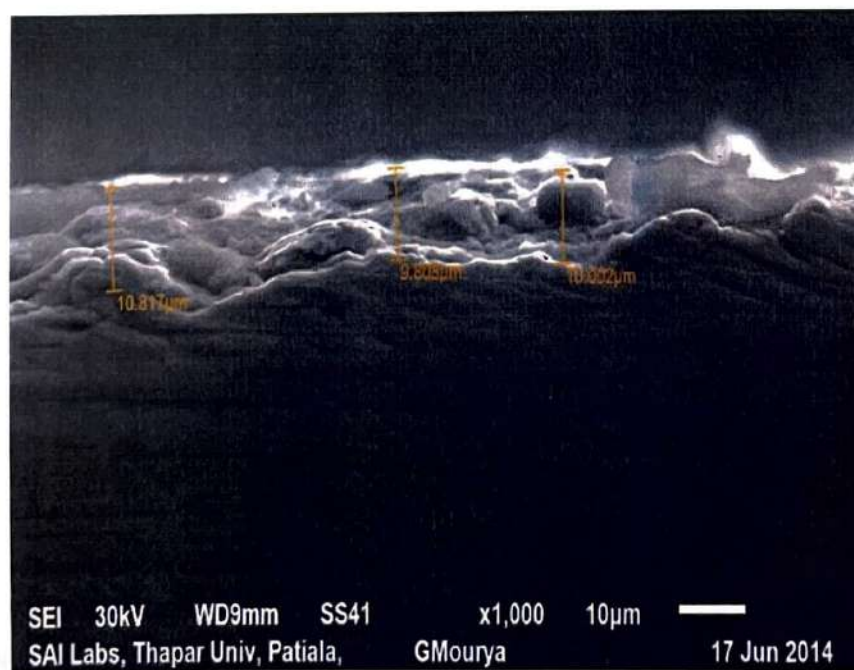


**Figure 8.6:** SEM Image of Transverse Section of Sample 4 (Ton 112μs, SV 40V, W<sub>d</sub> 10μm, FR 2 L/min)



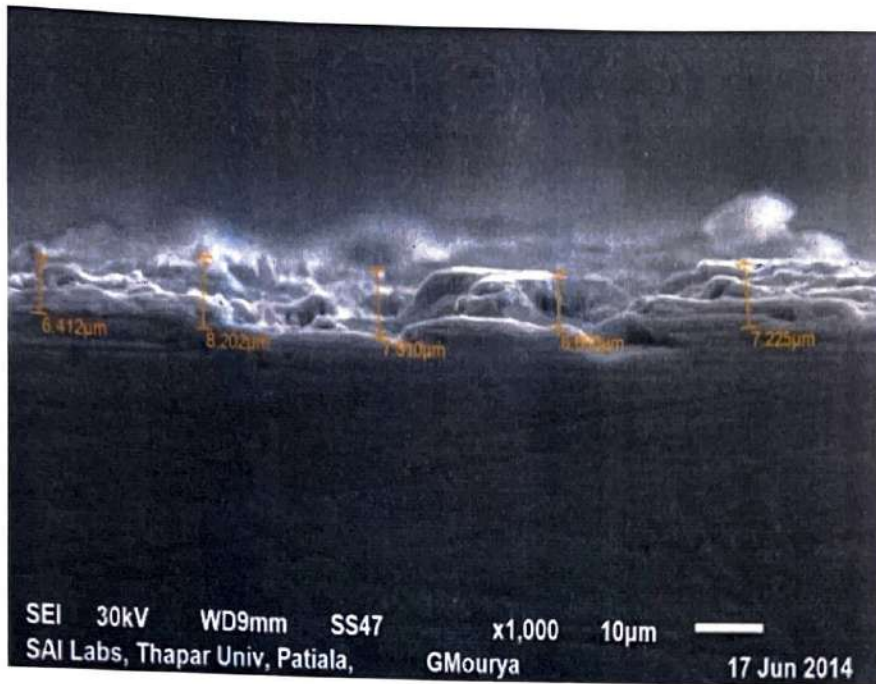


**Figure 8.7:** SEM Image of Transverse Section of Sample 15 (Ton 104μs, SV 40V, W<sub>d</sub> 30μm, FR 6 L/min)

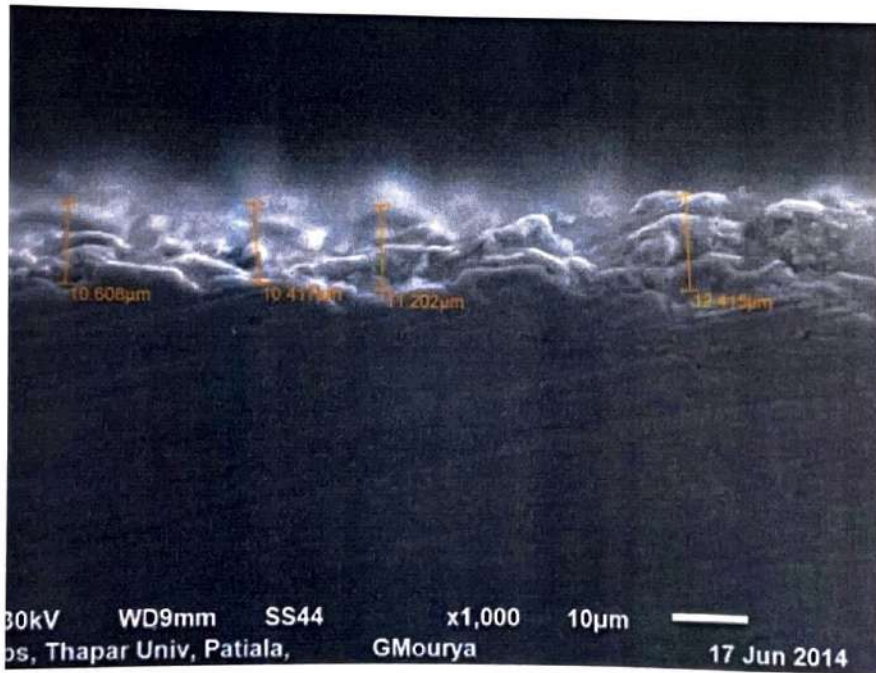


**Figure 8.8:** SEM Image of Transverse Section of Sample 26 (Ton 108μs, SV 30V, W<sub>d</sub> 20μm, FR 4 L/min)

RCL is observed which is discontinuous and non-uniform and the average thickness of damaged surface varies from 6μm to 12 μm. At high DE, melting and evaporation of material

generate gas bubbles causing high pressure energy in plasma channel (Li et al., 2013, Wang et al. 2009) which plough out the material from the work surface and create large size irregularities on work surface.

#### 8.4.2 Analysis of Dimensional Shift ( $D_s$ ) in Trim Cutting Operation

Dimensional shift ( $D_s$ ) is the thickness of material removed perpendicular to the cutting direction of wire electrode in trim cutting operation only. It depends on the melting, evaporation and flushing of the surface material. Fit summary for  $D_s$  suggested that quadratic model is statistically significant for analysis. Table 8.7 shows ANOVA for  $D_s$  after backward elimination process. The Model F-value of 193.29 implies that model is significant. There is only a 0.01% chance that a "Model F-Value" this large could occur due to noise. Values of "Prob > F" less than 0.050 indicates that model terms are significant. In this case A, B, C, D, AD, BC, CD,  $A^2$ ,  $B^2$ ,  $C^2$ ,  $D^2$  are significant model terms. The "Lack of Fit F-value" of 1.02 implies there is a 953.58 % chance that a "Lack of Fit F-value" this large value could occur due to noise. The "Pred R-Squared" of 0.9916 is in reasonable agreement with the "Adj R-Squared" of 0.9865. "Adeq Precision" measures the signal to noise ratio. A ratio greater than 4 is desirable. Figure 8.9 shows that the residuals are normally distributed about a straight line which means that the errors are normally distributed. It is observed from Figure 8.10 that all the actual values are following the predicted values. The final response equation after eliminating the non – significant terms for dimensional shift is as follows:

(In terms of actual parameters)

$$\begin{aligned} \text{Dimensional Shift} = & -1963.695 + 37.021 * \text{Ton} + 1.392 * \text{SV} - 1.501 * W_d - 31.036 * \text{FR} - \\ & 0.173 * \text{Ton}^2 - 8.0454 E - 0.0277 * \text{SV}^2 + 0.0572 * W_d^2 + 0.932 * \text{FR}^2 + 0.242 * \text{Ton} * W_d + \\ & 0.0193 * \text{SV} * W_d - 0.0343 * W_d * \text{FR} \end{aligned} \quad (8.2)$$

Increase in the value of Ton results into high heat generation that increases the melting and evaporation of work material and hence the value of  $D_s$  increases as shown by response surface plot in Figure 8.11a. Increase in FR increases the flushing rate of eroded particles and hence  $D_s$  increases with increasing FR and Ton.  $D_s$  increases with decrease in the value of SV as shown in Figure 8.11b. Increasing the value of wire depth ( $W_d$ ) increases the effective sparking on work surface and hence melting and erosion of the surface material increases as a result,  $D_s$  increases {Figure 8.11c}. The interactions among the parameters are noticed by the contour plot on 3D surface plot.

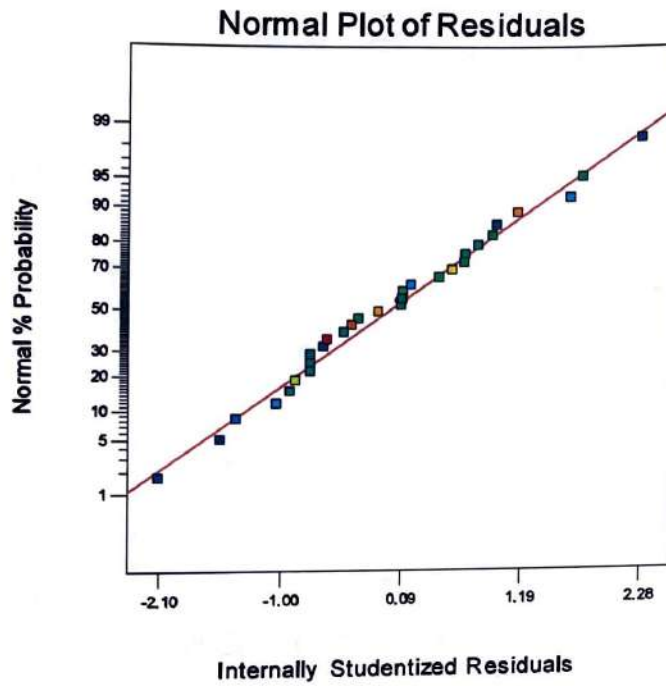


**Figure 8.9:** Normal probability Residuals plot for SR in Trim Cutting Operation

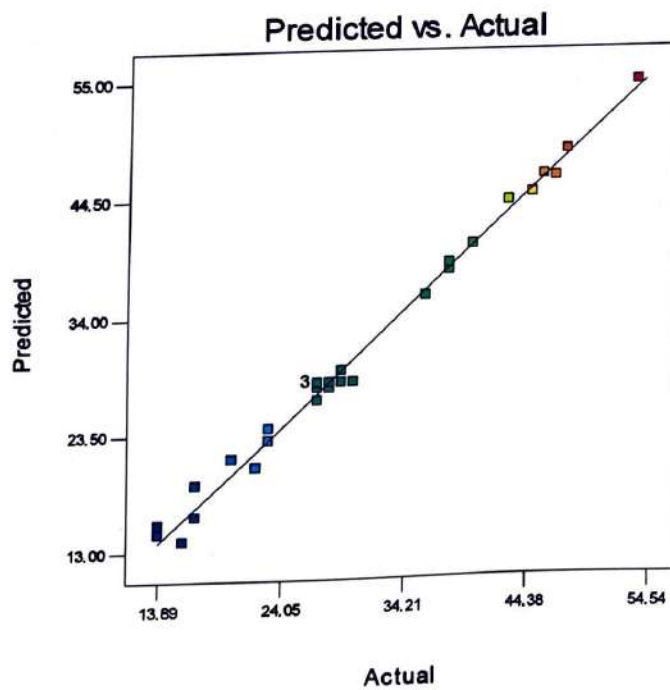
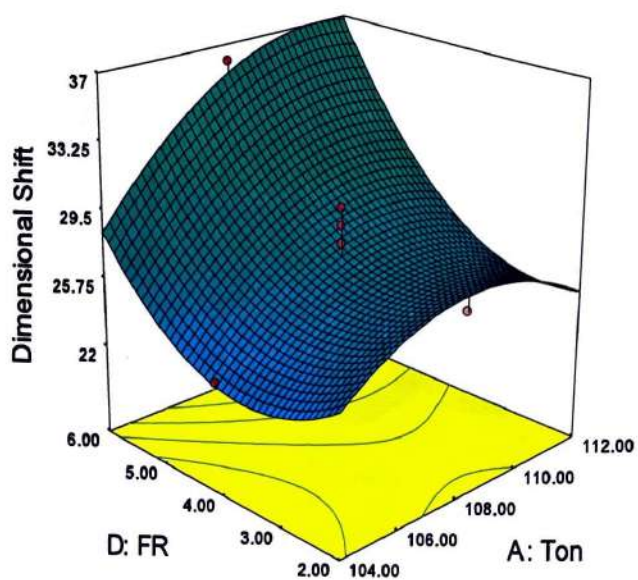


**Figure 8.10:** Predicted vs. Actual Plot for SR in Trim Cutting Operation

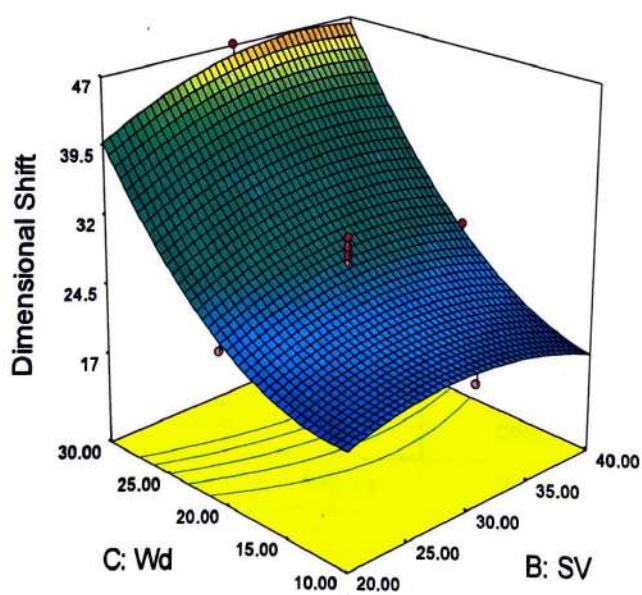


Table 8.7: ANOVA for Ds in Trim Cutting Operation

Source	Sum of Squares	Degree of freedom	Mean Square	F-value	p-value	
Model*	3444.21	11	313.11	193.29	< 0.0001	Significant
Ton	93.38	1	93.39	57.65	< 0.0001	
SV	24.5	1	24.5	15.12	< 0.0011	
W <sub>d</sub>	2738	1	2738	1690.27	< 0.0001	
FR	256.88	1	256.88	158.58	< 0.0001	
Ton * FR	60.06	1	60.06	37.07	< 0.0001	
SV * W <sub>d</sub>	60.06	1	60.06	37.07	< 0.0001	
W <sub>d</sub> * FR	7.56	1	7.56	4.66	0.0444	
(Ton) <sup>2</sup>	19.90	1	19.91	12.28	0.0025	
(SV) <sup>2</sup>	19.90	1	19.91	12.28	0.0025	
(W <sub>d</sub> ) <sup>2</sup>	85.01	1	85.01	52.47	< 0.0001	
(FR) <sup>2</sup>	36.01	1	36.01	22.23	0.0002	
Residual	29.16	18	1.62			
Lack of fit	21.16	13	1.63	1.0171	0.5358	Not significant
Pure error	8.00	5	1.60			
Cor. Total	3473.37	29				
<div><div>R<sup>2</sup> = 0.9916</div><div>Pred R-Squared = 0.9751</div><div>R<sup>2</sup> (Adj.) = 0.9865</div><div>Adeq Precision = 50.503</div></div>						



**Figure 8.11a:** Combined effect of FR and Ton on  $D_s$  (SV: 30V;  $W_d$ : 20 $\mu$ m)



**Figure 8.11b:** Combined effect of  $W_d$  and SV on  $D_s$  (Ton: 108 $\mu$ s; FR: 4L/min)

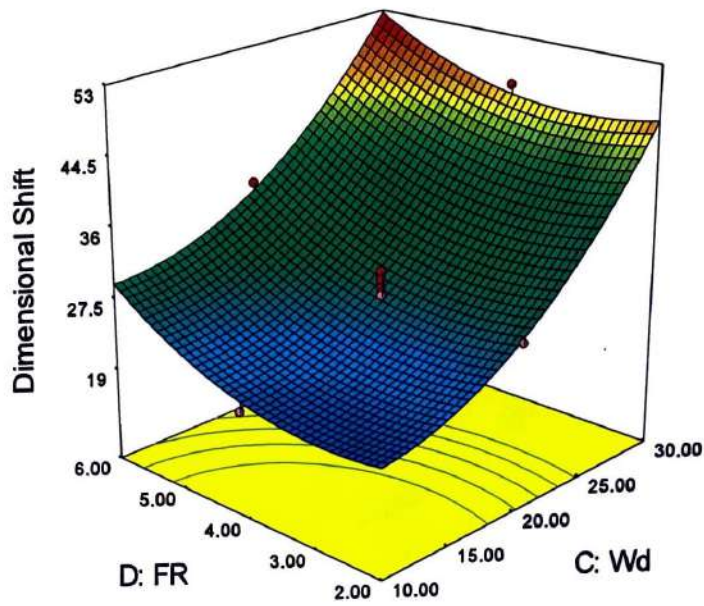


**Figure 8.11c:** Combined effect of FR and  $W_d$  on  $D_s$  (Ton: 108 $\mu$ s; SV: 30V)

### 8.5 MULTI RESPONSE OPTIMIZATION USING DESIRABILITY FUNCTION IN TRIM CUTTING

In order to obtain an optimum parametric setting for two performance characteristics, desirability function is utilised. The goal is to find optimal parameters' setting that maximizes the overall desirability function for minimum SR and  $D_s$ . Ranges and targets of inputs parameters namely Ton, SV,  $W_d$  and FR and the response characteristics SR and  $D_s$  are given in Table 8.8.

**Table 8.8:** Range of Input Parameters and Responses for Desirability (SR and  $D_s$ )

Constraints	Goal	Lower Limit	Upper Limit	Important
Ton	in range	104	112	3
SV	in range	20	40	3
$W_d$	In range	10	30	3
FR	In range	2	6	3
SR	Minimize	1.12	3.52	3
$D_s$	Minimize	14	54	3



### 8.5.1 Model 1: Surface Roughness (SR) and Dimensional Shift (D<sub>s</sub>)

The aim of optimization is to determine best combination of all parameters for finding the best results. A set of conditions corresponding to highest desirability value is selected as optimum condition for the desired responses. Table 8.9 shows the possible combination of WEDM process parameters that give the high value of desirability.

**Table 8.9: Process Parameters Combination for High Value of Desirability (SR and D<sub>s</sub>)**

Number	Process Parameters				Predicted Response		Desirability
	Ton( $\mu$ s)	SV(V)	W <sub>d</sub> ( $\mu$ m)	FR(L/min)	SR( $\mu$ m)	D <sub>s</sub> ( $\mu$ m)	
1	104.31	40.00	10.00	2.15	1.13	14.000	0.992
2	104.00	39.16	10.00	2.27	1.13	13.810	0.991
3	104.00	40.00	10.00	2.55	1.15	12.816	0.987
4	104.00	40.00	12.05	2.39	1.15	14.001	0.987
5	104.00	40.00	10.60	2.67	1.16	12.871	0.982
6	104.01	37.86	10.00	2.59	1.20	14.000	0.972
7	104.00	40.00	10.00	5.01	1.18	14.910	0.965
8	104.00	40.00	10.00	5.54	1.13	16.836	0.955
9	105.31	40.00	10.00	2.00	1.20	15.514	0.955
10	104.03	20.00	10.52	2.00	1.25	15.465	0.940
11	104.00	20.16	10.75	2.00	1.25	15.516	0.940
12	104.00	20.00	10.60	2.65	1.32	14.208	0.933
13	104.18	20.00	11.12	2.00	1.27	15.715	0.931
14	104.00	20.00	10.80	2.82	1.34	14.017	0.931
15	104.00	20.02	10.00	3.16	1.36	13.837	0.924
16	104.00	20.00	12.45	4.85	1.36	16.004	0.902
17	104.00	20.00	10.89	5.29	1.33	17.312	0.895
18	104.00	20.00	13.89	5.64	1.29	19.039	0.885
19	109.38	40.00	10.20	2.00	1.46	16.858	0.862
20	111.09	40.00	10.00	2.00	1.51	15.609	0.860

The ramp view drawn using Design Expert software shows the desirability for the output machining characteristics {Figure 8.12}. Bar graph shows the overall desirability function of the responses {Figure 8.13}.

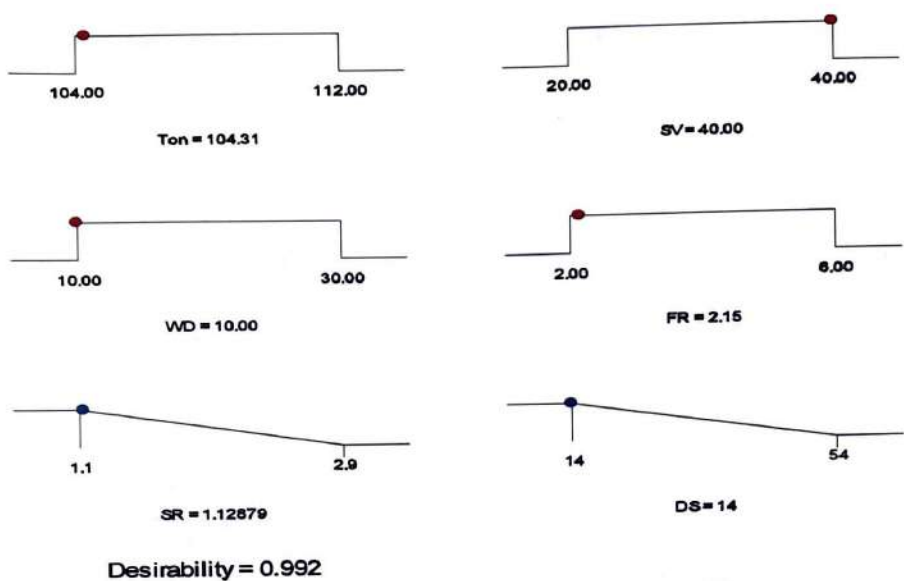


**Figure 8.12:** Ramp Function Graph of Desirability for SR and D<sub>s</sub>

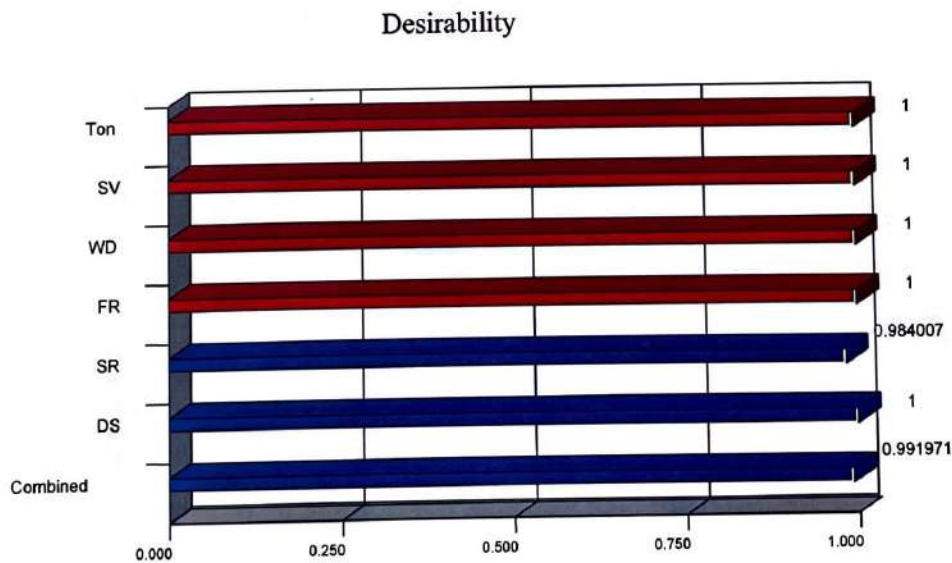


**Figure 8.13:** Bar Graph of Desirability for SR and D<sub>s</sub>

Desirability 3D-plots are drawn keeping input parameters in range, both SR and RoC at minimum {Figure 8.14-8.18}. Figure 8.19 shows the contour plot of overall desirability for multi-machining characteristics.

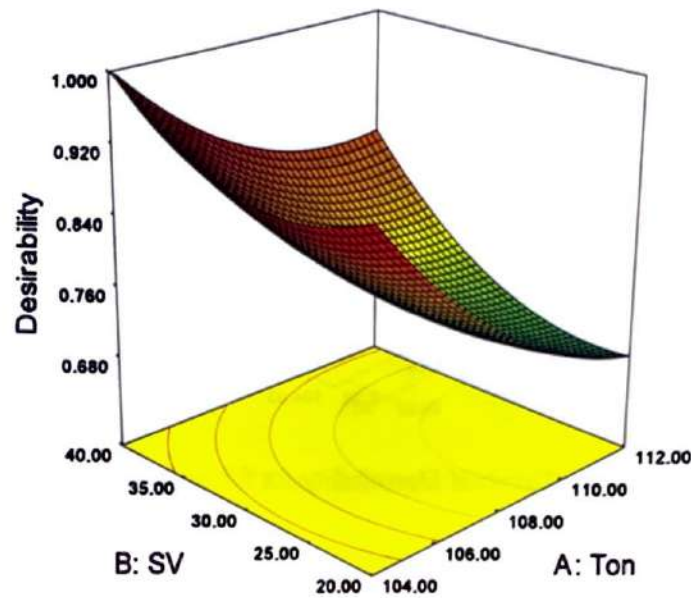


**Figure 8.14:** 3D Surface Graph of Desirability for SR and  $D_s$  ( $W_d$ : 10 $\mu$ m; FR: 2L/min)

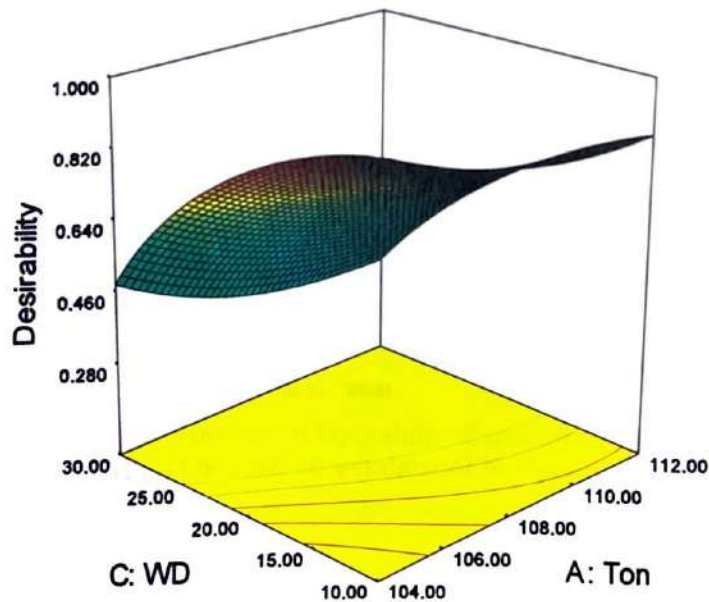


**Figure 8.15:** 3D Surface Graph of Desirability for SR and  $D_s$  (SV: 40V; FR: 2L/min)



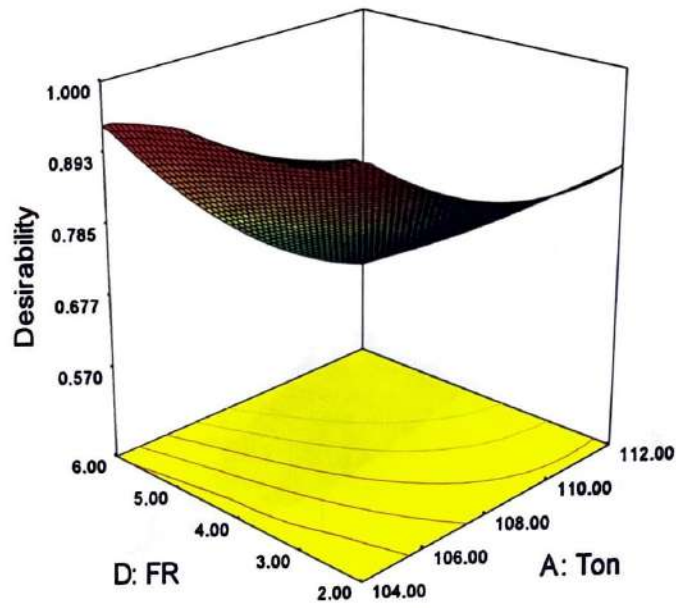


Figure 8.16: 3D Surface Graph of Desirability for SR and  $D_s$  (SV: 40V;  $W_d$ : 10 $\mu$ m)

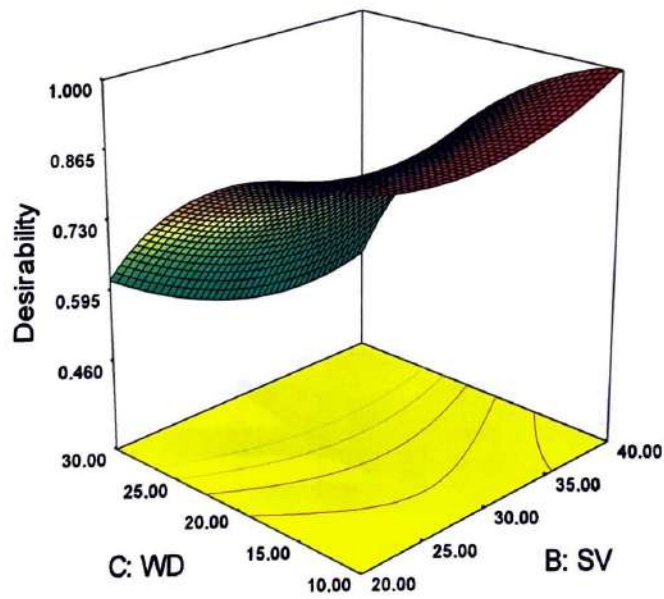
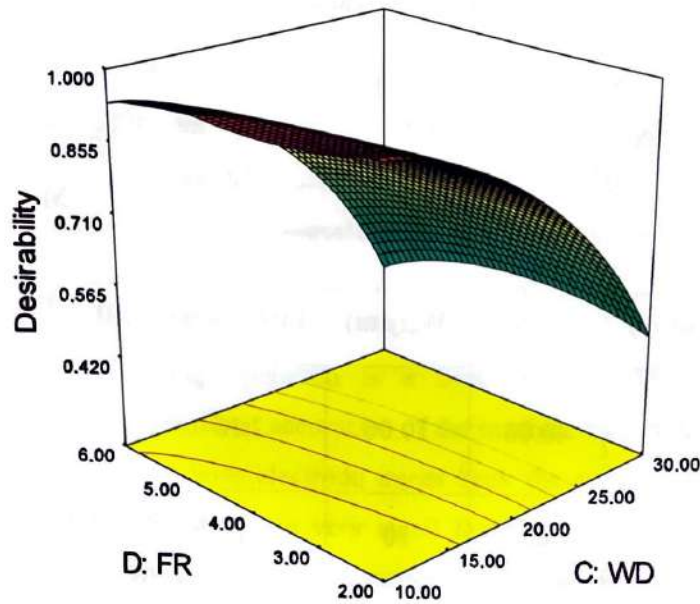
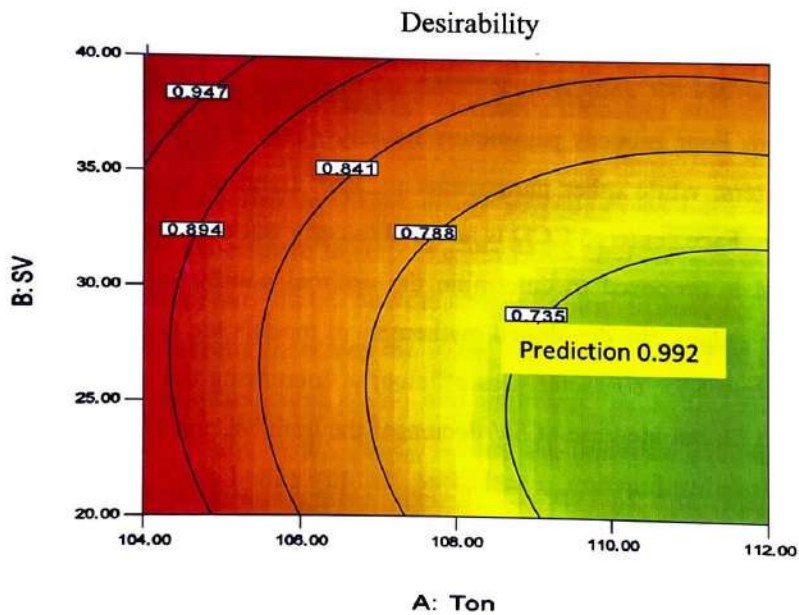


Figure 8.17: 3D Surface Graph of Desirability for SR and  $D_s$  (Ton: 104 $\mu$ m; FR: 2L/min)



**Figure 8.18:** 3D Surface Graph of Desirability for SR and  $D_s$  (Ton:  $104\mu\text{m}$ ; SV: 40V)



**Figure 8.19:** Contour Plot for Overall Desirability Function ( $W_d$ :  $10\mu\text{m}$ ; FR: 2L/min)

Corresponding to highest desirability, optimal combination of WEDM parameters for multi-machining characteristics are obtained. Confirmation experiments are conducted at this optimal setting and the average experimental values obtained for SR and  $D_s$ . The confirmatory results are very close to the predicted values that shows the goodness of the

proposed models and desirability approach. Table 8.10 shows predicted and confirmatory values of SR and D<sub>s</sub>.

**Table 8.10: Predicted and Confirmatory Values of SR and D<sub>s</sub>**

	Machining Parameters				Machining Characteristics	
	Ton(μs)	SV(V)	W <sub>d</sub> (μm)	FR(L/min)	SR(μm)	D <sub>s</sub> (μm)
Predicted values	104.31	40.00	10.00	2.15	1.13	14.000
confirmatory values	104	40	10	2	1.1	16

### 8.6 DISCUSSION

Trim cutting operation in WEDM is performed on Nimonic 90. Two performance characteristics namely SR and D<sub>s</sub> in WEDM are modelled and analysed using RSM in trim cutting operation. Four process parameters namely- Ton, SV, W<sub>d</sub> and FR are selected as variable parameters; while other parameters are kept fixed at their optimal setting in trim cutting operation. Face centered CCD is adopted to carry out experimental study. Quadratic model is proposed to determine the optimal combination of SR and D<sub>s</sub>. Using response surface graphs, the developed mathematical models are able to explain the effect of variables on performance characteristics efficiently. Increasing the value of Ton, W<sub>d</sub> and FR increases SR and D<sub>s</sub> but increase of SV decreases the both SR and D<sub>s</sub>.

Using desirability function, a scale free quantity called desirability is obtained for two performance characteristics to optimize multi-performance characteristics. Corresponding to highest desirability, the optimal combination of discharge parameters are Ton: 110 μs; SV 40V; W<sub>d</sub>: 10 μm and FR 2 L/min. Confirmation experiments prove the goodness of the proposed models and desirability function approach.

Using SEM image, effect of DE on surface morphology is examined. Average thickness of recast layer varies from 6 μm to 12 μm is found on the machines surfaced after trim cutting operation.



## CHAPTER-IX

# EXPERIMENTAL STUDY ON ROUGH AND TRIM CUT AND METAL POWDERS MIXED DIELECTRIC FOR WEDM OF NIMONIC-90

---

### 9.1 INTRODUCTION

In WEDM, trim cutting operation is a best option to improve the surface characteristics and dimensional accuracies of the machined surface. In trim cutting or finish cutting operation, wire electrode traces back the rough cut path with certain value of wire offset to remove a very small layer of work surface (Jangra, 2015; Sarkar et al., 2008). In rough cutting operation; spark zone is quite large as compared to trim cutting operation. As a result, the volume of molten metal is very high in rough cut which generates large pressure energy is spark zone that causes large size craters and cracks on work surface. In trim cutting operation, spark zone is influenced by WO value and discharge parameters. Therefore, using low DE parameters and accurate value of WO in trim cutting operation, damaged surface layer may be minimized or eliminated.

In the field of die sinking EDM, many investigations have been carried out using powders mixed dielectric to improve the MRR and surface characteristics. In EDM process, conductive metal powders reduces the insulating strength of the dielectric fluid and thereby increases the spark gap between the tool and work-piece, thus, the process becomes more stable and improves the MRR and surface finish (Kansal et al., 2005; Sidhu et al., 2014). As per the literature available, no research work is to be found on powders mixed dielectric in WEDM. Therefore, the concept of metal powders mixed dielectric is attempted for WEDM in present work. In this chapter, a comparative analysis of rough and trim cut using distilled water and trim cut with metal powders mixed distilled water is presented. The influence of two metal powders namely Al and Si (varying concentration of 1g/L, 2g/L and 3g/L) is an evaluated on CS and surface characteristics of Nimonic-90

## 9.2 EXPERIMENTAL PROCEDURE

### 9.2.1 Setup for Supplying of Metal Powders Mixed Dielectric Fluid

In rough cut operation of WEDM, the area covered by the spark zone around the wire electrode is large and the spark gap between wire electrode and work surface in the direction of cutting is very small and therefore, the dielectric fluid is used at high pressure to flush the eroded particles from the spark zone. If the metal powders mixed dielectric fluid is used at high pressure, the effect of powders additives on machining performance will not be justified. Also, due to the recirculation of dielectric fluid in WEDM setup, mixing of metal powders directly in dielectric tank (having large size  $\geq 400$  litres) is not economical. Therefore, the use of metal powders in dielectric fluid for rough cut of WEDM is quite challenging as compared to die sinking EDM where dielectric fluid (kerosene or distilled water) mixed with metal powders is easily pumped under the electrode facing the work material. However, in trim cutting operation, work surface in contact with wire electrode periphery is small which requires a laminar dielectric flow for effective sparking. Therefore, the idea of metal powders mixed dielectric is attempted in trim cutting operation only.

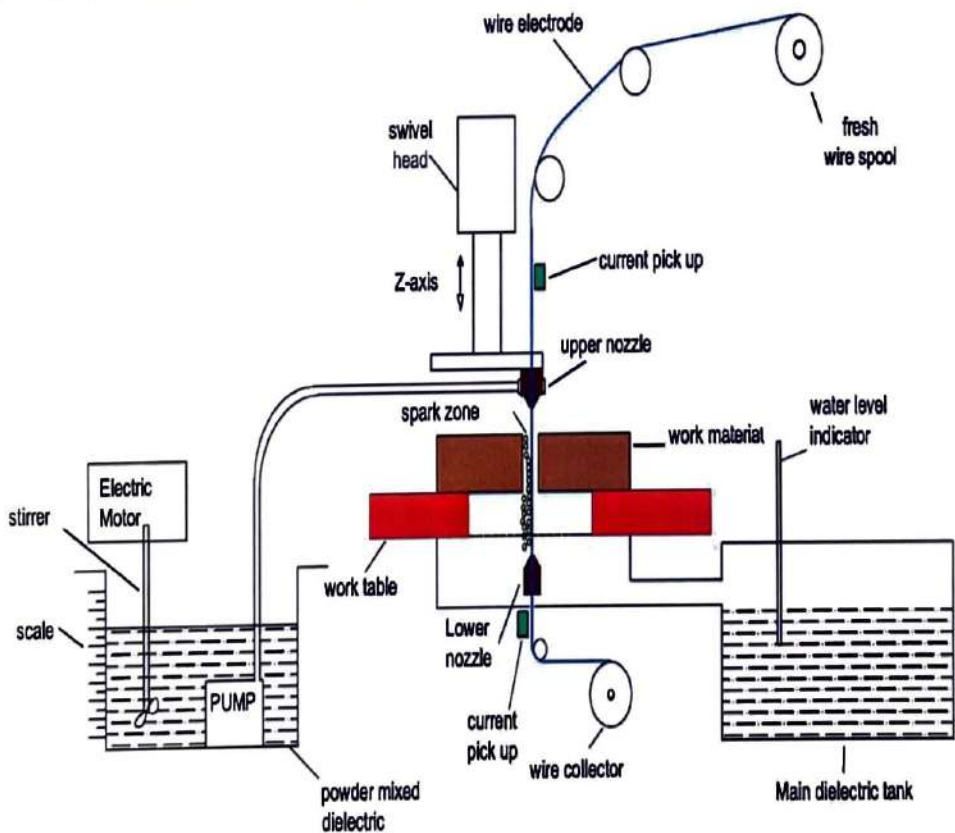


**Figure 9.1:** Experimental Setup for Powders Mixed WEDM (PWEDM)

A separate tank of size 40 litres is used to mix the powders in dielectric water and to pump the metal powders mixed dielectric fluid in trim cutting operation. Figure 9.1 shows the experimental setup. To supply the metal powders mixed distilled water in trim cut operation, a small capacity water pump is connected to the upper nozzle through a connector pipe and the lower nozzle is disconnected from main dielectric tank.

### 9.2.1 Machined Geometry

Nimonic 90 as Work material is available in the form of rectangular sheet of thickness 12.5 mm and the work samples are obtained in the form of rectangular punches of size 8 mm  $\times$  6 mm  $\times$  12.5 mm. Figure 9.2 shows the geometry or the wire path that is followed for rough and trim cut.

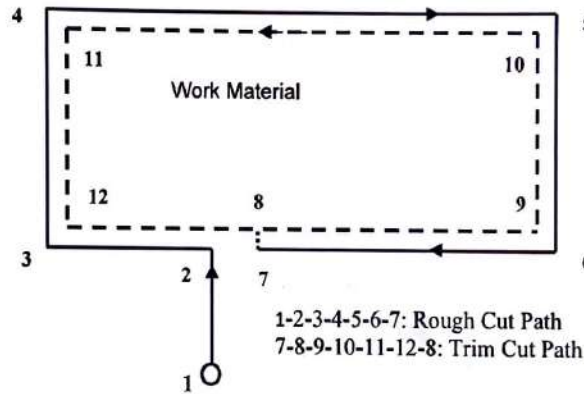


**Figure 9.2:** Geometry of Wire Path for Rough and Trim Cutting Operation

### 9.2.3 Machining Conditions

Experimental work is divided into three categorised as;

- Rough cutting operation performed at high DE.
- Rough cut at high DE followed by a single trim cut using distilled water as dielectric fluid.
- Rough cut at high DE followed by a single trim cut using metal powders (Al/Si) mixed distilled water as dielectric fluid.

Distilled water is used as a dielectric fluid. To control the discharge energy across the work material, values of discharge parameters namely Ton, Toff, Ip and SV are varied. High flow rate of dielectric fluid is desirable in rough cutting operation for quick and complete flushing of the melted debris out of the spark gap. Therefore, for rough cutting operation, dielectric flow rate was kept at high value of 12 litres per



minute ( $LM^{-1}$ ). To minimize the wire consumption, wire feed rate was kept at low value of 5m/min.

According to Jangra KK (2015), low DE along with a laminar dielectric flow is required for trim cutting operation to obtain effective spark generation for fine surface finish. Therefore, for trim cutting operation, a low dielectric supply is allowed through upper nozzle while bottom nozzle is closed. Table 9.1 shows the process parameters for rough and trim cutting operation.

**Table 9.1: Parameters Setting for Rough and Trim Cutting Operations**

Type of Operation	Dielectric Used	Dielectric Conditions	WO ( $\mu m$ )	Discharge Parameters		Wire Electrode Parameters	Other Fixed parameters
Rough Cutting Operation	Distilled water	Dielectric Pressure: High Flow rate: Upper nozzle: 12L/M Lower nozzle: 12L/M	Zero	High DE	Ton:118 Toff:43, Ip:120; SV:25	WT: 8 WF: 5  Servo Feed: 0200	Work piece height: 12.5mm; Wire diameter: 250 $\mu m$ ;  Wire material: Zinc coated brass
Trim Cutting Operation	Distilled water	Dielectric Pressure: Low Flow rate: Upper nozzle: 3L/M Lower nozzle: closed	105	Ton:105; Ip:100; Toff:30, SV:30		WT: 10; WF: 2  Servo Feed: 0150	
	Metal powders mixed distilled water	Dielectric Pressure: Low Flow rate: Upper nozzle: 4L/M Lower nozzle: closed	105				

Ton:  $\mu s$ ; Toff:  $\mu s$ ; Ip: A; SV: V; WT: N; WF: m/min;

### 9.3 RESULTS AND ANALYSIS

Experiments are conducted for rough and trim cutting operation corresponds to the parameters settings mentioned in Table 9.1. The influence of these parameter settings for rough cut and trim cutting operation is compared for SR and surface morphology. Also the influence of Al and Si metal powders (with a concentration of 1g/L, 2g/L and 3g/L) is evaluated and compared on these characteristics.

#### 9.3.1 Effect on Cutting Speed (CS)

CS represents the average speed of machining (m/min.) of work material in linear direction which is observed from the monitor of the machine tool.

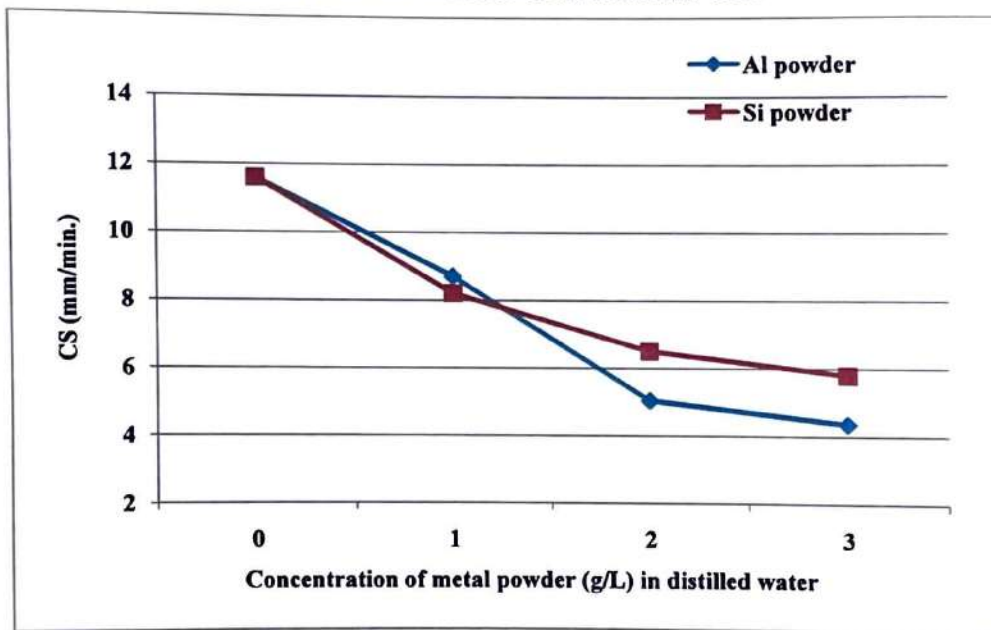


**Figure 9.3(a):** Influence of Concentration of Metal Powders on CS for Trim Cut

Figure 9.3(a) show a comparative chart of the CS for the experiments for trim cutting operation using simple distilled water and using Al and Si powders mixed distilled water as dielectric fluid. Increasing the concentration of metal powders in dielectric fluid decreases the CS remarkably as shown in Figure 9.3(a). It is observed that addition of both types of metal powders in distilled water resulted in improved and continuous sparking across the electrodes. In powders mixed EDM (PMEDM), CS increases due to the addition of metal powders in dielectric (Kansal et al., 2005; Singh et al., 2014) but in presented work CS decreases.

In both, EDM and WEDM, addition of metal powders reduces the insulating strength of the dielectric fluid and thus, increases the discharge channel for a given value of discharge parameters (Kansal et al., 2005). This process increases the melting and erosion of work material in PMEDM and hence CS increases. In case of trim cutting operation of WEDM, due to increase in spark radius and spark frequency, discharge area between wire periphery and work surface increases. This increasing discharge area reduces the servo feed as compared to trim cutting without metal powders and thus CS decreases in trim cut using metal powders mixed dielectric. The addition of metals powders up to the concentration of 2g/L shows a remarkable reduction in CS but beyond 2g/L, the reduction is very low. Because of addition of more metal powders, do not participate in lower down the insulating strength of dielectric. As compared to Al, Si powders exhibits less discharging and hence the reduction in CS is low for Si powders.

### 9.3.2 Effect on Surface Roughness (SR)

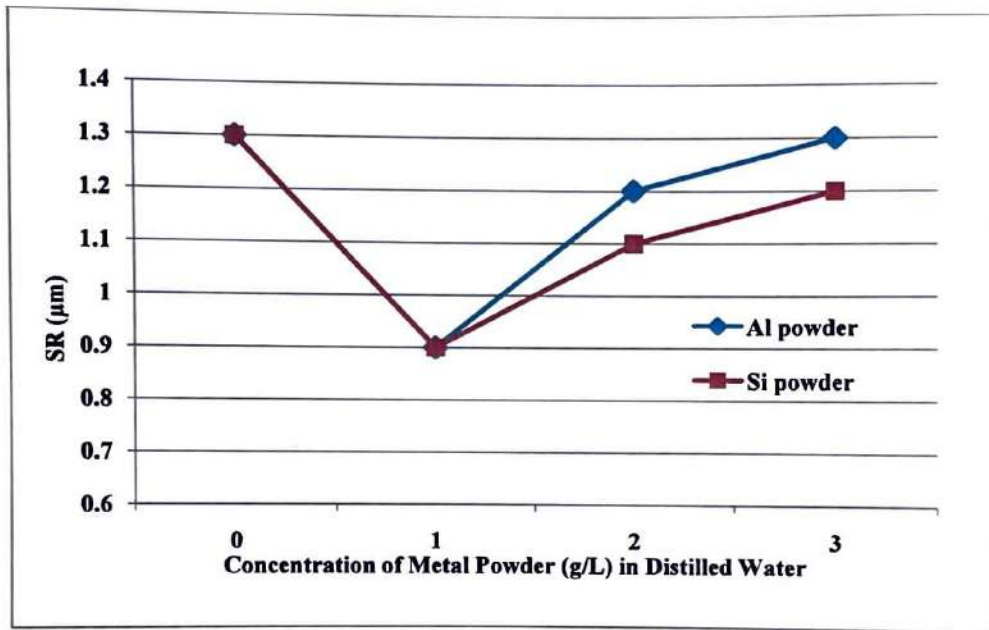
SR is characterized by the size and depth of the craters that are developed after the melting and expulsion of work material. Increasing DE increases the diameter and depth of surface craters resulting in high SR (Hewidy et al., 2005).

Figure 9.4 compares the surface roughness ( $R_a$  values) for the experiments performed under categories (a) and (b); that is rough cutting operations corresponding to high level of DE, a trim cut followed after rough cut using distilled water as dielectric fluid and trim cut using metals powders (Al/Si) mixed distilled water as dielectric fluid.

SR may be improved significantly using trim cutting operation irrespective of high DE in rough cutting operation. In trim cutting operation, a very thin layer of surface material is removed at appropriate wire offset value and thereby surface irregularities (peaks) are minimized to improve the SR. WO has a significant impact on SR for trim cut (Jangra, 2015; Sarkar et al., 2008). Decreasing the value of WO beyond 125 $\mu$ m (radius of wire), the area of contact between wire electrode and work surface increases. This increases the spark frequency and which in turn increases melting and erosion of work material increases. Increasing WO beyond 125  $\mu$ m will not be useful in generating the effective sparking because of large gap between wire electrode and work surface. Therefore, in present work, an effective WO of 105  $\mu$ m is selected, that represent  $D_{ww}$  of 20  $\mu$ m.



The addition of metal powders in a concentration of 1 g/L yields best surface finish of 0.90  $\mu\text{m}$ . Further addition of 1g/L of metal powders in distilled water causes better spark generation and distribution on work surface, which produces shallow craters on machined surface. The minimum achievable SR in WEDM is limited by the wire electrode diameter. Smaller the wire diameter, smaller the spark radius, and thus, smaller surface craters. By increasing the concentration of metal powders beyond 1g/L, the spark frequency and spark zone increases due to the reduction in insulating strength of dielectric, thus SR increases.



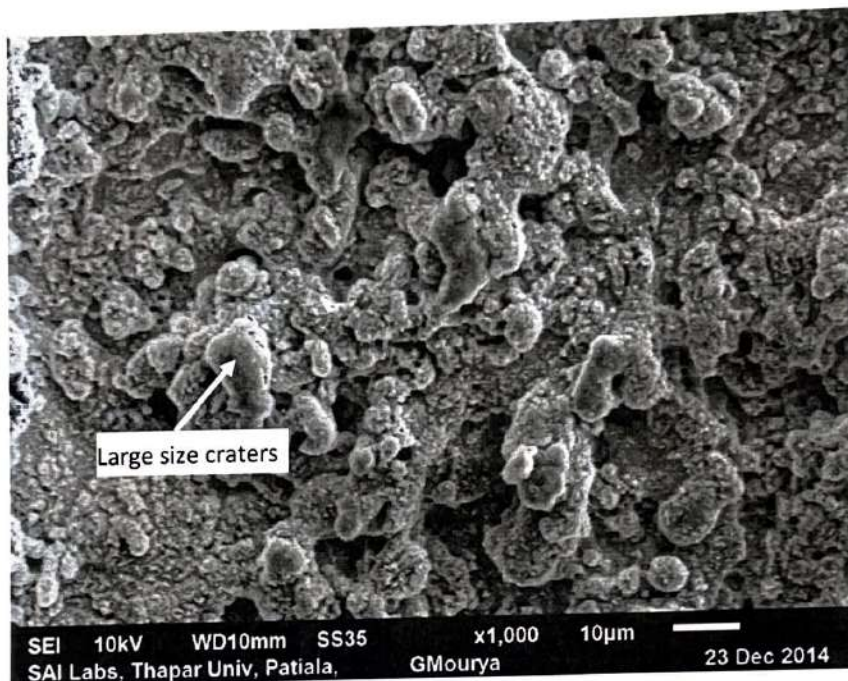
**Figure 9.4:** Influence of Concentration of Metal Powders in Dielectric Fluid for Trim Cut on SR

The melting point and resistivity for Si is high as compared to Al powders and sparking is low in case of Si powders mixed dielectric. Therefore, SR is low for Si powders. SR corresponds to 3g/L of Al powders is 1.3  $\mu\text{m}$  which is equal to SR value obtained in trim cut without metals powders. But the surface morphology for two different conditions is very different as discussed in subsequent section.

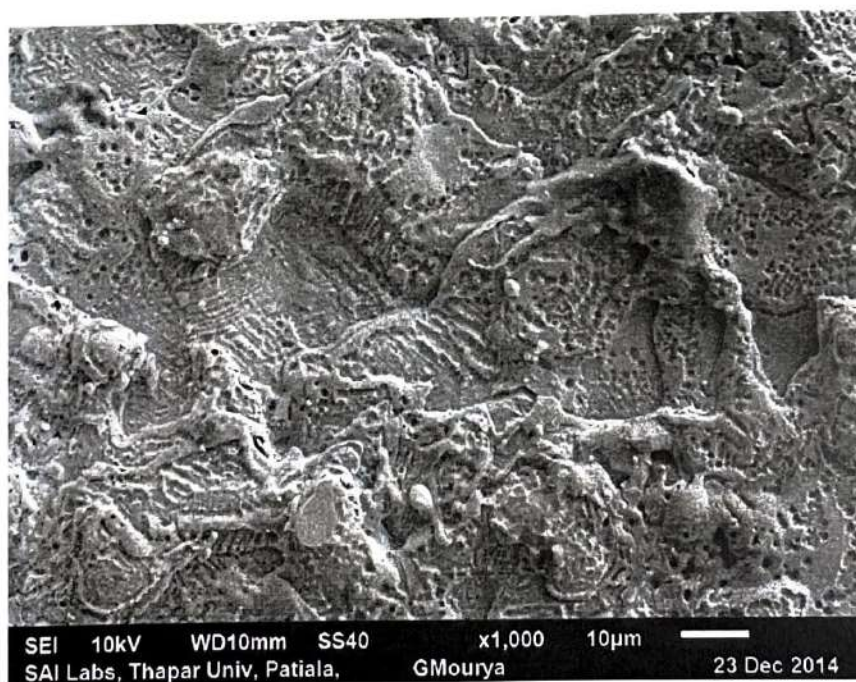
### 9.3.3 Surface Morphology and RCL

Figure 9.5 (a-d) and 9.6 (a-d) shows SEM images of the machined and transverse surface of work samples after (a) rough cut at high DE (b) trim cut (without metal powders) (c) trim cut using 3g/L Al powders (d) trim cut using 3 g/L Si powders in dielectric fluid. It is obtained from SEM images Figure 9.5 (a) that the machined

surface after rough cut at high DE consists of deep and large size craters. This is due to the fact that high DE causes overheating and evaporation of molten metal forming high pressure energy that creates large size craters (Li et al. 2013)



**Figure 9.5a:** SEM Image of Machined Surface after Rough Cut at High DE



**Figure 9.5b:** SEM Image of Machined Surface after Trim Cut (Without Metal Powders)



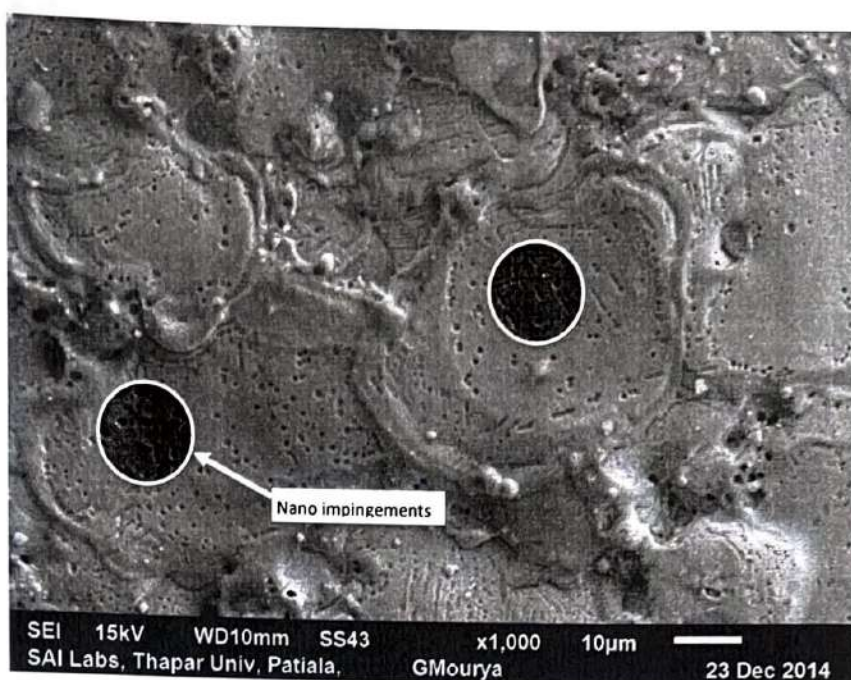


**Figure 9.5c:** SEM Image of Machined Surface after Trim Cut using 3g/L Al Powders in Dielectric

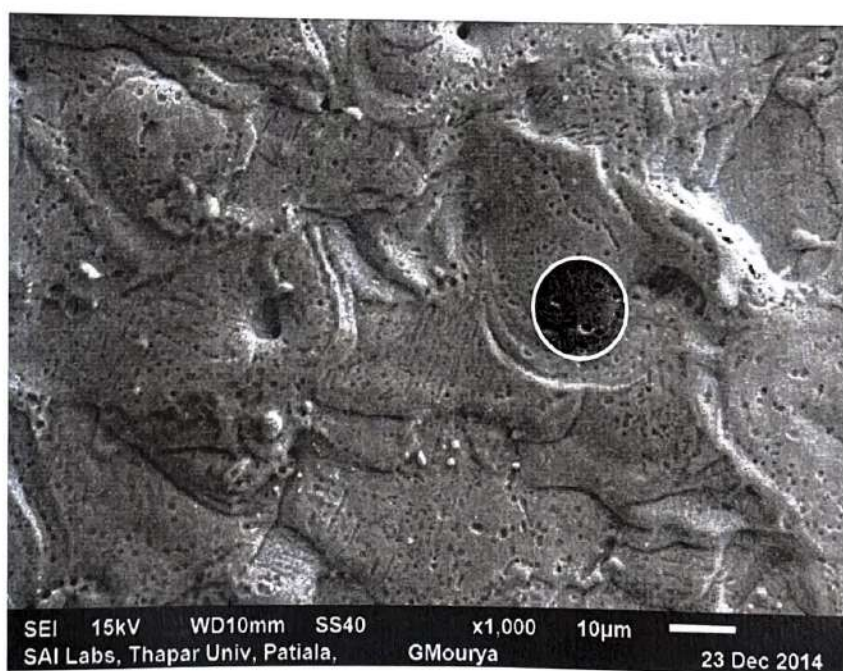


**Figure 9.5d:** SEM Image of Machined Surface after Trim Cut using 3 g/L Si Powders in Dielectric



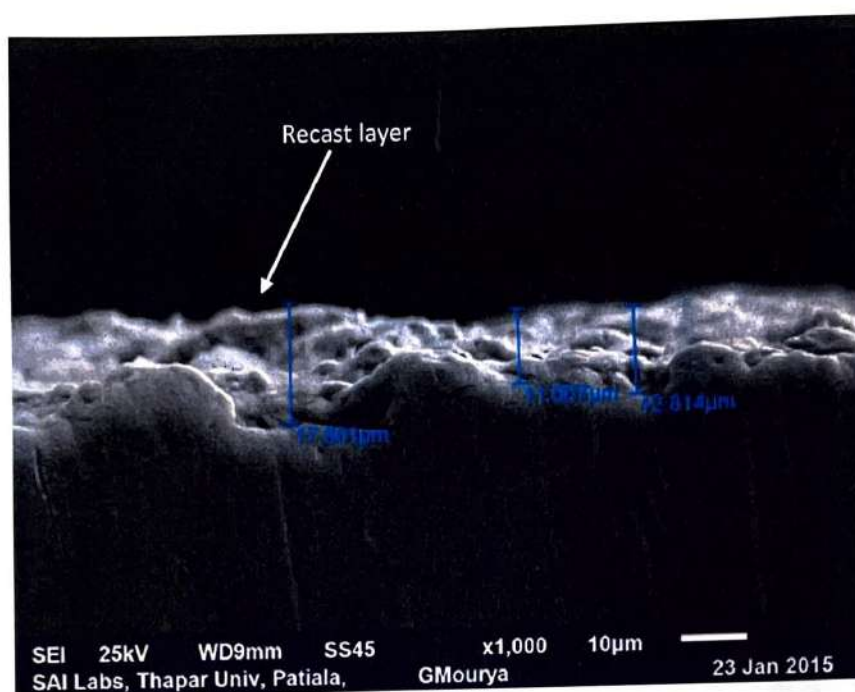


**Figure 9.6a:** SEM Image of Transverse Surface after Rough Cut at High DE

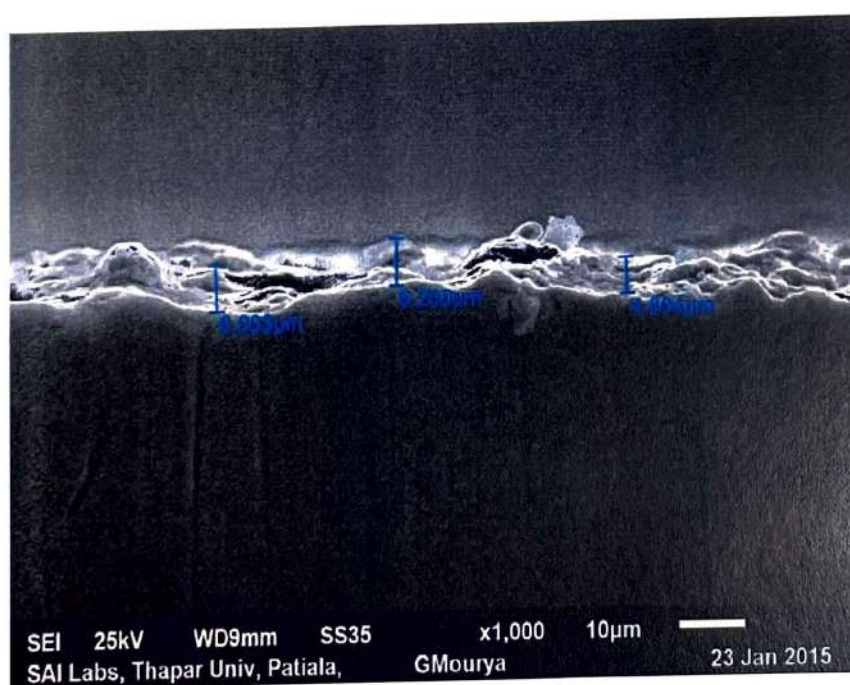


**Figure 9.6b:** SEM Image of Transverse Surface after Trim Cut (Without Metal Powders)

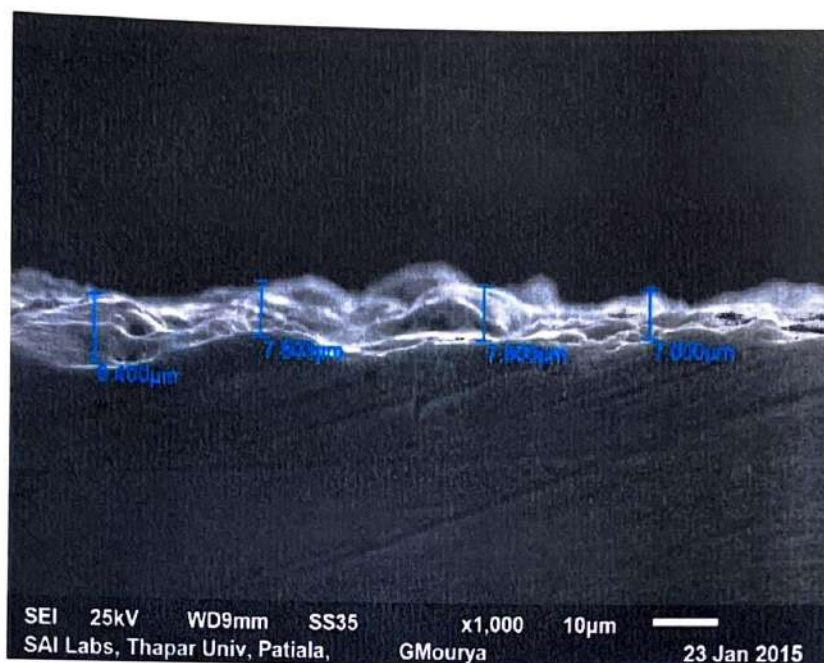


**Figure 9.6c:** SEM Image of Transverse Surface after Trim Cut using 3g/L Al Powders in Dielectric

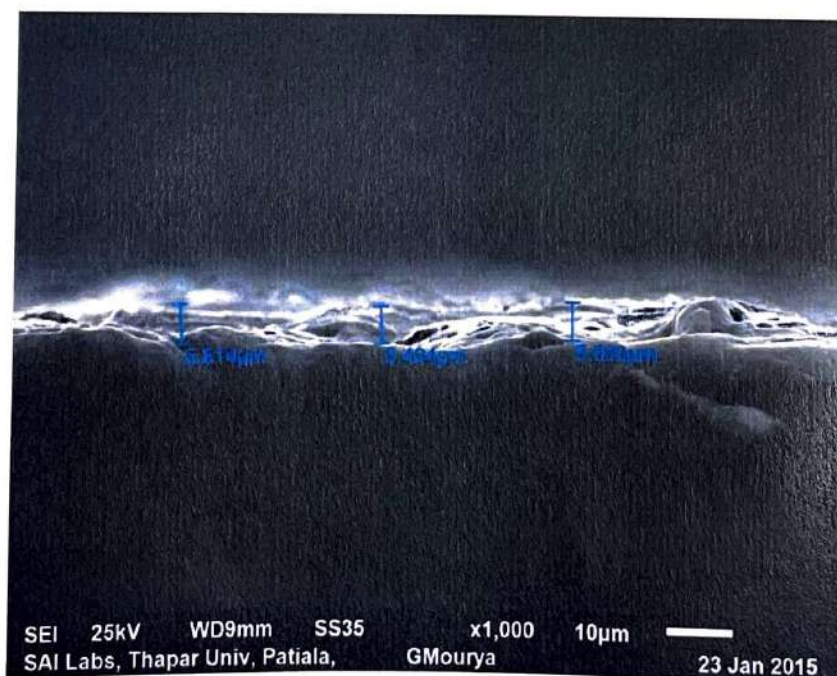


**Figure 9.6d:** SEM Image of Transverse Surface after Trim Cut using 3g/L Si Powders in Dielectric

Using trim cut at low discharge parameters, a thin layer of work surface is removed that completely eliminates the surface layer produced in rough cut. A fine and uniform surface texture obtained after trim cut as shown in Figure 9.5(b). Figure 9.5(c) and 9.5(d) shows a remarkable modification in surface textures after trim cut using metal powders mixed dielectric fluid. SEM image shows that the sparking on these surfaces is highly stable and uniformly distributed. Absence of carbon in Nimonic-90 and a stable sparking, gives a micro cracks free machined surface. Some nm sized impingements are observed on these surfaces as encircled in figure 9.5(c-d). This impingement may be due to the Al and Si powders that are not completely evaporated while sparking and thus, impinge at high pressure to the molten surface.

Figure 9.6 (a-d) shows the RCL on machined surface after rough and trim cutting operations. Figure 9.7 shows the average thickness of RCL corresponding to the different machining conditions. The average thickness of RCL (in  $\mu\text{m}$ ) for high DE for rough cut is found to be  $17.8 \mu\text{m}$  which is quite low as compared to steel alloys and WC-Co composites (Jangra, 2015) Trim cutting operation makes a remarkable reduction in thickness of RCL and is noticed from Figure 9.6(b) and Figure 9.7.

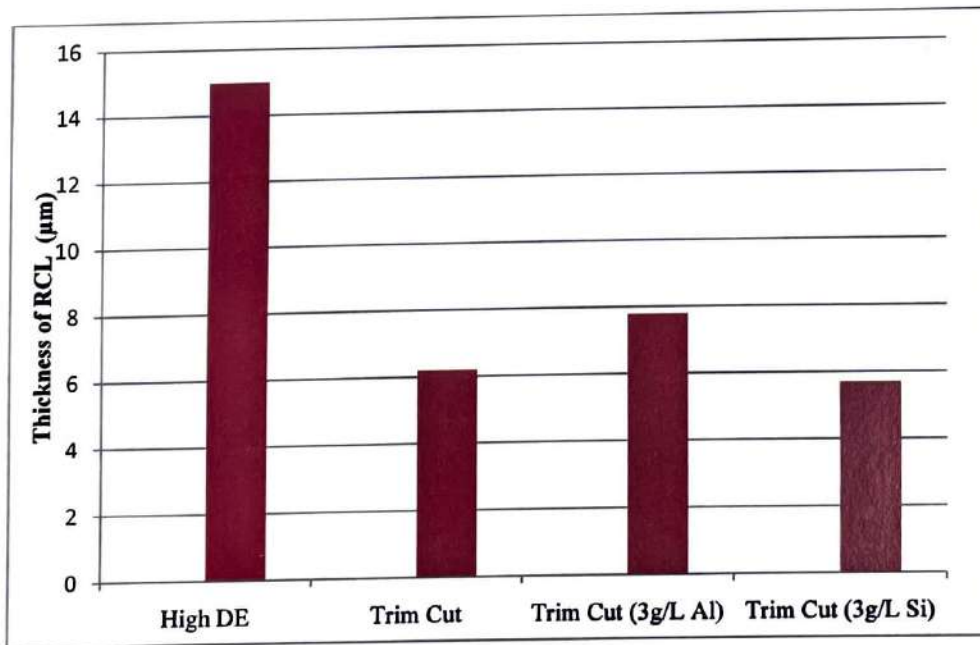
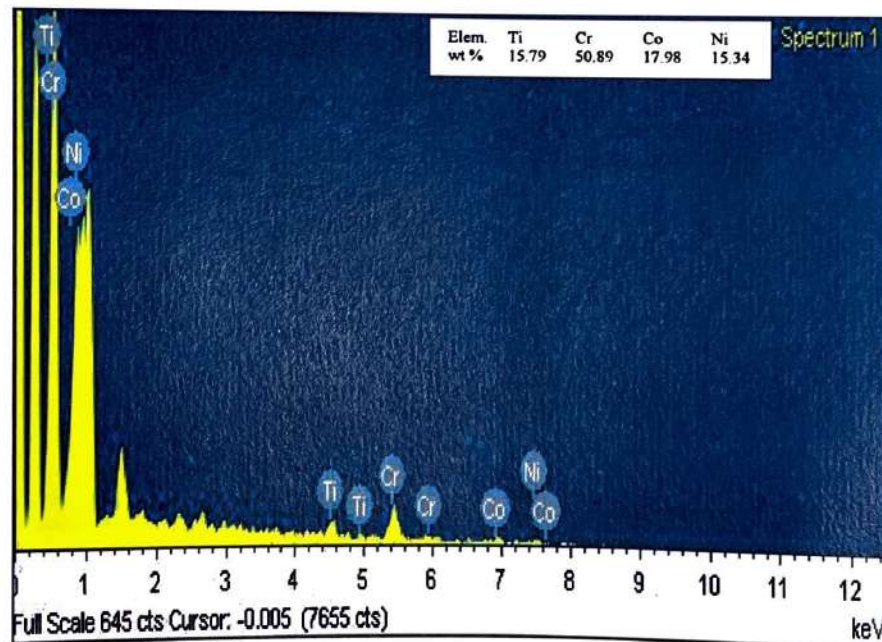


**Figure 9.7:** Comparison of Different WEDM Operations for Thickness of RCL

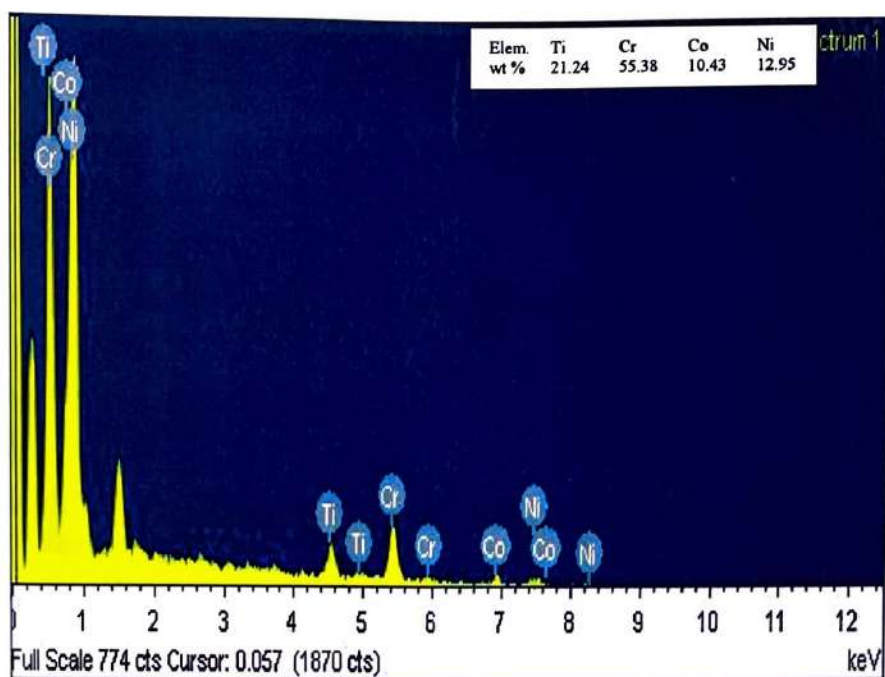


Figure 9.6(c) and (d) shows the thickness of RCL for metal powders mixed dielectric having the powders concentration of 3g/L for Al and Si powders respectively. Al powders results in little increase in TRL while Si powders results in a small reduction in thickness of RCL. An addition of Al powders beyond 1g/L results in increased discharge frequency and spark radius, thus, more melting and heating results in little increase in thickness of RCL. Due to high melting point and electrical resistivity of Si powders, less sparking occurs in Si powders in comparison to Al powders mixed dielectric. As result, thickness of RCL is low in case of Si powders mixed dielectric.

Energy dispersive spectroscopic (EDS) analysis is done on machined surface taking a spot area of 1000 sq.  $\mu\text{m}$ . Figure 9.8(a-d) presents the EDS analysis of machined surfaces shown in Figure 9.5. Figure 9.8(a) and 9.8(b) confirmed the presences of Ti, Cr, Co and Ni on machined surface while the presence of Al and Si elements is confirmed by EDS analysis shown in Figure 9.8(c) and 9.8(d) respectively.



**Figure 9.8(a):** EDS Analysis of Machined Surface after Rough Cut at High DE



**Figure 9.8(b):** EDS Analysis of Machined Surface after Trim Cut

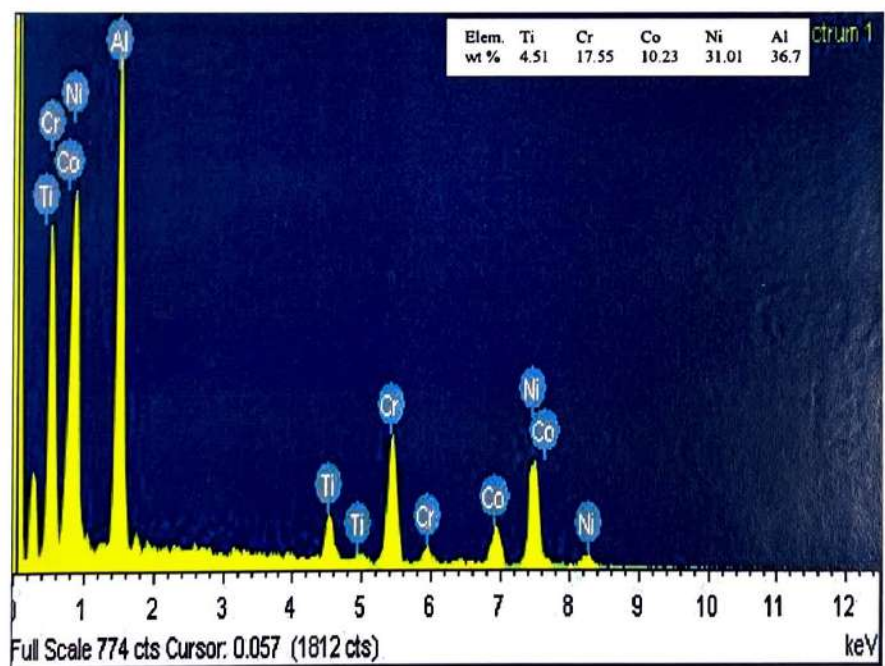


**Figure 9.8(c):** EDS Analysis of Machined Surface after Trim Cut using 3g/L Al Powders

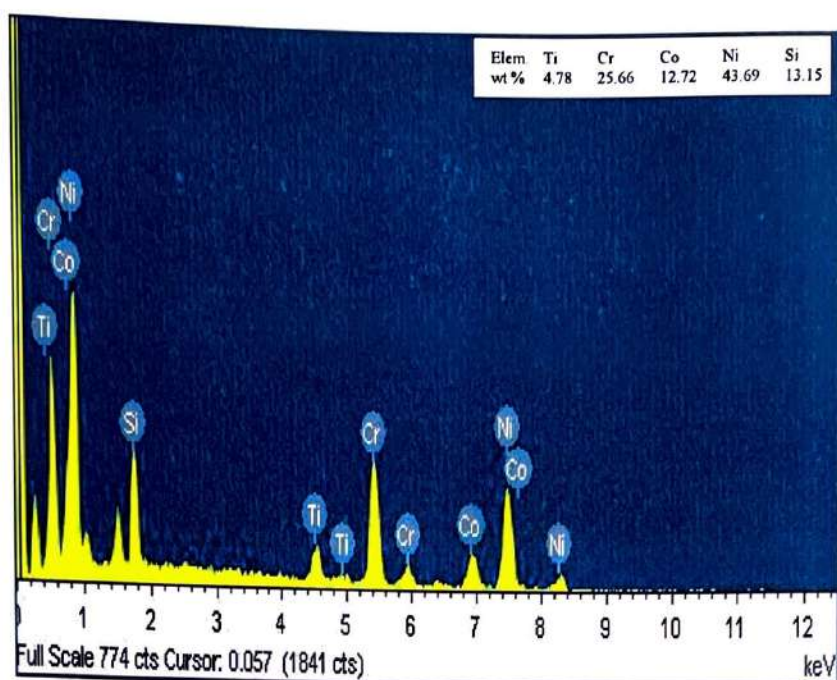


**Figure 9.8(d):** EDS Analysis of Machined Surface after Trim Cut using 3g/L Si Powders

### 9.3.4 Micro Hardness

Micro hardness test is used to measure the extent of surface damage caused by thermal energy of WEDM process. Therefore, micro-hardness is measured on transverse section of the machined surface. Micro-hardness profiles underneath the machined surface is shown in Figure 9.9 for the samples under rough cut (high DE), trim cut without metal powders and trim cuts using Al and Si powders in dielectric fluid.



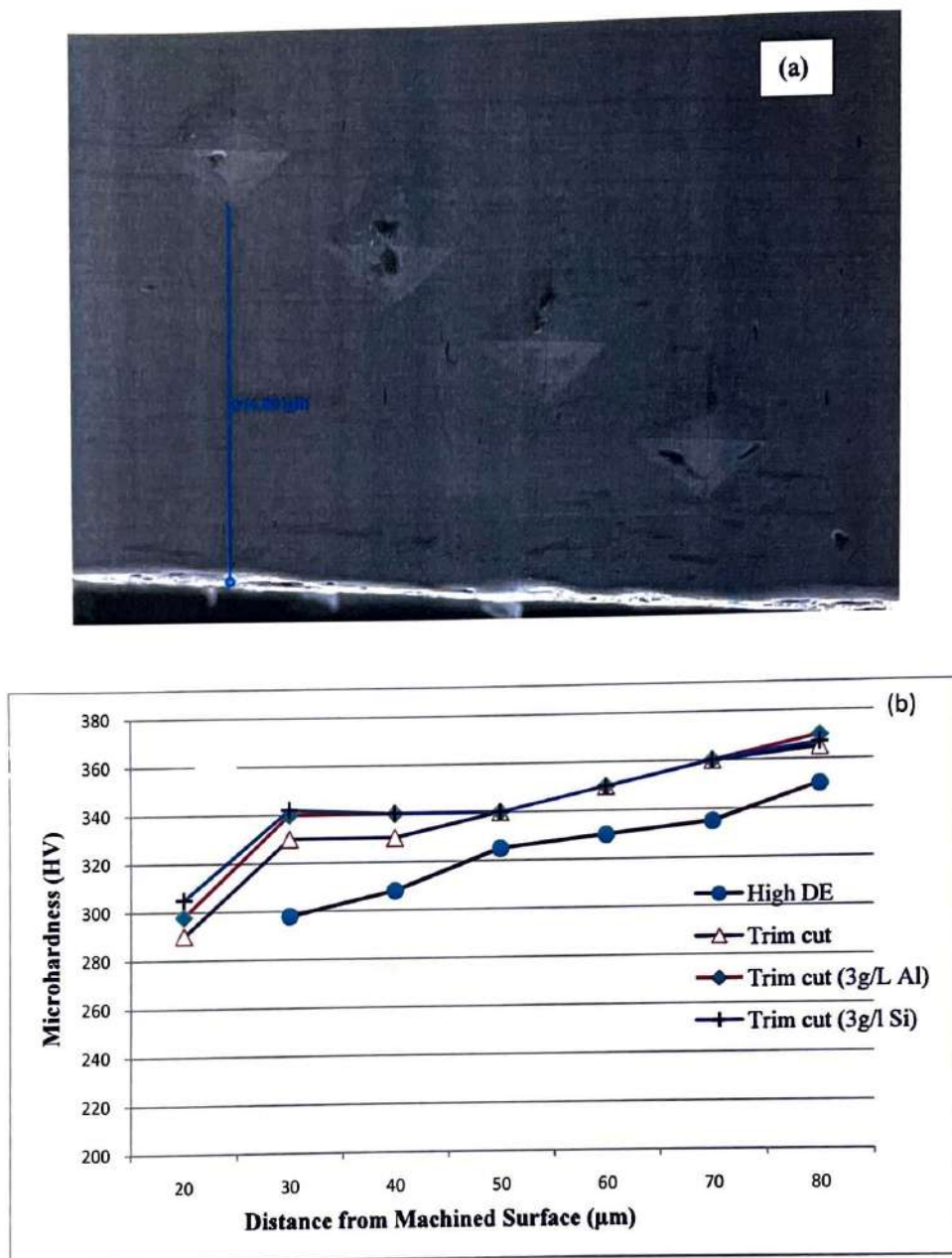


**Figure 9.9(a):** Micro Indent on Transverse Surface (b) Comparison of Micro-Hardness Underneath the Machined Surface Under Different Process Conditions.

Profiles show that the micro-hardness is low at the machined top layer as compared to bulk material. This reduction is due to the thermal damage of machined surface which is predominately due to the pressure energy generated inside the plasma channel and transfer of heat energy to the work material underneath the machined surface causing large heat affected zone (Li et al., 2013). The top damaged layer

consists of RCL while heat affected zone having longer grain size as compared to the bulk of the work material.

Using trim cut, this surface damage may be reduced as shown by the improved micro hardness profiles for trim cutting operation {Figure 8b}. It is worth to mention that measurement of micro hardness value corresponding to top machined layer is difficult because of the large surface damage at top surface that causes inaccurate impression of micro indent on this region. Therefore, the reading for micro hardness is missing up to 20  $\mu\text{m}$  underneath the top layer.

Using metal powders in dielectric fluid, the recast layer becomes smooth and dense as noticed from Figure 9.6(c-d). Therefore, the micro hardness improves using metals powders mixed dielectric fluid in trim cutting operation. In comparison to Al powders, Si powders results in denser machined surface and hence yields better machined surface.

## 9.5. DISCUSSION

This chapter presents a comparative experimental study on WEDM of Nimonic-90, for rough cut and trim cut without any metals powders additives and using Al and Si metal powders in dielectric fluid. The influence of DE for rough cut is evaluated for CS and SR and then, compared with trim cut without any metal powders additives in dielectric fluid. In succeeding experiments, influence of Al and Si metal powders in dielectric fluid is evaluated separately and a comparative analysis is made for CS, SR, RCL and micro hardness. The important findings of this chapter are summarized as follows:

- The value of SR increases from 1.42  $\mu\text{m}$  corresponding to the parameters of low DE to 3.1  $\mu\text{m}$  for the parameters of high DE for rough cut. SR is improved significantly using trim cut irrespective of high DE for rough cut. An addition of metal powders in a concentration of 1 g/L yields best surface finish of 0.90  $\mu\text{m}$  because of the better spark generation and distribution on work surface. Si powders yields better SR as compared to Al powders.
- SEM images show that the machined surface after rough cut at high DE consist of deep and large size craters whereas a fine and uniform surface texture was obtained after a trim cut. Micro hardness profiles show that the top machined layer is under high thermal damages in rough cut and the extent of this damage is

low for trim cut operation. Al powders with a concentration of 3g/L results in little increase in thickness of RCL while Si powders with a concentration 3g/L results in a smaller TRL.

- Using Al and Si metals powders in dielectric fluid, a remarkable modification are obtained for surface textures after trim cut. Using metal powders in dielectric fluid, the recast layer becomes smooth and dense which increases the micro hardness. Some nm sized impingement is observed on machined surfaces after trim cut using metal powders additives.